



# SATURN

MPR-SAT-FE-70-2

JUNE 20, 1970

(NASA-TM-X-64422) SATURN 5 LAUNCH VEHICLE  
FLIGHT EVALUATION REPORT: AS-508 APOLLO 13  
MISSION (NASA) 242 p

N90-70432

Unclas  
00/15 0257075

## SATURN V LAUNCH VEHICLE FLIGHT EVALUATION REPORT AS-508 APOLLO 13 MISSION

FF No. 602(C)	(ACCESSION NUMBER)	(THRU)
	242	9-C
	(PAGES)	(CODE)
	Tmx-64422	30
	(NASA CR OR TMX OR AD NUMBER)	(CATEGORY)



PREPARED BY  
SATURN FLIGHT EVALUATION WORKING GROUP



NATIONAL AERONAUTICS AND SPACE ADMINISTRATION

GEORGE C. MARSHALL SPACE FLIGHT CENTER

MPR-SAT-FE-70-2

**SATURN V LAUNCH VEHICLE  
FLIGHT EVALUATION REPORT - AS-508  
APOLLO 13 MISSION**

PREPARED BY

SATURN FLIGHT EVALUATION WORKING GROUP







MPR-SAT-FE-70-2

SATURN V LAUNCH VEHICLE FLIGHT EVALUATION REPORT - AS-508

APOLLO 13 MISSION

BY

Saturn Flight Evaluation Working Group  
George C. Marshall Space Flight Center

ABSTRACT

Saturn V AS-508 (Apollo 13 Mission) was launched at 14:13:00.00 Eastern Standard Time on April 11, 1970, from Kennedy Space Center, Complex 39, Pad A. The vehicle lifted off on schedule on a launch azimuth of 90 degrees east of north and rolled to a flight azimuth of 72.043 degrees east of north. The launch vehicle successfully placed the manned spacecraft in the planned translunar injection coast mode despite a premature S-II center engine cutoff. The S-IVB/IU impacted the lunar surface at  $2.5 \pm 0.5$  degrees south and  $27.9 \pm 0.1$  degrees west at 280,601.0 seconds (77:56:41.0) which was 65.5 +7.8, -4.8 kilometers (35.4 +4.2, -2.6 n mi) from the target of 3 degrees south and 30 degrees west. Impact velocity was 2579 m/s (8461 ft/s).

All Mandatory and Desirable Objectives of this mission for the launch vehicle were accomplished except the precise determination of the lunar impact point. It is expected that this will be accomplished at a later date. No failures, anomalies, or deviations occurred that seriously affected the mission.

Any questions or comments pertaining to the information contained in this report are invited and should be directed to:

Director, George C. Marshall Space Flight Center  
Huntsville, Alabama 35812  
Attention: Chairman, Saturn Flight Evaluation Working  
Group, S&E-CSE-LF (Phone 205-453-2575)



## TABLE OF CONTENTS

	Page		Page
TABLE OF CONTENTS	iii	SECTION 4A - LUNAR IMPACT	
LIST OF ILLUSTRATIONS	vi	4A.1 Summary	4A-1
LIST OF TABLES	ix	4A.2 Time Base 8 Maneuvers	4A-1
ACKNOWLEDGEMENT	xi	4A.3 Trajectory Evaluation	4A-5
ABBREVIATIONS	xii	4A.4 Lunar Impact Condition	4A-5
MISSION PLAN	xv	4A.5 Tracking	4A-8
FLIGHT SUMMARY	xviii	SECTION 5 - S-IC PROPULSION	
MISSION OBJECTIVES ACCOMPLISHMENT	xxii	5.1 Summary	5-1
FAILURES, ANOMALIES AND DEVIATIONS	xxiii	5.2 S-IC Ignition Transient Performance	5-1
SECTION 1 - INTRODUCTION		5.3 S-IC Mainstage Performance	5-3
1.1 Purpose	1-1	5.4 S-IC Engine Shutdown Transient Performance	5-7
1.2 Scope	1-1	5.5 S-IC Stage Propellant Management	5-7
SECTION 2 - EVENT TIMES		5.6 S-IC Pressurization Systems	5-8
2.1 Summary of Events	2-1	5.6.1 S-IC Fuel Pressurization System	5-8
2.2 Variable Time and Commanded Switch Selector Events	2-1	5.6.2 S-IC LOX Pressurization System	5-9
SECTION 3 - LAUNCH OPERATIONS		5.7 S-IC Pneumatic Control Pressure System	5-10
3.1 Summary	3-1	5.8 S-IC Purge Systems	5-10
3.2 Prelaunch Milestones	3-1	5.9 S-IC POGO Suppression System	5-10
3.3 Countdown Events	3-1	5.10 S-IC Hydraulic System	5-10
3.4 Propellant Loading	3-1	SECTION 6 - S-II PROPULSION	
3.4.1 RP-1 Loading	3-1	6.1 Summary	6-1
3.4.2 LOX Loading	3-3	6.2 S-II Chilldown and Buildup Transient Performance	6-2
3.4.3 LH <sub>2</sub> Loading	3-3	6.3 S-II Mainstage Performance	6-3
3.5 Insulation	3-3	6.4 S-II Shutdown Transient Performance	6-6
3.6 Ground Support Equipment	3-4	6.5 S-II Stage Propellant Management	6-8
3.6.1 Ground/Vehicle Interface	3-4	6.6 S-II Pressurization System	6-8
3.6.2 MSFC Furnished Ground Support Equipment	3-4	6.6.1 S-II Fuel Pressurization System	6-8
3.6.3 Camera Coverage	3-5	6.6.2 S-II LOX Pressurization System	6-10
SECTION 4 - TRAJECTORY		6.7 S-II Pneumatic Control Pressure System	6-12
4.1 Summary	4-1	6.8 S-II Helium Injection System	6-14
4.2 Trajectory Evaluation	4-1	6.9 S-II Hydraulic System	6-14
4.2.1 Ascent Phase	4-1		
4.2.2 Parking Orbit Phase	4-8		
4.2.3 Injection Phase	4-10		
4.2.4 Post TLI Phase	4-11		

PRECEDING PAGE BLANK NOT FILMED.

## TABLE OF CONTENTS (CONTINUED)

	Page		Page
<b>SECTION 7 - S-IVB PROPULSION</b>			
7.1	Summary	7-1	
7.2	S-IVB Chilldown and Buildup Transient Performance for First Burn	7-2	
7.3	S-IVB Mainstage Performance for First Burn	7-2	
7.4	S-IVB Shutdown Transient Performance for First Burn	7-5	
7.5	S-IVB Parking Orbit Coast Phase Conditioning	7-5	
7.6	S-IVB Chilldown and Restart for Second Burn	7-7	
7.7	S-IVB Mainstage Performance for Second Burn	7-7	
7.8	S-IVB Shutdown Transient Performance for Second Burn	7-11	
7.9	S-IVB Stage Propellant Management	7-11	
7.10	S-IVB Pressurization Systems	7-13	
7.10.1	S-IVB Fuel Pressurization System	7-13	
7.10.2	S-IVB LOX Pressurization System	7-15	
7.11	S-IVB Pneumatic Control System	7-22	
7.12	S-IVB Auxiliary Propulsion System	7-22	
7.13	S-IVB Orbital Safing Operations	7-26	
7.13.1	Fuel Tank Safing	7-27	
7.13.2	LOX Tank Dump and Safing	7-27	
7.13.3	Cold Helium Dump	7-27	
7.13.4	Ambient Helium Dump	7-29	
7.13.5	Stage Pneumatic Control Sphere Safing	7-29	
7.13.6	Engine Start Tank Safing	7-29	
7.13.7	Engine Control Sphere Safing	7-29	
7.14	Hydraulic System	7-29	
<b>SECTION 8 - STRUCTURES</b>			
8.1	Summary	8-1	
8.2	Total Vehicle Structures Evaluation	8-2	
8.2.1	Longitudinal Loads	8-2	
8.2.2	Bending Moments	8-2	
8.2.3	Vehicle Dynamic Characteristics	8-2	
8.3	Vibration Evaluation	8-15	
<b>SECTION 9 - GUIDANCE AND NAVIGATION</b>			
9.1	Summary	9-1	
9.1.1	Performance of the Guidance and Navigation System as Implemented in the Flight Program	9-1	
9.1.2	Instrument Unit Components	9-1	
9.2	Guidance Comparisons	9-1	
9.3	Navigation and Guidance Scheme Evaluation	9-4	
9.4	Guidance System Component Evaluation	9-11	
9.4.1	LVDC and LVDA Performances	9-11	
9.4.2	ST-124M-3 Inertial Platform	9-14	
9.4.3	Ladder Outputs	9-17	
9.4.4	Telemetry Outputs	9-17	
9.4.5	Discrete Outputs	9-17	
9.4.6	Switch Selector Functions	9-17	
<b>SECTION 10 - CONTROL AND SEPARATION</b>			
10.1	Summary	10-1	
10.2	S-IC Control System Evaluation	10-2	
10.3	S-II Control System Evaluation	10-4	
10.4	S-IVB Control System Evaluation	10-7	
10.4.1	Control System Evaluation During First Burn	10-7	
10.4.2	Control System Evaluation During Parking Orbit	10-8	
10.4.3	Control System Evaluation During Second Burn	10-8	
10.4.4	Control System Evaluation After S-IVB Second Burn	10-10	
10.5	Instrument Unit Control Components Evaluation	10-16	
10.6	Separation	10-17	
<b>SECTION 11 - ELECTRICAL NETWORKS AND EMERGENCY DETECTION SYSTEM</b>			
11.1	Summary	11-1	
11.2	S-IC Stage Electrical System	11-1	
11.3	S-II Stage Electrical System	11-2	
11.4	S-IVB Stage Electrical System	11-3	
11.5	Instrument Unit Electrical System	11-8	
11.6	Saturn V Emergency Detection System (EDS)	11-13	
<b>SECTION 12 - VEHICLE PRESSURE AND ACOUSTIC ENVIRONMENT</b>			
12.1	Summary	12-1	
12.2	Base Pressures	12-1	
12.2.1	S-IC Base Pressures	12-1	
12.3	Acoustic Environment	12-5	
12.3.1	External Acoustics	12-5	
<b>SECTION 13 - VEHICLE THERMAL ENVIRONMENT</b>			
13.1	Summary	13-1	
13.2	S-IC Base Heating	13-1	
13.3	S-II Base Heating	13-1	
13.4	Vehicle Aeroheating Thermal Environment	13-6	
<b>SECTION 14 - ENVIRONMENTAL CONTROL SYSTEMS</b>			
14.1	Summary	14-1	
14.2	S-IC Environmental Control	14-1	
14.3	S-II Environmental Control	14-2	
14.4	IU Environmental Control	14-3	
14.4.1	Thermal Conditioning System	14-3	
14.4.2	ST-124M-3 Gas Bearing System	14-7	

## TABLE OF CONTENTS (CONTINUED)

	Page
SECTION 15 - DATA SYSTEMS	
15.1 Summary	15-1
15.2 Vehicle Measurements Evaluation	15-1
15.3 Airborne VHF Telemetry Systems Evaluation	15-2
15.4 C-Band Radar System Evaluation	15-2
15.5 Secure Range Safety Command Systems Evaluation	15-6
15.6 Command and Communication System Evaluation	15-8
15.7 Ground Engineering Cameras	15-8
SECTION 16 - MASS CHARACTERISTICS	
16.1 Summary	16-1
16.2 Mass Evaluation	16-1
SECTION 17 - SPACECRAFT SUMMARY	
17-1	
APPENDIX A - ATMOSPHERE	
A.1 Summary	A-1
A.2 General Atmospheric Conditions at Launch Time	A-1
A.3 Surface Observations at Launch Time	A-1
A.4 Upper Air Measurements	A-1
A.4.1 Wind Speed	A-3
A.4.2 Wind Direction	A-6
A.4.3 Pitch Wind Component	A-6
A.4.4 Yaw Wind Component	A-6
A.4.5 Component Wind Shears	A-6
A.4.6 Extreme Wind Data in the High Dynamic Region	A-6
A.5 Thermodynamic Data	A-6
A.5.1 Temperature	A-6
A.5.2 Atmospheric Pressure	A-15
A.5.3 Atmospheric Density	A-15
A.5.4 Optical Index of Refraction	A-15
A.6 Comparison of Selected Atmospheric Data for Saturn V Launches	A-15
APPENDIX B - AS-508 SIGNIFICANT CONFIGURATION CHANGES	
B.1 Introduction	B-1

## LIST OF ILLUSTRATIONS

Figure	Page	Figure	Page	
2-1	Range Time to Vehicle Time Conversion	2-2	6-6 S-II LOX Tank Ullage Pressure	6-12
4-1	Ascent Trajectory Position Comparison	4-2	6-7 S-II LOX Pump Inlet Conditions	6-13
4-2	Ascent Trajectory Space-Fixed Velocity and Flight Path Angle Comparisons	4-3	7-1 S-IVB Start Box and Run Requirements - First Burn	7-3
4-3	Ascent Trajectory Acceleration Comparison	4-3	7-2 S-IVB Steady State Performance - First Burn	7-4
4-4	Dynamic Pressure and Mach Number Comparisons	4-4	7-3 S-IVB CVS Performance - Coast Phase	7-6
4-5	Ground Track	4-9	7-4 S-IVB Ullage Conditions During Repressurization Using O <sub>2</sub> /H <sub>2</sub> Burner	7-8
4-6	Injection Phase Space-Fixed Velocity and Flight Path Angle Comparisons	4-10	7-5 S-IVB O <sub>2</sub> /H <sub>2</sub> Burner Thrust and Pressurant Flowrates	7-9
4-7	Injection Phase Acceleration Comparison	4-11	7-6 S-IVB Start Box and Run Requirements - Second Burn	7-10
4A-1	S-IVB/IU Unscheduled Velocity Change	4A-3	7-7 S-IVB Steady State Performance - Second Burn	7-12
4A-2	Accumulated Longitudinal Velocity Change During Time Base 8	4A-4	7-8 S-IVB LH <sub>2</sub> Ullage Pressure - First Burn and Parking Orbit	7-14
4A-3	Lunar Impact Trajectory Radius and Space-Fixed Velocity Profiles	4A-6	7-9 S-IVB LH <sub>2</sub> Ullage Pressure - Second Burn and Translunar Coast	7-15
4A-4	Comparison of Projected Lunar Impact Points	4A-7	7-10 S-IVB Fuel Pump Inlet Conditions - First Burn	7-16
4A-5	Summary of CCS Tracking Data Used for Post-TLI Orbit Determination	4A-10	7-11 S-IVB Fuel Pump Inlet Conditions - Second Burn	7-17
5-1	S-IC LOX Start Box Requirements	5-2	7-12 S-IVB LOX Tank Ullage Pressure - First Burn and Parking Orbit	7-18
5-2	S-IC Engines Thrust Buildup	5-3	7-13 S-IVB LOX Tank Ullage Pressure - Second Burn and Translunar Coast	7-19
5-3	S-IC Stage Propulsion Performance	5-4	7-14 S-IVB LOX Pump Inlet Conditions - First Burn	7-20
5-4	F-1 LOX Pump Bearing Jet Pressure, Engine No. 2	5-6	7-15 S-IVB LOX Pump Inlet Conditions - Second Burn	7-21
5-5	S-IC Stage Fuel Ullage Pressure	5-8	7-16 S-IVB Cold Helium Supply History	7-23
5-6	S-IC Stage LOX Tank Ullage Pressure	5-9	7-17 APS Helium Bottle Temperature and Regulator Outlet Pressure	7-25
6-1	S-II Engine Start Tank Performance	6-2	7-18 S-IVB LOX Dump and Orbital Safing Sequence	7-26
6-2	S-II Engine Pump Inlet Start Requirements	6-4	7-19 S-IVB LOX Dump Parameter Histories	7-28
6-3	S-II Steady State Operation	6-5	8-1 Longitudinal Acceleration at CM and IU During Thrust Buildup and Launch	8-3
6-4	S-II Fuel Tank Ullage Pressure	6-9	8-2 Longitudinal Load at Time of Maximum Bending Moment, CECO and OECO	8-3
6-5	S-II Fuel Pump Inlet Conditions	6-11		

## LIST OF ILLUSTRATIONS (CONTINUED)

Figure	Page	Figure	Page
8-3	Maximum Bending Moment Near Max Q	8-4	
8-4	Comparison of Longitudinal Responses During S-IC Boost	8-5	
8-5	Longitudinal Acceleration at CM and IU at S-IC CECO and OECO	8-5	
8-6	Comparison of S-II Engine No. 5 Thrust Pad Acceleration With Previous Flights	8-6	
8-7	Comparison of S-II Engine No. 1 Thrust Pad Acceleration With Previous Flights	8-6	
8-8	S-II Pre-CECO Thrust Chamber Pressure Characteristics	8-7	
8-9	Comparison of S-II LOX Sump Acceleration With Previous Flights	8-7	
8-10	S-II Stage Center Engine LOX Feed System	8-9	
8-11	Center Engine LOX Pump Inlet Pressure Shift and Beam Vibration	8-9	
8-12	Center Engine Gain During S-II Oscillations	8-10	
8-13	S-II LOX Ullage Pressure	8-10	
8-14	Comparison of AS-507/AS-508 S-II Engine No. 5 LOX Line Characteristics	8-11	
8-15	S-II Engine Inboard/Outboard Power Ratio	8-11	
8-16	AS-508/AS-507 Longitudinal Acceleration Response Comparison During S-II Oscillations	8-13	
8-17	AS-508/AS-507 Acceleration and Pressure Characteristics From S-II CECO to OECO (8 to 14 Bandpass Filter)	8-14	
8-18	S-IVB First Burn Spectral Analyses	8-16	
8-19	S-IVB Second Burn Spectral Analyses	8-16	
8-20	S-IVB Aft Interstage Skin and Stringer Vibration	8-17	
9-1	Trajectory and ST-124M-3 Platform Velocity Comparison Boost-to-EPO (Trajectory Minus Guidance)	9-2	
9-2	Trajectory and ST-124M-3 Platform Velocity Comparison Second S-IVB Burn	9-3	
9-3	LH <sub>2</sub> Continuous Vent Thrust During Parking Orbit	9-8	
9-4	Attitude Commands During Boost to EPO	9-9	
9-5	Attitude Commands During S-IVB Second Burn	9-10	
9-6	Crossrange Velocity Measured by the ST-124M-3 Inertial Platform	9-15	
9-7	ST-124M-3 Accelerometer Pickoff	9-15	
10-1	Pitch and Yaw Plane Dynamics During S-IC Burn	10-3	
10-2	Angle-of-Attack During S-IC Burn	10-5	
10-3	Pitch and Yaw Plane Attitude Errors During S-II Burn	10-6	
10-4	Pitch and Yaw Attitude Errors During S-IVB First Burn	10-7	
10-5	Pitch Attitude Error During Parking Orbit	10-9	
10-6	Pitch and Yaw Attitude Errors During S-IVB Second Burn	10-9	
10-7	Pitch Attitude Error During Translunar Coast	10-11	
10-8	Yaw Rate Gyro Switch	10-14	
10-9	Pitch and Yaw Control System Response to Loss of Attitude Reference	10-15	
11-1	S-IVB Stage Forward No. 1 Battery Voltage and Current	11-4	
11-2	S-IVB Stage Forward No. 2 Battery Voltage and Current	11-5	
11-3	S-IVB Stage Aft No. 1 Battery Voltage and Current	11-6	
11-4	S-IVB Stage Aft No. 2 Battery Voltage and Current	11-7	
11-5	IU Battery 6D10 Voltage, Current and Temperature	11-9	
11-6	IU Battery 6D20 Voltage, Current and Temperature	11-10	
11-7	IU Battery 6D30 Voltage, Current and Temperature	11-11	
11-8	IU Battery 6D40 Voltage, Current and Temperature	11-12	
12-1	S-IC Base Heat Shield Differential Pressure	12-2	
12-2	S-II Base Heat Shield Forward Face Pressure	12-3	
12-3	S-II Thrust Cone Pressure	12-3	
12-4	S-II Heat Shield Aft Face Pressure	12-4	
12-5	AS-508 Acoustic Instrumentation	12-6	
12-6	External Overall Sound Pressure Level At Liftoff	12-6	
12-7	Vehicle External Overall Fluctuating Pressure Level	12-7	
12-8	Vehicle External Fluctuating Pressure Spectral Densities	12-9	
13-1	S-IC Base Heat Shield Total Heating Rate	13-2	

## LIST OF ILLUSTRATIONS (CONTINUED)

Figure		Page
13-2	S-IC Base Gas Temperature	13-3
13-3	S-IC Ambient Gas Temperature Under Engine Cocoon	13-4
13-4	S-II Heat Shield Aft Heat Rate	13-5
13-5	S-II Heat Shield Recovery Temperature	13-5
13-6	S-II Heat Shield Aft Radiation Heat Rate	13-7
13-7	Forward Location of Separated Flow on S-IC Stage	13-7
14-1	S-IC Aft Compartment Temperature Near Battery 12K10	14-2
14-2	IU TCS Coolant Control Parameters	14-3
14-3	IU Sublimator Performance During Ascent	14-4
14-4	IU TCS Hydraulic Performance	14-5
14-5	IU TCS GN <sub>2</sub> Sphere Pressure (D025-601)	14-5
14-6	Selected IU Component Temperatures	14-6
14-7	Comparison of AS-507 and AS-508 IU Temperatures	14-7
14-8	IU Inertial Platform GN <sub>2</sub> Pressures	14-8
14-9	IU GBS GN <sub>2</sub> Sphere Pressure (D010-603)	14-9
15-1	VHF Telemetry Coverage Summary	15-5
15-2	C-Band Radar Coverage Summary	15-7
15-3	CCS Coverage Summary	15-10
A-1	Surface Weather Map Approximately 7 Hours Before Launch of AS-508	A-2
A-2	500 Millibar Map Approximately 7 Hours Before Launch of AS-508	A-3
A-3	Scalar Wind Speed at Launch Time of AS-508	A-5
A-4	Wind Direction at Launch Time of AS-508	A-7
A-5	Pitch Wind Velocity Component (W <sub>x</sub> ) at Launch Time of AS-508	A-8
A-6	Yaw Wind Velocity Component (W <sub>y</sub> ) at Launch Time of AS-508	A-9
A-7	Pitch (S <sub>x</sub> ) and Yaw (S <sub>y</sub> ) Component Wind Shears at Launch Time of AS-508	A-10
A-8	Relative Deviation of Temperature and Pressure From the PRA-63 Reference Atmosphere, AS-508	A-13
A-9	Relative Deviation of Density and Absolute Deviation of the Index of Refraction From the PRA-63 Reference Atmosphere, AS-508	A-14

## LIST OF TABLES

Table	Page	Table	Page
1	Mission Objectives Accomplishment	9-1	Inertial Platform Velocity Comparisons (PACSS 12 Coordinate System)
2	Summary of Anomaly		9-5
3	Summary of Deviations	9-2	Guidance Comparisons (PACSS 13)
2-1	Time Base Summary	2-3	
2-2	Significant Event Times Summary	2-4	
2-3	Variable Time and Commanded Switch Selector Events	2-10	
3-1	AS-508/Apollo 13 Prelaunch Milestones	3-2	
4-1	Comparison of Significant Trajectory Events	4-5	
4-2	Comparison of Cutoff Events	4-6	
4-3	Comparison of Separation Events	4-7	
4-4	Stage Impact Location	4-8	
4-5	Parking Orbit Insertion Conditions	4-9	
4-6	Translunar Injection Conditions	4-12	
4A-1	Comparison of Time Base 8 Velocity Increments	4A-4	
4A-2	Comparison of Attitude Time Line, Time Base 8	4A-5	
4A-3	Comparison of Orbit Parameters After the Unscheduled Delta V	4A-7	
4A-4	S-IVB/IU Lunar Impact Parameters	4A-8	
4A-5	Summary of Lunar Impact Times	4A-9	
4A-6	S-IVB/IU CCS Tracking Network	4A-11	
5-1	S-IC Individual Engine Performance	5-5	
5-2	S-IC Stage Propellant Mass History	5-7	
6-1	S-II Engine Performance	6-7	
6-2	S-II Engine Performance Shifts	6-7	
6-3	S-II Propellant Mass History	6-9	
7-1	S-IVB Steady State Performance - First Burn (STDV +130 Second Time Slice at Standard Altitude Conditions)	7-5	
7-2	S-IVB Steady State Performance - Second Burn (STDV +130 Second Time Slice at Standard Altitude Conditions)	7-11	
7-3	S-IVB Stage Propellant Mass History	7-13	
7-4	S-IVB APS Propellant Consumption	7-24	
		9-7	Start and Stop Times for IGM Guidance Commands
		10-1	Maximum Control Parameters During S-IC Flight
		10-2	AS-508 Liftoff Misalignment Summary
		10-3	Maximum Control Parameters During S-II Burn
		10-4	Maximum Control Parameters During S-IVB First Burn
		10-5	Maximum Control Parameters During S-IVB Second Burn
		11-1	S-IC Stage Battery Power Consumption
		11-2	S-II Stage Battery Power Consumption
		11-3	S-IVB Stage Battery Power Consumption
		11-4	IU Battery Power Consumption
		15-1	AS-508 Measurement Summary
		15-2	AS-508 Flight Measurements Waived Prior to Flight
		15-3	AS-508 Measurement Malfunctions
		15-4	AS-508 Questionable Flight Measurements
		15-5	AS-508 Launch Vehicle Telemetry Links
		15-6	Command and Communication System Commands History, AS-508
		16-1	Total Vehicle Mass, S-IC Burn Phase (Kilograms)
		16-2	Total Vehicle Mass, S-IC Burn Phase (Pounds)
		16-3	Total Vehicle Mass, S-II Burn Phase (Kilograms)

## LIST OF TABLES (CONTINUED)

Table		Page
16-4	Total Vehicle Mass, S-II Burn Phase (Pounds)	16-4
16-5	Total Vehicle Mass, S-IVB First Burn Phase (Kilograms)	16-5
16-6	Total Vehicle Mass, S-IVB First Burn Phase (Pounds)	16-5
16-7	Total Vehicle Mass, S-IVB Second Burn Phase (Kilograms)	16-6
16-8	Total Vehicle Mass, S-IVB Second Burn Phase (Pounds)	16-6
16-9	Flight Sequence Mass Summary	16-7
16-10	Mass Characteristics Comparison	16-9
A-1	Surface Observations at AS-508 Launch Time	A-2
A-2	Solar Radiation at AS-508 Launch Time, Launch Pad 39A	A-4
A-3	Systems Used to Measure Upper Air Wind Data for AS-508	A-4
A-4	Maximum Wind Speed in High Dynamic Pressure Region for Apollo/Saturn 501 through Apollo/Saturn 508 Vehicles	A-11
A-5	Extreme Wind Shear Values in the High Dynamic Pressure Region for Apollo/Saturn 501 through Apollo/Saturn 508 Vehicles	A-12
A-6	Selected Atmospheric Observations for Apollo/Saturn 501 through Apollo/Saturn 508 Vehicle Launches at Kennedy Space Center, Florida	A-15
B-1	S-IC Significant Configuration Changes	B-1
B-2	S-II Significant Configuration Changes	B-2
B-3	S-IVB Significant Configuration Changes	B-2
B-4	IU Significant Configuration Changes	B-3

## ACKNOWLEDGEMENT

This report is published by the Saturn Flight Evaluation Working Group, composed of representatives of Marshall Space Flight Center, John F. Kennedy Space Center, and MSFC's prime contractors, and in cooperation with the Manned Spacecraft Center. Significant contributions to the evaluation have been made by:

George C. Marshall Space Flight Center

Science and Engineering

Central Systems Engineering  
Aero-Astroynamics Laboratory  
Astrionics Laboratory  
Computation Laboratory  
Astronautics Laboratory

Program Management

John F. Kennedy Space Center

Manned Spacecraft Center

The Boeing Company

McDonnell Douglas Astronautics Company

International Business Machines Company

North American Rockwell/Space Division

North American Rockwell/Rocketdyne Division

## ABBREVIATIONS

ACS	Alternating Current Power Supply	ECS	Environmental Control System
AOS	Acquisition of Signal	EDS	Emergency Detection System
APS	Auxiliary Propulsion System	EMR	Engine Mixture Ratio
ARIA	Apollo Range Instrument Aircraft	EPO	Earth Parking Orbit
ASC	Accelerometer Signal Conditioner	ESC	Engine Start Command
BDA	Bermuda	EST	Eastern Standard Time
CCS	Command and Communications System	ETW	Error Time Word
CDDT	Countdown Demonstration Test	EVA	Extra-Vehicular Activity
CECO	Center Engine Cutoff	FCC	Flight Control Computer
CG	Center of Gravity	FM/FM	Frequency Modulation/ Frequency Modulation
CM	Command Module	FRT	Flight Readiness Test
CNV	Cape Kennedy	GBS	Gas Bearing System
CRO	Carnarvon	GFCV	GOX Flow Control Valve
CSM	Command and Service Module	GDS	Goldstone
CVS	Continuous Vent System	GDSX	Goldstone Wing Station
CYI	Grand Canary Island	GG	Gas Generator
DEE	Digital Events Evaluator	GOX	Gaseous Oxygen
DO	Desirable Objective	GRR	Guidance Reference Release
DTS	Data Transmission System	GSE	Ground Support Equipment
EBW	Exploding Bridge Wire	GSCU	Ground Support Cooling Unit
ECO	Engine Cutoff	GWM	Guam
ECP	Engineering Change Proposal	GYM	Guaymas
		HAW	Hawaii
		HDA	Holddown Arm
		HFCV	Helium Flow Control Valve

ABBREVIATIONS (CONTINUED)

HSK	Honeysuckle Creek	MSFN	Manned Space Flight Network
HSKX	Honeysuckle Creek Wing Station	MSS	Mobile Service Structure
IGM	Iterative Guidance Mode	MTF	Mississippi Test Facility
IMU	Inertial Measurement Unit	M/W	Methanol Water
IU	Instrument Unit	NPSP	Net Positive Suction Pressure
KSC	Kennedy Space Center	NPV	Nonpropulsive Vent
LET	Launch Escape Tower	NASA	National Aeronautics and Space Administration
LH <sub>2</sub>	Liquid Hydrogen	OAT	Overall Test
LM	Lunar Module	OCP	Orbital Correction Program
LOI	Lunar Orbit Insertion	OECO	Outboard Engine Cutoff
LOS	Loss of Signal	OMPT	Operational Mass Point Trajectory
LOX	Liquid Oxygen	OT	Operational Trajectory
LV	Launch Vehicle	PAFB	Patrick Air Force Base
LVDA	Launch Vehicle Data Adapter	PCM	Pulse Code Modulation
LVDC	Launch Vehicle Digital Computer	PCM/ FM	Pulse Code Modulation/ Frequency Modulation
LVGSE	Launch Vehicle Ground Support Equipment	PEA	Platform Electronics Assembly
MAD	Madrid	POI	Parking Orbit Insertion
MADX	Madrid Wing Station	PMR	Programed Mixture Ratio
MCC-H	Mission Control Center - Houston	PRA	Patrick Reference Atmosphere
MILA	Merritt Island Launch Area	PTCS	Propellant Tanking Control System
ML	Mobile Launcher	PU	Propellant Utilization
MMH	Monomethyl Hydrazine	RF	Radiofrequency
MO	Mandatory Objective	RFI	Radiofrequency Interference
MOV	Main Oxidizer Valve	RMS	Root Mean Square
MR	Mixture Ratio	RP-1	Designation for S-IC Stage Fuel (kerosene)
MSC	Manned Spacecraft Center		
MSFC	Marshall Space Flight Center		

## ABBREVIATIONS (CONTINUED)

SA	Service Arm
SC	Spacecraft
SCFM	Standard Cubic Feet per Minute
SLA	Spacecraft/LM Adapter
SM	Service Module
SPS	Service Propulsion System
SRSCS	Secure Range Safety Command System
SS/FM	Single Sideband/Frequency Modulation
STDV	Start Tank Discharge Valve
SV	Space Vehicle
$T_1$	Time Base 1
TCS	Thermal Conditioning System
TD&E	Transposition, Docking and Ejection
TEI	Transearth Injection
TEX	Corpus Christi (Texas)
TLI	Translunar Injection
TMR	Triple Module Redundant
TSM	Tail Service Mast
TVC	Thrust Vector Control
UCR	Unsatisfactory Condition Report
USB	Unified S-Band
UT	Universal Time
VA	Volt Amperes
VAN	Vanguard (ship)
VHF	Very High Frequency

## MISSION PLAN

The AS-508 flight (Apollo 13 Mission) is the eighth flight in the Apollo/Saturn V flight program, the third lunar landing mission and the first landing planned for the lunar highlands. The primary mission objectives are: a) Perform selenological inspection, survey, and sampling of materials in a preselected region of the Fra Mauro formation; b) deploy and activate the Apollo Lunar Surface Experiments Package (ALSEP III); c) develop man's capability to work in the lunar environment; and d) obtain photographs of candidate exploration sites. The crew consists of James A. Lovell (Mission Commander), John L. Swigert, Jr. (Command Module Pilot), and Fred W. Haise, Jr. (Lunar Module Pilot).

The AS-508 launch vehicle is composed of the S-IC-8, S-II-8, and S-IVB-508 stages, and Instrument Unit-508. The Spacecraft (SC) consists of Spacecraft/Lunar Module Adapter (SLA)-16, Command and Service Module (CSM)-109, and Lunar Module (LM)-7.

Vehicle launch from Complex 39A at Kennedy Space Center (KSC) is along a 90 degree azimuth with a roll to a flight azimuth of approximately 72 degrees measured east of true north. Vehicle mass at ignition is 6,505,746 lbm.

The S-IC stage powered flight is approximately 164 seconds; the S-II stage provides powered flight for approximately 392 seconds. Following S-IVB burn (approximately 144 seconds duration), the S-IVB/IU/SLA/LM/CSM is inserted into a circular 100 n mi altitude (referenced to the earth equatorial radius) Earth Parking Orbit (EPO). Vehicle mass at orbit insertion is 300,263 lbm.

At approximately 10 seconds after EPO insertion, the vehicle is aligned with the local horizontal. Continuous hydrogen venting is initiated shortly after EPO insertion and the Launch Vehicle (LV) and CSM systems are checked in preparation for the Translunar Injection (TLI) burn. During the second or third revolution in EPO, the S-IVB stage is restarted and burns for approximately 356 seconds. This burn injects the S-IVB/IU/SLA/LM/CSM into a free-return, translunar trajectory.

Within 15 minutes after TLI, the vehicle initiates an inertial attitude hold for CSM separation, docking and LM ejection. Following the attitude freeze, the CSM separates from the LV and the SLA panels are jettisoned. The CSM then transposes and docks to the LM. After docking, the CSM/LM is spring ejected from the S-IVB/IU. Following separation of the combined CSM/LM from the S-IVB/IU, the S-IVB/IU will perform a yaw maneuver and an 80 second burn of the S-IVB Auxiliary Propulsion System (APS) ullage engines to propel the S-IVB/IU a safe distance away from the spacecraft. Subsequent to the completion of the S-IVB/IU evasive maneuver, the S-IVB/IU is placed on a trajectory such that it will impact the lunar surface in the vicinity of the Apollo 12 landing site. The impact trajectory is achieved by propulsive venting of liquid hydrogen (LH<sub>2</sub>), dumping of liquid oxygen (LOX) and by firing the APS engines. The S-IVB/IU impact will be recorded by the seismograph deployed during the Apollo 12 mission. S-IVB/IU lunar impact is predicted at approximately 77 hours 45 minutes after launch.

During the three day translunar coast, the astronauts will perform star-earth landmark sightings, Inertial Measurement Unit (IMU) alignments, general lunar navigation procedures and possibly four midcourse corrections. One of these maneuvers will transfer the SC into a low-periselenium non-free-return translunar trajectory at approximately 28 hours after TLI. At approximately 77 hours and 25 minutes, a Service Propulsion System (SPS), Lunar Orbit Insertion (LOI) burn of approximately 356 seconds inserts the CSM/LM into a 59 by 170 n mi altitude parking orbit.

Approximately two revolutions after LOI, a 23.1-second SPS burn will adjust the orbit into a 9 by 59 n mi altitude. The LM is entered by astronauts Lovell and Haise and checkout is accomplished. During the twelfth revolution in orbit at 59 hours, the LM separates from the CSM and prepares for the lunar descent. The LM descent propulsion system is used to brake the LM into the proper landing trajectory and maneuver the LM during descent to the lunar surface.

Following lunar landing, two 4.0 hour Extravehicular Activity (EVA) time periods are scheduled during which the astronauts will explore the lunar surface, examine the LM exterior, photograph the lunar terrain, and deploy scientific instruments. The total stay time on the lunar surface is open-ended, with a planned maximum of 35 hours, depending upon the outcome of current lunar surface operations planning and of real-time operational decisions. After the EVA, the astronauts prepare the LM ascent propulsion system for lunar ascent.

The CSM performs a plane change approximately 24 hours before lunar ascent. At approximately 137 hours and 16 minutes, the ascent stage inserts the LM into a 9 by 44 n mi altitude lunar orbit, and rendezvous and docks with the CSM. Following docking, equipment transfer and

decontamination procedures, the LM ascent stage is jettisoned and targeted to impact the lunar surface between Apollo 12 and Apollo 13 landing sites. Seismometer readings will be provided from both sites. Following LM ascent stage deorbit burn, the CSM performs a plane change to photograph future landing sites. Photographing and landmark tracking will be performed during revolutions 40 through 44. Transearth Injection (TEI) is accomplished at the end of revolution 46 at approximately 167 hours and 29 minutes with a 135-second SPS burn.

During the 73-hour transearth coast, the astronauts will perform navigation procedures, star-earth-moon sightings and possibly three midcourse corrections. The Service Module (SM) will separate from the Command Module (CM) 15 minutes before reentry. Splashdown will occur in the Pacific Ocean approximately 241 hours and 3 minutes after liftoff.

After the recovery operations, a biological quarantine is imposed on the crew and CM. An incubation period of 18 days from splashdown (21 days from lunar ascent) is required for the astronauts. The hardware incubation period is the time required to analyze certain lunar samples.

## FLIGHT SUMMARY

The sixth manned Saturn V Apollo space vehicle, AS-508 (Apollo 13 Mission) was launched at 14:13:00 Eastern Standard Time on April 11, 1970 from Kennedy Space Center, Complex 39, Pad A. Except for high amplitude, low frequency oscillations which resulted in premature S-II Center Engine Cutoff (CECO), the basic performance of the launch vehicle was satisfactory. The high amplitude oscillations were not transmitted above the S-II stage. Despite the anomaly, this eighth launch of the Saturn V/Apollo successfully performed all the mandatory and desirable launch vehicle objectives. All aspects of the S-IVB/IU lunar impact objective were accomplished successfully except for the precise determination of the impact point. It is expected that the final impact solution will satisfy the mission objective.

The launch countdown support systems performed well. However, several systems experienced component failures and malfunctions that required corrective action. All repairs were accomplished in time to maintain the launch schedule and no unscheduled holds were experienced. Damage to the pad, mobile launcher, and support equipment was minor.

The vehicle was launched on an azimuth 90 degrees east of north. A roll maneuver at 12.6 seconds placed the vehicle on a flight azimuth of 72.043 degrees east of north. Trajectory parameters were close to nominal during S-IC stage and S-II stage burns until early shutdown of the S-II center engine. The premature S-II CECO caused considerable deviations for certain launch vehicle trajectory parameters. Despite these deviations, near nominal trajectory parameters were achieved at parking orbit insertion and at Translunar Injection (TLI) although the events occurred 44.0 and 13.6 seconds later than predicted, respectively at a heading angle 1.230 degrees later than nominal. Command Service Module (CSM) separation occurred 38.9 seconds later than predicted, causing some deviation in trajectory parameters at this time. The earth impact locations for the S-IC and S-II stages were determined by a theoretical free-flight simulation. The analyses for the S-IC and S-II stages showed the surface range for the impact points to be 7.6 kilometers (4.1 n mi) and 8.6 kilometers (4.6 n mi) greater than nominal, respectively.

At 280,599.7  $\pm$ 0.1 seconds (77:56:39.7) vehicle time the S-IVB/IU impacted the lunar surface at approximately 2.5  $\pm$ 0.5 degrees south latitude and 27.9  $\pm$ 0.1 degrees west longitude, which is approximately 65.5 +7.8, -4.8 kilometers (35.4 +4.2, -2.6 n mi) from the target of 3 degrees south latitude and 30 degrees west longitude. Impact velocity was 2579 m/s (8461 ft/s). The mission objectives were to maneuver the S-IVB/IU such that it would have at least a 50 percent probability of impacting the lunar surface within 350 kilometers (189 n mi) of the target, and to determine the actual impact point within 5 kilometers (2.7 n mi) and the time of impact within 1 second. Preliminary results of the seismic experiment indicate that the S-IVB/IU impact signal was 20 to 30 times greater in amplitude and four times longer in duration than the Apollo 12 Lunar Module (LM) impact.

All S-IC propulsion systems performed satisfactorily, as did the hydraulic system. Stage thrust, specific impulse, total propellant consumption rate, and total consumed mixture ratio (averaged from liftoff to OECO) were 0.26, 0.20, 0.06, and 0.24 percent higher than predicted, respectively. Total propellant consumption from holddown arm release to Outboard Engine Cutoff (OECO) was low by 0.06 percent. CECO was commanded by the IU as planned. OECO, initiated by the LOX low level sensors, occurred 0.4 second earlier than predicted.

The S-II propulsion system performance was satisfactory throughout flight except for the premature CECO which occurred 132.4 seconds early due to high amplitude, low frequency oscillations in the propulsion/structural system. OECO occurred 34.5 seconds late as a result of the early CECO. Stage thrust, propellant flowrate, and propellant mixture ratio were 0.19, 0.25, and 0.18 percent lower than predicted, respectively, at the standard time slice 62 seconds after engine start. The specific impulse at this time slice was 0.09 percent higher than predicted. The IU command to shift Engine Mixture Ratio from high to low upon attainment of a pre-programmed stage velocity increase occurred 32.2 seconds later than predicted primarily because of the early CECO. The engine servicing, recirculation, helium injection, valve actuation, and LOX and LH<sub>2</sub> tank pressurization systems all performed satisfactorily. S-II hydraulic system performance was normal throughout flight.

The J-2 engine operated satisfactorily throughout the operational phase of S-IVB first and second burns with normal engine shutdowns. S-IVB first burn duration was 9.3 seconds longer than predicted, primarily due to the performance of lower stages. The engine performance during first burn, as determined from standard altitude reconstruction analysis, differed from the predicted by +0.29 percent for thrust while the specific impulse was near that predicted. The Continuous Vent System (CVS) adequately regulated LH<sub>2</sub> tank ullage pressure at an average level of 19.3 psia during orbit and the Oxygen/Hydrogen burner satisfactorily achieved LH<sub>2</sub> and LOX tank repressurization for restart. Engine restart conditions

were within specified limits. The restart with the propellant utilization valve fully open was successful. S-IVB second burn duration was 4.9 seconds less than predicted. The engine performance during second burn, as determined from the standard altitude reconstruction analysis, differed from the predicted by -0.24 percent for thrust and 0.09 percent for specific impulse. Subsequent to second burn the stage propellant tanks and helium spheres were safed satisfactorily. Sufficient impulse was derived from LOX dump, LH<sub>2</sub> CVS operation and APS ullage burn to achieve a successful lunar impact. An additional velocity change of 7 to 10 ft/s was experienced during the unanticipated APS firings at 70,150 seconds (19:29:10). The S-IVB hydraulic system performance was satisfactory throughout the mission.

The structural loads experienced during S-IC boost phase were well below design values. The maximum Q region bending moment was  $69 \times 10^6$  lbf-in. at the S-IC LOX tank, which was 25 percent of design value. Thrust cut-off transients experienced by AS-508 were similar to those of previous flights. The maximum dynamic transient at the IU resulting from S-IC CECO was  $\pm 0.20$  g longitudinal. At OECO a maximum dynamic longitudinal acceleration of  $\pm 0.28$  g and  $\pm 0.85$  g was experienced at the IU and Command Module (CM), respectively. The order of magnitude of the thrust cutoff responses are considered normal. During S-IC stage boost phase, 4 to 5 hertz oscillations were detected beginning at 100 seconds. The maximum amplitude measured in the IU at 125 seconds was  $\pm 0.04$  g. Oscillations in the 4 to 5 hertz range have been observed on previous flights and are considered to be normal vehicle response to flight environment. AS-508 experienced low frequency (14 to 16 hertz) POGO oscillations during S-II stage boost. Three distinct periods of structural/propulsion coupled oscillations exhibited peaks at 180, 250, and 330 seconds. The third period of oscillations resulted in LOX pump discharge pressure variations of sufficient magnitude to activate the center engine thrust OK pressure switches and shut down the engine 132.4 seconds early. All oscillations decayed to a normal level following CECO. Analysis of flight data indicates that no structural failure occurred as a result of the oscillations. Flight measurements also show that the oscillations were confined to the S-II stage and were not transmitted up the vehicle. The structural loads experienced during the S-IVB stage burn were well below design values. During first burn the S-IVB experienced low amplitude 18 to 20 hertz oscillations. The amplitudes measured on the gimbal block were comparable to previous flights and well within the expected range of values. Similarly, S-IVB second burn produced intermittent low amplitude oscillations in the 12 to 14 hertz frequency range which peaked near second burn cutoff. Three vibration measurements were made on the S-IVB aft interstage. The maximum vibration levels measured occurred at liftoff and during the Mach 1 to Max Q flight period.

The guidance and navigation system performed satisfactorily resulting in accurate parking orbit and TLI parameters. Guidance parameters were modified to compensate for the early S-II CECO, and the S-IVB burn was lengthened to compensate for the additional gravity losses during S-II burn. The Launch Vehicle Digital Computer (LVDC), the Launch Vehicle

Data Adapter (LVDA), and the ST-124M-3 inertial platform functioned satisfactorily. Crossrange velocity, as measured by the inertial platform, exhibited a negative shift of approximately 0.65 m/s (2.13 ft/s) at approximately 3.4 seconds, introducing a 0.5 m/s (1.6 ft/s) velocity error. The velocity shift probably resulted from the accelerometer head momentarily contacting a mechanical stop due to the high vibration levels after liftoff. The effect on navigation accuracy was negligible. A similar crossrange velocity shift was exhibited on AS-506. At 68,948 seconds (19:09:08), the LVDC exhibited a memory failure due to 6D10 battery depletion, and the flight program essentially ceased operation.

Vehicle control system performance was satisfactory during the flight. At Iterative Guidance Mode (IGM) initiation a pitchup transient occurred similar to that experienced on previous flights. All separations were normal. During the CSM separation from the S-IVB/IU and during the Transposition, Docking and Ejection (TD&E) maneuver the control system maintained a fixed inertial attitude to provide a stable docking platform. Following TD&E, S-IVB/IU attitude control was maintained during the evasive maneuver, the maneuver to lunar impact attitude, and the LOX dump and APS burns. An unscheduled decrease in range rate of approximately 2 to 3 m/s (7 to 10 ft/s) was experienced for approximately 60 seconds beginning at 70,150 seconds (19:29:10). This unscheduled maneuver had no adverse effect on lunar targeting.

The launch vehicle electrical systems and emergency detection system performed satisfactorily throughout all phases of flight. Operation of the batteries, power supplies, inverters, exploding bridgewire firing units, and switch selectors was normal. AS-508 was the first flight for which significant data were available to battery depletion.

Vehicle base pressure, base thermal and acoustic environments, in general, were similar to those experienced on earlier flights. The environmental control system performance was satisfactory.

All elements of the data system performed satisfactorily throughout the flight. Measurements from onboard telemetry were 99.9 percent reliable. Telemetry performance was normal and Radiofrequency (RF) propagation was generally good although the usual problems due to flame effects and staging were experienced. Usable VHF data were received to 14,280 seconds (03:58:00). Command systems RF performance for both the secure range safety command systems and the Command and Communications System (CCS) was normal. Usable CCS telemetered data were received to 70,380 seconds (19:33:00). CCS signal carrier was tracked until lunar impact. The only significant problem encountered during the mission was signal interference between the IU CCS and the LM unified S-band during translunar coast. This problem was caused by the necessity to power the LM before S-IVB/IU lunar impact. Good tracking data were received from the C-band radar with Carnarvon reporting final loss of signal at 44,220 seconds (12:17:00). The 67 ground engineering cameras provided good data during the launch.

## MISSION OBJECTIVES ACCOMPLISHMENT

Table 1 presents the MSFC Mandatory Objectives and Desirable Objectives as defined in the Saturn V Mission Implementation Plan, "H" Series Missions, Apollo 12, 13, 14, and 15; MSFC Document PM-SAT-8010.5 (Revision C), dated February 9, 1970. An assessment of the degree of accomplishment of each objective is shown. Discussion supporting the assessment can be found in other sections of this report as shown in Table 1.

Table 1. Mission Objectives Accomplishment

NO.	MSFC MANDATORY OBJECTIVES (MO) AND DESIRABLE OBJECTIVES (DO)	DEGREE OF ACCOMPLISHMENT	DISCREPANCIES	PARAGRAPH IN WHICH DISCUSSED
1	Launch on a flight azimuth between 72 and 96 degrees and insert the S-IVB/IU/SC into the planned circular earth parking orbit (MO).	Complete	None	4.1, 9.1.1
2	Restart the S-IVB during either the second or third revolution and inject the S-IVB/IU/SC onto the planned translunar trajectory (MO).	Complete	None	4.2.3, 7.6
3	Provide the required attitude control for the S-IVB/IU/SC during TD&E (MO).	Complete	None	10.4.4
4	Perform an evasive maneuver after ejection of the CSM/LM from the S-IVB/IU (DO).	Complete	None	10.4.4
5	Attempt to impact the S-IVB/IU on the lunar surface within 350 kilometers of 3 degrees South, 30 degrees West (DO).	Complete	None	4A.1
6	Determine actual impact point within 5 kilometers and time of impact within one second (DO).	Probably Complete	Analysis not Complete	4A.1
7	Vent and dump the remaining gases and propellants to save the S-IVB/IU (DO).	Complete	None	7.13

## FAILURES, ANOMALIES AND DEVIATIONS

Evaluation of the launch vehicle data revealed no failures, one anomaly and three deviations. The anomaly and the deviations are summarized in the following tables.

Table 2. Summary of Anomaly

ANOMALY IDENTIFICATION					RECOMMENDED CORRECTIVE ACTION			
ITEM	VEHICLE SYSTEM	DESCRIPTION (CAUSE)	EFFECT ON MISSION	OCCURRENCE (RANGE TIME SECONDS)	DESCRIPTION	ACTION STATUS	VEHICLE EFFECTIVITY	PARAGRAPH REFERENCE
1	S-II Structure/ Propulsion	High amplitude oscillations in the 14 to 16 hertz range during S-II mainstage were sufficiently severe to cause the center engine to shut down 132 seconds early. (Oscillations of this frequency are an inherent characteristic of the present configuration of the S-II stage, although the high amplitude occurring during AS-508 flight was not expected.)	None	330.6	<p>Addition of an accumulator in the LOX feed line of center engine to lower the natural frequency of the line, and hence decouple the line from the cross-beam mode which should in turn suppress the high amplitude vibrations.</p> <p>Investigation of an additional safety cutoff device is underway. Leading candidate is a structural vibration detection system.</p>	<p>Accumulator presently being installed in AS-509</p> <p>No firm action yet on vibration detection system</p>	AS-509 and Subs	8.2.3 6.3

Table 3. Summary of Deviations

ITEM	VEHICLE SYSTEM	DEVIATION	PROBABLE CAUSE	SIGNIFICANCE	PARAGRAPH REFERENCE
1	S-1C Propulsion	Unexpected shifts in engine No. 2 turbopump bearing jet pressure	Contaminant restrictions within the bearing jets.	Probably none. Several F-1 turbopumps have experienced similar shifts during engine static tests without problems. The occurrence of this type bearing jet pressure discrepancy during flight is not considered detrimental to F-1 engine turbopump reliability. No shifts have occurred since incorporation of an improved cleaning procedure. The only remaining flight engines not incorporating the improved cleaning procedure are engines S/N F2059 and S/N F2061.	5.3
2	S-1VB/IU Control	Unscheduled S-1VB/IU velocity change of 7 to 10 ft/s at 70,150 seconds (19:29:10).	APS firings in pitch and yaw due to Flight Control Computer output resulting from loss of yaw rate feedback and in response to the attitude error signal after loss of attitude control.	The stage would not necessarily have impacted the lunar surface within the prescribed limits if the velocity change had been in a different direction with respect to the flight path. The direction of the resultant velocity increment is unpredictable.	4A, 10.4.4 7.12
3	IU	At approximately 3.4 seconds the crossrange velocity measurement exhibited a shift of 2.13 ft/s, resulting in a velocity error of approximately 1.64 ft/s.	The velocity shift resulted from the accelerometer head momentarily contacting a mechanical stop due to the high vibration levels after liftoff.	This deviation had negligible effect on launch vehicle operation.	9.1.2



## SECTION 1

### INTRODUCTION

#### 1.1 PURPOSE

This report provides the National Aeronautics and Space Administration (NASA) Headquarters, and other interested agencies, with the launch vehicle evaluation results of the AS-508 flight (Apollo 13 Mission). The basic objective of flight evaluation is to acquire, reduce, analyze, evaluate and report on flight data to the extent required to assure future mission success and vehicle reliability. To accomplish this objective, actual flight failures, anomalies and deviations are identified, their causes determined, and information made available for corrective action.

#### 1.2 SCOPE

This report contains the performance evaluation of the major launch vehicle systems, with special emphasis on failures, anomalies and deviations. Summaries of launch operations and spacecraft performance are included.

The official George C. Marshall Space Flight Center (MSFC) position at this time is represented by this report. It will not be followed by a similar report unless continued analysis or new information should prove the conclusions presented herein to be significantly incorrect. Reports covering major subjects and special subjects will be published as required.



## SECTION 2

### EVENT TIMES

#### 2.1 SUMMARY OF EVENTS

Range zero time, the basic time reference for this report is 14:13:00 Eastern Standard Time (EST) (19:13:00 Universal Time [UT]) April 11, 1970. Range time is the elapsed time from range zero time and, unless otherwise noted, is the time used throughout this report. All data, except as otherwise defined, presented in "Range Time" are the times at which the data were received at the telemetry ground station, i.e., actual time of occurrence at the vehicle plus telemetry transmission time. The Time-From-Base times are presented as elapsed vehicle time from start of time base. Vehicle time is the Launch Vehicle Digital Computer (LVDC) clock time, and differs from actual time of occurrence by any clock error that may exist. Figure 2-1 shows the conversion between range and vehicle times.

Range times for each time base used in the flight sequence program and the signal for initiating each time base are presented in Table 2-1. Start times of  $T_0$ ,  $T_1$ ,  $T_2$  and  $T_3$  were nominal.  $T_4$  and  $T_5$  were initiated approximately 34.6 and 44.0 seconds late, respectively, due to variations in the stage burn times. The variations, discussed in Sections 6, 7 and 8, affected the start of all subsequent time bases. Start times of  $T_6$  and  $T_7$  were 18.2 and 13.6 seconds late, respectively.  $T_8$ , which was initiated by the receipt of a ground command, started 239.3 seconds late.

A summary of significant events for AS-508 is given in Table 2-2. The events in Table 2-2 associated with guidance, navigation, and control were nominal and are accurate to within a major computation cycle.

The predicted times for establishing actual minus predicted times in Table 2-2 were taken from 40M33628, "Interface Control Document Definition of Saturn SA-508 Flight Sequence Program", and from the "AS-508 H-2 Mission Launch Vehicle Operational Flight Trajectory", dated December 18, 1969 and updated January 19, 1970, except as noted.

#### 2.2 VARIABLE TIME AND COMMANDED SWITCH SELECTOR EVENTS

Table 2-3 lists the switch selector events which were issued during the flight but were not programed for specific times. The water coolant valve open and close switch selector commands were issued based on the condition

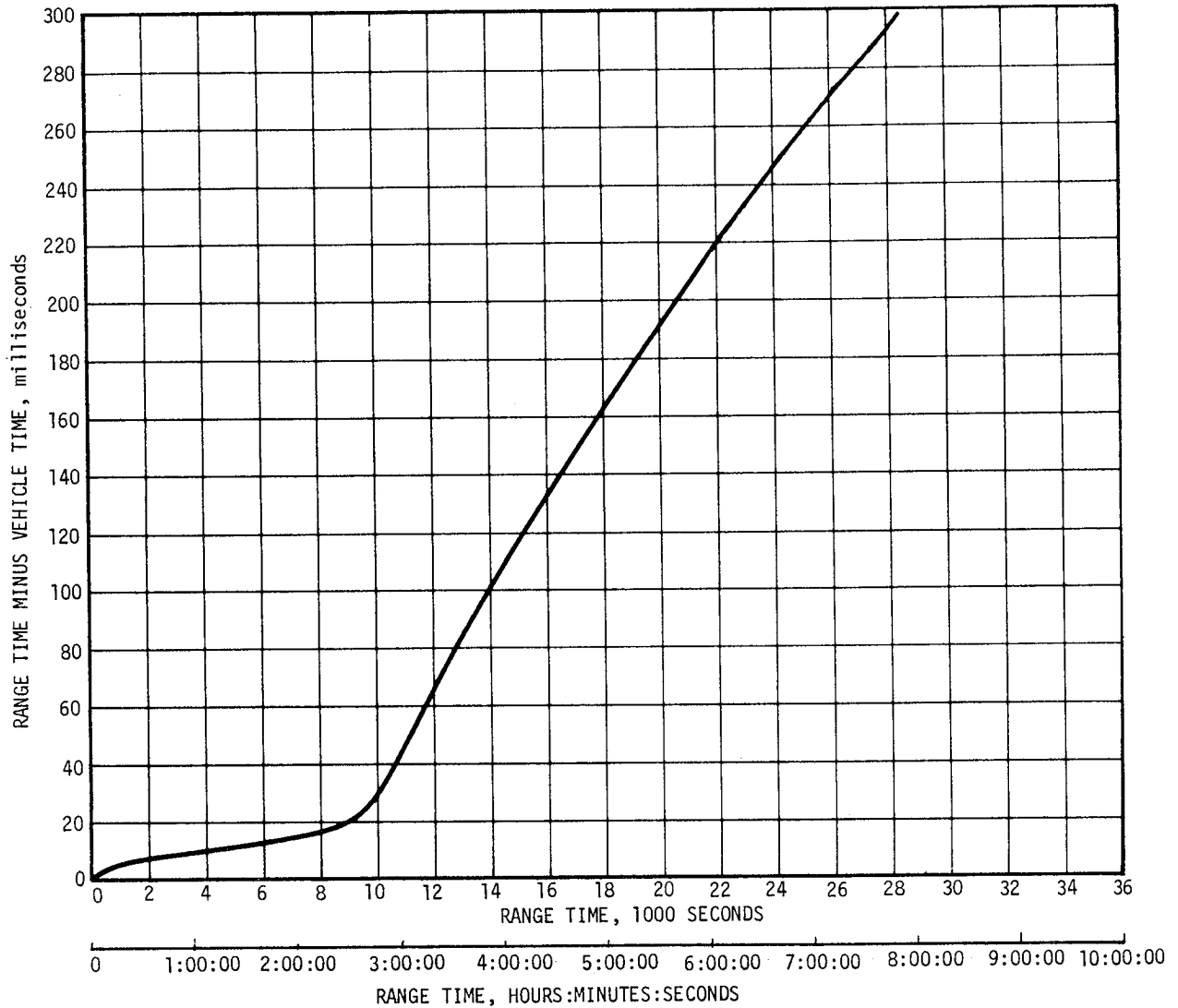


Figure 2-1. Range Time to Vehicle Time Conversion

of two thermal switches in the Environmental Control System (ECS). The outputs of these switches were sampled once every 300 seconds, beginning at 480 seconds, and a switch selector command was issued to open or close the water valve. The valve was opened if the sensed temperature was too high, and was closed if the temperature was too low. Data indicate the water coolant valve responded properly to temperature fluctuations.

The IU command to shift Engine Mixture Ratio (EMR) from high to low occurred 32.2 seconds late, mainly due to the early S-II stage Center Engine Cutoff (CECO), as discussed in paragraph 6.5. This command is issued upon attainment of a preprogrammed velocity increase as sensed by the LVDC. The program logic delays the EMR shift and provides for Translunar Injection capability with one S-II engine out.

Table 2-1. Time Base Summary

TIME BASE	RANGE TIME SEC (HR:MIN:SEC)	SIGNAL START
T <sub>0</sub>	-16.96	Guidance Reference Release
T <sub>1</sub>	0.61	IU Umbilical Disconnect Sensed by LVDC
T <sub>2</sub>	135.33	Downrange Velocity $\geq$ 500 m/s at T <sub>1</sub> +134.7 seconds as Sensed by LVDC
T <sub>3</sub>	163.64	S-IC OECO Sensed by LVDC
T <sub>4</sub>	592.66	S-II OECO Sensed by LVDC
T <sub>5</sub>	750.05	S-IVB ECO (Velocity) Sensed by LVDC
T <sub>6</sub>	8768.11 (02:26:08.11)	Restart Equation Solution
T <sub>7</sub>	9697.40 (02:41:37.40)	S-IVB ECO (Velocity) Sensed by LVDC
T <sub>8</sub>	15,479.43 (04:17:59.43)	Initiated by Ground Command

Table 2-3 also contains the special sequence of switch selector events which were programed to be initiated by telemetry station acquisition and included the following calibration sequence:

Function	Stage	Time (Sec)
Telemetry Calibrator In-Flight Calibrate ON	IU	Acquisition +60.0
IM Calibrate ON	S-IVB	Acquisition +60.4
TM Calibrate OFF	S-IVB	Acquisition +61.4
Telemetry Calibrator In-Flight Calibrate OFF	IU	Acquisition +65.0

Table 2-2. Significant Event Times Summary

ITEM	EVENT DESCRIPTION	RANGE TIME		TIME FROM BASE	
		ACTUAL SEC	ACT-PRED SEC	ACTUAL SEC	ACT-PRED SEC
1	GUIDANCE REFERENCE RELEASE (GRR)	-17.0	0.0	-17.6	0.1
2	S-IC ENGINE START SEQUENCE COMMAND (GROUND)	-8.9	0.0	-9.5	0.0
3	S-IC ENGINE NO.5 START	-6.7	0.0	-7.3	0.0
4	S-IC ENGINE NO.1 START	-6.3	0.0	-6.9	0.0
5	S-IC ENGINE NO.3 START	-6.2	0.0	-6.8	0.0
6	S-IC ENGINE NO.4 START	-6.0	0.0	-6.6	0.1
7	S-IC ENGINE NO.2 START	-6.0	0.0	-6.6	0.0
8	ALL S-IC ENGINES THRUST OK	-1.4	0.1	-2.0	0.2
9	RANGE ZERO	0.0		-0.6	
10	ALL HCLDDOWN ARMS RELEASED (FIRST MOTION)	0.3	0.0	-0.4	0.0
11	IU UMBILICAL DISCONNECT, START OF TIME BASE 1 (T1)	0.6	-0.1	0.0	0.0
12	BEGIN TOWER CLEARANCE YAW MANEUVER	2.3	0.6	1.7	0.7
13	END YAW MANEUVER	10.0	-0.9	9.4	-0.9
14	BEGIN PITCH AND ROLL MANEUVER	12.6	0.1	12.0	0.1
15	S-IC OUTBOARD ENGINE CANT	20.6	-0.1	20.0	0.0
16	END ROLL MANEUVER	32.1	1.7	31.5	1.8
17	MACH 1	68.4	-0.2	67.8	-0.2
18	MAXIMUM DYNAMIC PRESSURE (MAX Q)	81.3	-4.0	80.7	-3.9
19	S-IC CENTER ENGINE CUTOFF (CECO)	135.18	-0.09	134.57	-0.05
20	START OF TIME BASE 2 (T2)	135.3	-0.1	0.0	0.0
21	END PITCH MANEUVER (TILT ARREST)	163.3	1.3	27.9	1.2
22	S-IC OUTBOARD ENGINE CUTOFF (OECO)	163.60	-0.40	28.27	-0.38
23	START OF TIME BASE 3 (T3)	163.6	-0.4	0.0	0.0

Table 2-2. Significant Event Times Summary (Continued)

ITEM	EVENT DESCRIPTION	RANGE TIME		TIME FROM BASE	
		ACTUAL SEC	ACT-PRED SEC	ACTUAL SEC	ACT-PRED SFC
24	START S-II LH2 TANK HIGH PRESSURE VENT MODE	163.7	-0.4	0.1	0.0
25	S-II LH2 RECIRCULATION PUMPS OFF	163.8	-0.4	0.2	0.0
26	S-II ULLAGE MOTOR IGNITION	164.1	-0.4	0.5	0.0
27	S-IC/S-II SEPARATION COMMAND TO FIRE SEPARATION DEVICES AND RETRO MOTORS	164.3	-0.4	0.7	0.0
28	S-II ENGINE START SEQUENCE COMMAND (ESC)	165.0	-0.4	1.4	0.0
29	S-II ENGINE SOLENOID ACTIVATION (AVERAGE OF FIVE)	165.0	-0.4	1.4	0.0
30	S-II IGNITION-STDV OPEN	166.0	-0.4	2.4	0.0
31	S-II MAINSTAGE	168.0	-0.4	4.4	0.0
32	S-II ULLAGE MOTOR BURN TIME TERMINATION (THRUST REACHES 75%)	168.1	-0.5	4.4	-0.2
33	S-II CHILLDOWN VALVES CLOSE	170.0	-0.4	6.4	0.0
34	S-II HIGH (5.5) EMR ON	170.5	-0.4	6.9	0.0
35	S-II SECOND PLANE SEPARATION COMMAND (JETTISON S-II AFT INTERSTAGE)	194.3	-0.4	30.7	0.0
36	LAUNCH ESCAPE TOWER (LET) JETTISON	201.0	0.6	37.4	1.0
37	ITERATIVE GUIDANCE MODE (IGM) PHASE 1 INITIATED*	204.5	-0.5	40.9	-0.1
38	S-II LOX STEP PRESSURIZATION	263.6	-0.4	100.0	0.0
39	S-II ENGINE #5 SOLENOID DEACTIVATION SIGNAL (K1-205) (CECO)	330.65	-132.36	167.00	-132.00
40	S-II CENTER ENGINE CUTOFF COMMAND	462.6	-0.4	299.0	0.0
41	S-II LH2 STEP PRESSURIZATION	463.6	-0.4	300.0	0.0
42	GUIDANCE SENSED TIME TO BEGIN EMR SHIFT (IGM PHASE 2 INITIATED & START OF ARTIFICIAL TAU MODE)*	534.7	32.2	371.0	32.5

\*Time is accurate to major computation cycle dependent upon length of computation cycle.

Table 2-2. Significant Event Times Summary (Continued)

ITEM	EVENT DESCRIPTION	RANGE TIME		TIME FROM BASE	
		ACTUAL SEC	ACT-PRED SEC	ACTUAL SEC	ACT-PRED SEC
43	S-II LOW ENGINE MIXTURE RATIO (EMR) SHIFT (ACTUAL)	537.5	33.7	373.8	34.0
44	END OF ARTIFICIAL TAU MODE*	545.8	32.8	382.2	33.2
45	S-II OUTBOARD ENGINE CUTOFF (OECO)	592.64	34.53	429.00	34.90
46	S-II ENGINE CUTOFF INTERRUPT, START OF TIME BASE 4 (T4) (START OF IGM PHASE 3)	592.7	34.6	0.0	0.0
47	S-IVB ULLAGE MOTOR IGNITION	593.4	34.5	0.8	0.0
48	S-II/S-IVB SEPARATION COMMAND TO FIRE SEPARATION DEVICES AND RETRO MOTORS	593.5	34.5	0.9	0.0
49	S-IVB ENGINE START COMMAND (FIRST ESC)	593.6	34.5	1.0	0.0
50	FUEL CHILDDOWN PUMP OFF	594.8	34.5	2.2	0.0
51	S-IVB IGNITION (STDV OPEN)	596.9	34.8	4.3	0.3
52	S-IVB MAINSTAGE	599.4	34.8	6.8	0.3
53	START OF ARTIFICIAL TAU MODE*	600.2	34.7	7.5	0.1
54	S-IVB ULLAGE CASE JETTISON	605.4	34.5	12.8	0.0
55	END OF ARTIFICIAL TAU MODE*	611.2	36.9	18.5	2.4
56	BEGIN TERMINAL GUIDANCE*	716.9	44.6	124.2	10.1
57	END IGM PHASE 3*	743.2	45.3	150.5	10.7
58	BEGIN CHI FREEZE*	743.2	45.3	150.5	10.7
59	S-IVB VELOCITY CUTOFF COMMAND (FIRST GUIDANCE CUTOFF) (FIRST ECO)	749.83	44.06	-0.22	-0.02
60	S-IVB ENGINE CUTOFF INTERRUPT, START OF TIME BASE 5 (T5)	750.0	44.0	0.0	0.0
61	S-IVB APS ULLAGE ENGINE NO. 1 IGNITION COMMAND	750.3	44.0	0.3	0.0
62	S-IVB APS ULLAGE ENGINE NO. 2 IGNITION COMMAND	750.4	44.0	0.4	0.0
63	LOX TANK PRESSURIZATION OFF	751.2	44.0	1.2	0.0
64	PARKING ORBIT INSERTION	759.8	44.0	9.8	0.0

\*Time is accurate to major computation cycle dependent upon length of computation cycle.

Table 2-2. Significant Event Times Summary (Continued)

ITEM	EVENT DESCRIPTION	RANGE TIME		TIME FROM BASE	
		ACTUAL SEC	ACT-PRED SEC	ACTUAL SEC	ACT-PRED SEC
65	BEGIN MANEUVER TO LOCAL HORIZONTAL ATTITUDE*	770.1	43.7	20.1	-0.3
66	S-IVB CONTINUOUS VENT SYSTEM (CVS) ON	809.0	44.0	59.0	0.0
67	S-IVB APS ULLAGE ENGINE NO. 1 CUTOFF COMMAND	837.0	44.0	87.0	0.0
68	S-IVB APS ULLAGE ENGINE NO. 2 CUTOFF COMMAND	837.1	44.0	87.1	0.0
69	BEGIN ORBITAL NAVIGATION *	850.4	44.0	100.3	-0.1
70	BEGIN S-IVB RESTART PREPARATIONS, START OF TIME BASE 6 (T6)	8768.1	18.2	0.0	0.0
71	S-IVB O2/H2 BURNER LH2 ON	8809.4	18.2	41.3	0.0
72	S-IVB O2/H2 BURNER EXCITERS ON	8809.7	18.2	41.6	0.0
73	S-IVB O2/H2 BURNER LOX ON (HELIUM HEATER ON)	8810.1	18.2	42.0	0.0
74	S-IVB CVS OFF	8810.3	18.2	42.2	0.0
75	S-IVB LH2 REPRESSURIZATION CONTROL VALVE ON	8816.2	18.2	48.1	0.0
76	S-IVB LOX REPRESSURIZATION CONTROL VALVE ON	8816.4	18.2	48.3	0.0
77	S-IVB AUX HYDRAULIC PUMP FLIGHT MODE ON	8987.1	18.2	219.0	0.0
78	S-IVB LOX CHILLDOWN PUMP ON	9017.1	18.2	249.0	0.0
79	S-IVB LH2 CHILLDOWN PUMP ON	9022.1	18.2	254.0	0.0
80	S-IVB PREVALVES CLOSED	9027.1	18.2	259.0	0.0
81	S-IVB PU MIXTURE RATIO 4.5 ON	9218.2	18.2	450.1	0.0
82	S-IVB APS ULLAGE ENGINE NO. 1 IGNITION COMMAND	9264.4	18.2	496.3	0.0
83	S-IVB APS ULLAGE ENGINE NO. 2 IGNITION COMMAND	9264.5	18.2	496.4	0.0
84	S-IVB O2/H2 BURNER LH2 OFF (HELIUM HEATER OFF)	9264.9	18.2	496.8	0.0
85	S-IVB O2/H2 BURNER LOX OFF	9269.4	18.2	501.3	0.0

\*Time is accurate to major computation cycle dependent upon length of computation cycle.

Table 2-2. Significant Event Times Summary (Continued)

ITEM	EVENT DESCRIPTION	RANGE TIME		TIME FROM BASE	
		ACTUAL SEC	ACT-PRED SEC	ACTUAL SEC	ACT-PRED SEC
86	S-IVB LH2 CHILLDOWN PUMP OFF	9337.5	18.2	569.4	0.0
87	S-IVB LOX CHILLDOWN PUMP OFF	9337.7	18.2	569.6	0.0
88	S-IVB ENGINE RESTART COMMAND (FUEL LEAD INITIATION) (SECOND ESC)	9338.1	18.2	570.0	0.0
89	S-IVB APS ULLAGE ENGINE NO. 1 CUTOFF COMMAND	9341.1	18.2	573.0	0.0
90	S-IVB APS ULLAGE ENGINE NO. 2 CUTOFF COMMAND	9341.2	18.2	573.1	0.0
91	S-IVB SECOND IGNITION (STDV OPEN)	9346.4	18.5	578.3	0.3
92	S-IVB MAINSTAGE	9348.9	18.5	580.8	0.3
93	ENGINE MIXTURE RATIO (EMR) SHIFT	9448.7	18.3	680.6	0.1
94	S-IVB LH2 STEP PRESSURIZATION (SECOND BURN RELAY OFF)	9618.1	18.2	850.0	0.0
95	BEGIN TERMINAL GUIDANCE *	9668.3	14.1	900.2	-4.0
96	BEGIN CHI FREEZE*	9695.7	14.2	927.6	-4.0
97	S-IVB SECOND GUIDANCE CUTOFF COMMAND (SECOND ECD)	9697.17	13.55	-0.23	-0.03
98	S-IVB ENGINE CUTOFF INTERRUPT, START OF TIME BASE 7	9697.4	13.6	0.0	0.0
99	S-IVB CVS ON	9697.9	13.6	0.5	0.0
100	TRANSLUNAR INJECTION	9707.2	13.6	9.8	0.0
101	BEGIN MANEUVER TO LOCAL HORIZONTAL ATTITUDE*	9848.0	13.3	150.6	-0.3
102	BEGIN ORBITAL NAVIGATION*	9848.0	13.3	150.6	-0.3
103	S-IVB CVS OFF	9848.3	13.6	150.9	0.0
104	BEGIN MANEUVER TO TRANSPOSITION AND DOCKING ATTITUDE (TD&E)*	10598.3	14.5	900.9	0.9
105	CSM SEPARATION	11198.9	38.9**	1501.5	25.3
106	CSM DOCK	11948.8	188.8**	2251.4	175.3
107	SC/LV FINAL SEPARATION	14460.8	0.8**	4763.3	-12.8

\*Time is accurate to major computation cycle dependent upon length of computation cycle.  
 \*\*The predicted time for establishing this actual minus predicted time has been taken from the Apollo 13 Final Flight Plan, Revision B, dated March 16, 1970.

Table 2-2. Significant Event Times Summary (Continued)

ITEM	EVENT DESCRIPTION	RANGE TIME		TIME FROM BASE	
		ACTUAL SEC	ACT-PRED SEC	ACTUAL SEC	ACT-PRED SEC
108	START OF TIME BASE 8 (T8)	15479.4	239.3**	0.0	0.0
109	S-IVB APS ULLAGE ENGINE NO. 1 IGNITION COMMAND	15480.6	239.3**	1.2	0.0
110	S-IVB APS ULLAGE ENGINE NO. 2 IGNITION COMMAND	15480.8	239.3**	1.4	0.0
111	S-IVB APS ULLAGE ENGINE NO. 1 CUTOFF COMMAND	15560.6	239.3**	81.2	0.0
112	S-IVB APS ULLAGE ENGINE NO. 2 CUTOFF COMMAND	15560.8	239.3**	81.4	0.0
113	INITIATE MANEUVER TO LOX DUMP ATTITUDE*	16060.0	240.0**	580.6	0.7
114	S-IVB CVS ON	16479.4	239.3**	1000.0	0.0
115	BEGIN LOX DUMP	16759.4	239.3**	1280.0	0.0
116	S-IVB CVS OFF	16779.4	239.3**	1300.0	0.0
117	END LOX DUMP	16807.4	239.3**	1328.0	0.0
118	H2 NONPROPULSIVE VENT (NPV) ON	16886.4	239.3**	1407.0	0.0
119	INITIATE MANEUVER TO ATTITUDE REQUIRED FOR FINAL S-IVB APS BURN*	20887.8	187.8**	5408.3	-51.5
120	S-IVB APS ULLAGE ENGINE NO. 1 IGNITION COMMAND	21599.5	-0.5**	6120.0	-239.8
121	S-IVB APS ULLAGE ENGINE NO. 2 IGNITION COMMAND	21599.7	-0.5**	6120.2	-239.8
122	S-IVB APS ULLAGE ENGINE NO. 1 CUTOFF COMMAND	21816.5	-19.5**	6337.0	-258.8
123	S-IVB APS ULLAGE ENGINE NO. 2 CUTOFF COMMAND	21816.7	-19.5**	6337.2	-258.8
124	S-IVB/IU LUNAR IMPACT	280601.0 (77:56:41.0) (HRS:MIN:SEC)	701.0**	265121.6 (73:38:41.6) (HRS:MIN:SEC)	461.7

\*Time is accurate to major computation cycle dependent upon length of computation cycle.  
 \*\*The predicted time for establishing this actual minus predicted time has been taken from the Apollo 13 Final Flight Plan, Revision B, dated March 16, 1970.

Table 2-3. Variable Time and Commanded Switch Selector Events

FUNCTION	STAGE	RANGE TIME (SEC)	TIME FROM BASE (SEC)	REMARKS
High (5.5) Engine Mixture Ratio Off	S-II	535.3	T <sub>3</sub> +371.6	LVDC Function
Low (4.5) Engine Mixture Ratio On	S-II	535.5	T <sub>3</sub> +371.8	LVDC Function
Water Coolant Valve Open	IU	781.2	T <sub>5</sub> +31.1	LVDC Function
Telemetry Calibrator Inflight Calibrate On	IU	1079.0	T <sub>5</sub> +329.0	Acquisition By Canary Revolution 1
TM Calibrate On	S-IVB	1079.4	T <sub>5</sub> +329.4	Acquisition By Canary Revolution 1
TM Calibrate Off	S-IVB	1080.4	T <sub>5</sub> +330.4	Acquisition By Canary Revolution 1
Telemetry Calibrator Inflight Calibrate Off	IU	1084.0	T <sub>5</sub> +334.0	Acquisition By Canary Revolution 1
Telemetry Calibrator Inflight Calibrate On	IU	3223.0	T <sub>5</sub> +2473.0	Acquisition By Carnarvon Revolution 1
TM Calibrate On	S-IVB	3223.4	T <sub>5</sub> +2473.4	Acquisition By Carnarvon Revolution 1
TM Calibrate Off	S-IVB	3224.4	T <sub>5</sub> +2474.4	Acquisition By Carnarvon Revolution 1
Telemetry Calibrator Inflight Calibrate Off	IU	3228.0	T <sub>5</sub> +2478.0	Acquisition By Carnarvon Revolution 1
Telemetry Calibrator Inflight Calibrate On	IU	6703.0	T <sub>5</sub> +5953.0	Acquisition By Canary Revolution 2
TM Calibrate On	S-IVB	6703.4	T <sub>5</sub> +5953.4	Acquisition By Canary Revolution 2
TM Calibrate Off	S-IVB	6704.4	T <sub>5</sub> +5954.4	Acquisition By Canary Revolution 2
Telemetry Calibrator Inflight Calibrate Off	IU	6718.0	T <sub>5</sub> +5958.0	Acquisition By Canary Revolution 2
Water Coolant Valve Closed	IU	8805.4	T <sub>6</sub> +37.3	LVDC Function
Telemetry Calibrator Inflight Calibrate On	IU	9988.6	T <sub>7</sub> +291.2	Acquisition By Hawaii Revolution 2
TM Calibrate On	S-IVB	9989.0	T <sub>7</sub> +291.6	Acquisition By Hawaii Revolution 2
TM Calibrate Off	S-IVB	9989.9	T <sub>7</sub> +292.6	Acquisition By Hawaii Revolution 2
Telemetry Calibrator Inflight Calibrate Off	IU	9993.6	T <sub>7</sub> +296.2	Acquisition By Hawaii Revolution 2
Water Coolant Valve Open	IU	12,480.7	T <sub>7</sub> +2783.3	LVDC Function
Water Coolant Valve Closed	IU	12,780.2	T <sub>7</sub> +3082.8	LVDC Function
Water Coolant Valve Open	IU	15,180.2	T <sub>7</sub> +5482.7	LVDC Function
Start of Time Base 8 (T <sub>8</sub> )		15,479.4	T <sub>8</sub> +0.0	CCS Command
Water Coolant Valve Closed	IU	15,480.9	T <sub>8</sub> +1.4	LVDC Function
Water Coolant Valve Open	IU	18,180.3	T <sub>8</sub> +2700.8	LVDC Function
Water Coolant Valve Closed	IU	18,480.8	T <sub>8</sub> +3001.3	LVDC Function

Table 2-3. Variable Time and Commanded Switch Selector Events (Continued)

FUNCTION	STAGE	RANGE TIME (SEC)	TIME FROM BASE (SEC)	REMARKS
Water Coolant Valve Open	IU	21,180.4	T <sub>g</sub> +5700.9	LVDC Function
Water Coolant Valve Closed	IU	21,480.8	T <sub>g</sub> +6001.2	LVDC Function
S-IVB Ullage Engine No. 1 On	S-IVB	21,599.5	T <sub>g</sub> +6120.0	CCS Command
S-IVB Ullage Engine No. 2 On	S-IVB	21,599.7	T <sub>g</sub> +6120.2	CCS Command
S-IVB Ullage Engine No. 1 Off	S-IVB	21,816.5	T <sub>g</sub> +6337.0	CCS Command
S-IVB Ullage Engine No. 2 Off	S-IVB	21,816.7	T <sub>g</sub> +6337.2	CCS Command



## SECTION 3

### LAUNCH OPERATIONS

#### 3.1 SUMMARY

The ground systems supporting the AS-508/Apollo 13 countdown and launch performed satisfactorily. System component failures and malfunctions requiring corrective action were corrected during countdown and no unscheduled holds were incurred. Propellant tanking was accomplished satisfactorily. Launch occurred at 14:13:00 Eastern Standard Time (EST), April 11, 1970, from Pad 39A of the Kennedy Space Center, Saturn Complex. Damage to the pad, Launch Umbilical Tower (LUT) and support equipment was considered minimal.

#### 3.2 PRELAUNCH MILESTONES

A chronological summary of prelaunch milestones for the AS-508 launch is contained in Table 3-1.

#### 3.3 COUNTDOWN EVENTS

The AS-508/Apollo 13 terminal countdown was picked up at T-28 hours on April 9, 1970, at 24:00:00 EST. Scheduled holds in the launch countdown sequence were 9 hours 13 minutes duration at T-9 hours and 1 hour duration at T-3 hours 30 minutes. Launch activities were directed from Launch Control Center (LCC) Firing Room 1. Launch occurred on schedule at 14:13:00 EST, April 11, 1970.

#### 3.4 PROPELLANT LOADING

##### 3.4.1 RP-1 Loading

The RP-1 system successfully supported the launch countdown without incident. S-IC stage replenishment was initiated at approximately T-13 hours and level adjust at T-1 hour. The air vent trap (A4120, P/N 76K00072) closed prematurely during replenish operations causing a quantity of fill line gas residuals to be pumped through the S-IC stage fuel tank. This problem also occurred during the Countdown Demonstration Test (CDDT) and is under design investigation.

Table 3-1. AS-508/Apollo 13 Prelaunch Milestones

DATE	ACTIVITY OR EVENT
June 13, 1969	S-IVB-508 Stage Arrival
June 16, 1969	S-IC-8 Stage Arrival
June 18, 1969	S-IC Erection on Mobile Launcher 3
June 26, 1969	Command and Service Module (CSM)-109 Arrival
June 27, 1969	Lunar Module (LM)-7 Ascent Stage Arrival
June 28, 1969	LM-7 Descent Stage Arrival
June 29, 1969	S-II-8 Stage Arrival
July 7, 1969	Instrument Unit (IU)-508 Arrival
July 17, 1969	S-II Erection
July 18, 1969	Spacecraft/Lunar Module Adapter (SLA)-16 Arrival
July 31, 1969	S-IVB Erection
August 1, 1969	IU Erection
August 29, 1969	Launch Vehicle (LV) Electrical System Test
October 21, 1969	LV Propellant Dispersion/Malfunction Overall Test (OAT) Complete
December 4, 1969	LV Service Arm OAT
December 10, 1969	Spacecraft (SC) Erection
December 15, 1969	Space Vehicle (SV)/Mobile Launcher Transfer to Pad 39A
January 19, 1970	SV Electrical Mate
January 20, 1970	SV OAT No. 1 (Plugs In)
February 26, 1970	SV Flight Readiness Test (FRT) Completed
March 16, 1970	RP-1 Loading
March 25, 1970	Countdown Demonstration Test (CDDT) Completed (Wet)
March 26, 1970	CDDT Completed (Dry)
April 9, 1970	SV Terminal Countdown Started
April 11, 1970	SV Launch On Schedule

### 3.4.2 LOX Loading

The LOX system satisfactorily supported the launch countdown. The fill sequence was nominal beginning with start of S-IVB stage loading at T-8 hours 22 minutes. LOX loading was completed and replenishment initiated on all stages at T-5 hours 41 minutes.

During the countdown, at approximately T-2 hours 5 minutes, the S-IC stage LOX vent valve No. 2 stuck in the open position. A procedure to cycle the vent valves at 15 to 20-minute intervals had been in effect since completion of S-IC fast fill at approximately T-5 hours 41 minutes. LOX vent valve No. 2 had been successfully cycled about 15 minutes prior to sticking. The problem was resolved by closing LOX vent valve No. 1 and applying a GN<sub>2</sub> purge through the sticking LOX vent valve No. 2. After 88 seconds of purge and 13 cycles of the close command switch, the LOX vent valve No. 2 returned to the closed position. The LOX vent valve No. 2 was left in the closed position for the remainder of the countdown, and no further problems developed. An investigation to determine the cause of the problem is underway.

### 3.4.3 LH<sub>2</sub> Loading

The LH<sub>2</sub> system successfully supported launch countdown. The fill sequence was nominal beginning with start of S-II stage loading at T-5 hours 33 minutes. LH<sub>2</sub> loading was completed and replenishment initiated at T-4 hours 4 minutes.

During S-IVB stage loading, major excursions occurred on the LH<sub>2</sub> fine and the LH<sub>2</sub> coarse mass measurements. As loading progressed the system recovered allowing the countdown to continue normally. The system again operated abnormally beginning at T-3 seconds and lasting through tower clearance. This system was known to be a potential problem from previous testing. An alternate loading procedure had been prepared prior to start of the launch countdown but was not required to complete the countdown.

## 3.5 INSULATION

The S-II-8 was the first stage to utilize spray-on foam as the external insulation for the LH<sub>2</sub> tank sidewalls and forward skirt. This is discussed further in Appendix B. The performance of the stage insulation, including Ground Support Equipment (GSE) purge and vacuum systems, was satisfactory with no parameters exceeding redline limits. Detailed inspection of the external insulation, using operational television, indicated that the spray-on foam performed satisfactorily. The total heat leak through the insulation to the LH<sub>2</sub> tank was well below the specification value.

### 3.6 GROUND SUPPORT EQUIPMENT

#### 3.6.1 Ground/Vehicle Interface

In general performance of the ground service systems supporting all stages of the launch vehicle was satisfactory. Overall damage to the pad, LUT, and support equipment from the blast and flame impingement was considered minimal. Detailed discussion of the GSE is contained in KSC Apollo/Saturn V (AS-508) "Ground Support Evaluation Report".

The ground Environmental Control System (ECS) performed satisfactorily throughout countdown and launch, with one exception. With ground ECS flowrate and temperature at maximum values, the S-IC aft flight battery compartment temperature, with specification limits of  $80 \pm 15^\circ\text{F}$ , dropped to  $61^\circ\text{F}$ . The low temperature had been anticipated from CDDT performance and a waiver had been approved permitting limits of 50 to  $95^\circ\text{F}$  for the compartment temperature during the AS-508 launch (see paragraph 14.2).

The Holddown Arms and Service Arms (SA) satisfactorily supported the launch and caused no countdown holds or delays. Because of a Digital Events Evaluator (DEE)-6 failure at T-1 second, SA retract times and valve actuation times are not available. However, the SA control panels indicated that all retract and withdrawal firing systems actuated, and that all arms fully retracted and latched.

Overall performance of the Tail Service Mast system was satisfactory. Valve actuation and retract times are not available because of the DEE-6 failure. Television observation and panel lights indicated that all three return valves opened, the masts retracted together and hoods closed within the 4.0 second maximum allowed from aft umbilical plate separation.

#### 3.6.2 MSFC Furnished Ground Support Equipment

The S-IC stage mechanical and electrical Ground Support Equipment performed satisfactorily during launch operations with only one minor system failure encountered. At T-14 hours a gradual increase in  $\text{GN}_2$  primary pressure, from 3540 to 3650 psig, was noted on the S-IC pneumatics console. Investigation indicated possible internal leakage in the dome loading regulator (P/N A9927). The regulator was replaced and the system retested satisfactorily. Subsequent analysis of the removed regulator could not confirm the failure. No further action is planned.

At T-1.156 seconds the DEE-6 began displaying erroneous data. This condition existed until 1800 seconds when the problem cleared and the output was normal. Permanent record data from magnetic tape was also erroneous. It is suspected that the problem occurred in the "W" Time Multiplex Communication Channel (I/O Channel) since the only area affected was outputting of data to magnetic tape and printers. The cause of failure is unknown at this time, but is apparently due to launch vibration.

Blast damage to the equipment was considered minimal.

### 3.6.3 Camera Coverage

Upon review of the film coverage the following conditions were observed:

- a. S-II stage intermediate SA No. 4 umbilical door (station 1772) did not secure upon SA withdrawal from the vehicle.
- b. S-II stage forward SA umbilical cover (between stringer 68 and 69) did not secure upon SA withdrawal from the vehicle. This condition also occurred during the AS-506 and AS-507 launches.



## SECTION 4

### TRAJECTORY

#### 4.1 SUMMARY

The vehicle was launched on an azimuth 90 degrees east of north. A roll maneuver at 12.6 seconds placed the vehicle on a flight azimuth of 72.043 degrees east of north. The reconstructed trajectory was generated by merging the ascent phase, the parking orbit phase, the injection phase, and the post Translunar Injection (TLI) phase trajectories. The analysis for each phase was conducted separately with appropriate end point constraints to provide trajectory continuity. Available C-Band radar and Unified S-Band (USB) tracking data plus telemetered guidance velocity data were used in the trajectory reconstruction.

The trajectory parameters were close to nominal through S-IC and S-II stage burns until the early shutdown of the S-II center engine. The premature S-II Center Engine Cutoff (CECO) caused considerable deviations for certain trajectory parameters. S-II Outboard Engine Cutoff (OECO) occurred 34.5 seconds late as a result of the early CECO. The S-IVB burn time was extended by the guidance unit so that the vehicle achieved near nominal earth parking orbit insertion conditions 44.07 seconds later than predicted at a heading angle 1.230 degrees greater than nominal. The trajectory parameters at TLI were also close to nominal although the event itself was 13.56 seconds later than nominal. The trajectory parameters at Command Service Module (CSM) separation deviated somewhat from nominal since the event occurred 38.9 seconds later than predicted.

The earth impact locations for the S-IC and S-II stages were determined by a theoretical free-flight simulation. The analysis for the S-IC stage showed the surface range for the impact point to be 7.6 kilometers (4.1 n mi) greater than nominal. The analysis for the S-II stage showed the surface range for the impact point to be 8.6 kilometers (4.6 n mi) greater than nominal.

#### 4.2 TRAJECTORY EVALUATION

##### 4.2.1 Ascent Phase

The ascent phase spans the interval from guidance reference release through parking orbit insertion. The ascent trajectory was established by using

telemetered guidance velocities as generating parameters to fit tracking data from five C-Band stations and two S-Band stations. Approximately 20 percent of the tracking data were eliminated due to inconsistencies. The launch phase portion of the ascent phase, (liftoff to approximately 20 seconds), was established by constraining integrated telemetered guidance accelerometer data to the best estimate trajectory. The launch phase trajectory was initialized from launch camera data.

Actual and nominal altitude, surface range, and crossrange for the ascent phase are presented in Figure 4-1. Actual and nominal space-fixed velocity and flight path angle during ascent are shown in Figure 4-2. Actual and nominal comparisons of total inertial accelerations are shown in Figure 4-3. The maximum acceleration during S-IC burn was 3.83 g. The early shutdown of the S-II center engine resulted in subsequent longer burns of the S-II and S-IVB stages. These extended burn times compensated for the early S-II CECO and the vehicle was inserted into a near nominal parking orbit.

Mach number and dynamic pressure are shown in Figure 4-4. These parameters were calculated using meteorological data measured to an altitude of 80.5 kilometers (43.5 n mi). Above this altitude the measured data were merged into the U. S. Standard Reference Atmosphere.

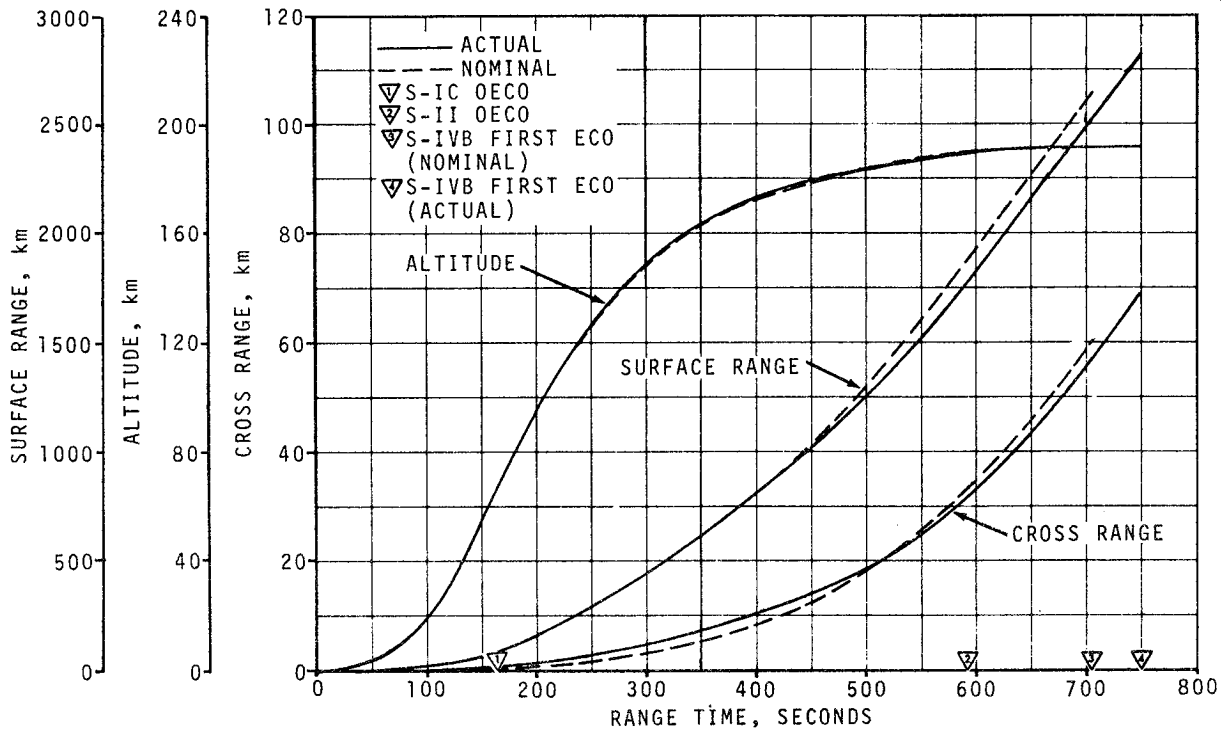


Figure 4-1. Ascent Trajectory Position Comparison

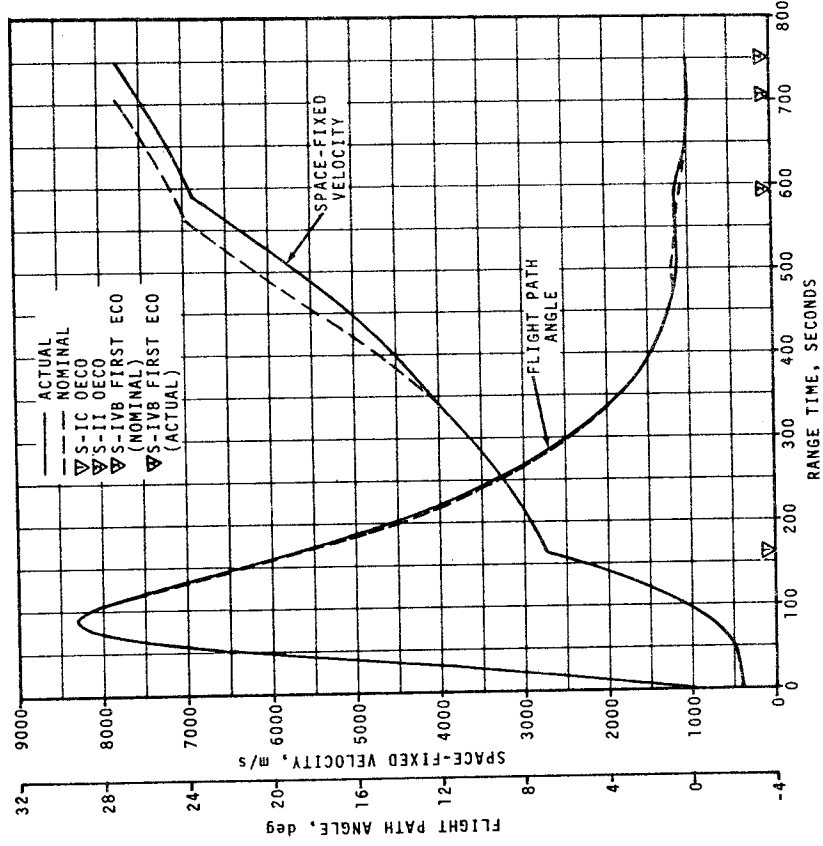


Figure 4-2. Ascent Trajectory Space-Fixed Velocity and Flight Path Angle Comparisons

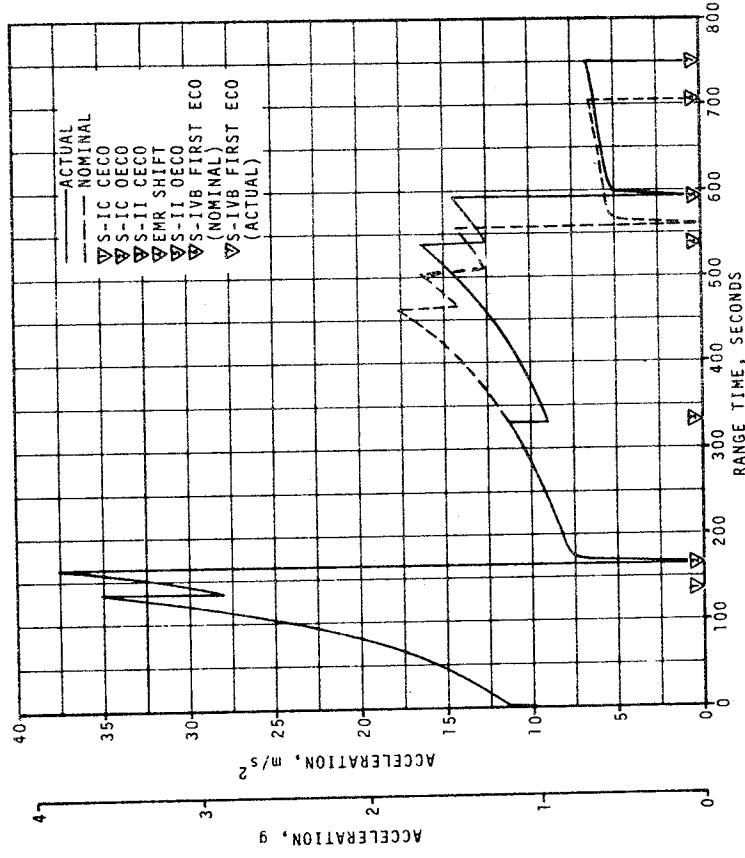


Figure 4-3. Ascent Trajectory Acceleration Comparison

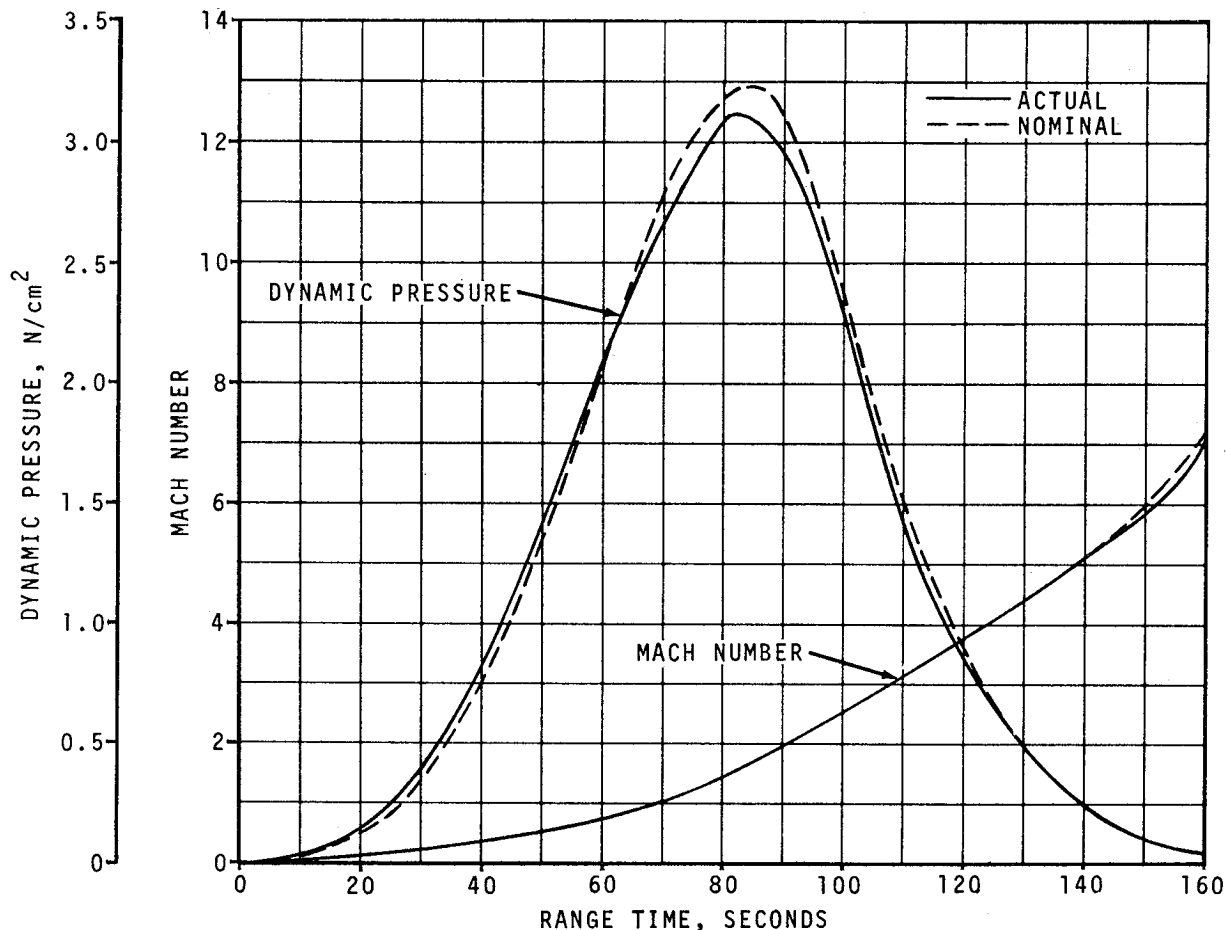


Figure 4-4. Dynamic Pressure and Mach Number Comparisons

Actual and nominal values of parameters at significant trajectory event times, cutoff events, and separation events are shown in Tables 4-1, 4-2, and 4-3, respectively.

The free-flight trajectories of the spent S-IC and S-II stages were simulated using initial conditions from the final postflight trajectory. The simulation was based upon the separation impulses for both stages and nominal tumbling drag coefficients. No tracking data were available for verification. Table 4-1 presents a comparison of free-flight parameters to nominal at apex for the S-IC and S-II stages. Table 4-4 presents a comparison of free-flight parameters to nominal at impact for the S-IC and S-II stages.

Table 4-1. Comparison of Significant Trajectory Events

EVENT	PARAMETER	ACTUAL	NOMINAL	ACT-NOM
First Motion	Range Time, sec	0.3	0.3	0.0
	Total Inertial Acceleration, m/s <sup>2</sup> (ft/s <sup>2</sup> ) (g)	10.35 (33.96) (1.06)	10.41 (34.15) (1.06)	-0.06 (-0.19) (0.00)
Mach 1	Range Time, sec	68.4	68.6	-0.2
	Altitude, km (n mi)	8.1 (4.4)	7.9 (4.3)	0.2 (0.1)
Maximum Dynamic Pressure	Range Time, sec	81.3	85.3	-4.0
	Dynamic Pressure, N/cm <sup>2</sup> (lbf/ft <sup>2</sup> )	3.12 (651.6)	3.23 (674.6)	-0.11 (-23.0)
	Altitude, km (n mi)	12.5 (6.7)	13.6 (7.3)	-1.1 (-0.6)
Maximum Total Inertial Acceleration:	S-IC			
	Range Time, sec	163.70	163.18	0.52
	Acceleration, m/s <sup>2</sup> (ft/s <sup>2</sup> ) (g)	37.60 (123.36) (3.83)	37.53 (123.13) (3.83)	0.07 (0.23) (0.00)
	S-II			
	Range Time, sec	537.00	463.09	73.91
	Acceleration, m/s <sup>2</sup> (ft/s <sup>2</sup> ) (g)	16.25 (53.31) (1.66)	17.65 (57.91) (1.80)	-1.40 (-4.60) (-0.14)
	S-IVB 1st Burn			
	Range Time, sec	750.00	705.84	44.16
	Acceleration, m/s <sup>2</sup> (ft/s <sup>2</sup> ) (g)	6.66 (21.85) (0.68)	6.53 (21.42) (0.67)	0.13 (0.43) (0.01)
	S-IVB 2nd Burn			
	Range Time, sec	9,697.23	9,683.67	13.56
	Acceleration, m/s <sup>2</sup> (ft/s <sup>2</sup> ) (g)	14.03 (46.03) (1.43)	13.89 (43.57) (1.42)	0.14 (0.46) (0.01)
Maximum Earth-Fixed Velocity:	S-IC			
	Range Time, sec	164.10	164.51	-0.41
	Velocity, m/s (ft/s)	2,383.8 (7,820.9)	2,379.0 (7,805.1)	4.8 (15.8)
	S-II			
	Range Time, sec	593.50	559.02	34.48
	Velocity, m/s (ft/s)	6,492.7 (21,301.5)	6,558.5 (21,517.4)	-65.8 (-215.9)
	S-IVB 1st Burn			
	Range Time, sec	750.50	715.76	34.74
	Velocity, m/s (ft/s)	7,389.3 (24,243.1)	7,389.5 (24,243.8)	-0.2 (-0.7)
	S-IVB 2nd Burn			
	Range Time, sec	9,697.80	9,683.80	14.00
	Velocity, m/s (ft/s)	10,433.6 (34,231.0)	10,429.8 (34,218.5)	3.8 (12.5)
Apex:	S-IC Stage			
	Range Time, sec	271.7	270.3	1.4
	Altitude, km (n mi)	116.9 (63.1)	114.6 (61.9)	2.3 (1.2)
	Surface Range, km (n mi)	325.9 (176.0)	322.0 (173.9)	3.9 (2.1)
	S-II Stage			
	Range Time, sec	632.2	600.3	31.9
Altitude, km (n mi)	190.7 (103.0)	189.4 (102.3)	1.3 (0.7)	
Surface Range, km (n mi)	2,035.0 (1,098.8)	1,919.7 (1,036.6)	115.3 (62.2)	

NOTE: The Range Time used are times of occurrence at the vehicle, reference Figure 2-1.

Table 4-2. Comparison of Cutoff Events

PARAMETER	ACTUAL	NOMINAL	ACT-NOM	ACTUAL	NOMINAL	ACT-NOM
S-IC CECO (ENGINE SOLENOID)			S-IC OECO (ENGINE SOLENOID)			
Range Time, sec	135.18	135.27	-0.09	163.60	164.00	-0.40
Altitude, km (n mi)	43.5 (23.5)	42.6 (23.0)	0.9 (0.5)	67.4 (36.4)	66.5 (35.9)	0.9 (0.5)
Surface Range, km (n mi)	44.9 (24.2)	44.3 (23.9)	0.6 (0.3)	94.4 (51.0)	94.2 (50.9)	0.2 (0.1)
Space-Fixed Velocity, m/s (ft/s)	1,928.9 (6,328.4)	1,915.8 (6,285.4)	13.1 (43.0)	2,744.0 (9,002.6)	2,739.9 (8,989.2)	4.1 (13.4)
Flight Path Angle, deg	23.612	23.442	0.170	19.480	19.250	0.230
Heading Angle, deg	76.609	76.369	0.240	75.696	75.356	0.340
Crossrange, km (n mi)	0.5 (0.3)	0.1 (0.1)	0.4 (0.2)	1.0 (0.5)	0.3 (0.2)	0.7 (0.3)
Crossrange Velocity, m/s (ft/s)	11.1 (36.4)	3.0 (9.8)	8.1 (26.6)	23.4 (76.8)	8.0 (26.2)	15.4 (50.6)
S-II CECO (ENGINE SOLENOID)			S-II OECO (ENGINE SOLENOID)			
Range Time, sec	330.64	463.01	-132.37	592.64	558.11	34.53
Altitude, km (n mi)	159.6 (86.2)	179.4 (96.9)	-19.8 (-10.7)	189.1 (102.1)	187.6 (101.3)	1.5 (0.8)
Surface Range, km (n mi)	552.0 (298.1)	1,105.1 (596.7)	-553.1 (-298.6)	1,786.4 (964.6)	1,651.7 (891.8)	134.7 (72.8)
Space-Fixed Velocity, m/s (ft/s)	3,919.6 (12,859.6)	5,652.5 (18,544.9)	-1,732.9 (-5,685.3)	6,891.8 (22,610.9)	6,958.6 (22,830.1)	-66.8 (-219.2)
Flight Path Angle, deg	4.158	0.894	3.264	0.657	0.699	-0.042
Heading Angle, deg	76.956	79.576	-2.620	83.348	82.565	0.783
Crossrange, km (n mi)	6.4 (3.5)	13.7 (7.4)	-7.3 (-3.9)	32.0 (17.3)	27.1 (14.6)	4.9 (2.7)
Crossrange Velocity, m/s (ft/s)	44.7 (146.7)	109.0 (357.6)	-64.3 (-210.9)	183.2 (601.0)	176.8 (580.1)	6.4 (20.9)
S-IVB 1ST GUIDANCE CUTOFF SIGNAL			S-IVB 2ND GUIDANCE CUTOFF SIGNAL			
Range Time, sec	749.83	705.76	44.07	9,697.15	9,683.59	13.56
Altitude, km (n mi)	191.6 (103.5)	191.4 (103.3)	0.2 (0.2)	324.0 (174.9)	328.4 (177.3)	-4.4 (-2.4)
Surface Range, km (n mi)	2,840.2 (1,533.6)	2,646.8 (1,429.2)	193.4 (104.4)			
Space-Fixed Velocity, m/s (ft/s)	7,790.8 (25,560.4)	7,791.4 (25,562.3)	-0.6 (-1.9)	10,839.5 (35,562.7)	10,836.6 (35,553.1)	2.9 (9.6)
Flight Path Angle, deg	0.004	-0.001	0.005	7.182	7.224	-0.042
Heading Angle, deg	89.713	88.484	1.229	59.443	59.425	0.018
Crossrange, km (n mi)	69.3 (37.4)	60.2 (32.5)	9.1 (4.9)			
Crossrange Velocity, m/s (ft/s)	297.0 (974.4)	275.6 (904.2)	21.4 (70.2)			
Eccentricity				0.9758	0.9760	-0.0002
C <sub>3</sub> *, m <sup>2</sup> /s <sup>2</sup> (ft <sup>2</sup> /s <sup>2</sup> )				-1,463,628 (-15,754,361)	-1,447,169 (-15,577,197)	-16,459 (-177,164)
Inclination, deg				31.818	31.834	-0.016
Descending Node, deg				122.996	123.030	-0.034
<p>NOTE: The Range Times used are times of occurrence at the vehicle, reference Figure 2-1.</p> <p>*C<sub>3</sub> is twice the specific energy of orbit</p> $C_3 = V^2 - \frac{2\mu}{R}$ <p>where V = Inertial Velocity  <math>\mu</math> = Gravitational Constant  R = Radius Vector From Center of Earth</p>						

Table 4-3. Comparison of Separation Events

PARAMETER	ACTUAL	NOMINAL	ACT-NOM
S-IC/S-II SEPARATION			
Range Time, sec	164.3	164.7	-0.4
Altitude, km (n mi)	68.0 (36.7)	67.2 (36.3)	0.8 (0.4)
Surface Range, km (n mi)	96.0 (51.8)	95.7 (51.7)	0.3 (0.1)
Space-Fixed Velocity, m/s (ft/s)	2,754.3 (9,036.4)	2,749.5 (9,020.7)	4.8 (15.7)
Flight Path Angle, deg	19.383	19.145	0.238
Heading Angle, deg	75.693	75.353	0.340
Crossrange, km (n mi)	1.0 (0.5)	0.3 (0.2)	0.7 (0.3)
Crossrange Velocity, m/s (ft/s)	23.6 (77.4)	8.2 (26.9)	15.4 (50.5)
Geodetic Latitude, deg N	28.864	28.869	-0.005
Longitude, deg E	-79.666	-79.670	0.004
S-II/S-IVB SEPARATION			
Range Time, sec	593.5	559.0	34.5
Altitude, km (n mi)	189.2 (102.2)	187.7 (101.3)	1.5 (0.9)
Surface Range, km (n mi)	1,791.8 (967.5)	1,657.5 (895.0)	134.3 (72.5)
Space-Fixed Velocity, m/s (ft/s)	6,895.9 (22,624.3)	6,961.6 (22,839.9)	-65.7 (-215.6)
Flight Path Angle, deg	0.650	0.689	-0.039
Heading Angle, deg	83.380	82.599	0.781
Crossrange, km (n mi)	32.2 (17.4)	27.3 (14.7)	4.9 (2.7)
Crossrange Velocity, m/s (ft/s)	183.7 (602.7)	177.3 (581.7)	6.4 (21.0)
Geodetic Latitude, deg N	32.087	31.940	0.147
Longitude, deg E	-62.380	-63.791	1.411
S-IVB/CSM SEPARATION			
Range Time, sec	11,198.9	11,160.0	38.9
Altitude, km (n mi)	6,997.9 (3,778.6)	6,866.8 (3,707.8)	131.1 (70.8)
Space-Fixed Velocity, m/s (ft/s)	7,628.9 (25,029.2)	7,667.7 (25,156.5)	-38.8 (-127.3)
Flight Path Angle, deg	45.030	44.741	0.289
Heading Angle, deg	72.315	71.988	0.327
Geodetic Latitude, deg N	26.952	26.764	0.188
Longitude, deg E	-129.677	-130.188	0.511
NOTE: The Range Times used are times of occurrence at the vehicle, reference Figure 2-1.			

Table 4-4. Stage Impact Location

PARAMETER	ACTUAL	NOMINAL	ACT-NOM
S-IC STAGE IMPACT			
Range Time, sec	546.9	544.3	2.6
Surface Range, km (n mi)	658.0 (355.3)	650.4 (351.2)	7.6 (4.1)
Crossrange, km (n mi)	12.1 (6.5)	7.3 (3.9)	4.8 (2.6)
Geodetic Latitude, deg N	30.177	30.197	-0.020
Longitude, deg E	-74.065	-74.153	0.088
S-II STAGE IMPACT			
Range Time, sec	1,258.1	1,241.4	16.7
Surface Range, km (n mi)	4,542.3 (2,452.6)	4,533.7 (2,448.0)	8.6 (4.6)
Crossrange, km (n mi)	150.1 (81.0)	149.1 (80.5)	1.0 (0.5)
Geodetic Latitude, deg N	31.320	31.316	0.004
Longitude, deg E	-33.289	-33.383	0.094

#### 4.2.2 Parking Orbit Phase

Orbital tracking data for six passes was obtained from four C-Band stations and one S-Band station of the NASA Manned Space Flight Network.

The parking orbit trajectory was calculated by integrating corrected insertion conditions forward to 8950 seconds. The insertion conditions, as determined by the Orbital Correction Program, were obtained by a differential correction procedure which adjusted the estimated insertion conditions to fit the tracking data in accordance with the weights assigned to the data. The venting model, utilized to fit the tracking data, was derived from telemetered guidance velocity data from the ST-124M-3 guidance platform.

The actual and nominal parking orbit insertion parameters are presented in Table 4-5. The ground track from insertion to S-IVB/CSM separation is given in Figure 4-5.

Table 4-5. Parking Orbit Insertion Conditions

PARAMETER	ACTUAL	NOMINAL	ACT-NOM
Range Time, sec	759.83	715.76	44.07
Altitude, km (n mi)	191.6 (103.5)	191.4 (103.3)	0.2 (0.2)
Space-Fixed Velocity, m/s (ft/s)	7,792.5 (25,565.9)	7,793.0 (25,567.6)	-0.5 (-1.7)
Flight Path Angle, deg	0.005	0.000	0.005
Heading Angle, deg	90.148	88.918	1.230
Inclination, deg	32.525	32.539	-0.014
Descending Node, deg	123.084	123.125	-0.041
Eccentricity	0.0001	0.0000	0.0001
Apogee*, km (n mi)	185.7 (100.3)	185.2 (100.0)	0.5 (0.3)
Perigee*, km (n mi)	183.9 (99.3)	185.1 (99.9)	-1.2 (-0.6)
Period, min	88.19	88.19	0.00
Geodetic Latitude, deg N	32.694	32.692	0.002
Longitude, deg E	-50.490	-52.552	2.062

NOTE: The Range Times used are times of occurrence at the vehicle, reference Figure 2-1.

\*Based on a spherical earth of radius 6,378.165 km (3,443.934 n mi).

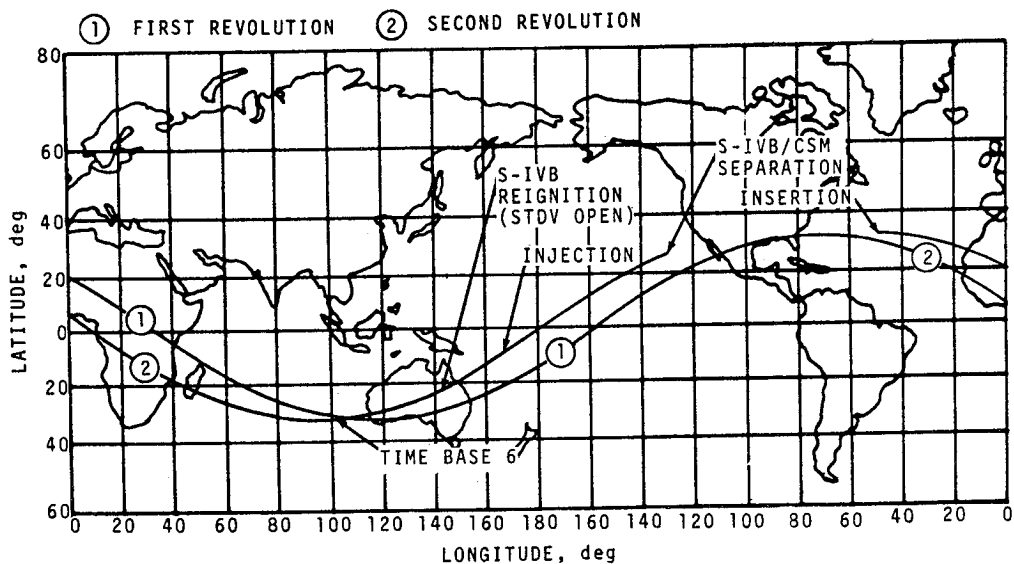


Figure 4-5. Ground Track

### 4.2.3 Injection Phase

The injection phase trajectory was generated by the integration of the telemetered guidance accelerometer data. These accelerometer data were initialized from a parking orbit state vector at 8950 seconds and were constrained to a state vector at TLI obtained from the post TLI trajectory. There were no tracking data available during S-IVB second burn.

Comparisons between the actual and nominal space-fixed velocity and flight path angle are shown in Figure 4-6. The actual and nominal total inertial acceleration comparisons are presented in Figure 4-7. The space-fixed velocity and flight path angle were greater than nominal with deviations more noticeable towards the end of the time period. The actual and nominal targeting parameters at S-IVB second guidance cutoff are presented in Table 4-2.

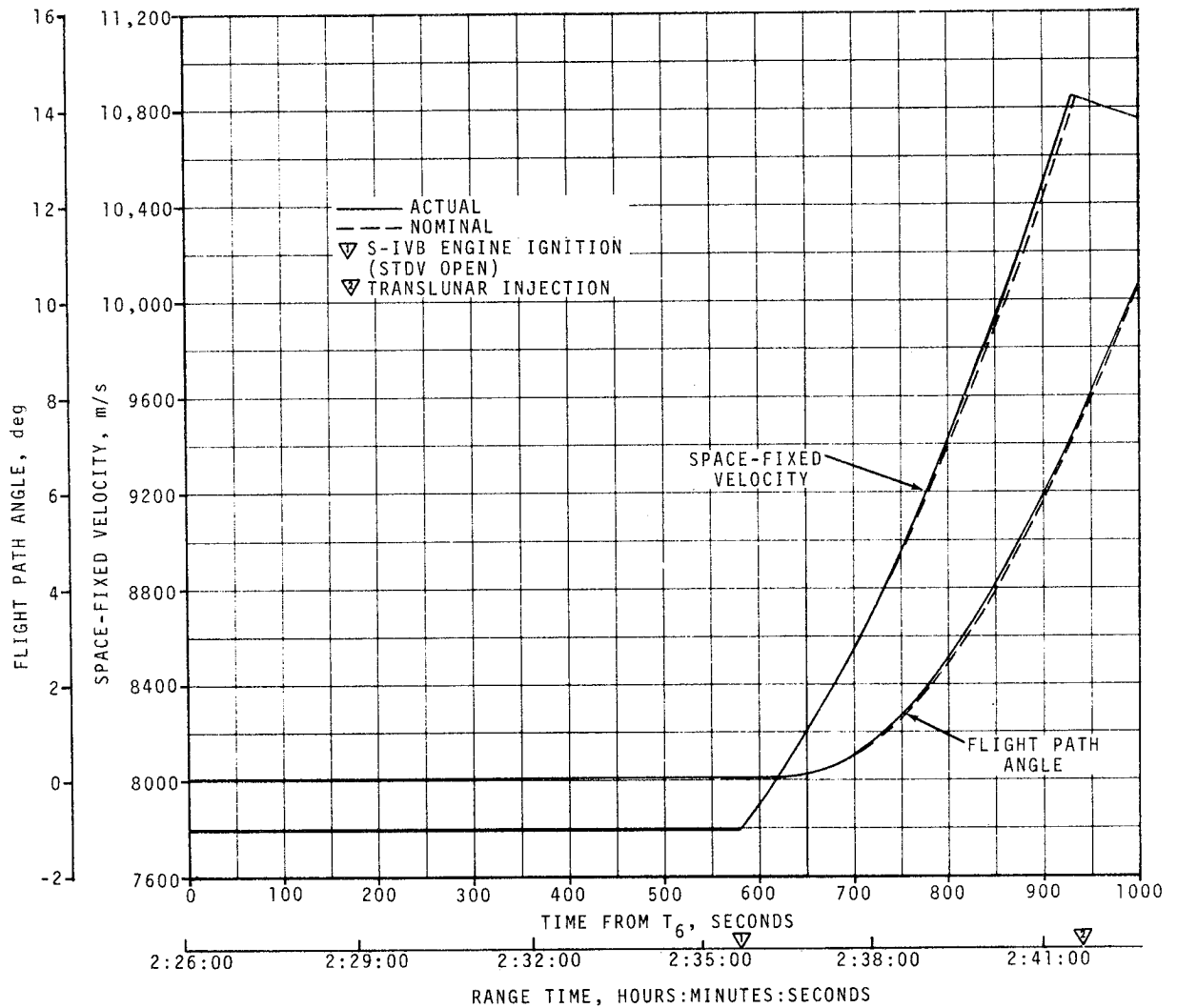


Figure 4-6. Injection Phase Space-Fixed Velocity and Flight Path Angle Comparisons

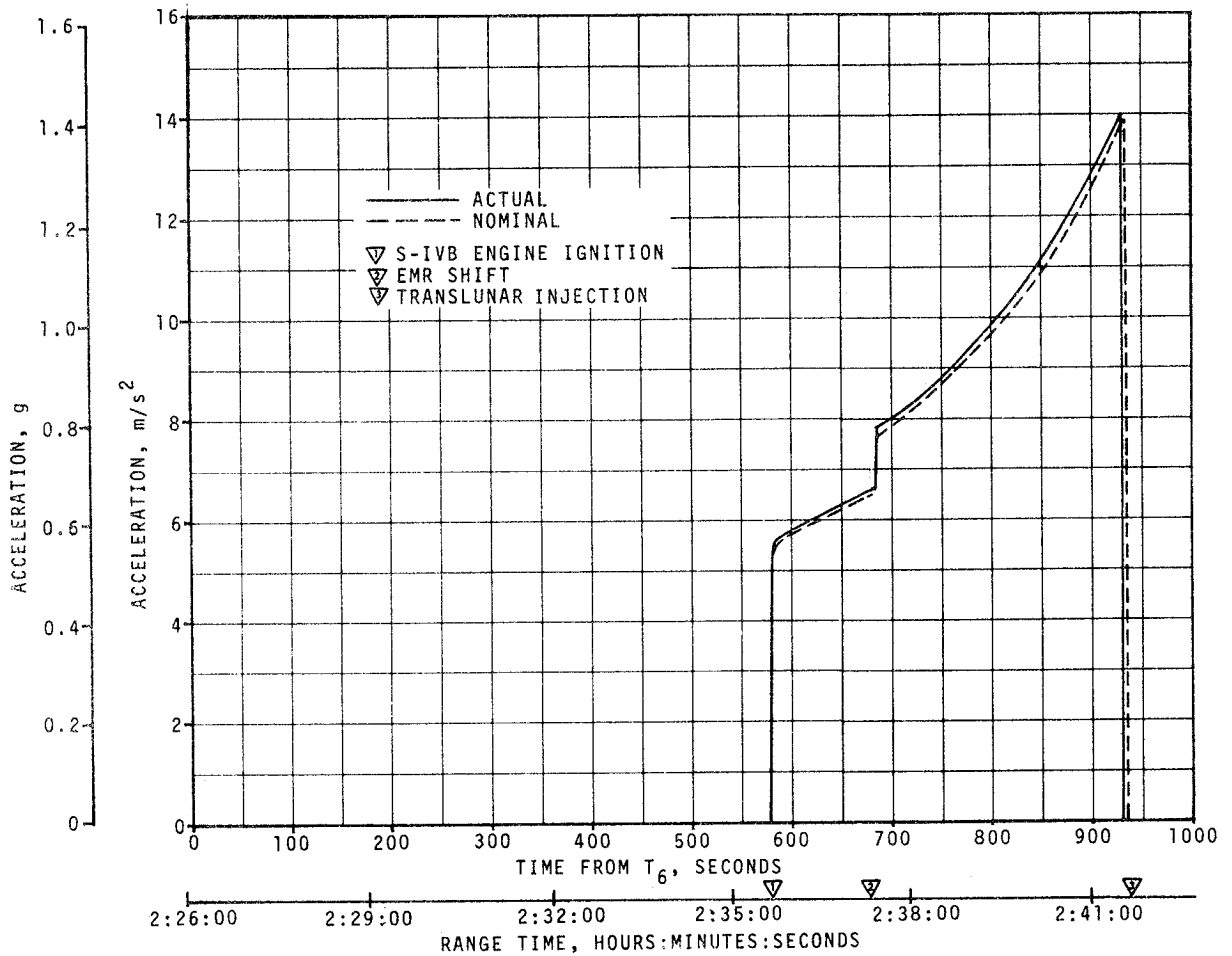


Figure 4-7. Injection Phase Acceleration Comparison

#### 4.2.4 Post TLI Phase

The post TLI trajectory spans the interval from translunar injection to S-IVB/CSM separation. Tracking data from three C-Band stations and three S-Band stations were utilized in the reconstruction of this trajectory segment. The post TLI trajectory reconstruction utilizes the same methodology as outlined in paragraph 4.2.2. The actual and nominal translunar injection conditions are compared in Table 4-6. The S-IVB/CSM separation conditions are presented in Table 4-3.

Table 4-6. Translunar Injection Conditions

PARAMETER	ACTUAL	NOMINAL	ACT-NOM
Range Time, sec	9,707.15	9,693.59	13.56
Altitude, km (n mi)	337.9 (182.5)	342.4 (184.9)	-4.5 (-2.4)
Space-Fixed Velocity, m/s (ft/s)	10,832.1 (35,538.4)	10,828.4 (35,526.2)	3.7 (12.2)
Flight Path Angle, deg	7.635	7.676	-0.041
Heading Angle, deg	59.318	59.299	0.019
Inclination, deg	31.817	31.833	-0.016
Descending Node, deg	122.997	123.031	-0.034
Eccentricity	0.9772	0.9772	0.0000
C <sub>3</sub> , m <sup>2</sup> /s <sup>2</sup> (ft <sup>2</sup> /s <sup>2</sup> )	-1,376,274 (-14,814,090)	-1,376,265 (-14,813,993)	-9 (-97)
NOTE: The Range Times used are times of occurrence at the vehicle, reference Figure 2-1			

## SECTION 4A

### LUNAR IMPACT

#### 4A.1 SUMMARY

All aspects of the S-IVB/IU Lunar Impact objective were accomplished successfully except the precise determination of impact point. The final impact solution is expected to satisfy the mission objective. At 280,599.7  $\pm$ 0.1 seconds (77:56:39.7) vehicle time the S-IVB/IU impacted the lunar surface at approximately 2.5  $\pm$ 0.5 degrees south latitude and 27.9  $\pm$ 0.1 degrees west longitude, which is approximately 65.5  $\pm$ 7.8, -4.8 kilometers (35.4  $\pm$ 4.2, -2.6 n mi) from the target of 3 degrees south latitude and 30 degrees west longitude. Impact velocity was 2579 m/s (8461 ft/s). The mission objectives were to maneuver the S-IVB/IU such that it would have at least a 50 percent probability of impacting the lunar surface within 350 kilometers (189 n mi) of the target, and to determine the actual impact point within 5 kilometers (2.7 n mi) and the time of impact within 1 second.

Preliminary results of the seismic experiment indicate that the S-IVB/IU impact signal was 20 to 30 times greater in amplitude and four times longer in duration than the Apollo 12 Lunar Module (LM) impact.

#### 4A.2 TIME BASE 8 MANEUVERS

The Auxiliary Propulsion System (APS) evasive burn, Continuous Vent System (CVS) vent, LOX dump, and APS lunar impact burn occurred as planned and were close to nominal. Following CSM/LM ejection, the vehicle was maneuvered to an inertially fixed attitude as required for the evasive APS burn. After the evasive attitude was attained, Time Base 8 (T<sub>8</sub>) was initiated 239.3 seconds later than nominal at 15,479.4 seconds (04:17:59.4) and the APS ullage engines burned for 80 seconds to provide the required spacecraft/launch vehicle separation velocity. At 16,060.0 seconds (04:27:40.0), the stage maneuvered to the CVS/LOX dump attitude. The initial lunar targeting velocity change was accomplished by means of a 300-second duration CVS vent and 48-second duration LOX dump. The S-IVB/IU was targeted to a lunar impact of 9.0 degrees south latitude and 72.3 degrees west longitude (selenographic coordinates); however, this impact point was not sufficiently close to the desired target. A maneuver consisting of an attitude change and an APS ullage engine burn to occur at 21,600 seconds (06:00:00), in order to improve the targeting, was

defined at approximately 18,000 seconds (05:00:00) at the Huntsville Operations Support Center (HOSC). The maneuver was based on a post-Translunar Injection (TLI) tracking vector sent from the Mission Control Center (MCC) and received at Marshall Space Flight Center (MSFC) prior to Tg as planned. The maneuver considered actual event times and velocity increments of the APS evasive burn, CVS vent and LOX dump. The velocity increments were obtained in real-time by telemetered accelerometer measurements. At 19,200 seconds (05:20:00), the maneuver command was transmitted to MCC, and at 20,887 seconds (05:48:07), the command was uplinked to the IU. The S-IVB/IU maneuvered -1 degree in pitch and -3 degrees in yaw. The resulting attitude was 182 degrees in pitch and -8 degrees in yaw, referenced to the local horizontal system. At this attitude and at approximately 21,600 seconds (06:00:00), the APS ullage engines burned for a duration of 217 seconds, as commanded.

At 27,900 seconds (07:45:00) a tracking vector, which included data subsequent to the 217-second APS burn, was sent from the MCC to MSFC as planned. This vector was integrated out to lunar distance and indicated that the stage would impact the moon within 200 kilometers (108 n mi) of the desired target. This vector indicated that no additional targeting maneuvers would be required to assure that the spent stage would have at least a 50 percent probability of impacting within a 350-kilometer (189-n mi) radius of the target.

Tracking vectors were received at regular intervals, and indicated that the S-IVB/IU would impact approximately 200 kilometers (108 n mi) southwest of the target site. At 70,150 seconds (19:29:10), a shift was observed in range rate tracking data and was interpreted as a velocity change due to a propulsive force acting on the spent stage. This velocity change is discussed in paragraph 10.4.4. Figure 4A-1 shows a decrease in range rate of approximately 2 to 3 m/s (7 to 10 ft/s) beginning at 70,150 seconds (19:29:10). The decrease in range rate lasted approximately 60 seconds. The projected impact location of all subsequent tracking vectors out to actual lunar impact were slightly east of the target. The velocity change altered the predicted lunar impact point approximately 5 degrees in latitude, 150 kilometers (81 n mi), closer to the target. Analysis of the projected impact points before and after the unscheduled velocity change indicates that a velocity change of approximately 2.5 m/s (8.2 ft/s) at an attitude of 181 degrees pitch and -33 degrees yaw would cause an identical perturbation to the translunar trajectory. It should be noted that this is a representative perturbation effect and that there exists a family of such perturbations that would result in the same impact conditions. However, if the velocity change had occurred in less favorable directions the stage would not have impacted within the prescribed limits.

Table 4A-1 shows the actual and nominal velocity increments along the S-IVB/IU longitudinal body axis. Figure 4A-2 shows the velocity change

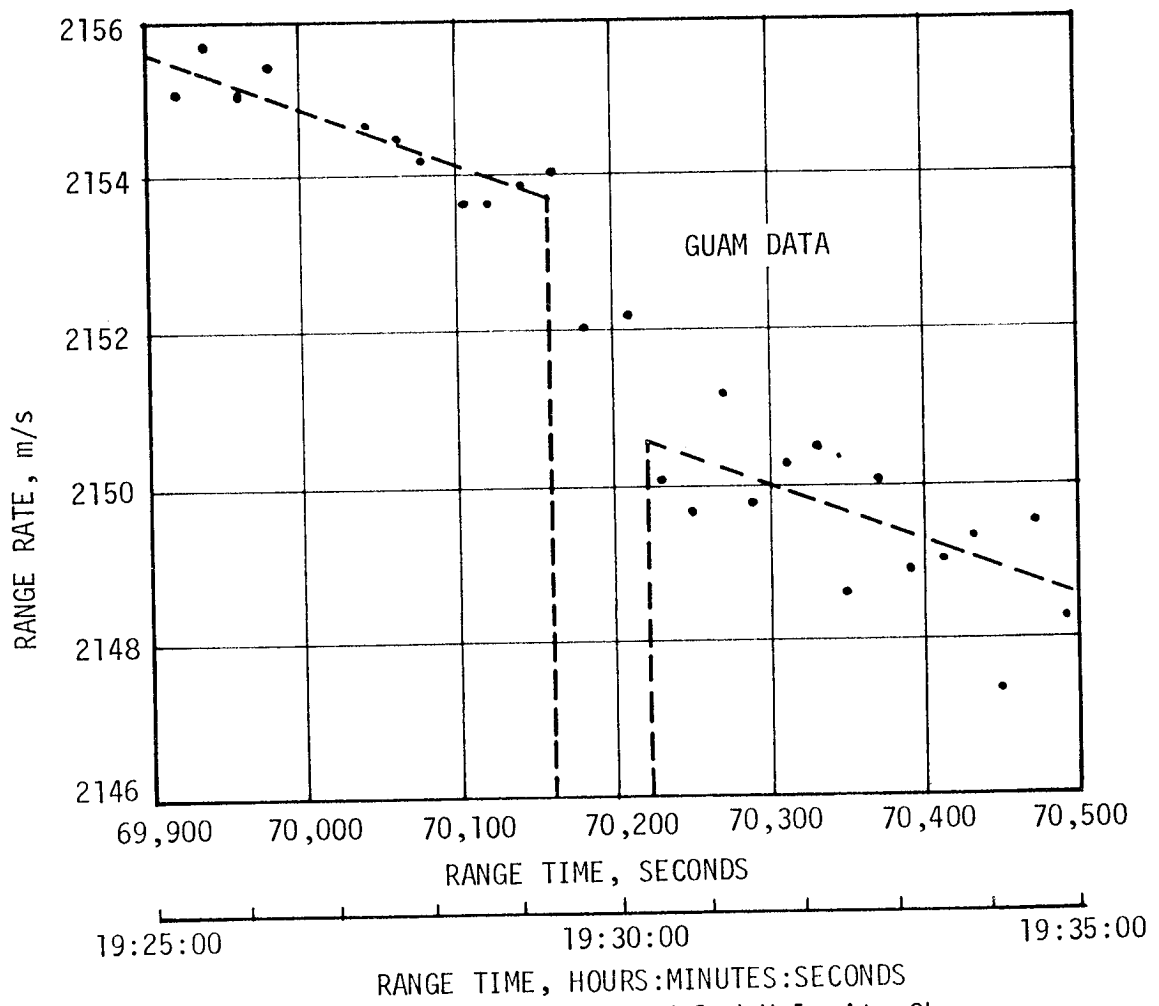
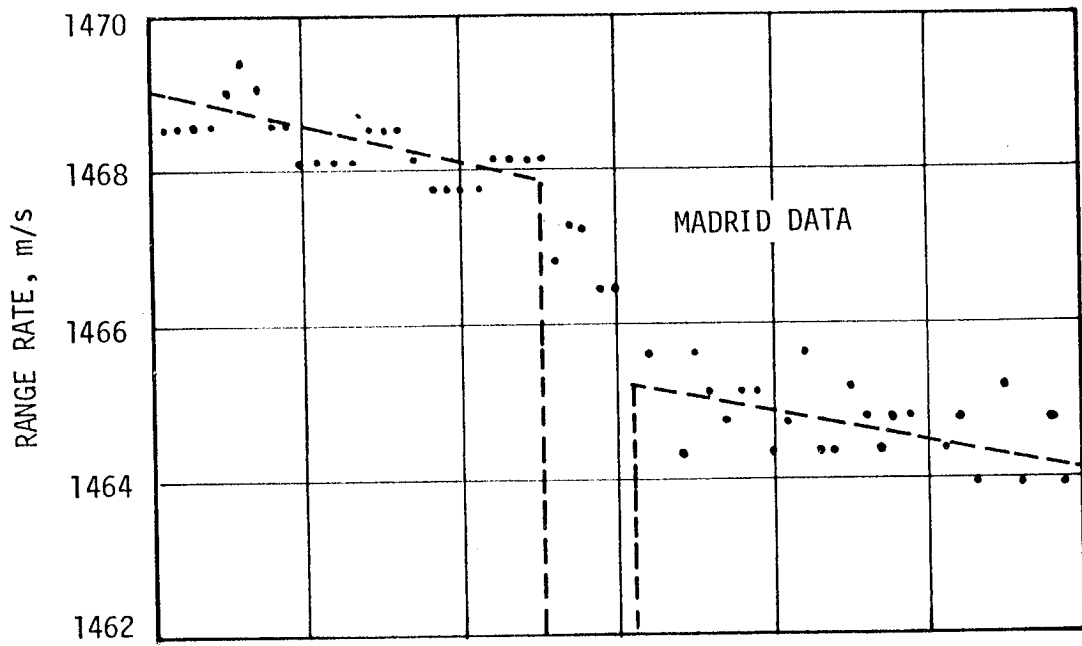


Figure 4A-1. S-IVB/IU Unscheduled Velocity Change

Table 4A-1. Comparison of Time Base 8 Velocity Increments

PARAMETER	ACTUAL	NOMINAL	ACT-NOM
APS Evasive Burn (80 seconds duration), m/s (ft/s)	2.98 (9.78)	2.90 (9.51)	0.08 (0.27)
CVS Vent (300 seconds duration), m/s (ft/s)	0.44 (1.44)	0.50 (1.64)	-0.06 (-0.20)
LOX Dump (48 seconds duration), m/s (ft/s)	8.73 (28.64)	8.30 (27.23)	0.43 (1.41)
APS Lunar Impact Burn (217 seconds duration), m/s (ft/s)	9.12 (29.92)	9.21* (30.22)	-0.09** (-0.30)

\*Based on actual velocity increments from APS evasive burn, CVS, and LOX dump. Calculated in Real-Time.  
 \*\*Actual-Calculated.

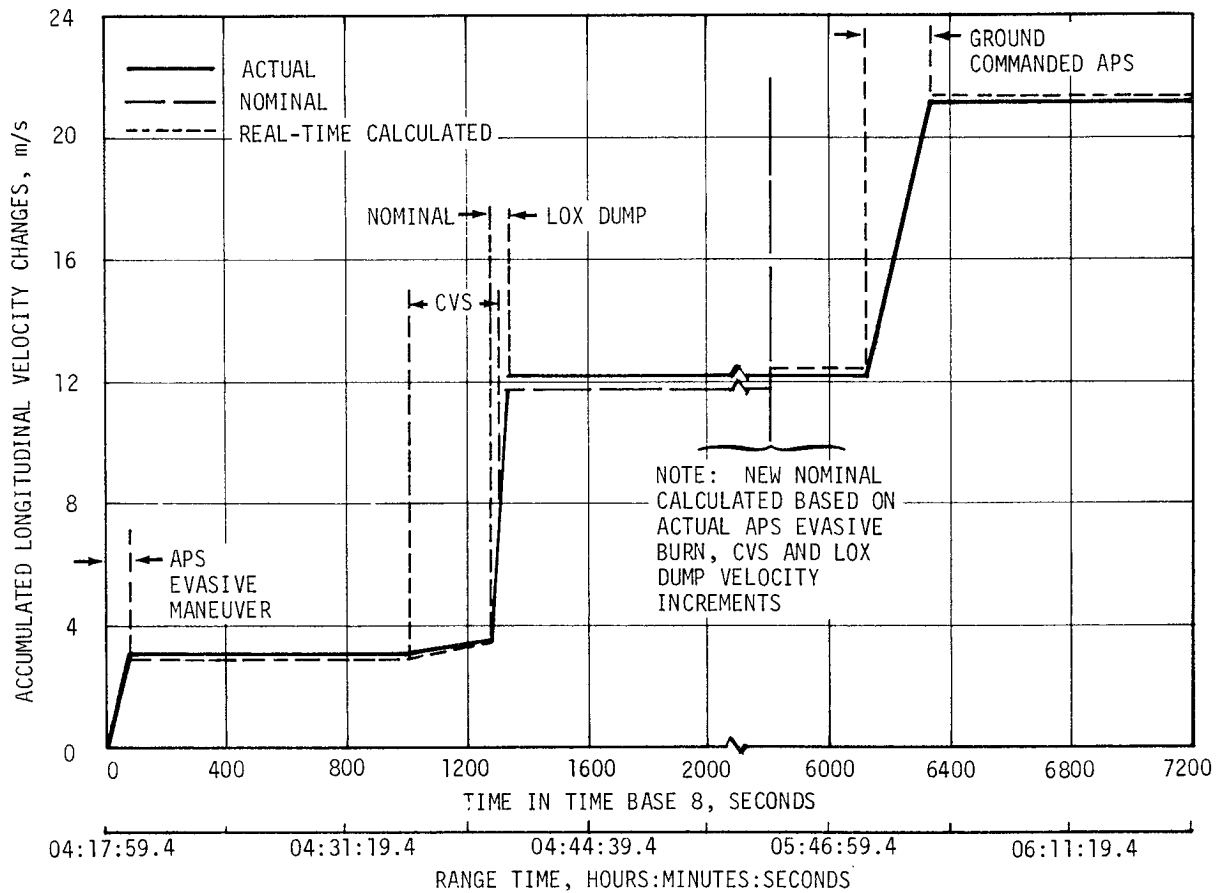


Figure 4A-2. Accumulated Longitudinal Velocity Change During Time Base 8

profile during  $T_8$ . Table 4A-2 shows the actual and nominal attitudes at which the various events during  $T_8$  were performed. The difference between the actual and nominal attitudes for the APS lunar impact burn is the magnitude of the commanded maneuver at 20,887 seconds (05:48:07).

#### 4A.3 TRAJECTORY EVALUATION

Figure 4A-3 shows the radius and space-fixed velocity (earth centered) profiles from the APS lunar impact burn to lunar impact. Table 4A-3 shows the actual and nominal orbit parameters following the unscheduled velocity change. The orbit parameters are two-body calculations. The orbit parameters indicate a slightly lower energy orbit than nominal which is consistent with the actual impact location being further east than the target site. An increasing underspeed condition causes the impact point to move in a west to east direction.

#### 4A.4 LUNAR IMPACT CONDITION

Figure 4A-4 shows various impact points relative to the target and seismometer locations. There are three significant comparisons to be made from this figure. First, comparison of the impact point of the TLI IU state vector (with actual velocity increments modeled through the APS lunar impact burn) with the projected impact site, prior to the unscheduled velocity change, shows the approximate projected error in the IU state vector at TLI. Second, comparison of the impact

Table 4A-2. Comparison of Attitude Time Line, Time Base 8

EVENT	ACTUAL		NOMINAL		ACT-NOM	
	PITCH	YAW	PITCH	YAW	PITCH	YAW
APS Evasive Burn, deg	176	40	176	40	0	0
CVS Vent, deg	183	-5	183	-5	0	0
LOX Dump, deg	183	-5	183	-5	0	0
APS Lunar Impact Burn, deg	182	-8	183	-5	-1	-3

NOTE: Attitudes referenced to Local Horizontal System.

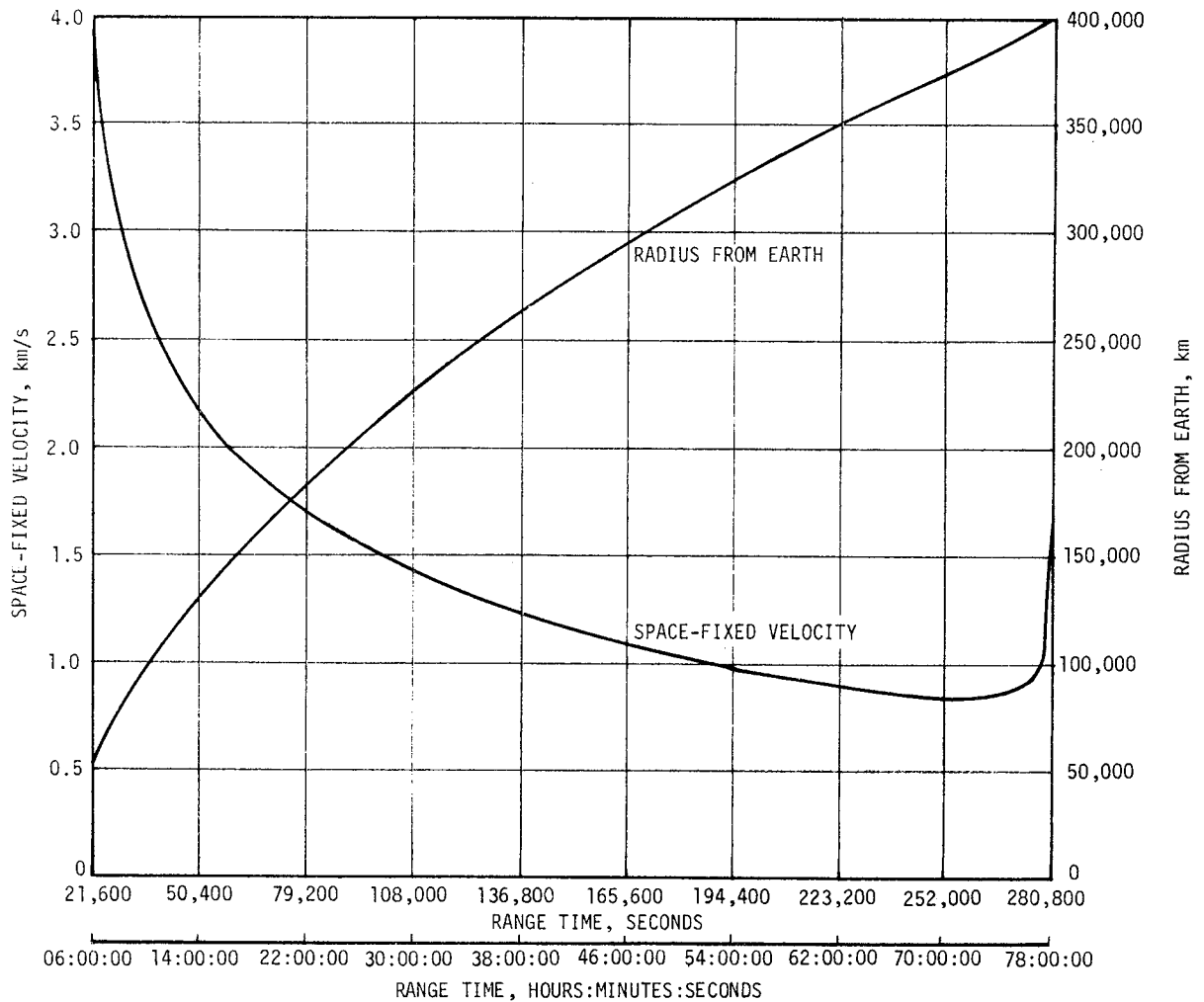


Figure 4A-3. Lunar Impact Trajectory Radius and Space-Fixed Velocity Profiles

point, prior to the unscheduled velocity change, with the target site shows the actual miss distance due to real-time targeting. Third, a comparison of the actual impact point with the target and seismometer locations illustrates actual miss distances. The miss distances with other impact parameters are shown in Table 4A-4. A summary of impact times recorded by the various tracking sites is shown in Table 4A-5. The average of the recorded times was used as the best available time of impact, and is considered accurate to within 0.1 second.

Preliminary results of the seismic experiment are that the overall characteristic of the seismic signal due to S-IVB/IU impact is similar to that of the Apollo 12 LM impact signal. The S-IVB/IU signal was 20 to 30 times greater in amplitude and four times longer in duration (approximately 4 hours versus 1 hour) than the Apollo 12 LM impact. A period of 30 seconds elapsed between time of impact and arrival of

Table 4A-3. Comparison of Orbit Parameters After the Unscheduled Delta V

PARAMETER	ACTUAL	NOMINAL	ACT-NOM
Semimajor Axis, km (n mi)	266,092 (143,678)	267,411 (144,390)	-1319 (-712)
Eccentricity	0.97585	0.97605	-0.00020
Inclination, deg*	31.8317	31.8498	-0.0181
$C_3$ , $m^2/s^2$ ( $ft^2/s^2$ )	-1,497,990 (-16,124,162)	-1,490,600 (-16,044,617)	-7390 (-79,545)
Right Ascension of Ascending Node, deg	170.1472	170.1475	-0.0003
Argument of Perigee, deg	249.655	248.623	1.032
Perigee Altitude, km (n mi)	47 (25)	25 (13)	22 (12)
Apogee Altitude, km (n mi)	519,381 (280,443)	522,040 (281,879)	-2659 (-1436)

\*Referenced to earth's equatorial plane.

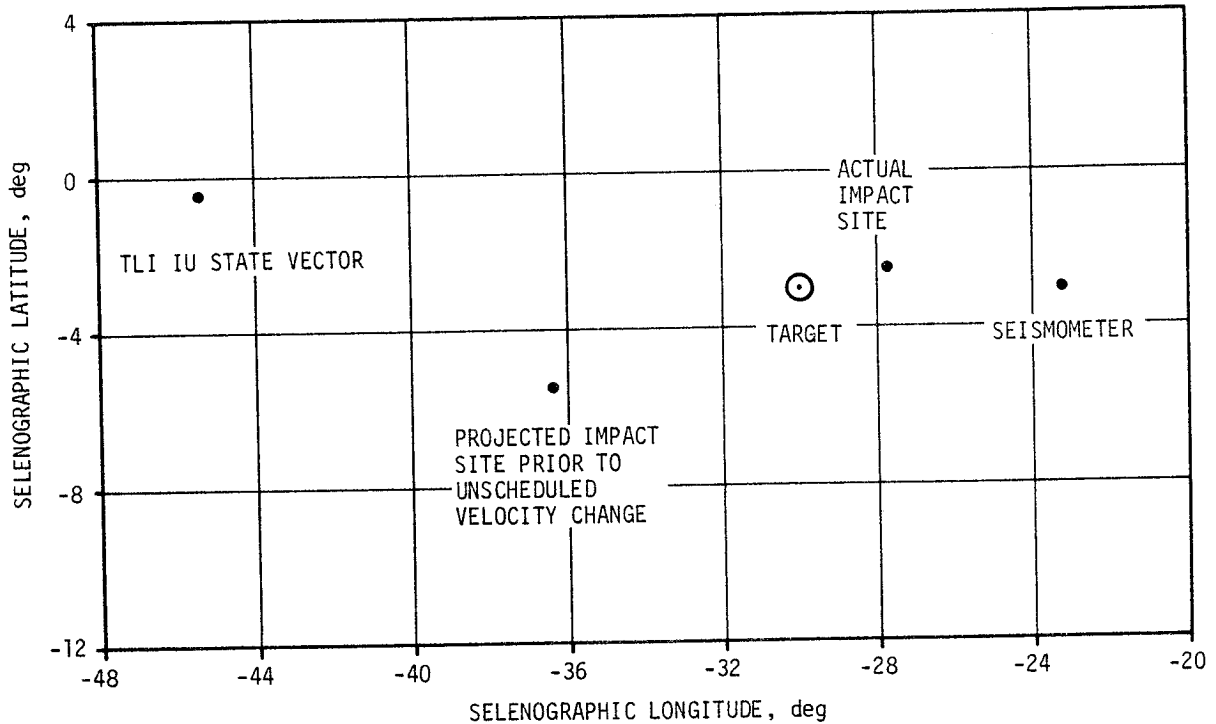


Figure 4A-4. Comparison of Projected Lunar Impact Points

Table 4A-4. S-IVB/IU Lunar Impact Parameters

PARAMETER AT IMPACT	ACTUAL	NOMINAL	ACT-NOM
Stage Mass, kg (lbm)	13,426* (29,599)*	13,395 (29,532)	31 (67)
Moon Centered Space-Fixed Velocity, m/s (ft/s)	2579 (8461)	2580 (8464)	-1 (-3)
Path Angle Measured from Local Vertical, deg	13.2	12.0	1.2
Heading Angle (North to West), deg	100.6	100.0	0.6
Tumble Rate, deg/s	12†	N.A.	N.A.
Selenographic West Longitude, deg	27.9 ±0.1	30.0	-2.1 ±0.1
Selenographic South Latitude, deg	2.5 ±0.5	3.0	-0.5 ±0.5
Impact Time, HR:MIN:SEC**	77:56:39.7	77:45:00	00:11:39.7
Distance to Target, km (n mi)	65.5 <sup>+7.8</sup> <sub>-4.8</sub> (35.4 <sup>+4.2</sup> <sub>-2.6</sub> )	0 (0)	65.5 <sup>+7.8</sup> <sub>-4.8</sub> (35.4 <sup>+4.2</sup> <sub>-2.6</sub> )
Distance to Seismometer, km (n mi)	139.1 <sup>+5.4</sup> <sub>-3.8</sub> (75.1 <sup>+2.9</sup> <sub>-2.1</sub> )	0 (0)	139.1 <sup>+5.4</sup> <sub>-3.8</sub> (75.1 <sup>+2.9</sup> <sub>-2.1</sub> )
*Stage dry weight - all residual propellants assumed dissipated. **Actual time (Signal delay time = 1.323 sec).			

the seismic wave at the seismometer. Peak intensity of the seismometer signal occurred approximately 450 seconds after impact. In addition to the seismic data, the Suprathermal Ion Detector Experiment (SIDE) recorded an increase in the ion count 22 seconds after impact.

A more accurate determination of the impact location and related analyses is continuing.

#### 4A.5 TRACKING

Approximately 75 hours of S-IVB/IU tracking data, from TLI to lunar impact, were obtained. Prior to activating the LM communication system, both Goddard Space Flight Center (GSFC) and Manned Spacecraft Center (MSC)

Table 4A-5. Summary of Lunar Impact Times

TRACKING STATION	RECORDED IMPACT TIME, HR:MIN:SEC	
	GREENWICH MEAN TIME APRIL 15, 1970	RANGE TIME
Madrid	01:09:41.025	77:56:41.025
Ascension	01:09:41.04	77:56:41.04
GSFC (ETC 3)	01:09:41.01	77:56:41.01
Goldstone	01:09:41.02	77:56:41.02
Hawaii	01:09:41.015	77:56:41.015
MILA	01:09:41.026	77:56:41.026
Average	01:09:41.023	77:56:41.023
NOTE: Signal Delay Time = 1.323 sec Actual Impact Time = 77:56:39.7 ±0.1 sec		

monitored and analyzed the data in real-time; however, after the CSM problem began, only GSFC continued to analyze real-time data and provide tracking vectors. Figure 4A-5 shows the data considered by GSFC in the orbit and impact location determinations. Table 4A-6 lists the tracking sites, their configuration sizes, and abbreviations used.

An increase in the spent stage tumble rate after the unscheduled velocity change caused the range rate data to be relatively noisy, which hindered an accurate determination of the actual impact point to date. There was a temporary tracking frequency conflict between the LM and IU which resulted in the loss of some tracking data. The frequency conflict was solved by driving the IU frequency off-center in order to differentiate between the LM and IU signals, as discussed in paragraph 15.6. The final solution of the actual impact coordinates are expected to be accurate to within 0.10 degree in latitude, and 0.05 degree in longitude which is within approximately 3.4 kilometers (1.8 n mi).

4A-10

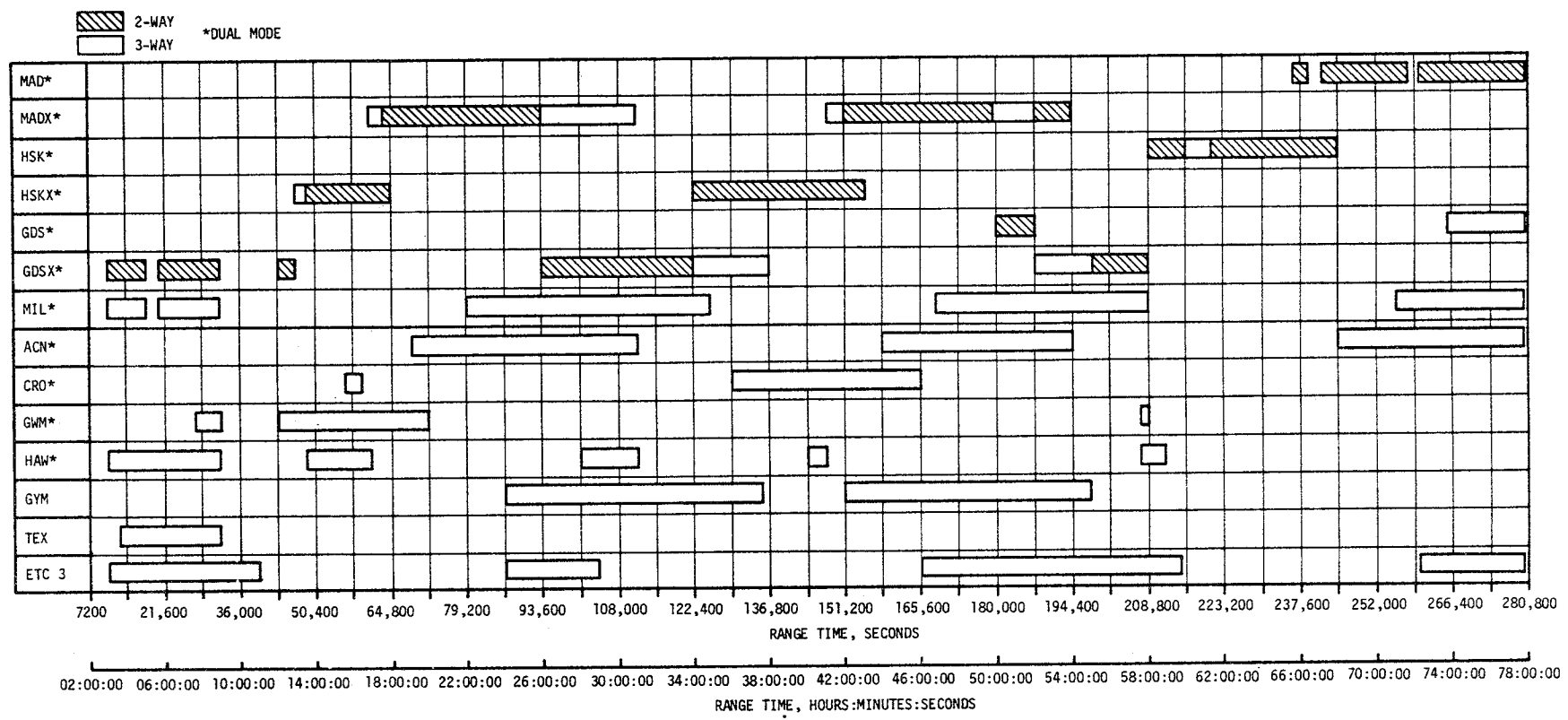


Figure 4A-5. Summary of CCS Tracking Data Used for Post-TLI Orbit Determination

Table 4A-6. S-IVB/IU CCS Tracking Network

STATION	CONFIGURATION	ABBREVIATION
Madrid, Spain	Main Site - 85 ft dish Wing Site - 85 ft dish	MAD MADX
Honeysuckle Creek, Australia	Main Site - 85 ft dish Wing Site - 85 ft dish	HSK HSKX
Goldstone, California	Main Site - 85 ft dish Wing Site - 85 ft dish	GDS GDSX
Merritt Island, Florida	30 ft dish	MIL
Canary Island	30 ft dish	CYI
Ascension Island	30 ft dish	ACN
Carnarvon, Australia	30 ft dish	CRO
Guam Island	30 ft dish	GWM
Hawaii	30 ft dish	HAW
Guaymas, Mexico	30 ft dish	GYM
Corpus Christi, Texas	30 ft dish	TEX
Goddard Experimental Test Center	30 ft dish	ETC 3



## SECTION 5

### S-IC PROPULSION

#### 5.1 SUMMARY

All S-IC propulsion systems performed satisfactorily and the propulsion performance level was very close to predicted. Stage site thrust (averaged from liftoff to Outboard Engine Cutoff [OECO]) was 0.26 percent higher than predicted. Total propellant consumption rate was 0.06 percent higher than predicted with the total consumed Mixture Ratio (MR) 0.24 percent higher than predicted. Specific impulse was 0.20 percent higher than predicted. Total propellant consumption from Holddown Arm (HDA) release to OECO was low by 0.06 percent.

Center Engine Cutoff (CECO) was initiated by the Instrument Unit (IU) at 135.18 seconds as planned. Outboard engine cutoff, initiated by LOX low level sensors, occurred at 163.60 seconds which was 0.40 second earlier than predicted. This is a small difference compared to the predicted 3-sigma limits of +5.58, -3.89 seconds. The LOX residual at OECO was 38,921 lbm compared to the predicted 39,403 lbm. The fuel residual at OECO was 27,573 lbm compared to the predicted 31,957 lbm.

There were three unplanned events that occurred during the S-IC countdown and boost, although they did not cause launch delay or problems during flight. These events were:

- a. LOX tank vent and relief valve temporarily stuck open during countdown.
- b. The planned 1-2-2 start sequence was not attained.
- c. Engine No. 2 LOX pump bearing jet pressure exhibited unexpected shifts and operated at a higher level than predicted.

S-IC hydraulic system performance was normal throughout the flight.

#### 5.2 S-IC IGNITION TRANSIENT PERFORMANCE

The fuel pump inlet preignition pressure was 45.7 psia and within F-1 Engine Model Specification limits of 43.5 to 110 psia.

The LOX pump inlet preignition pressure and temperature were 82.5 psia and -285.1°F and were within the F-1 Engine Model Specification limits, as shown in Figure 5-1.

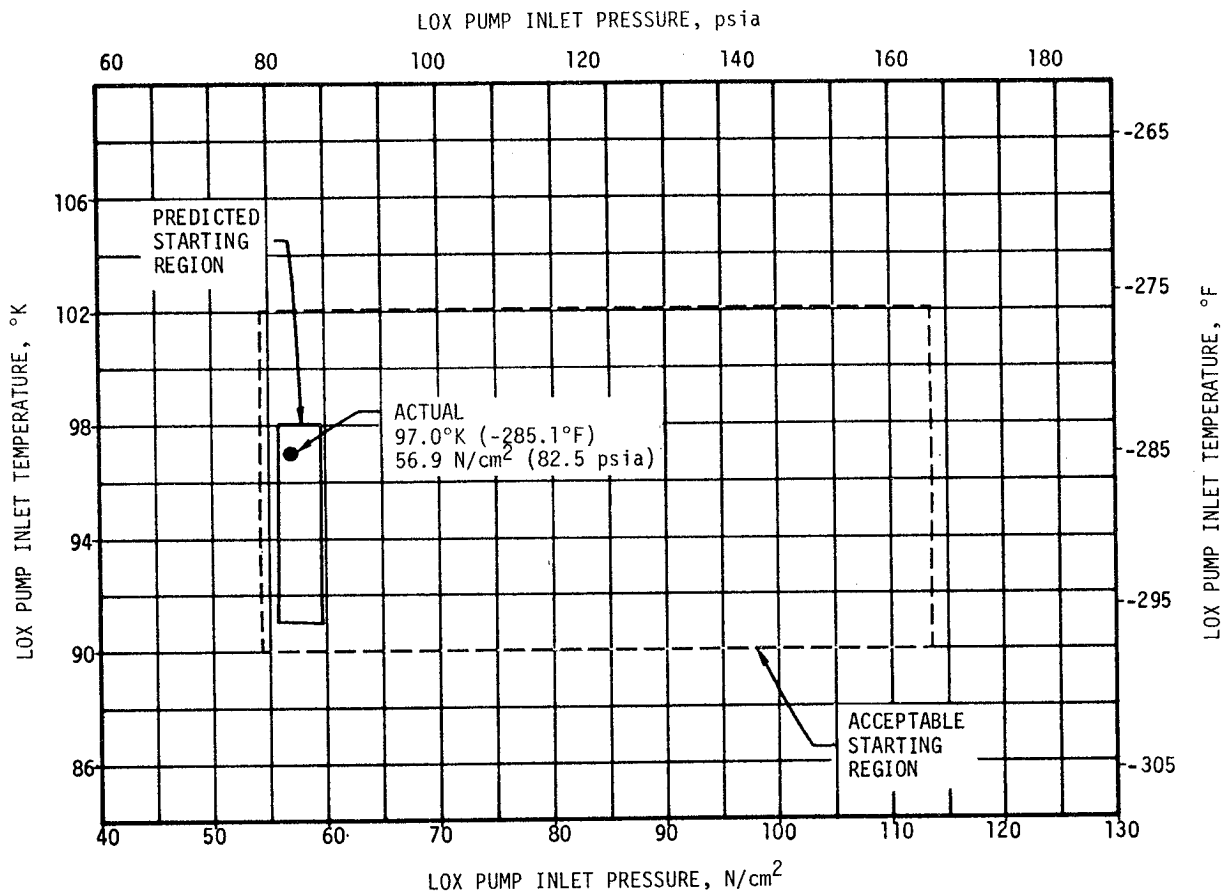


Figure 5-1. S-IC LOX Start Box Requirements

The planned 1-2-2 start was not attained since engines No. 2 and 4 combustion chamber pressures did not reach 100 psig within the desired 100-millisecond time period. See Figure 5-2. Engine No. 4 reached 100 psig chamber pressure 0.303 second slower than predicted and 0.317 second later than engine No. 2, resulting in a 1-2-1-1 start. Structurally, a 1-2-2 start is desired for minimizing the start and liftoff dynamics caused by thrust buildup of the engines. Each F-1 engine has distinctive starting characteristics requiring individually programmed start signals in order to minimize the dispersions in achieving the planned start sequence. Determination of start signal presettings is one objective of static firing the S-IC stage. Engine No. 4 was replaced after the stage static firing. Consequently, only single engine firing data for engine No. 4 was available for determining the start signal presetting. It is well known that presettings based only on single engine firings are inaccurate, therefore the AS-508 1-2-1-1 start was not unexpected. The 1-2-1-1 start caused no problems.

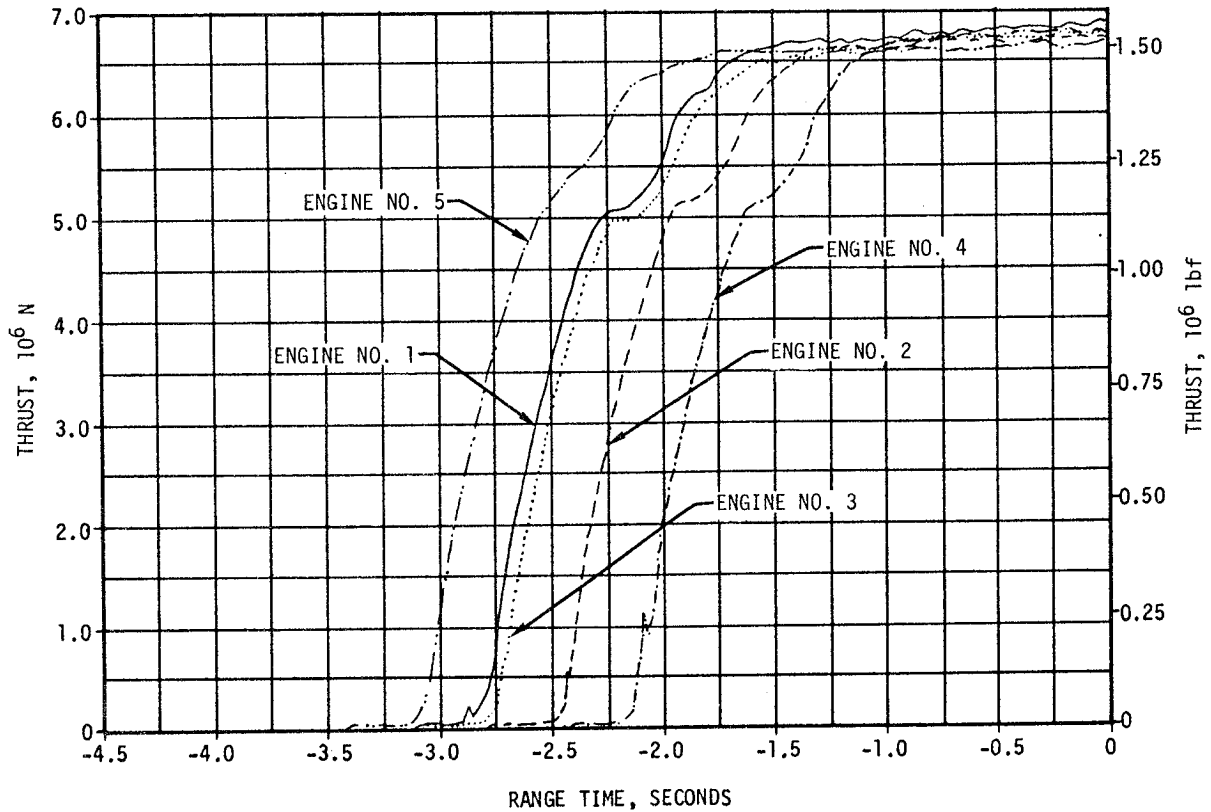


Figure 5-2. S-IC Engines Thrust Buildup

### 5.3 S-IC MAINSTAGE PERFORMANCE

S-IC stage propulsion performance was very close to the predicted level, as shown in Figure 5-3. The stage site thrust (averaged from range time zero to OECO) was 0.26 percent higher than predicted.

Total propellant consumption rate was 0.06 percent higher than predicted and the total consumed propellant MR was 0.24 percent higher than predicted. The specific impulse was 0.20 percent higher than predicted. Total propellant consumption from HDA release to OECO was low by 0.06 percent.

For comparison of F-1 engine flight performance with predicted performance, the flight performance has been analytically reduced to standard conditions and compared to the predicted performance which is based on ground firings and also reduced to standard conditions. These values are shown in Table 5-1 at the 35 to 38-second time slice. Individual engine deviations from predicted thrust ranged from 0.199 percent lower (engine No. 2) to 0.397 percent higher (engine No. 3). Individual engine deviations from specific impulse ranged from 0.038 percent lower (engines No. 2, 4, and 5) to 0.038 percent higher (engines No. 1 and 3).

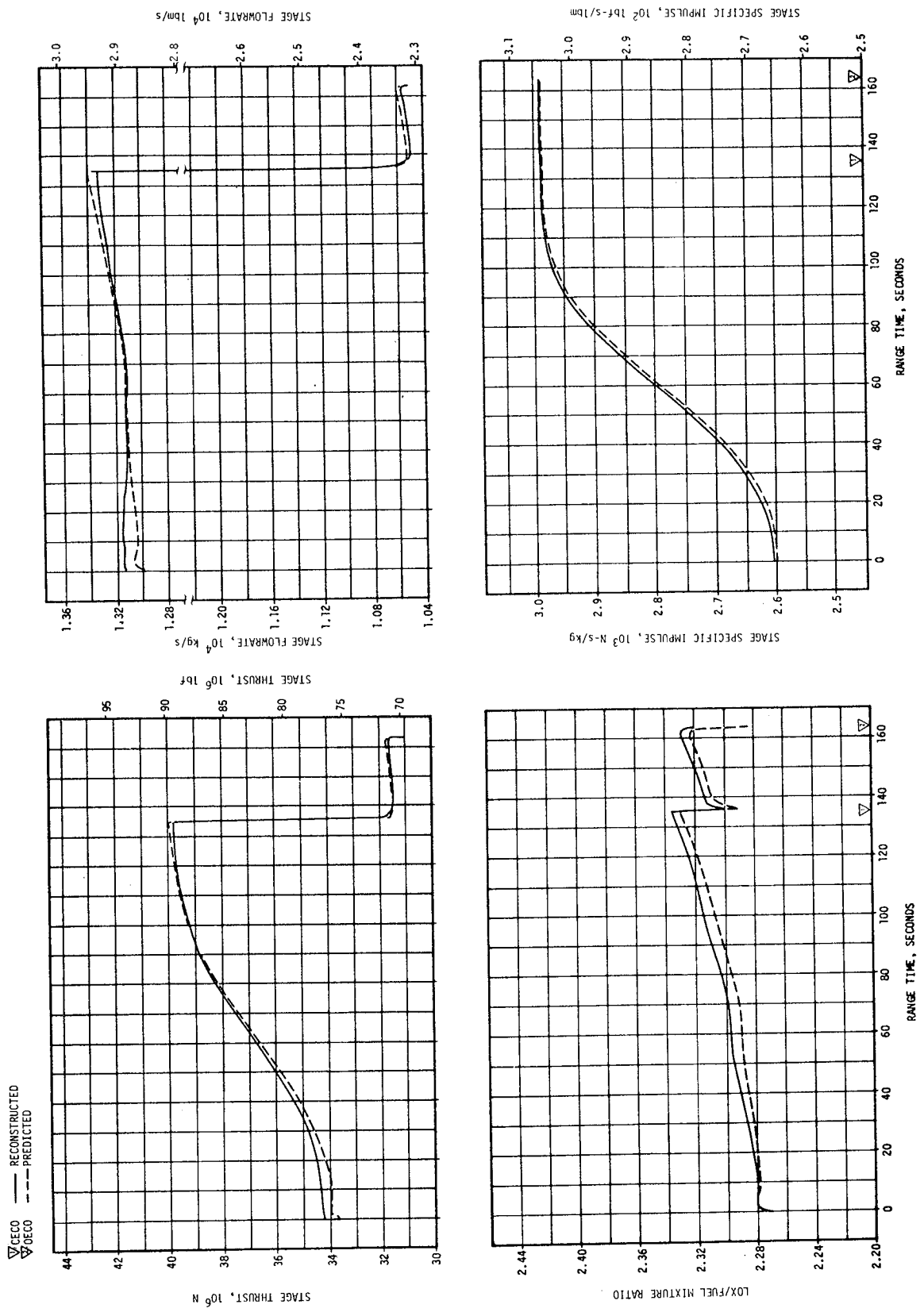


Figure 5-3. S-IC Stage Propulsion Performance

Table 5-1. S-IC Individual Engine Performance

PARAMETER	ENGINE	PREDICTED	RECONSTRUCTION ANALYSIS	DEVIATION PERCENT	AVERAGE DEVIATION PERCENT
Thrust, 10 <sup>3</sup> lbf	1	1514	1520	0.396	0.053
	2	1504	1501	-0.199	
	3	1510	1516	0.397	
	4	1516	1513	-0.198	
	5	1512	1510	-0.132	
Specific Impulse, lbf-s/lbm	1	264.5	264.6	0.038	-0.008
	2	264.9	264.8	-0.038	
	3	264.8	264.9	0.038	
	4	266.0	265.9	-0.038	
	5	264.7	264.6	-0.038	
Total Flowrate lbm/s	1	5724	5746	0.384	0.052
	2	5680	5670	-0.176	
	3	5702	5722	0.351	
	4	5698	5689	-0.158	
	5	5713	5705	-0.140	
Mixture Ratio LOX/Fuel	1	2.272	2.268	-0.176	-0.088
	2	2.256	2.255	-0.044	
	3	2.260	2.257	-0.133	
	4	2.261	2.260	-0.044	
	5	2.242	2.241	-0.045	
NOTE: Performance levels were reduced to standard sea level and pump inlet conditions. Data was taken from the 35 to 38-second time slice.					

Engine No. 2 (S/N F2058) LOX pump bearing jet pressure stabilized initially at 468 psia, approximately 88 psi higher than that demonstrated during acceptance and stage static tests. At 10 seconds, the jet pressure sharply increased 48 psi to a level of 516 psia and remained stable at that level until 88 seconds, at which time it sharply decayed 78 psi and remained stable at a pressure of approximately 438 psia until OECO. At no time did the pressure exceed the ground test redline value of 555 psia, see Figure 5-4.

The F-1 turbopump has three shaft bearings. Each bearing is cooled during operation by fuel which is routed from the fuel pump discharge volute, through the bearing coolant valve which filters the fuel and reduces fuel pressure to the desired level and then through three jets, for each bearing, which direct the fuel onto the bearing surfaces.

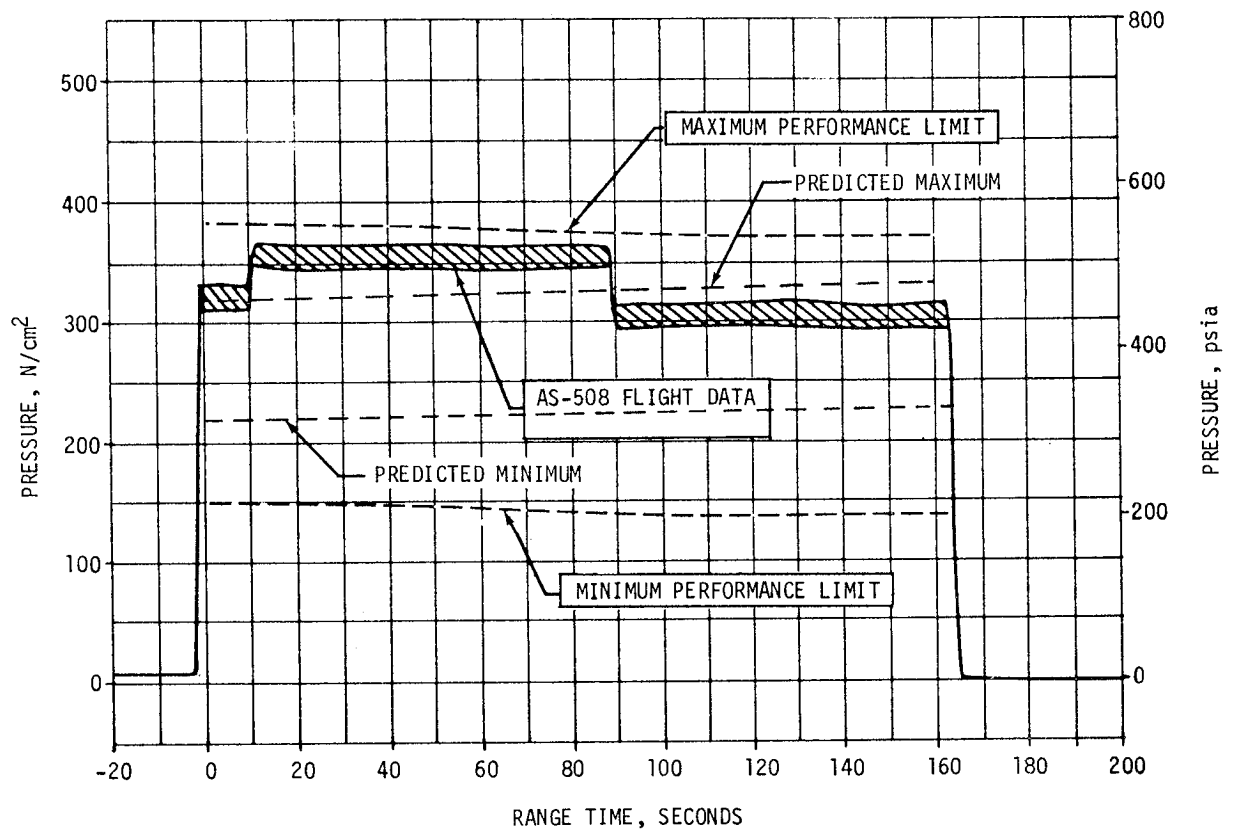


Figure 5-4. F-1 LOX Pump Bearing Jet Pressure, Engine No. 2

The bearing jet pressure changes, experienced by engine No. 2, were probably due to contaminant restrictions within the bearing jets. It is postulated that one of the nine jets was restricted prior to attaining the stabilized operating level, which would account for the initial level being higher than expected. At 10 seconds another jet could have become restricted, resulting in the pressure increase. At 88 seconds the initial restriction could have become dislodged resulting in a pressure decrease.

Similar turbopump bearing jet pressure changes have been experienced during single engine testing without any accompanying turbopump problems. Several turbopumps which experienced a pressure increase were disassembled prior to subsequent testing and disclosed no hardware damage; however, machining particle contamination of the jet assembly was found. Consequently, an improved manufacturing cleaning procedure was instituted. No similar jet pressure increases have occurred since incorporation of this cleaning procedure. The only remaining flight engines not incorporating the improved cleaning procedure are engine S/N F2059 installed in stage S-IC-11, and engine S/N F2061 installed in stage S-IC-9. Engines S/N F2059 and S/N F2061 acceptance and stage test data indicated normal turbopump bearing jet pressure characteristics.

The turbopump bearing coolant system incorporates redundancy by having three jets for each bearing. Furthermore, machine particle contamination, as previously noted, is usually associated with the number two bearing which receives additional coolant fluid from the number one bearing drainage. The occurrence of a bearing jet pressure discrepancy during flight, similar to that experienced by engine S/N F2058 during the AS-508 flight, is not considered detrimental to F-1 engine turbopump reliability.

#### 5.4 S-IC ENGINE SHUTDOWN TRANSIENT PERFORMANCE

Center engine cutoff, initiated by a signal from the IU, was at 135.18 seconds as planned. Outboard engine cutoff, initiated by LOX low level sensors, occurred at 163.60 seconds which was 0.40 second earlier than predicted. This is a small difference compared to the predicted 3-sigma limits of +5.58, -3.89 seconds.

Thrust decay of the F-1 engines was normal.

#### 5.5 S-IC STAGE PROPELLANT MANAGEMENT

Outboard engine cutoff was initiated by the LOX low level sensors as planned, and resulted in residual propellants being very close to the predicted values. The residual LOX at OECO was 38,921 lbm compared to the predicted value of 39,403 lbm. The fuel residual at OECO was 27,573 lbm compared to the predicted value of 31,957 lbm. A summary of the propellants remaining at major event times is presented in Table 5-2.

Table 5-2. S-IC Stage Propellant Mass History

EVENT	PREDICTED, LBM		LEVEL SENSOR DATA, LBM		RECONSTRUCTED, LBM	
	LOX	FUEL	LOX	FUEL	LOX	FUEL
Ignition Command	3,306,503	1,434,963	-	1,431,365	3,304,734	1,431,384
Holddown Arm Release	3,240,439	1,416,385	3,233,269	1,412,475	3,236,952	1,412,322
CECO	509,112	234,432	496,929	226,836	502,675	226,924
OECO	39,403	31,957	42,808	27,681	38,921	27,573
Separation	34,633	29,582	-	-	33,854	25,098
Zero Thrust	34,144	29,007	-	-	33,457	24,453

NOTE: Predicted and reconstructed values do not include pressurization gas so they will compare with level sensor data.

## 5.6 S-IC PRESSURIZATION SYSTEMS

### 5.6.1 S-IC Fuel Pressurization System

The fuel tank pressurization system performed satisfactorily. The low flow prepressurization system was commanded on at -97 seconds. High flow pressurization, accomplished by the onboard pressurization system, performed as expected. Helium flow control valve No. 1 was commanded on at -2.7 seconds and was supplemented by the high flow prepressurization system until umbilical disconnect.

Fuel tank ullage pressure was within the predicted limits throughout flight, as shown in Figure 5-5. Helium flow control valves No. 2, 3, and 4 were commanded open during flight by the switch selector, within acceptable limits. Helium bottle pressure was 3000 psia at -2.8 seconds and decayed to 520 psia at OECO. Total helium flowrate and heat exchanger performance were as expected.

Fuel pump inlet pressure was maintained above the required minimum Net Positive Suction Pressure (NPSP) during flight.

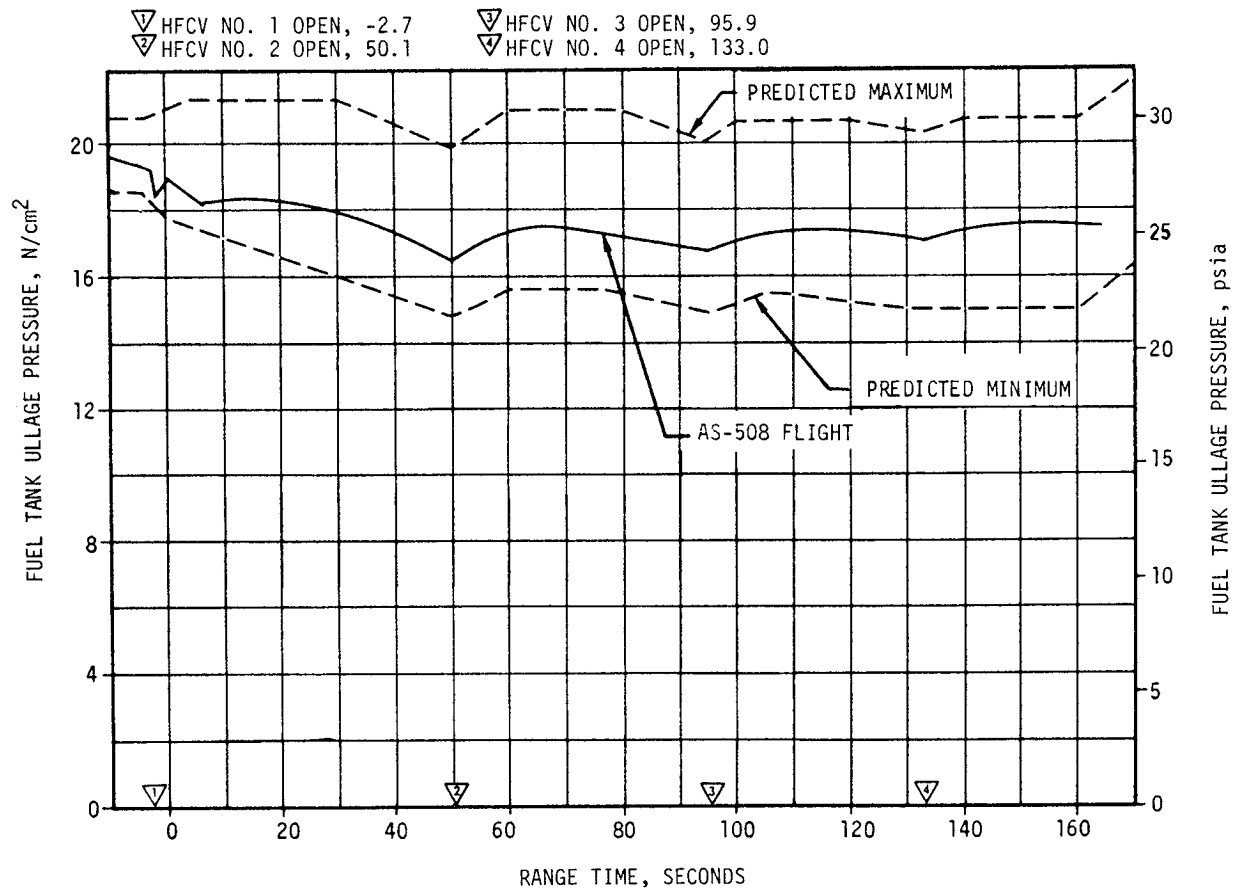


Figure 5-5. S-IC Stage Fuel Ullage Pressure

### 5.6.2 S-IC LOX Pressurization System

The LOX pressurization system performed satisfactorily and all performance requirements were met. The ground prepressurization system maintained ullage pressure within acceptable limits until launch commit. The onboard pressurization system subsequently maintained ullage pressure within the GOX Flow Control Valve (GFCV) band during flight. The prepressurization system was initiated at -72 seconds. Ullage pressure increased to the prepressurization switch band and flow was terminated at -57 seconds. The low flow system was cycled on two additional times at -37 and -11 seconds. At -4.7 seconds the high flow system was commanded on and maintained ullage pressure within acceptable limits until launch commit.

The LOX tank ullage pressure during flight, as shown in Figure 5-6, was maintained within the required limits throughout flight by the GFCV. The maximum GOX flowrate to the tank, at CECO, was 55.6 lbm/s. The heat exchangers performed as expected.

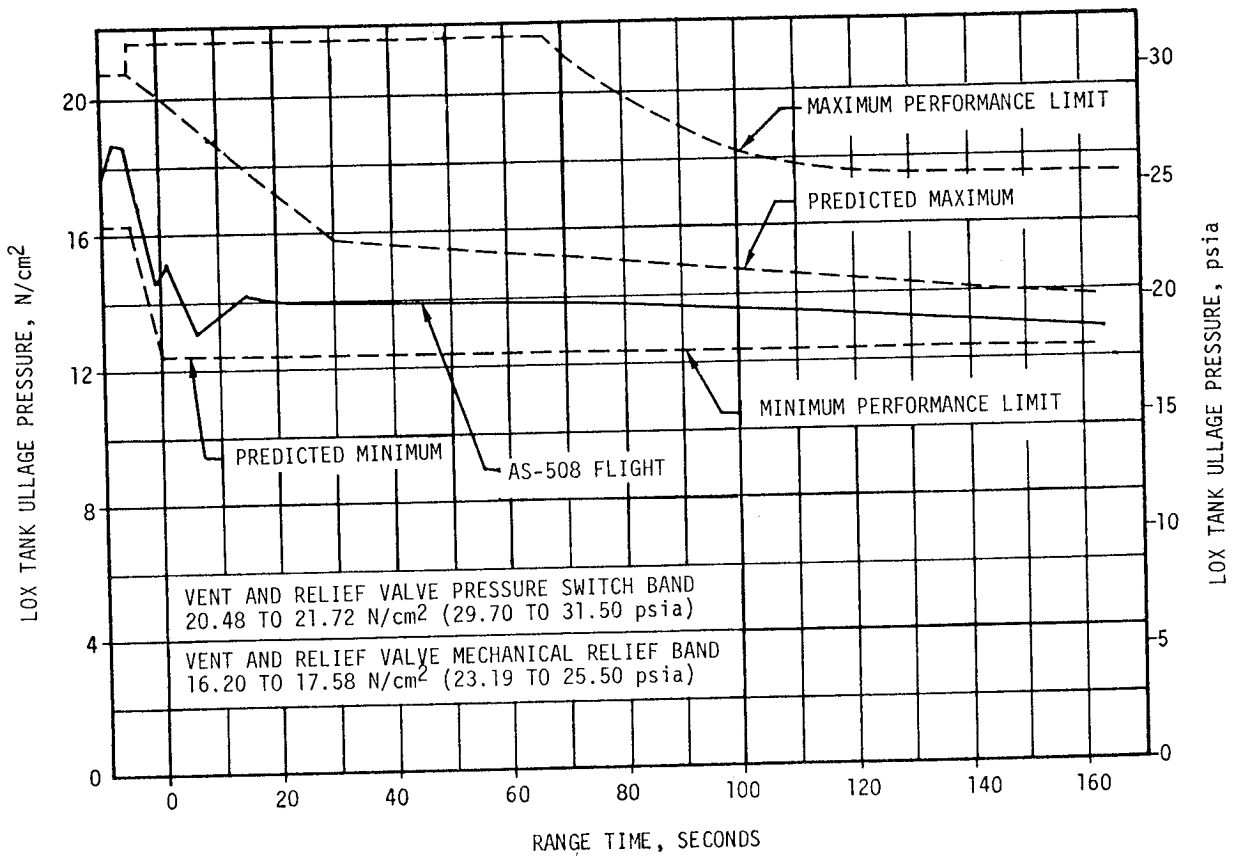


Figure 5-6. S-IC Stage LOX Tank Ullage Pressure

During the prelaunch activities the LOX tank vent and relief valve stuck in the open position for about 41 minutes beginning at -2 hours and 5 minutes. The valve closed at -1 hour and 24 minutes and no further problem occurred during the remainder of the countdown or during flight. See paragraph 3.4.2 for additional details.

LOX pump inlet pressure was maintained above the required minimum NPSP during flight.

#### 5.7 S-IC PNEUMATIC CONTROL PRESSURE SYSTEM

The control pressure system functioned satisfactorily throughout S-IC flight.

Sphere pressure was 2997 psia at liftoff and remained steady until CECO when it decreased to 2845 psia. The decrease was due to actuation of the center engine prevalves. There was a further decrease to 2445 psia after OECO. The engine prevalves were closed after engine cutoff as required.

#### 5.8 S-IC PURGE SYSTEMS

Performance of the S-IC purge systems was satisfactory during flight.

The turbopump LOX seal purge storage sphere pressure was within the limits of 2700 to 3300 psia until ignition, and 3300 to 1000 psia from liftoff to OECO.

#### 5.9 S-IC POGO SUPPRESSION SYSTEM

The POGO suppression system performed satisfactorily during S-IC flight.

Outboard LOX prevalve temperature measurements indicated that the prevalve cavities were filled with helium prior to liftoff as planned. The measurements in the outboard prevalves went cold momentarily at liftoff, indicating LOX sloshed on the probes. They remained warm throughout flight, indicating helium in the prevalves. At cutoff, the increased pressure forced LOX into the prevalves once more. The two measurements in the center engine prevalve indicated cold, which meant LOX was in this valve as planned.

#### 5.10 S-IC HYDRAULIC SYSTEM

The performance of the S-IC hydraulic system was satisfactory. All servoactuator supply pressures were within required limits. The engine control system return pressures were within predicted limits, and the hydraulic control system valves operated as planned.

## SECTION 6

### S-II PROPULSION

#### 6.1 SUMMARY

Engine No. 5 cut off earlier than planned because of high amplitude oscillations in the propulsion/structural system; otherwise, the S-II propulsion system performance was satisfactory. The S-II Engine Start Command (ESC), as sensed at the engines, occurred at 165.0 seconds. Center Engine Cutoff (CECO) occurred at 330.65 seconds or 132.36 seconds earlier than planned. Outboard Engine Cutoff (OECO) occurred at 592.64 seconds or 34.53 seconds later than predicted.

Total stage thrust at the standard time slice (62 seconds after S-II ESC) was 0.19 percent below predicted. Total propellant flowrate, including pressurization flow, was 0.25 percent below predicted and stage specific impulse was 0.09 percent above predicted at the standard time slice. Stage propellant mixture ratio was 0.18 percent below predicted. Engine thrust buildup and cutoff transients were normal.

Low amplitude oscillations were observed on all engines during S-II boost prior to CECO. Net engine performance levels of outboard engines were not affected.

The propellant management system performance was satisfactory, except for sporadic wet indications of the overflow point sensors prior to launch. The system used open-loop control of the engine Propellant Utilization (PU) valves, similar to the AS-507 flight. The Instrument Unit (IU) command to shift Engine Mixture Ratio (EMR) from high to low was initiated upon attainment of a preprogrammed stage velocity increase as sensed by the Launch Vehicle Digital Computer (LVDC). Due mainly to early CECO the guidance sensed EMR shift occurred 32.2 seconds later than predicted.

S-II OECO, initiated by the LOX engine cutoff sensors, was achieved following a planned 1.5-second time delay. Residual propellant in the tanks at OECO signal was 6057 lbm, compared to the prediction of 6026 lbm.

The performance of the LOX and LH<sub>2</sub> tank pressurization systems was within predicted limits. Ullage pressure in both tanks was more than adequate to meet established engine inlet propellant requirements throughout mainstage. As commanded by the IU, step pressurization occurred at 263.6 seconds for the LOX tank and 463.6 seconds for the LH<sub>2</sub> tank.

The engine servicing, recirculation, helium injection and valve actuation systems all performed satisfactorily.

S-II hydraulic system performance was normal throughout the flight.

## 6.2 S-II CHILLDOWN AND BUILDUP TRANSIENT PERFORMANCE

The engine servicing operations required to condition the engines prior to engine start were satisfactorily accomplished. Thrust chamber temperatures were within predicted limits at both prelaunch and engine start. Thrust chamber chilldown requirements are -200°F maximum at prelaunch commit and -150°F maximum at engine start. Thrust chamber temperatures ranged between -296 and -274°F at prelaunch commit and between -240 and -212°F at engine start. Thrust chamber temperature warmup rates during S-IC boost agreed closely with those experienced on previous flights.

Both temperature and pressure conditions of the J-2 engine start tanks were within the required prelaunch and engine start boxes as shown in Figure 6-1.

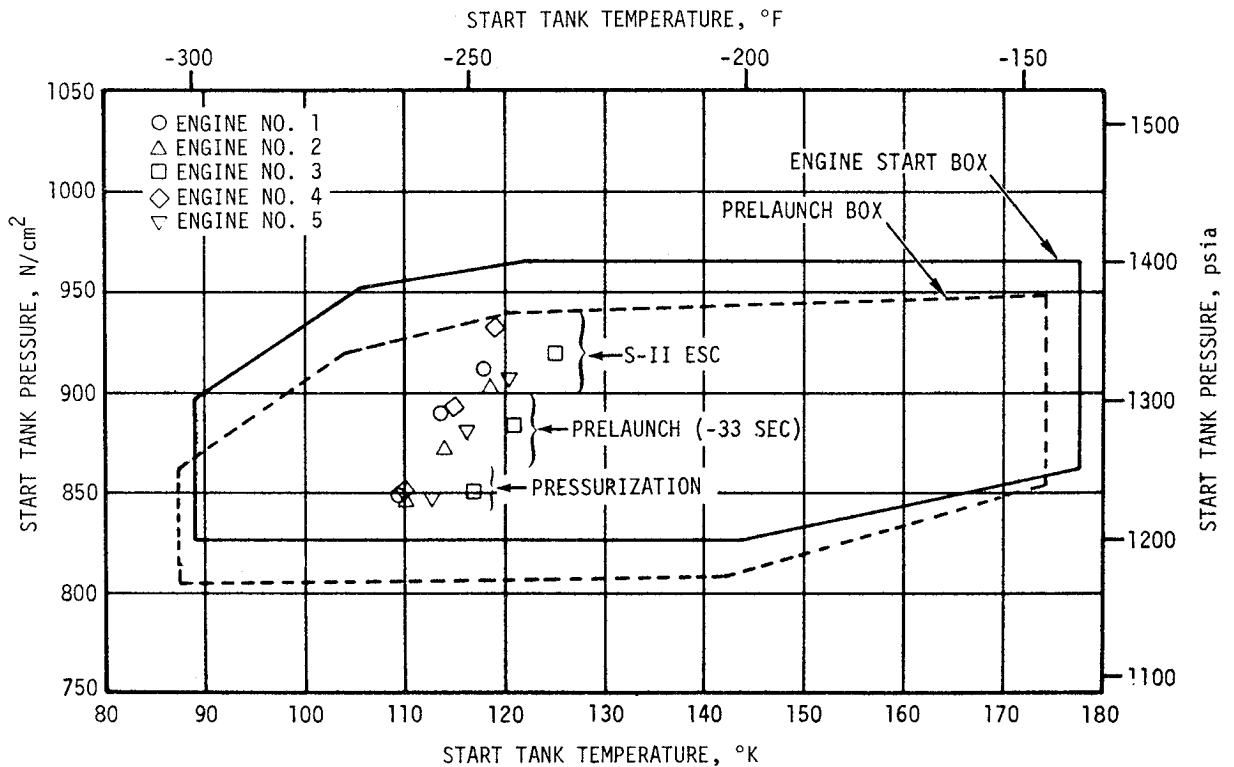


Figure 6-1. S-II Engine Start Tank Performance

Start tank temperatures at the conclusion of chilldown were approximately 18°F colder than on AS-507. This performance resulted from operating the A7-71 Heat Exchanger Unit, with all ullage vents open continuously, from the initiation of start tank chilldown at -22 minutes. The start tank system performance was entirely satisfactory.

Prelaunch and S-IC boost start tank temperature and pressure heat-up rates were normal and within the spread reported for AS-507. No indications of start tank relief valve operation were noted.

All engine helium tank pressures were within the prelaunch and engine start limits of 2800 to 3450 psia. Engine helium tank pressures ranged between 3190 and 3075 psia prior to launch (at -19 seconds) and between 3300 and 3175 psia at S-II ESC.

The LOX and LH<sub>2</sub> recirculation systems used to chill the feed ducts, turbo-pumps, and other engine components performed satisfactorily during prelaunch and S-IC boost. Engine pump inlet temperatures and pressures at engine start were well within the requirements as shown in Figure 6-2. The LOX pump discharge temperatures at S-II ESC were approximately 16.5°F subcooled, well below the 3°F subcooling requirement.

Prepressurization of the propellant tanks was accomplished satisfactorily. Ullage pressures at S-II ESC were 39.3 psia for LOX and 28.0 psia for LH<sub>2</sub>.

S-II ESC was received at 165.0 seconds and the Start Tank Discharge Valve (STDV) solenoid activation signal occurred 1.0 second later. The engine thrust buildup was satisfactory and within the required thrust buildup envelope. All engines reached their mainstage levels (pressure switch pickup) within 2.8 seconds after S-II ESC.

### 6.3 S-II MAINSTAGE PERFORMANCE

The propulsion reconstruction analysis showed that stage performance, during mainstage operation, was satisfactory except that engine No. 5 was shut down prematurely because of high amplitude, low frequency oscillations in propulsion and structural systems. These oscillations occurred in the frequency range of 14 to 16 hertz. Thrust chamber pressure oscillations reached an amplitude of approximately ±236 psi. High amplitude oscillations in the LOX feed system activated the thrust OK pressure switches and in turn initiated engine cutoff. Indications are that the oscillations caused no engine damage. See paragraph 8.2.3 for more detail.

A comparison of predicted and reconstructed performance of thrust, specific impulse, total flowrate, and mixture ratio versus time is shown in Figure 6-3. Stage performance during the high EMR portion of flight (prior to CECO) was very close to predicted. At the time slice of ESC +62 seconds, total stage thrust was 1,160,765 lbf which is 2184 lbf (0.19 percent) below the preflight prediction. Total propellant flowrate,

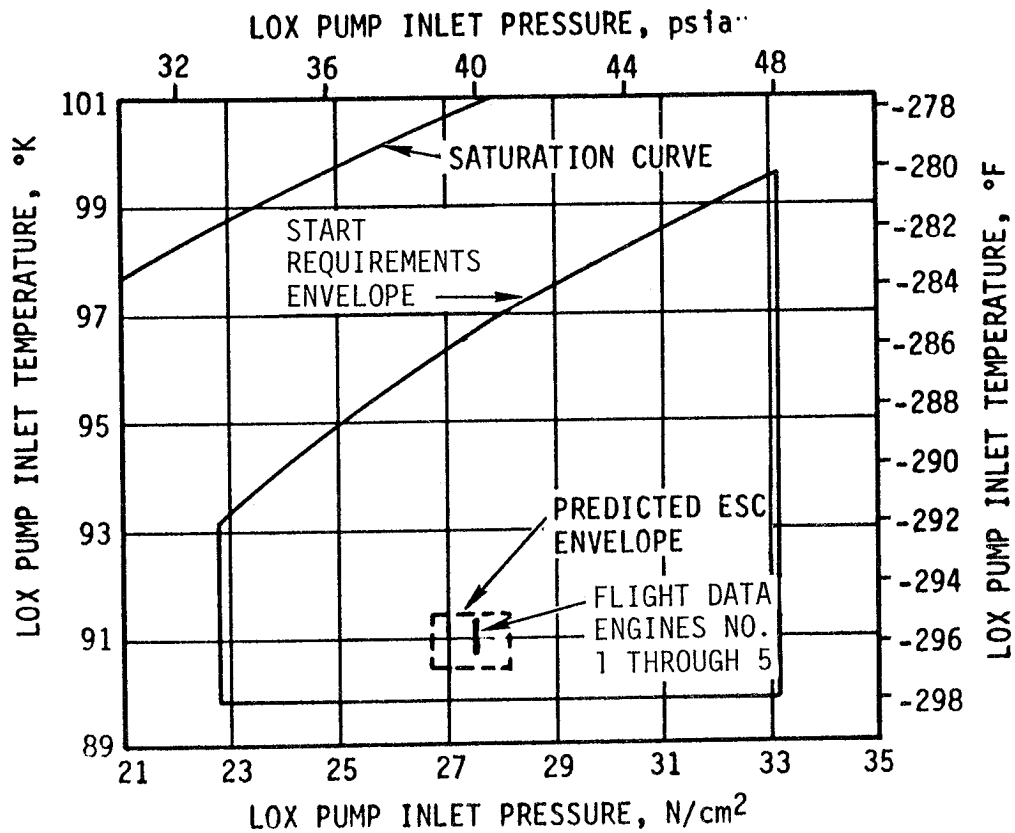
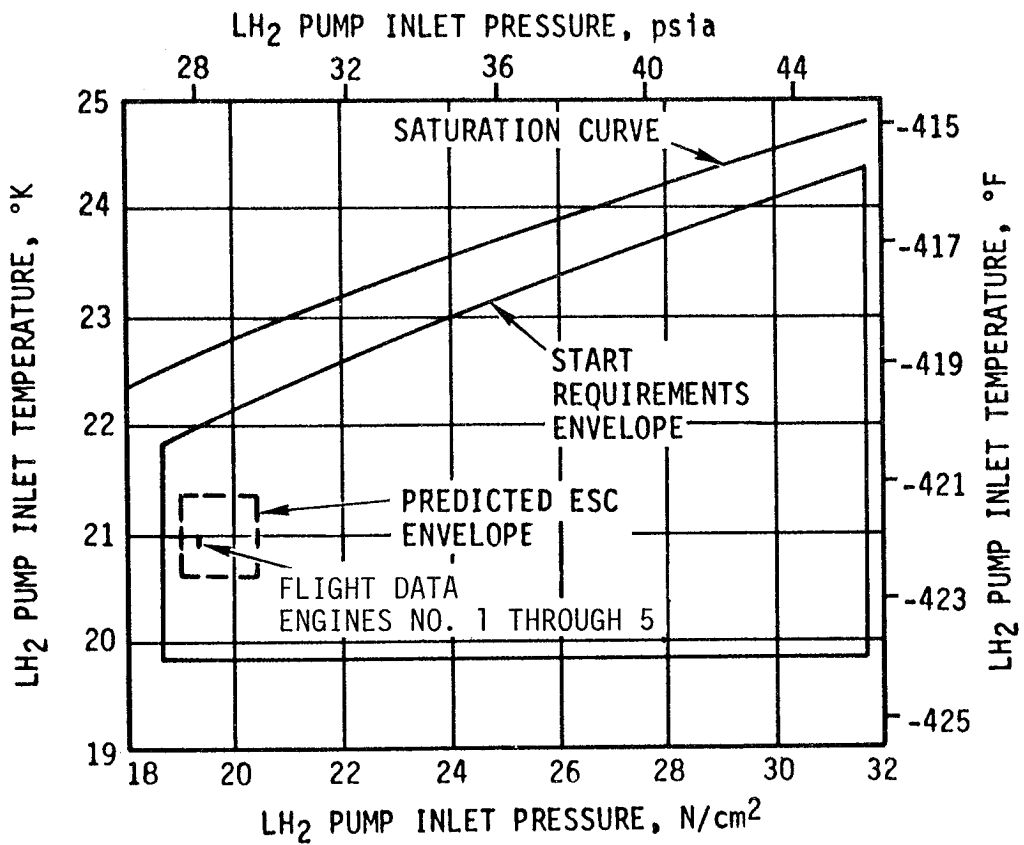


Figure 6-2. S-II Engine Pump Inlet Start Requirements

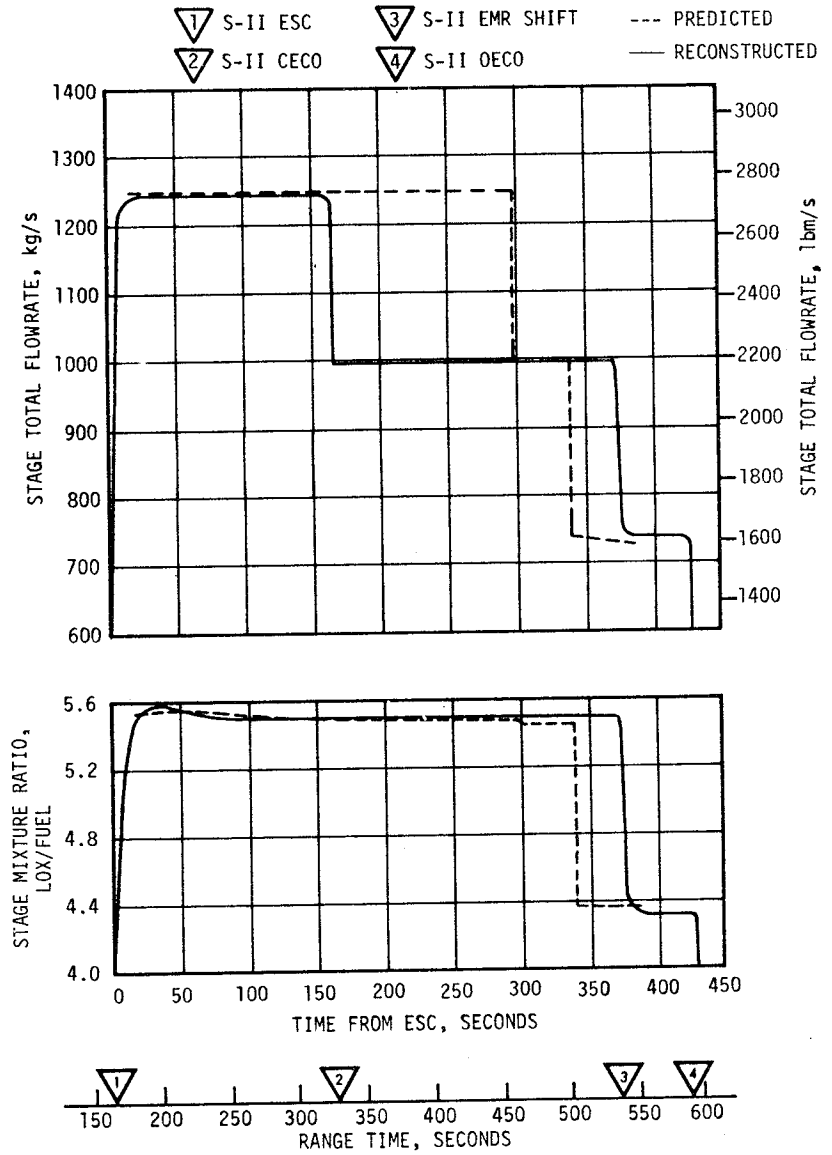
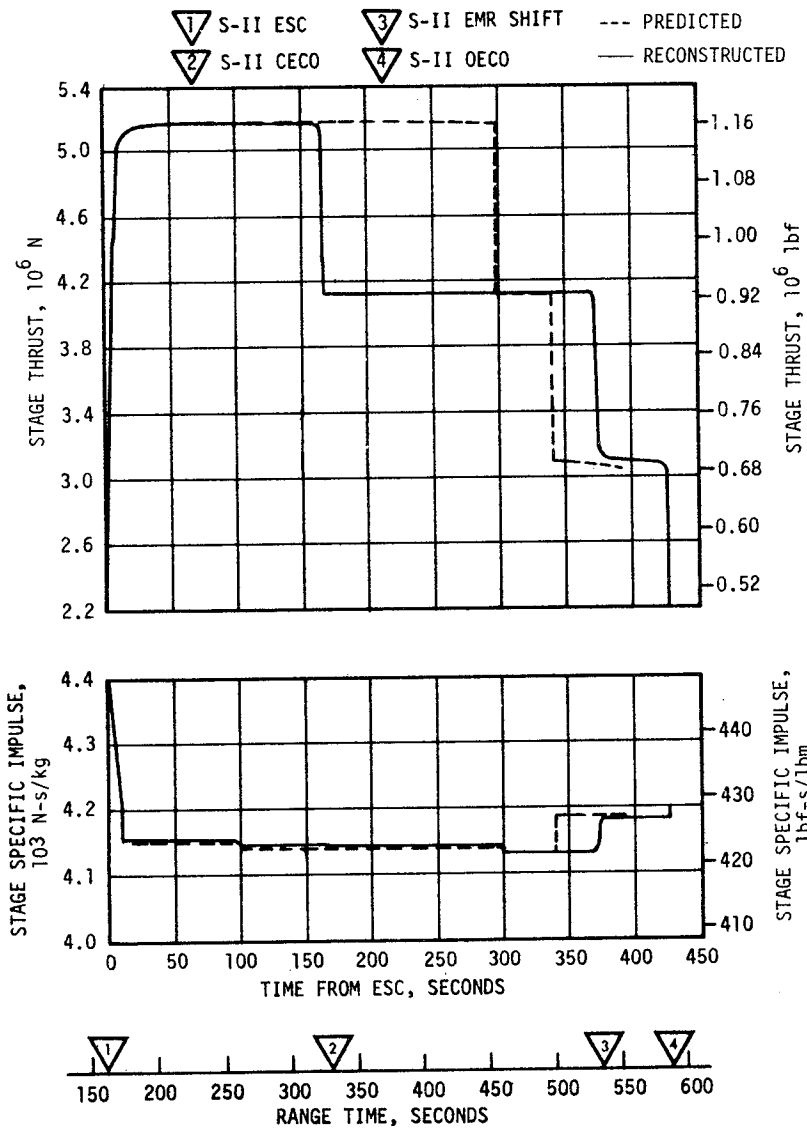


Figure 6-3. S-II Steady State Operation

including pressurization flow, was 2740.6 lbf/s; 0.25 percent below predicted. Stage specific impulse, including the effect of pressurization gas flowrate, was 423.5 lbf-s/lbf; 0.09 percent above predicted. Stage propellant MR was 0.18 percent below predicted.

At ESC +165.6 seconds, 132.4 seconds earlier than planned, the center engine was shut down by thrust OK pressure switch dropout. This action reduced total stage thrust by 233,917 lbf to a level of 924,762 lbf. The EMR shift from high to low occurred 372.5 seconds after ESC; 33.7 seconds later than predicted. The change of EMR resulted in further stage thrust reduction and at ESC +421.6 seconds the total vehicle thrust was 689,491 lbf; thus, a decrease in thrust of 235,271 lbf was indicated between high and low EMR operation. S-II burn duration was 427.64 seconds, which was 34.93 seconds longer than predicted, due primarily to early CECO.

Individual J-2 engine data, excluding the effects of pressurization flowrate, are presented in Table 6-1 for the ESC +62-second time slice. Good correlation between predicted and reconstructed flight performance is indicated by the small deviations.

The performance levels shown in Table 6-1 have not been adjusted to standard J-2 altitude conditions and do not include the effects of pressurization flow. Considering data that have been adjusted to standard conditions, very little difference from the results shown in Table 6-1 has been observed. The adjusted data show all engine thrust levels to be within 0.81 percent of those achieved during stage acceptance test.

Typical minor engine performance shifts were observed during analysis of stage flight data. Available flight instrumentation does not permit a detailed investigation of the cause for each performance shift. However, the more familiar ones can be recognized by their characteristic effects on basic flight parameters (see Table 6-2).

#### 6.4 S-II SHUTDOWN TRANSIENT PERFORMANCE

S-II OECO was initiated by the stage LOX depletion cutoff system. The LOX depletion cutoff system again included a 1.5-second delay timer. As in previous flights (AS-504 and subs), this resulted in engine thrust decay (observed as a drop in thrust chamber pressure) prior to receipt of the cutoff signal. However, due to early CECO, the precutoff decay was greatly reduced as compared with AS-504 without CECO. Only engine No. 1 exhibited a significant thrust chamber pressure decay, decreasing 110 psi in the final 0.4 second before cutoff. All other outboard engine thrust chamber pressure decays were approximately 42 psi.

At S-II OECO signal (592.64 seconds), total stage thrust was down to 635,725 lbf. Stage thrust dropped to 3 percent of this level within 0.94 second. The stage cutoff impulse through the 3 percent thrust level was estimated to be 193,024 lbf-s.

Table 6-1. S-II Engine Performance

PARAMETER	ENGINE NUMBER	PREDICTED	RECONSTRUCTED	PERCENT INDIVIDUAL DEVIATION	PERCENT AVERAGE DEVIATION
Thrust, lbf	1	234,462	233,602	- 0.37	- 0.19
	2	232,817	232,956	0.06	
	3	234,034	233,060	- 0.42	
	4	230,056	230,216	0.07	
	5	231,580	230,933	- 0.28	
Specific Impulse, lbf-s/lbm	1	425.2	425.5	0.07	0.15
	2	424.9	425.9	0.24	
	3	424.6	425.0	0.09	
	4	423.5	424.1	0.14	
	5	424.5	425.4	0.21	
Engine Flowrate, lbm/s	1	551.4	549.0	- 0.44	- 0.34
	2	547.9	546.9	- 0.18	
	3	551.2	548.3	- 0.53	
	4	543.2	542.8	- 0.07	
	5	545.6	542.9	- 0.49	
Engine Mixture Ratio, LOX/Fuel	1	5.54	5.54	0.00	- 0.22
	2	5.64	5.64	0.00	
	3	5.58	5.55	- 0.54	
	4	5.56	5.57	0.18	
	5	5.53	5.49	- 0.72	
NOTE: Values do not include pressurization flow.					

Table 6-2. S-II Engine Performance Shifts

ENGINE NO.	PERFORMANCE SHIFT (MAGNITUDE AND TIME OF OCCURRENCE)	REMARKS
1	-2300 lbf in-run thrust shift at 255 seconds (ESC +90 seconds)	Shift in Gas Generator (GG) oxidizer system resistance.
4	+1500 lbf in-run thrust shift at 215 seconds (ESC +50 seconds)	Shift in GG oxidizer system resistance
5	-1600 lbf run-to-run shift in thrust from engine acceptance	Shift in GG oxidizer system resistance
All Outboard Engines	In-run low frequency thrust oscillations at ESC +164 seconds	During center engine high amplitude oscillations. (See paragraph 8.2.3 for more detail.)
NOTE: None of the shifts are considered to be unusual in either magnitude or cause.		

## 6.5 S-II STAGE PROPELLANT MANAGEMENT

The propellant management system performed satisfactorily during the propellant loading operation and during flight, except as noted below. The S-II stage employed an open-loop system utilizing fixed, open-loop commands from the IU rather than feedback signals from the tank mass sensing probes. Open-loop PU is also planned for all subsequent vehicles.

The launch facility Propellant Tanking Control System (PTCS) and the propellant management system properly controlled S-II loading and replenishment. However, during the prelaunch countdown, both LOX and LH<sub>2</sub> overflow point sensors sporadically indicated wet. An investigation of this problem is now in progress.

The open-loop PU system responded as expected during flight and no instabilities were noted. Open-loop PU system operation commenced when "High EMR select" was commanded at ESC +5.5 seconds, as planned. The PU valves then moved to the high EMR position, providing an average EMR of 5.50. The IU command to shift EMR from high to low was initiated at ESC +369.7 seconds (32.2 seconds later than predicted) upon attainment of a preprogrammed velocity increase as sensed by the LVDC. These deviations are attributed to the early CECO and to a smaller degree engine performance variations from predicted, and larger than predicted propellant loading of the upper stages. The IU command caused the PU valves to be driven to the low EMR position, providing an average EMR of 4.35 which was 0.02 less than predicted.

OECO was initiated by the LOX tank propellant depletion system (with a 1.5-second ECO time delay) 34.5 seconds later than predicted due to the previously mentioned deviations. The open-loop PU error at OECO was approximately +38 lbm LH<sub>2</sub> versus a 3-sigma tolerance of  $\pm 2500$  lbm LH<sub>2</sub>. Based on corrected PU system data, propellant residuals (mass in tanks and sump) at OECO were 1797 lbm LOX and 4260 lbm LH<sub>2</sub>.

Table 6-3 presents a comparison of propellant masses as measured by the PU probes and engine flowmeters. The best estimate propellant mass is based on integration of flowmeter data utilizing the propellant residuals as determined from PU system data corrected for nominal tank mismatch at OECO. Best estimates of propellant mass loaded correlate with the post-launch trajectory simulation within the accuracy of the measurements utilized. These mass values were 0.07 percent more than predicted for LOX and 0.13 percent more than predicted for LH<sub>2</sub>.

## 6.6 S-II PRESSURIZATION SYSTEM

### 6.6.1 S-II Fuel Pressurization System

LH<sub>2</sub> tank ullage pressure, actual and predicted, is presented in Figure 6-4 for autosequence, S-IC boost, and S-II boost. The LH<sub>2</sub> vent valves were closed at -96.2 seconds and the ullage volume pressurized to 35.3 psia

Table 6-3. S-II Propellant Mass History

EVENT	PREDICTED, LBM		PU SYSTEM ANALYSIS, LBM		ENGINE FLOWMETER INTEGRATION (BEST ESTIMATE), LBM	
	LOX	LH <sub>2</sub>	LOX	LH <sub>2</sub>	LOX	LH <sub>2</sub>
Ground Ignition	834,558	159,500	834,004	159,778	835,116	159,700
S-II ESC	834,558	159,486	832,068	158,905	835,116	159,700
S-II PU Valve Step	77,929	21,513	78,725	20,921	76,270	21,367
S-II OECO	1801	4225	1800	4263	1797	4260
S-II Residual After Thrust Decay	1555	4117	Data not usable	Data not usable	1643	4187

NOTE: Table is based on mass in tanks and sump only. Propellant trapped external to tanks and LOX sump is not included.

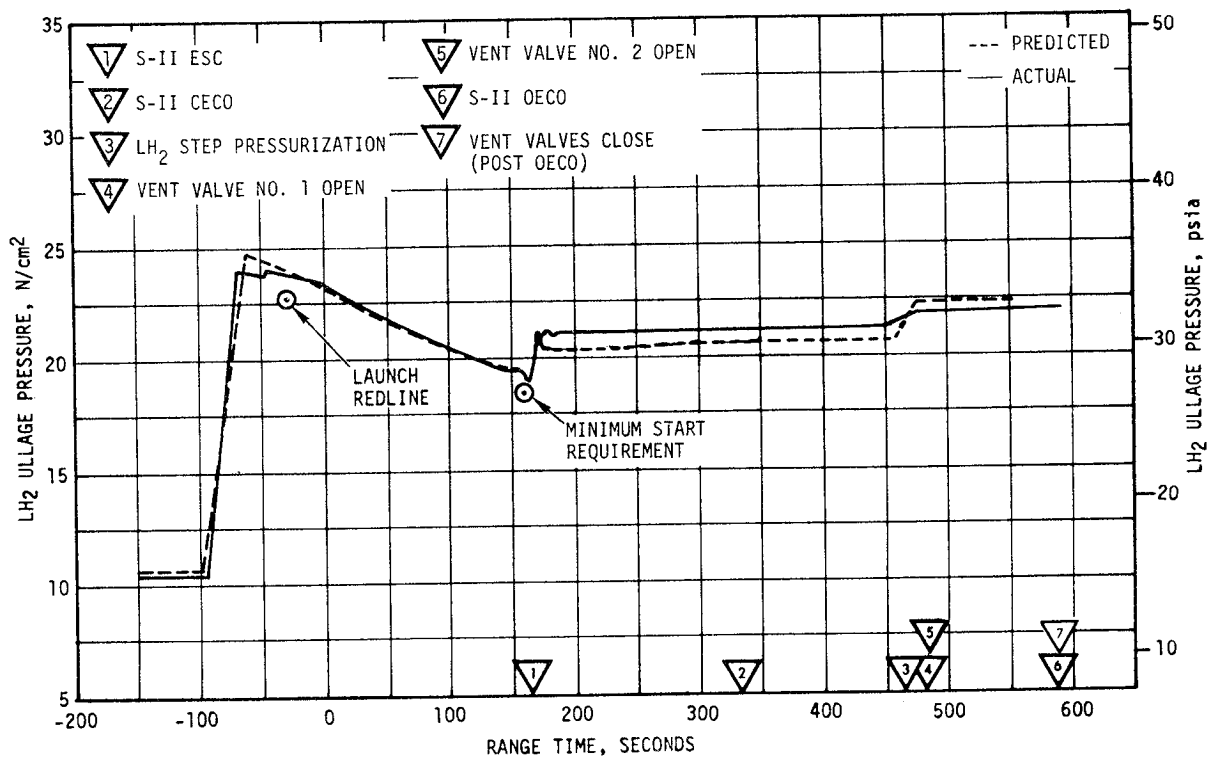


Figure 6-4. S-II Fuel Tank Ullage Pressure

in approximately 22.5 seconds. One make-up cycle was required at -41.1 seconds. The LH<sub>2</sub> tank vent valves opened during S-IC boost, limiting tank pressure; however, no main poppet operation was indicated. Differential pressure across the vent valve was kept below the low-mode upper limit of 29.5 psi. Ullage pressure at engine start was 28 psia exceeding the minimum engine start requirement of 27 psia. The LH<sub>2</sub> tank vent valves were switched to the high vent mode immediately prior to S-II engine start.

LH<sub>2</sub> tank ullage pressure remained slightly above its predicted value during S-II mainstage operation prior to step pressurization. The indicated ullage pressure was comparable to the pressure in this interval during S-II-8 static firing.

The LH<sub>2</sub> tank regulator was commanded open at 463.6 seconds and ullage pressure increased to 31.6 psia. The vent valves started to vent at 467.7 seconds and continued to vent throughout the remainder of the S-II burn. Ullage pressure remained within the high mode vent range of 30.5 to 33.0 psia.

Figure 6-5 shows LH<sub>2</sub> total inlet pressure, temperature and Net Positive Suction Pressure (NPSP) for the J-2 engines. The parameters were close to predicted values. The NPSP exceeded the minimum requirement throughout the S-II burn phase.

#### 6.6.2 S-II LOX Pressurization System

LOX tank ullage pressure, actual and predicted, is presented in Figure 6-6 for autosequence, S-IC boost, and S-II burn. After a 2 minute cold helium chilldown flow through the LOX tank, the vent valves were closed at -185.3 seconds and the LOX tank was prepressurized to the pressure switch setting of 38.3 psia in approximately 32.5 seconds. At approximately -78 seconds, the pressure increased to 39 psia because of the LH<sub>2</sub> tank prepressurization. LOX ullage pressure was 39.3 psia at engine start.

After the ullage pressure recovered from the initial drop at engine start, the pressure was controlled within the LOX pressure regulator range of 36 to 38.5 psia until step pressurization. Step pressurization increased the ullage pressure to 38.2 psia. This was slightly lower than predicted as discussed in paragraph 8.2.3. In addition the LOX tank ullage pressure experienced a slump of 0.4 psi just after step pressurization. Review of S-II-8 static firing ullage pressure data also shows a slight slump of about 0.15 psi after step pressurization. This pressure slump was the result of the interaction of colder heat exchanger outlet temperature, smaller ullage volume and a slight variation in regulator response compared to previous flights.

1 S-II ESC

3 LH<sub>2</sub> STEP PRESSURIZATION

2 S-II CECO

4 S-II OECO

----- PREDICTED

———— ACTUAL

— · — · — · MINIMUM NPSP REQUIREMENT

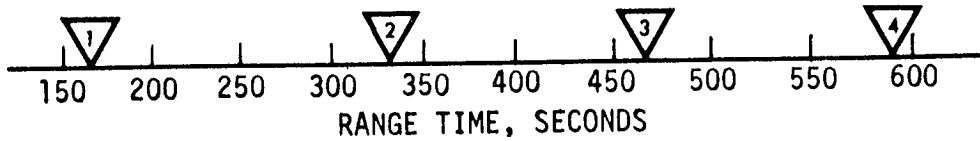
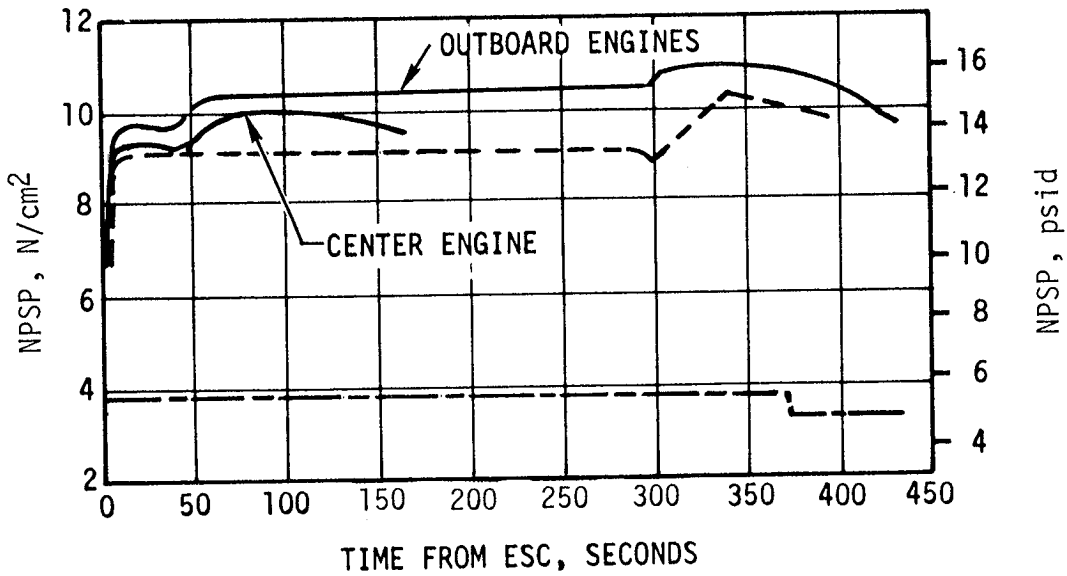
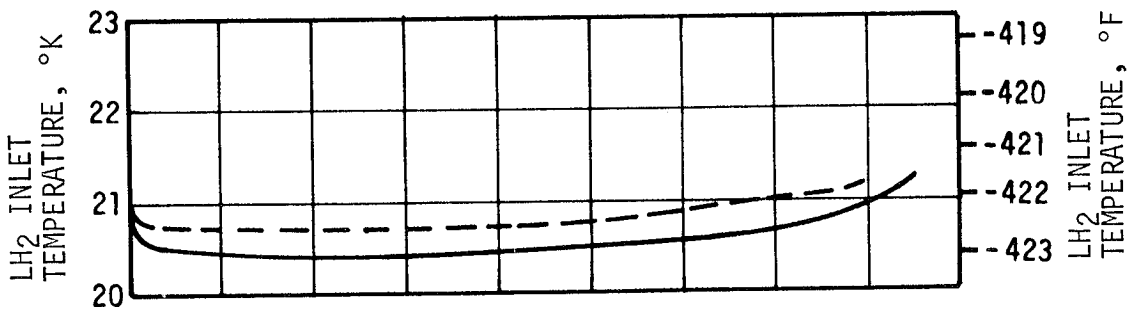
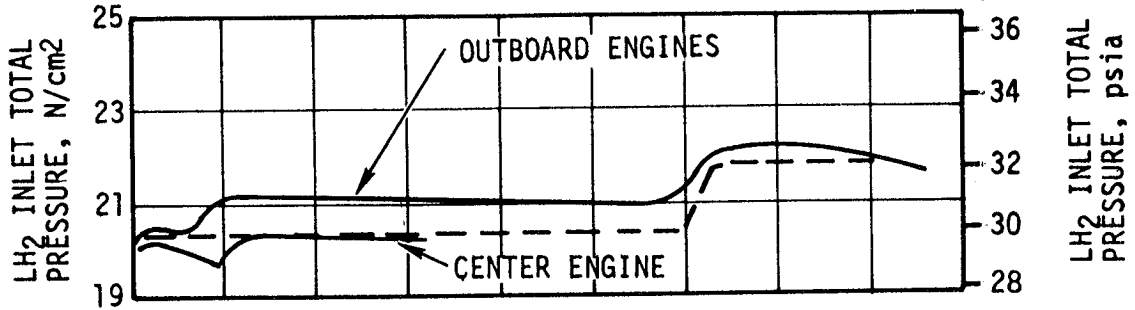


Figure 6-5. S-II Fuel Pump Inlet Conditions

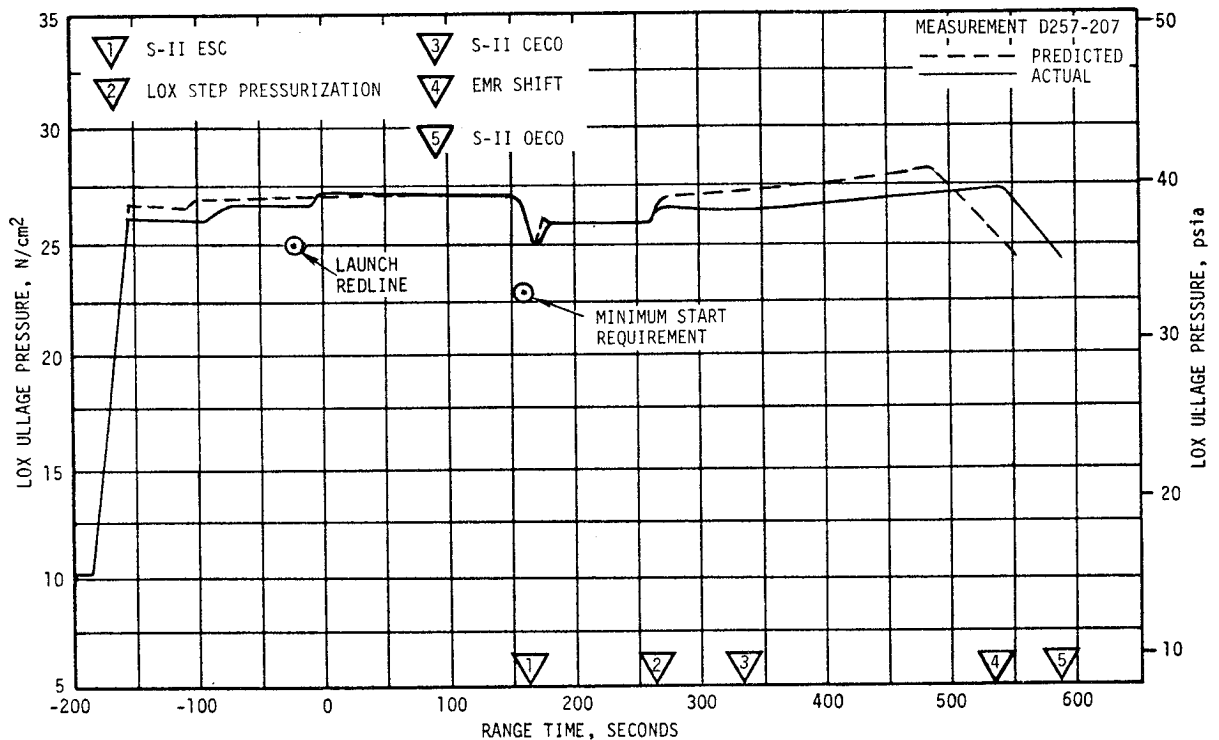


Figure 6-6. S-II LOX Tank Ullage Pressure

The ullage pressure recovered from the initial slump more slowly than it had during the S-II-8 static firing. The slow recovery of the ullage pressure is a result of early CECO. The heat transfer area within the LOX tank remains relatively constant after CECO but with only four engines supplying pressurant, instead of five, a slower ullage pressure buildup occurred.

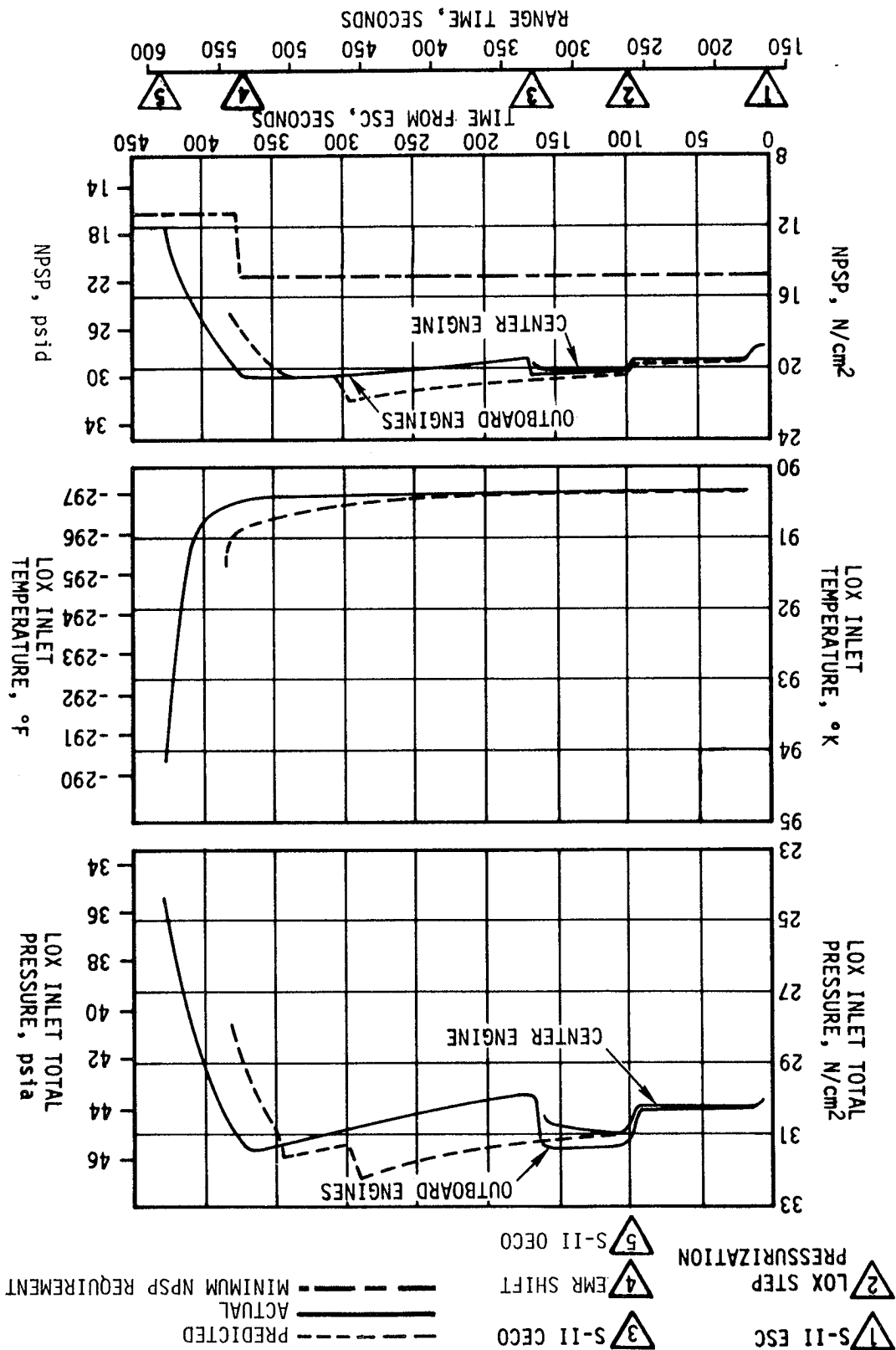
The ullage pressure reached a maximum of 39.7 psia at EMR shift. As a result of EMR shift, the pressure began to decrease and had reached 35.5 psia at OECO. No LOX tank venting was observed. LOX pump total inlet pressure, temperature and NPSP are presented in Figure 6-7.

#### 6.7 S-II PNEUMATIC CONTROL PRESSURE SYSTEM

The pneumatic control system functioned satisfactorily throughout the S-IC and S-II boost periods. Bottle pressure was 3030 psia at -30 seconds and due to normal valve activities during S-II burn, pressure decayed to approximately 2620 psia after S-II OECO.

Regulator outlet pressure during flight remained at a constant 715 psia, except for the expected momentary pressure drops when the recirculation or prevalues were actuated closed just after engine start, at CECO and OECO.

Figure 6-7. S-II LOX Pump Inlet Conditions



## 6.8 S-II HELIUM INJECTION SYSTEM

The performance of the helium injection system was satisfactory. Requirements were met and parameters were in agreement with predicted values. The supply bottle was pressurized to 3050 psia prior to liftoff and by ESC the pressure was 700 psia. Helium injection system average total flowrate during supply bottle blowdown (-30 to 163 seconds) was 72.5 SCFM.

## 6.9 S-II HYDRAULIC SYSTEM

S-II hydraulic system performance was normal throughout the flight. System supply and return pressures, reservoir volumes, and system fluid temperatures were within predicted ranges. Reservoir fluid temperatures were close to the predicted rate of increase. All servoactuators responded to commands with good precision.

Except for CECO-induced transients, forces acting on the actuators were well below a predicted maximum of 19,000 lbf. The maximum force in tension was 8450 lbf acting on the pitch actuator of engine No. 1. The maximum force in compression was 7150 lbf action on the pitch actuator of engine No. 2. All measurements showed the effects of the center engine oscillations and the resulting CECO. The greatest effect was noted on actuator differential pressure measurements where oscillating loads up to 20,800 lbf (0 to peak) were indicated. These loads were induced by the structural accelerations. There was no evidence of contribution to the oscillations in the actuator command data.

## SECTION 7

### S-IVB PROPULSION

#### 7.1 SUMMARY

The J-2 engine operated satisfactorily throughout the operational phase of first and second burn and had normal shutdowns. S-IVB first burntime was 152.9 seconds which was 9.3 seconds longer than predicted, primarily due to the performance of lower stages. The J-2 engine thrust performance, during first burn, differed by 0.29 percent from the predicted (Start Tank Discharge Valve [STDV] open +130 seconds) as determined from standard altitude reconstruction analysis. Specific impulse was near that predicted. The S-IVB stage first burn Engine Cutoff (ECO) was initiated by the Launch Vehicle Digital Computer (LVDC) at 749.83 seconds.

The Continuous Vent System (CVS) adequately regulated LH<sub>2</sub> tank ullage pressure at an average level of 19.3 psia during earth orbit, and the Oxygen/Hydrogen (O<sub>2</sub>/H<sub>2</sub>) burner satisfactorily achieved LH<sub>2</sub> and LOX tank repressurization for restart. Engine restart conditions were within specified limits. The restart with the Propellant Utilization (PU) valve fully open was successful.

S-IVB second burntime was 350.8 seconds which was 4.9 seconds less than predicted. The engine performance during second burn, as determined from the standard altitude reconstruction analysis, differed from the predicted (STDV +130 seconds) by -0.24 percent for thrust and 0.09 percent for specific impulse. Second burn ECO was initiated by the LVDC at 9697.17 seconds.

Subsequent to second burn, the stage propellant tanks and helium spheres were safed satisfactorily. Sufficient impulse was derived from LOX dump, LH<sub>2</sub> CVS operation and Auxiliary Propulsion System (APS) ullage burn to achieve a successful lunar impact. An additional velocity change of 7 to 10 ft/s was accumulated during the unanticipated APS firings at 70,150 seconds (19:29:10).

The S-IVB hydraulic system performance was satisfactory during its complete mission.

## 7.2 S-IVB CHILLDOWN AND BUILDUP TRANSIENT PERFORMANCE FOR FIRST BURN

The propellant recirculation systems performed satisfactorily, meeting start and run box requirements for fuel and LOX as shown in Figure 7-1. The thrust chamber temperature at launch was well below the maximum allowable redline limit of  $-130^{\circ}\text{F}$ . At S-IVB first burn Engine Start Command (ESC), the temperature was  $-151^{\circ}\text{F}$ , which was within the requirement of  $-189.6 \pm 110^{\circ}\text{F}$ .

The chilldown and loading of the engine Gaseous Hydrogen ( $\text{GH}_2$ ) start tank and pneumatic control sphere prior to liftoff was satisfactory. At first burn ESC the start tank conditions were within the required region of  $1325 \pm 75$  psia and  $-170 \pm 30^{\circ}\text{F}$  for start. The discharge was completed and the refill initiated at first burn ESC +3.8 seconds. The refill was satisfactory and in good agreement with the acceptance test.

The engine control bottle pressure and temperature at liftoff were 2964 psia and  $-173^{\circ}\text{F}$ .  $\text{LH}_2$  and LOX systems chilldown, which was continuous from before liftoff until just prior to first ESC, was satisfactory. At first ESC, the LOX pump inlet temperature was  $-295.5^{\circ}\text{F}$  and the  $\text{LH}_2$  pump inlet temperature was  $-421.8^{\circ}\text{F}$ .

The first burn start transient was satisfactory. The thrust buildup was within the limits set by the engine manufacturer. This buildup was similar to the thrust buildups observed on AS-506 and AS-507. The PU valve was in the null position prior to first start, but, as expected, shifted 0.6 degree during start. The total impulse from STDV open to STDV open +2.5 seconds was 189,441 lbf-s for first start.

First burn fuel lead followed the predicted pattern and resulted in satisfactory conditions as indicated by the thrust chamber temperatures and the associated fuel injector temperatures.

## 7.3 S-IVB MAINSTAGE PERFORMANCE FOR FIRST BURN

The propulsion reconstruction analysis showed that the stage performance during mainstage operation was satisfactory. A comparison of predicted and actual performance of thrust, specific impulse, total flowrate, and Engine Mixture Ratio (EMR) versus time is shown in Figure 7-2. Table 7-1 shows the specific impulse, flowrates and EMR deviations from the predicted at the STDV +130 second time slice.

The performance of the J-2 engine helium control system was satisfactory during mainstage operation. The engine control bottle was connected to the stage ambient repressurization bottles and therefore, there was little pressure decay. Helium usage was approximately 0.32 lbm during first burn.

The PU valve position shifted 0.6 degree during first burn and 0.5 degree during second burn. These shifts are approximately the same as those observed on previous flights.

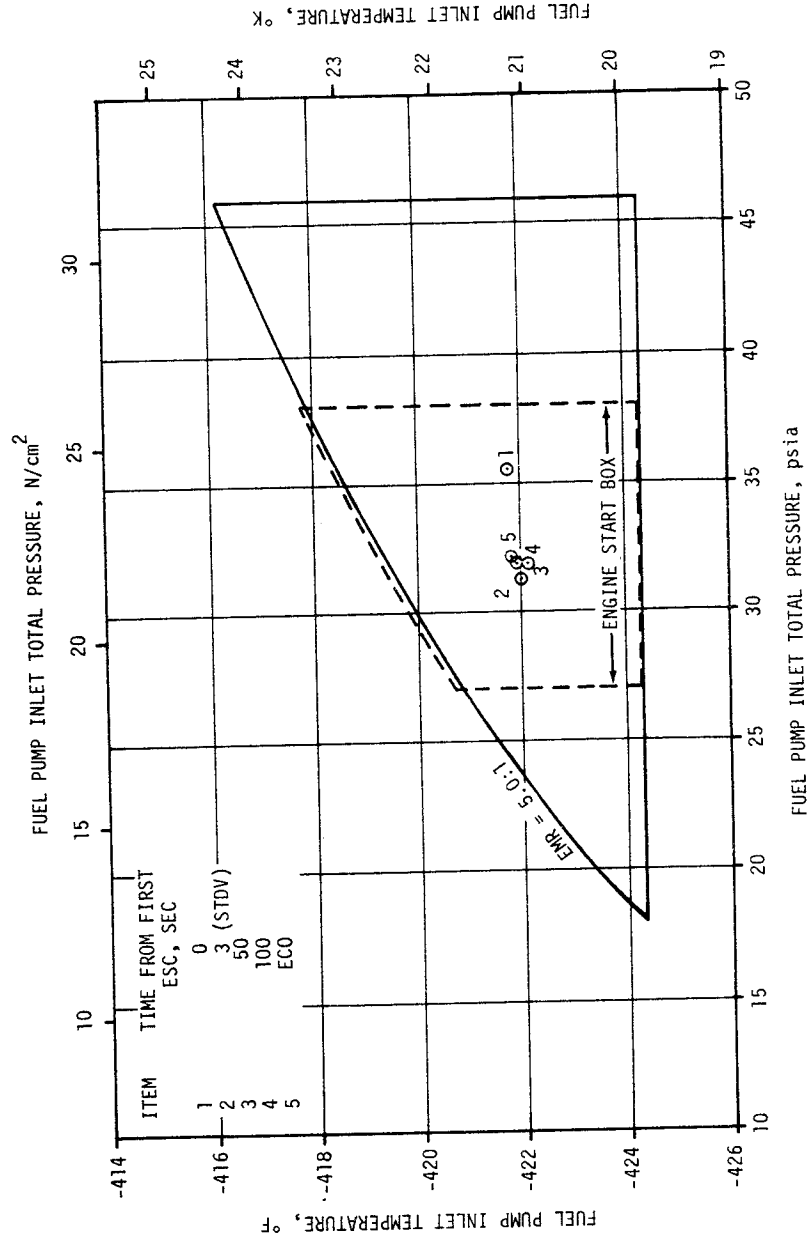
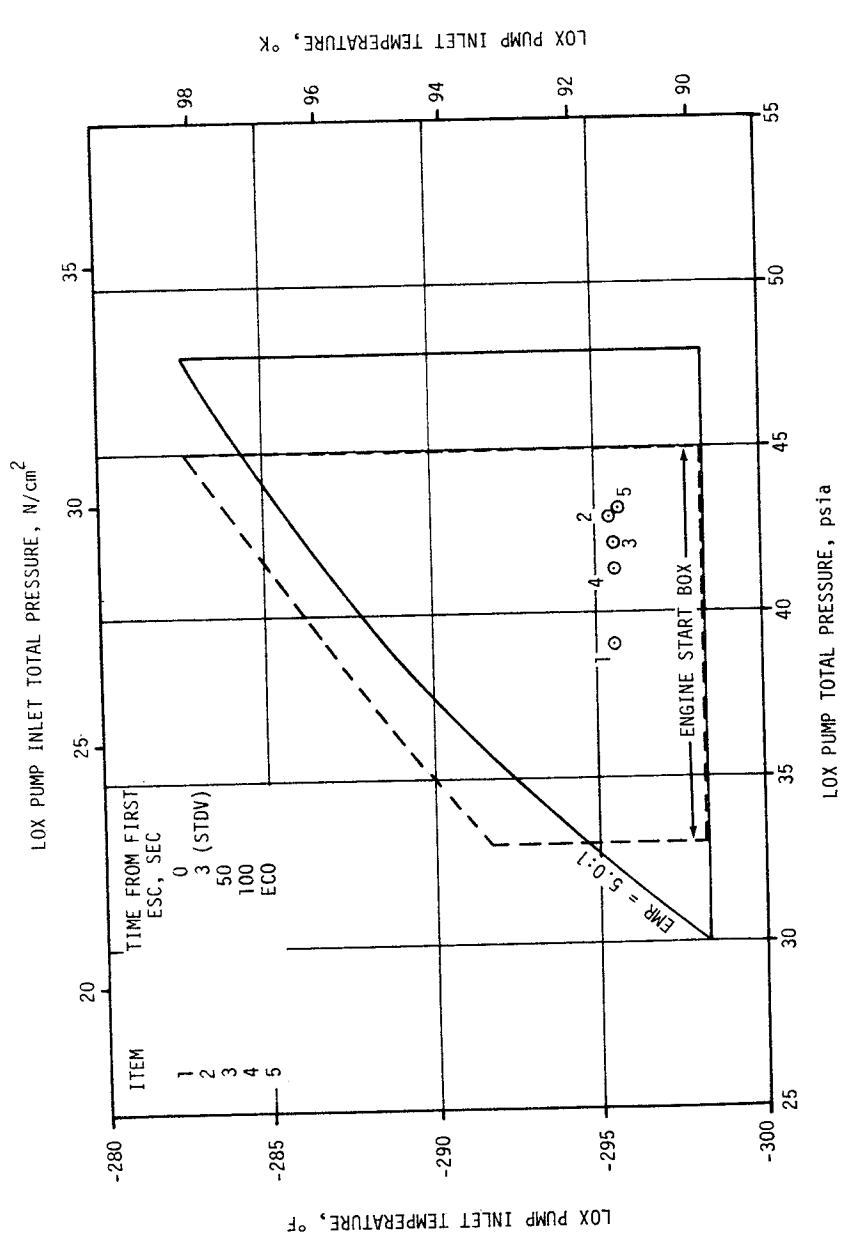


Figure 7-1. S-IVB Start Box and Run Requirements - First Burn

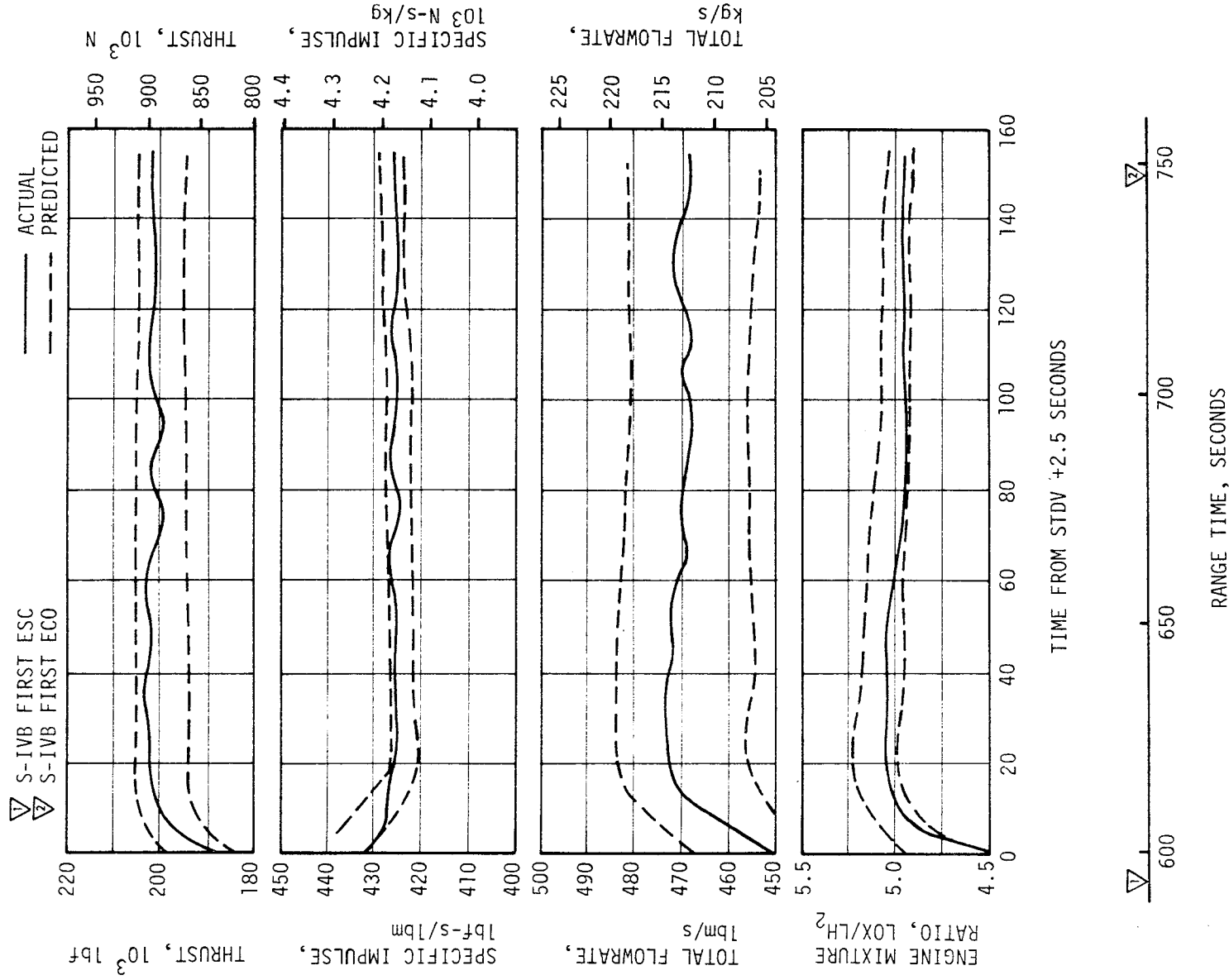


Figure 7-2. S-IVB Steady State Performance - First Burn

Table 7-1. S-IVB Steady State Performance - First Burn  
(STDV +130 Second Time Slice at Standard Altitude Conditions)

PARAMETER	PREDICTED	RECONSTRUCTION	FLIGHT DEVIATION	PERCENT DEVIATION FROM PREDICTED
Thrust, lbf	199,003	199,577	574	0.288
Specific Impulse, lbf-s/lbm	426.8	427.2	0.4	0.094
LOX Flowrate, lbm/s	387.65	388.07	0.42	0.108
Fuel Flowrate, lbm/s	78.58	79.05	0.47	0.598
Engine Mixture Ratio, LOX/Fuel	4.933	4.909	-0.024	-0.486

#### 7.4 S-IVB SHUTDOWN TRANSIENT PERFORMANCE FOR FIRST BURN

S-IVB first ECO was initiated at 749.83 seconds by a guidance velocity cutoff command which resulted in a burntime of 152.9 seconds. This was 9.3 seconds longer than predicted due to the performance of lower stages.

The ECO transient was satisfactory. The total cutoff impulse to zero percent of rated thrust was 44,319 lbf-s which was 3700 lbf-s less than predicted. Cutoff occurred with the PU valve in the null position.

#### 7.5 S-IVB PARKING ORBIT COAST PHASE CONDITIONING

The LH<sub>2</sub> CVS performed satisfactorily, maintaining the fuel tank ullage pressure at an average level of 19.3 psia. This was well within the 18 to 21 psia band of the new inflight specification.

The continuous vent regulator was activated at 809.0 seconds and was terminated at 8810.3 seconds. The CVS performance is shown in Figure 7-3. The thrust between 1000 and 1500 seconds was below predicted but is within allowable performance limits.

Calculations based on estimated temperatures indicate that the mass vented during parking orbit was 1880 lbm and that the boiloff mass was 2010 lbm.

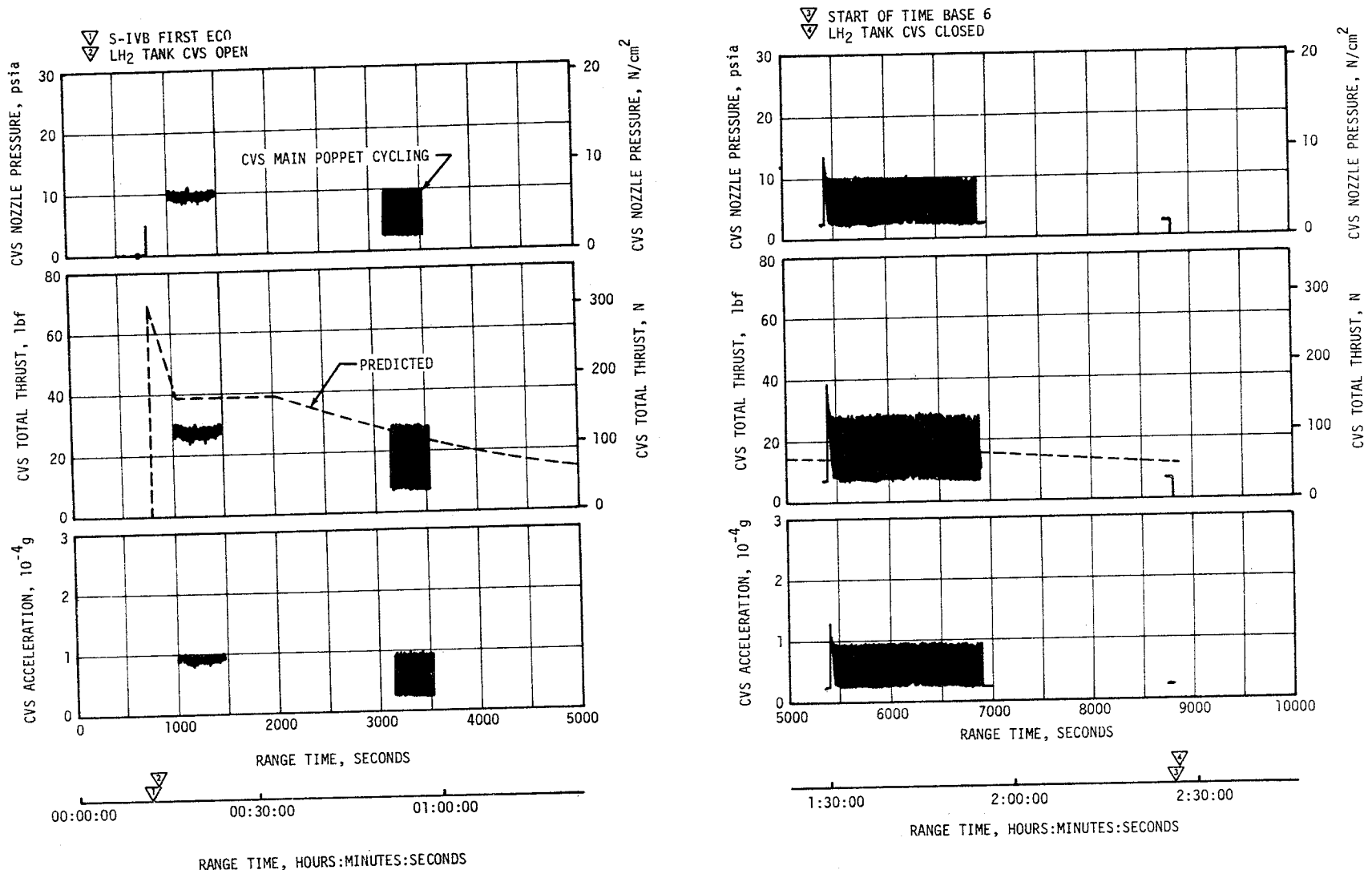


Figure 7-3. S-IVB CVS Performance - Coast Phase

## 7.6 S-IVB CHILLDOWN AND RESTART FOR SECOND BURN

Repressurization of the LOX and LH<sub>2</sub> tanks was satisfactorily accomplished by the O<sub>2</sub>/H<sub>2</sub> burner. Helium heater "ON" command was initiated at 8810.1 seconds. The LH<sub>2</sub> repressurization control valves were opened at helium heater "ON" +6.1 seconds and the fuel tank was repressurized from 19.5 to 30.4 psia in 190.7 seconds. There were 25.8 lbm of cold helium used to repressurize the LH<sub>2</sub> tank. The LOX repressurization control valves were opened at O<sub>2</sub>/H<sub>2</sub> burner "ON" +6.3 seconds and the LOX tank was repressurized from 38.5 to 40.0 psia in 65.2 seconds. There were 1.7 lbm of helium used to repressurize the LOX tank. LH<sub>2</sub> and LOX ullage pressures are shown in Figure 7-4. The burner continued to operate for a total of 454.8 seconds providing nominal propellant settling forces. The performance of the AS-508 O<sub>2</sub>/H<sub>2</sub> burner was satisfactory as shown in Figure 7-5.

The S-IVB LOX recirculation system satisfactorily provided conditioned oxidizer to the J-2 engine for restart. The LOX and fuel pump inlet conditions are plotted in the start and run boxes in Figure 7-6. At second ESC, the LOX and fuel pump inlet temperatures were -295.0°F and -418.6°F, respectively. Fuel recirculation temperature at ESC was slightly out of the start box. This condition has occurred on previous flights and a change to the second ESC requirement is under consideration. Fuel recirculation system performance was adequate and conditions at the pump inlet were satisfactory at second STDV open. Second burn fuel lead generally followed the predicted pattern and resulted in satisfactory conditions as indicated by thrust chamber temperature and the associated fuel injector temperature. The S-IVB-508 stage was the first stage to have a start tank helium recharge capability using the LOX ambient repressurization system (bottle No. 2). Since the start system performance was nominal during coast and restart, no helium recharge was required. The start tank performed satisfactorily during second burn blowdown and recharge sequence. The engine start tank was recharged properly and maintained sufficient pressure during coast. The engine control sphere first burn gas usage was as predicted; the ambient helium spheres recharged the control sphere to a nominal level for restart.

The second burn start transient was satisfactory. The thrust buildup was within the limits set by the engine manufacturer and was similar to the thrust buildup on AS-506 and AS-507. The PU valve was in the proper full open (4.5 EMR) position prior to the second start. The total impulse from STDV open to STDV open +2.5 seconds was 174,932 lbf-s.

The helium control system performed satisfactorily during second burn mainstage. There was little pressure decay during the burn due to the connection to the stage repressurization system. Approximately 1.09 lbm of helium was consumed during second burn.

## 7.7 S-IVB MAINSTAGE PERFORMANCE FOR SECOND BURN

The propulsion reconstruction analysis showed that the stage performance during mainstage operation was satisfactory. A comparison of predicted and actual performance of thrust, specific impulse, total flowrate, and EMR

- ▽ O<sub>2</sub>/H<sub>2</sub> BURNER ON
- ▽ LH<sub>2</sub> AND LOX CRYOGENIC REPRESS VALVES OPEN
- ▽ TERMINATION OF LOX TANK REPRESS
- ▽ TERMINATION OF LH<sub>2</sub> TANK REPRESS
- ▽ O<sub>2</sub>/H<sub>2</sub> BURNER OFF

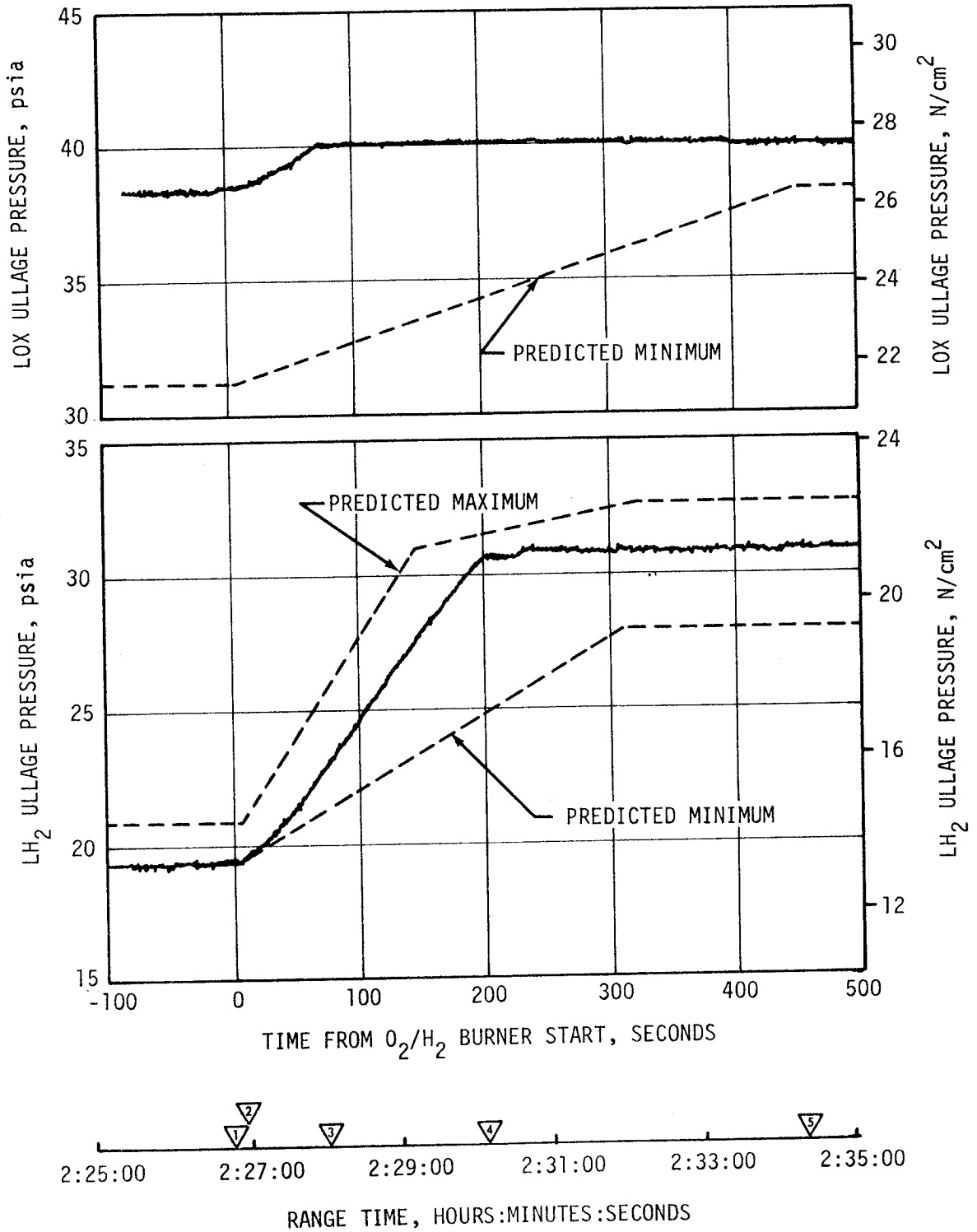
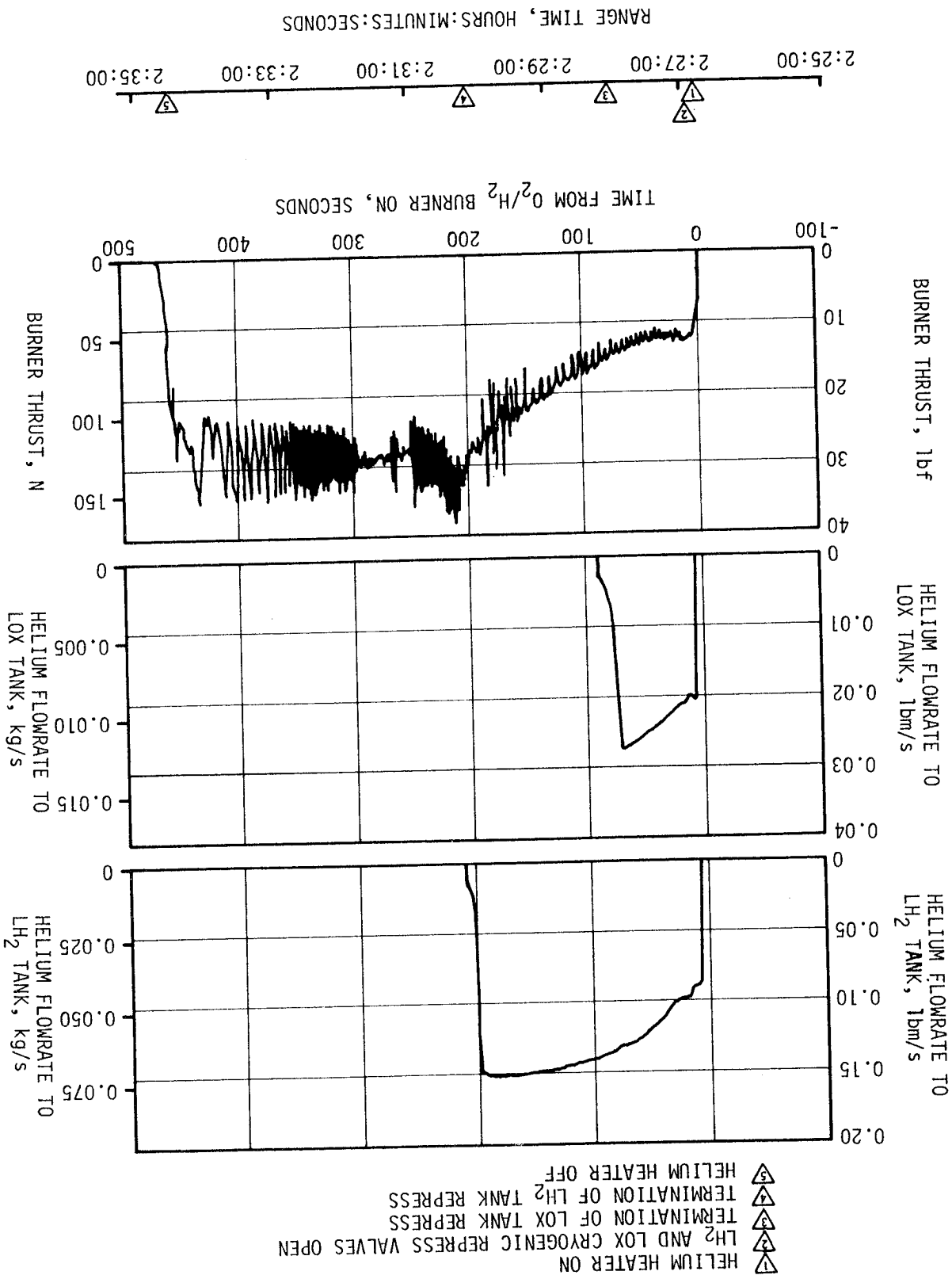


Figure 7-4. S-IVB Ullage Conditions During Repressurization Using O<sub>2</sub>/H<sub>2</sub> Burner

Figure 7-5. S-IVB O<sub>2</sub>/H<sub>2</sub> Burner Thrust and Pressurant Flowrates



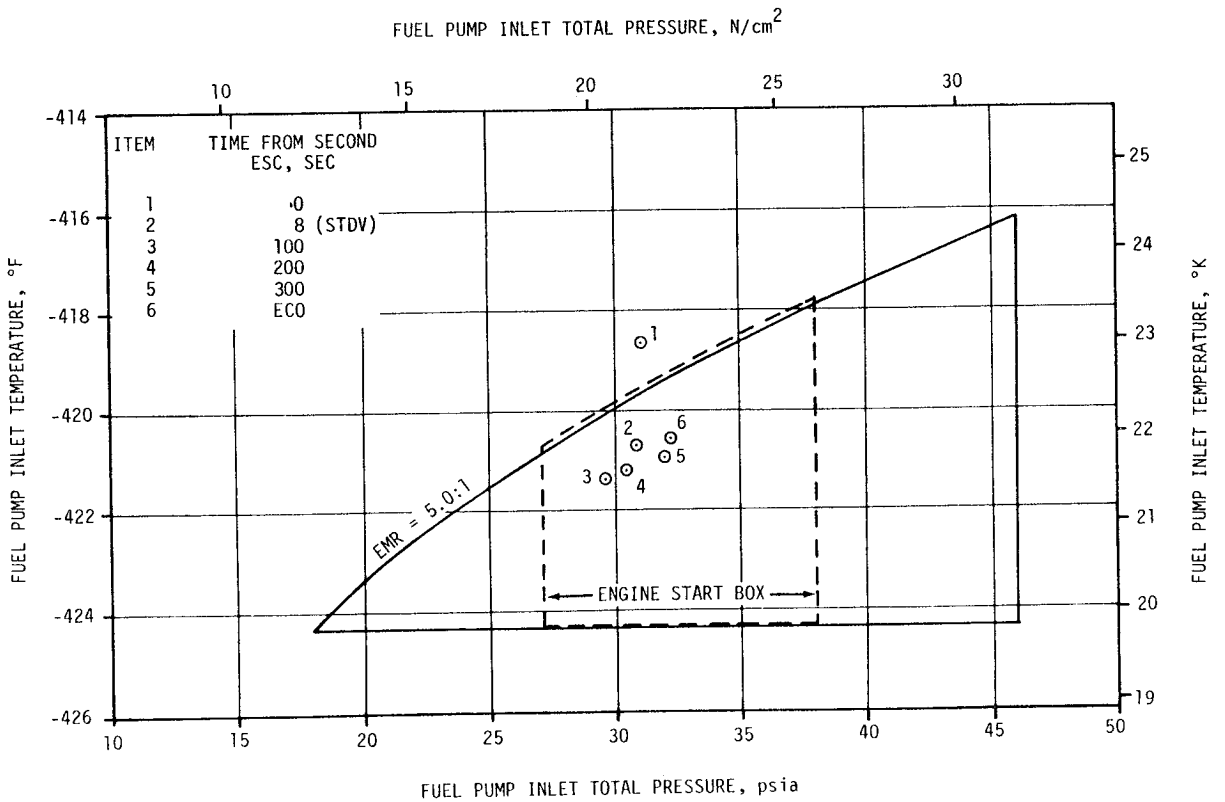
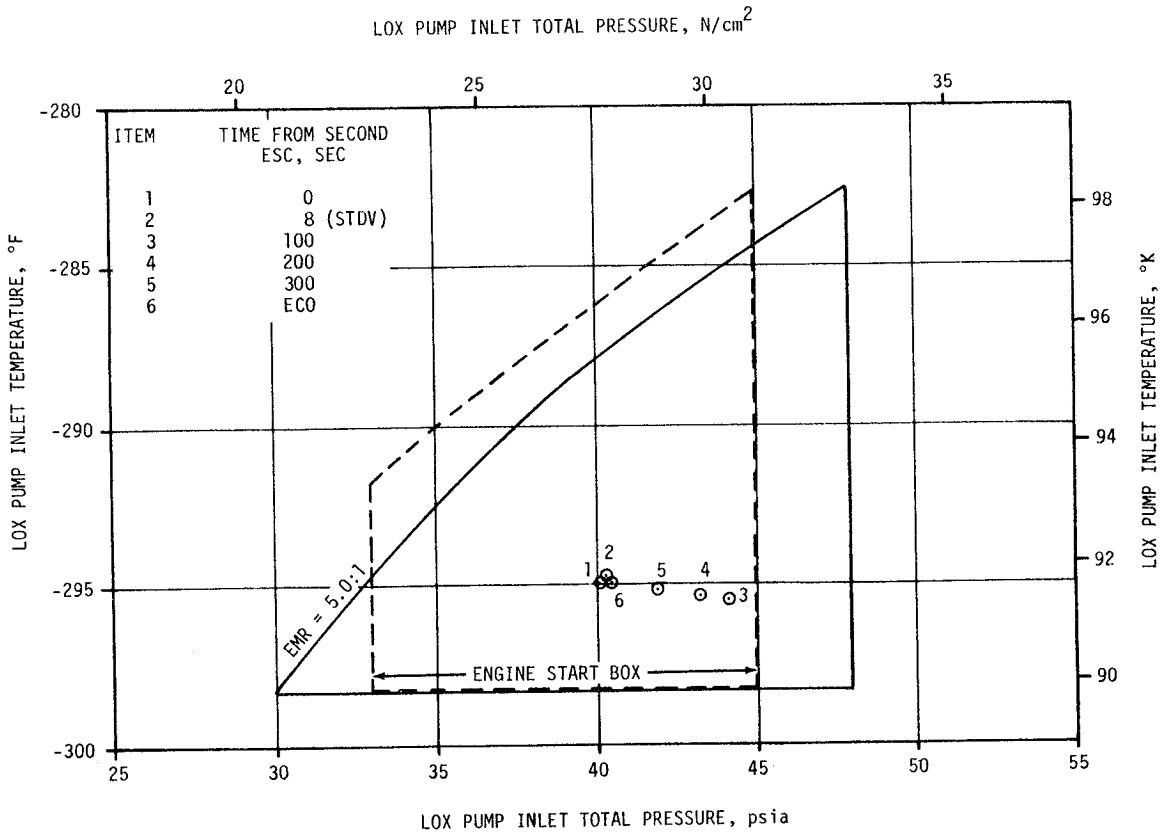


Figure 7-6. S-IVB Start Box and Run Requirements - Second Burn

versus time is shown in Figure 7-7. Table 7-2 shows the specific impulse, flowrates and EMR deviations from the predicted at the STDV +130 second time slice.

### 7.8 S-IVB SHUTDOWN TRANSIENT PERFORMANCE FOR SECOND BURN

S-IVB second ECO was initiated at 9697.17 seconds by a guidance velocity cutoff command for a burntime of 350.8 seconds. This burntime was 4.9 seconds less than that predicted.

The ECO transient was satisfactory. The total cutoff impulse to zero thrust was 46,235 lbf-s, which was 2224 lbf-s less than predicted. Cutoff occurred with the PU valve in the null position.

### 7.9 S-IVB STAGE PROPELLANT MANAGEMENT

The PU system was operated in the open-loop mode, which means the LOX flowrate is not controlled, to insure simultaneous depletion of propellants. The PU system successfully accomplished the requirements associated with propellant loading.

A comparison of propellant mass values at critical flight events, as determined by various analyses, is presented in Table 7-3. The best estimate full load propellant masses were 0.19 percent greater for LOX and 0.36 percent greater for LH<sub>2</sub> than the predicted values. This deviation was well within the required loading accuracy.

Extrapolation of propellant level sensor data to depletion, using the propellant flowrates, indicated that a LOX depletion would have occurred approximately 9.26 seconds after second burn velocity cutoff.

Table 7-2. S-IVB Steady State Performance - Second Burn  
(STDV +130 Second Time Slice at Standard Altitude Conditions)

PARAMETER	PREDICTED	RECONSTRUCTION	FLIGHT DEVIATION	PERCENT DEVIATION FROM PREDICTED
Thrust, lbf	199,003	198,536	-467	-0.235
Specific Impulse, lbf-s/lbm	426.8	427.2	0.4	0.094
LOX Flowrate, lbm/s	387.65	386.54	-1.11	-0.286
Fuel Flowrate, lbm/s	78.58	78.24	-0.34	-0.433
Engine Mixture Ratio, LOX/Fuel	4.933	4.940	0.007	0.142

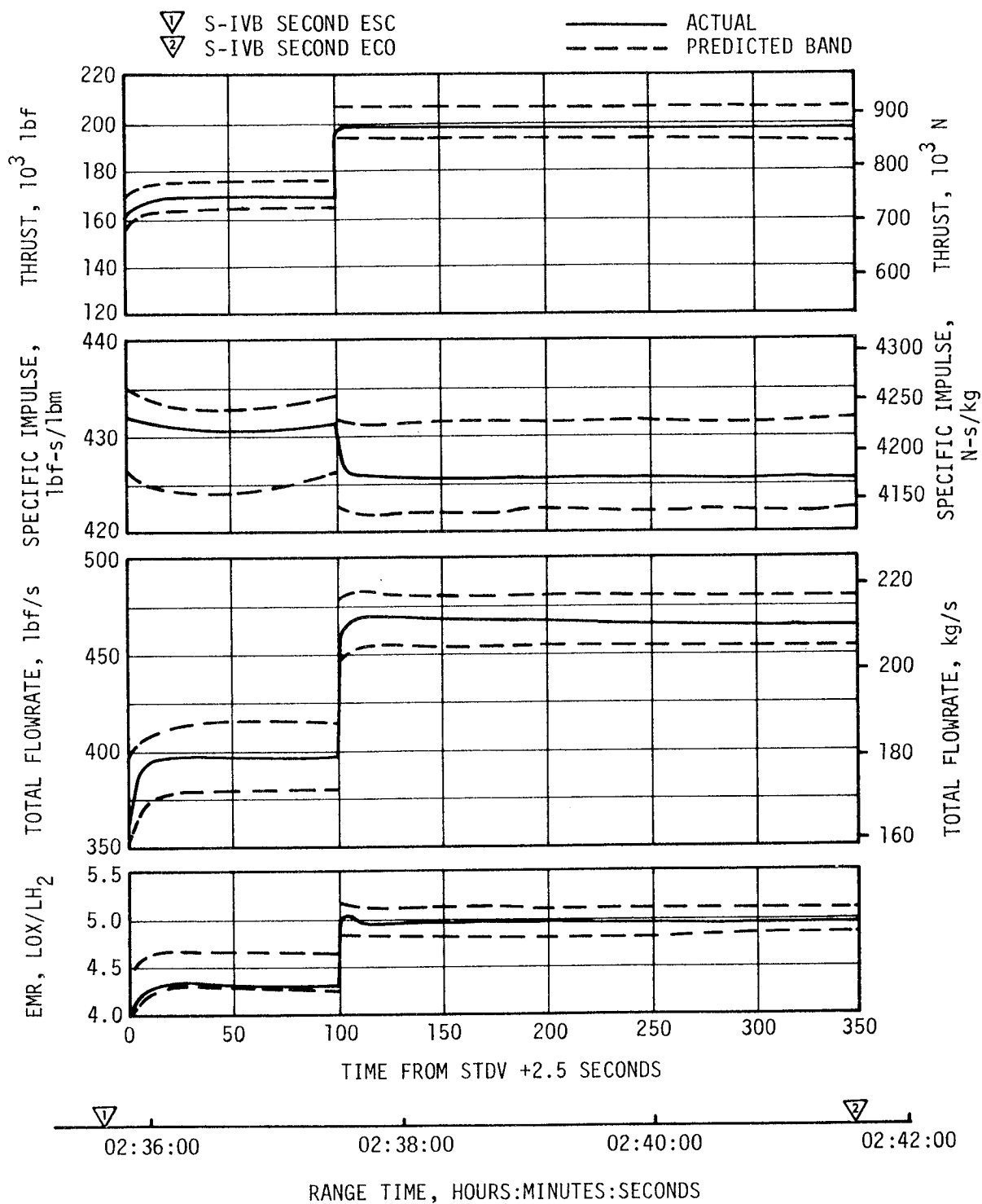


Figure 7-7. S-IVB Steady State Performance - Second Burn

Table 7-3. S-IVB Stage Propellant Mass History

EVENT	UNITS	PREDICTED*		PU INDICATED (CORRECTED)		PU VOLUMETRIC		FLOW INTEGRAL		BEST ESTIMATE**	
		LOX	LH2	LOX	LH2	LOX	LH2	LOX	LH2	LOX	LH2
S-IC Liftoff	1bm	191,532	43,500	191,588	43,585	191,615	43,892	192,123	43,418	191,890	43,657
First S-IVB ESC	1bm	191,526	43,500	191,588	43,585	191,615	43,892	192,123	43,418	191,890	43,657
First S-IVB ECO	1bm	131,552	31,398	132,641	31,420	132,826	31,590	132,799	31,336	132,738	31,445
Second S-IVB ESC	1bm	131,317	28,857	132,413	29,386	132,598	29,506	132,564	29,290	132,525	29,397
Second S-IVB ECO	1bm	1233	1451	4381	2280	4336	2252	4102	1977	4102	1977

\* The predicted mass values have been adjusted for the actual burn times according to the predicted flowrates.  
 \*\* The Best Estimate masses shown do not include mass below the main engine valves, as presented in Section 16.

During first burn the PU valve was positioned at null for start and remained there, as programmed, for the duration of the burn. The PU valve was commanded to the 4.5 EMR position 119.9 seconds prior to second ESC, and remained there for 230.5 seconds. At second ESC +110.6 seconds the valve was commanded to the null position (approximately 5.0 EMR) and remained there throughout the remainder of the flight. The actual times were within 28 milliseconds of predicted.

## 7.10 S-IVB PRESSURIZATION SYSTEMS

### 7.10.1 S-IVB Fuel Pressurization System

The LH<sub>2</sub> pressurization system met all of its operational requirements. The LH<sub>2</sub> pressurization system indicated acceptable performance during prepressurization, boost, first burn, coast phase, and second burn.

The LH<sub>2</sub> tank prepressurization command was received at -96.7 seconds and the tank pressurized signal was received 12.5 seconds later. Following the termination of prepressurization, the ullage pressure reached relief conditions, approximately 31.9 psia, and remained at that level until liftoff, as shown in Figure 7-8. A small ullage collapse occurred during the first 90 seconds of boost. The ullage pressure returned to the relief level by 130 seconds due to self pressurization.

During first burn, the average pressurization flowrate was approximately 0.66 lbm/s providing a total flow of 98.7 lbm. All during the burn the ullage pressure was at the relief level, as predicted.

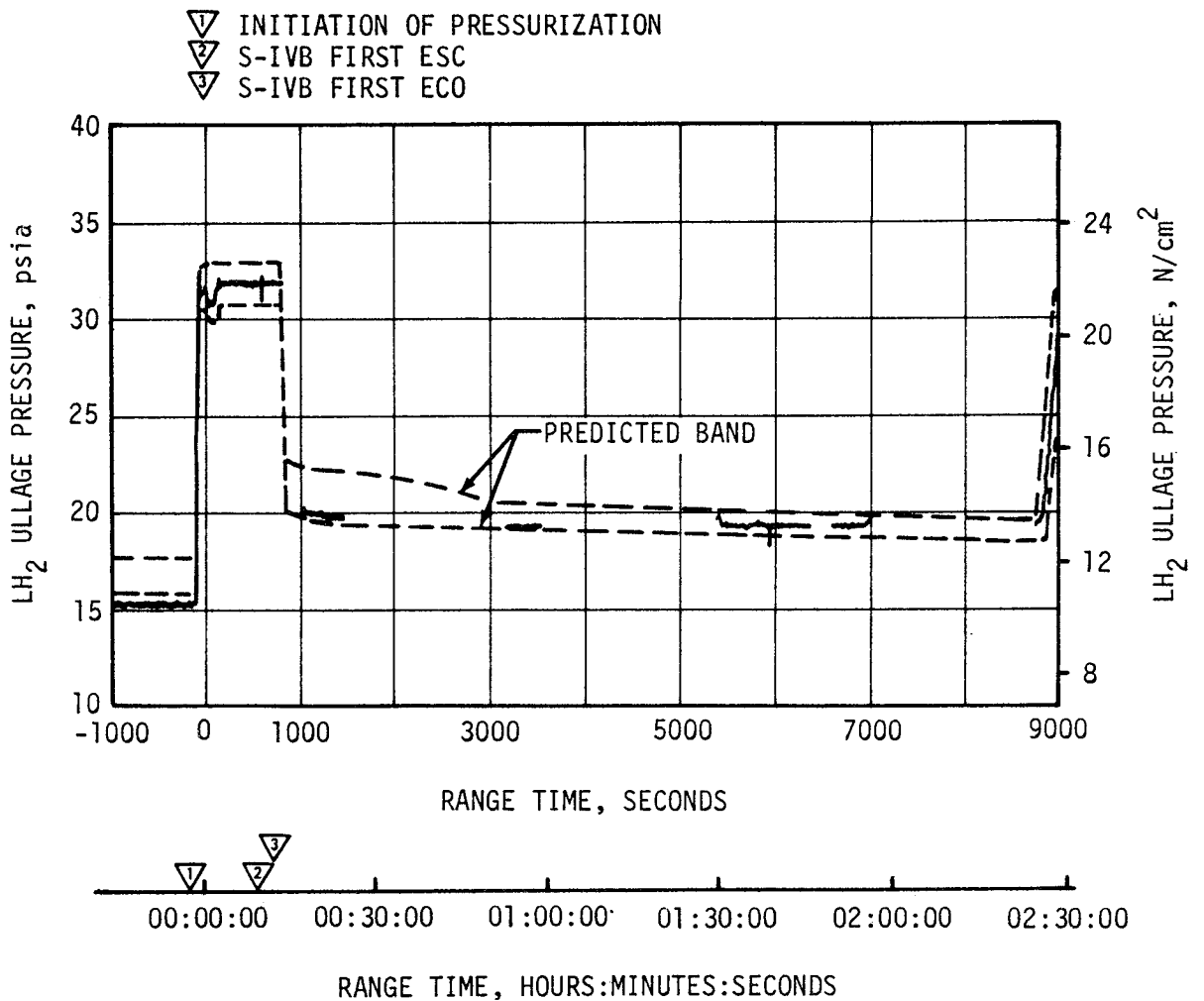


Figure 7-8. S-IVB LH<sub>2</sub> Ullage Pressure - First Burn and Parking Orbit

The LH<sub>2</sub> tank was satisfactorily repressurized for restart by the O<sub>2</sub>/H<sub>2</sub> burner. The LH<sub>2</sub> ullage pressure was 31.0 psia at second burn ESC, as shown in Figure 7-9. The average second burn pressurization flowrate was 0.64 lbm/s until step pressurization when it increased to 1.27 lbm/s. This provided a total flow of 273.3 lbm during second burn. Significant venting during second burn occurred at second ESC +280 seconds when step pressurization was initiated. This behavior was as predicted.

The LH<sub>2</sub> pump inlet Net Positive Suction Pressure (NPSP) was calculated from the pump interface temperature and total pressure. These values indicated that the NPSP at first burn ESC was 16.2 psi. At the minimum point, the NPSP was 7.2 psi above the required value. Throughout the burn, the NPSP had satisfactory agreement with the predicted values. The NPSP at second burn ESC was 1.1 psi which was 3.4 psi below the required value. The NPSP requirement was met by second STDV open. Figures 7-10 and 7-11 summarize the fuel pump inlet conditions for first and second burns.

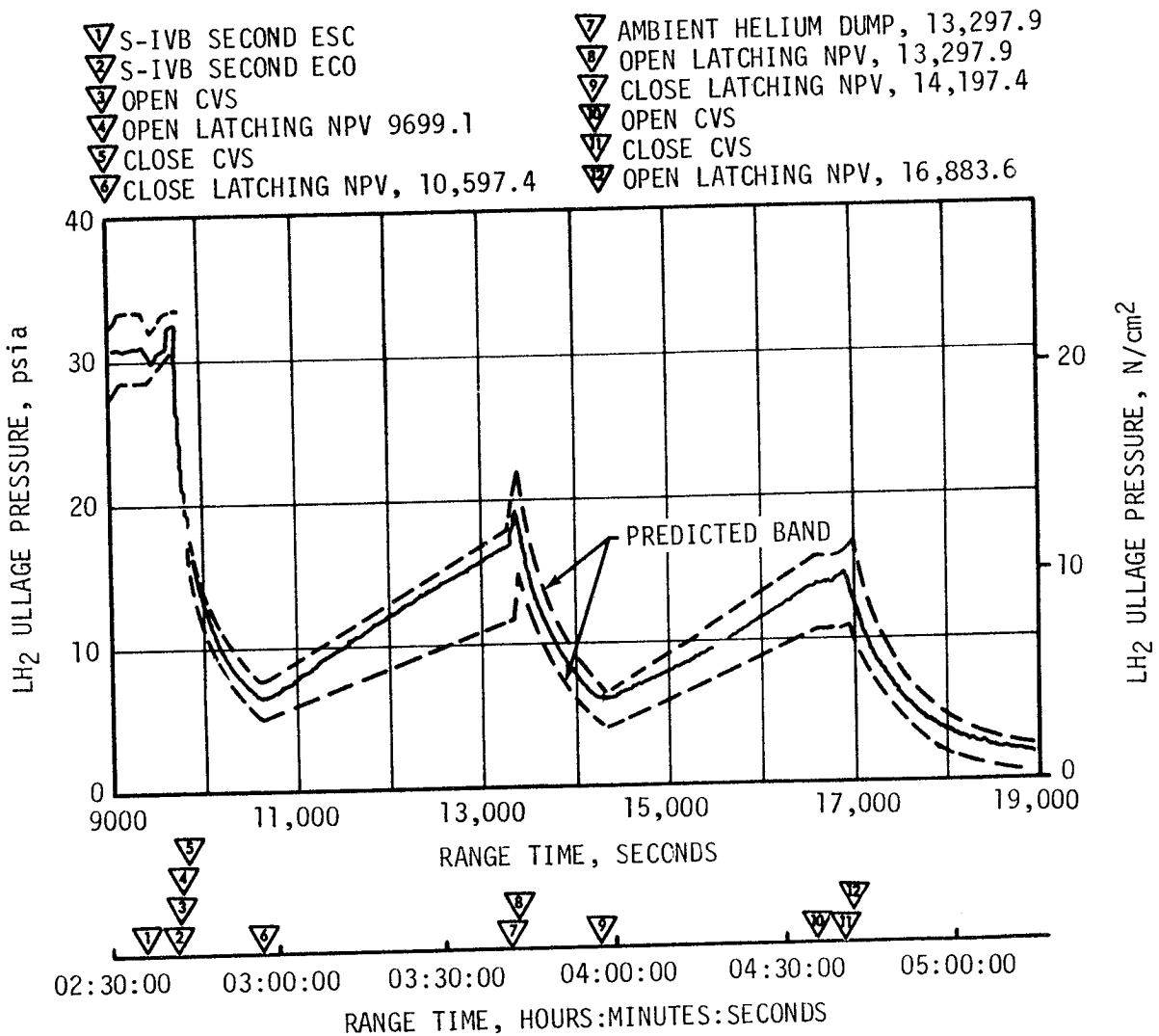


Figure 7-9. S-IVB LH<sub>2</sub> Ullage Pressure - Second Burn and Translunar Coast

### 7.10.2 S-IVB LOX Pressurization System

LOX tank prepressurization was initiated at -167 seconds and increased the LOX tank ullage pressure from ambient to 40.8 psi within 20 seconds, as shown in Figure 7-12. Four makeup cycles were required to maintain the LOX tank ullage pressure before the ullage temperature stabilized. At -96 seconds the LOX tank ullage pressure increased from 39.9 to 42.5 psia due to fuel tank prepressurization. The pressure then gradually decreased to 42.1 psia at liftoff.

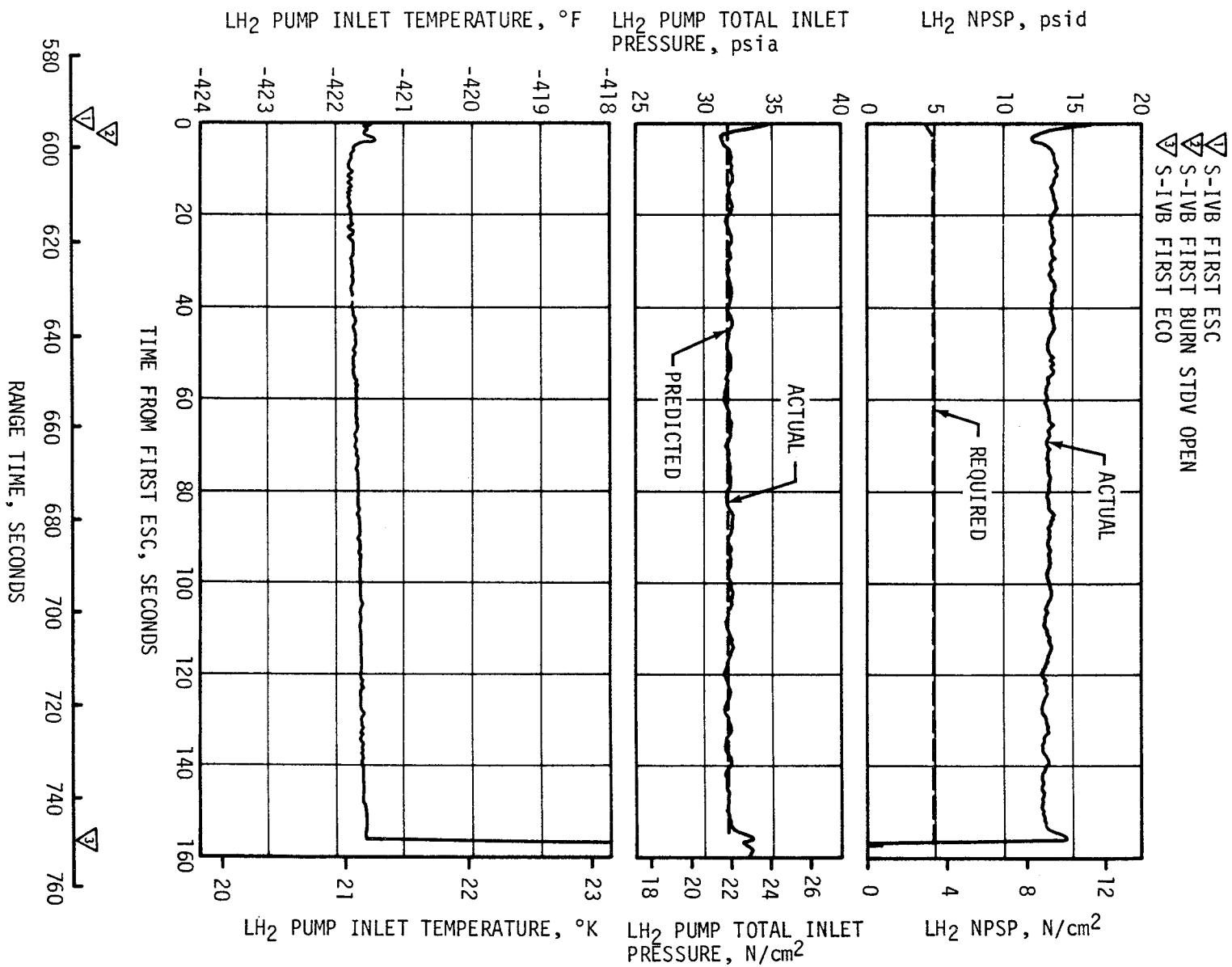


Figure 7-10. S-1VB Fuel Pump Inlet Conditions - First Burn

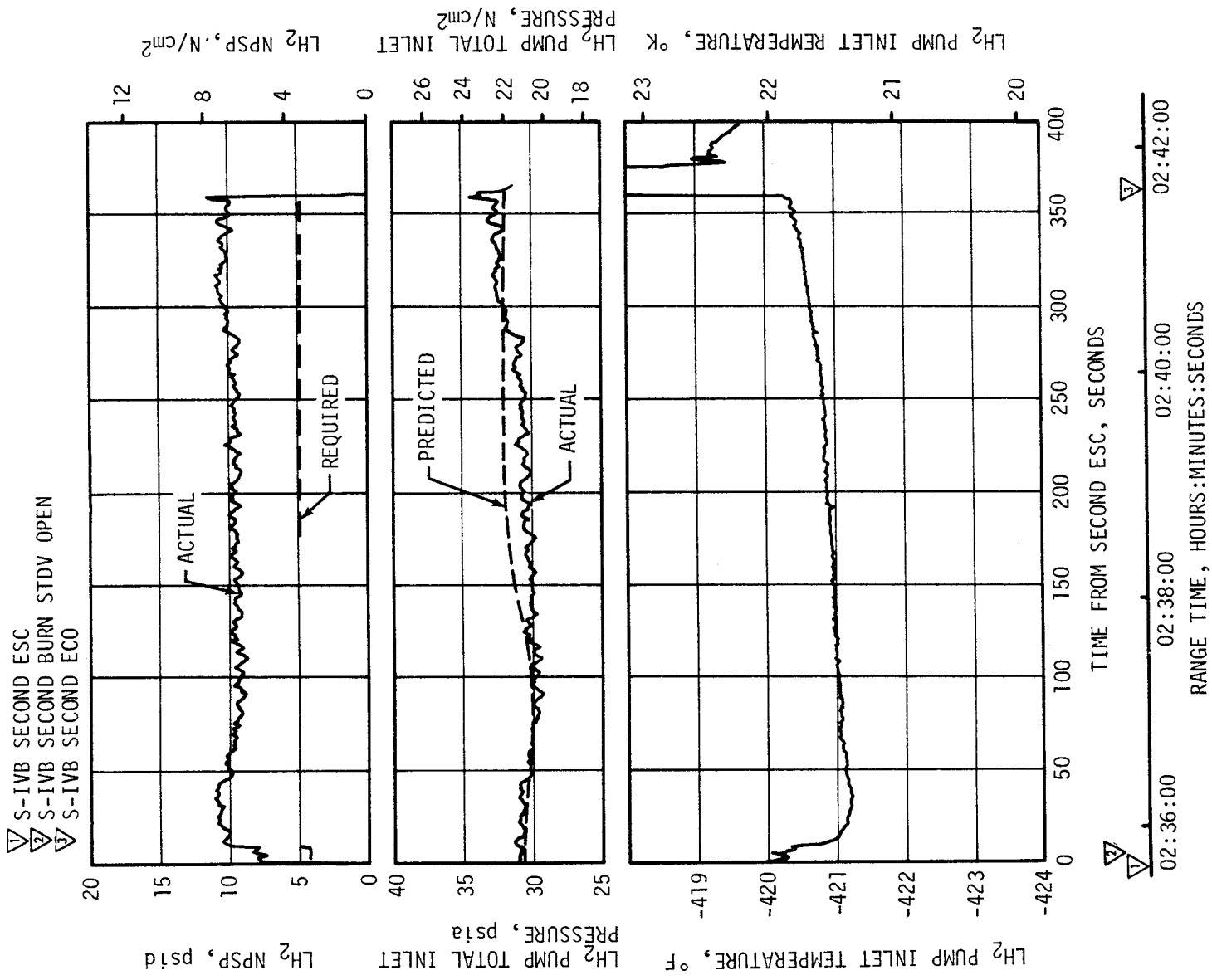


Figure 7-11. S-IVB Fuel Pump Inlet Conditions - Second Burn

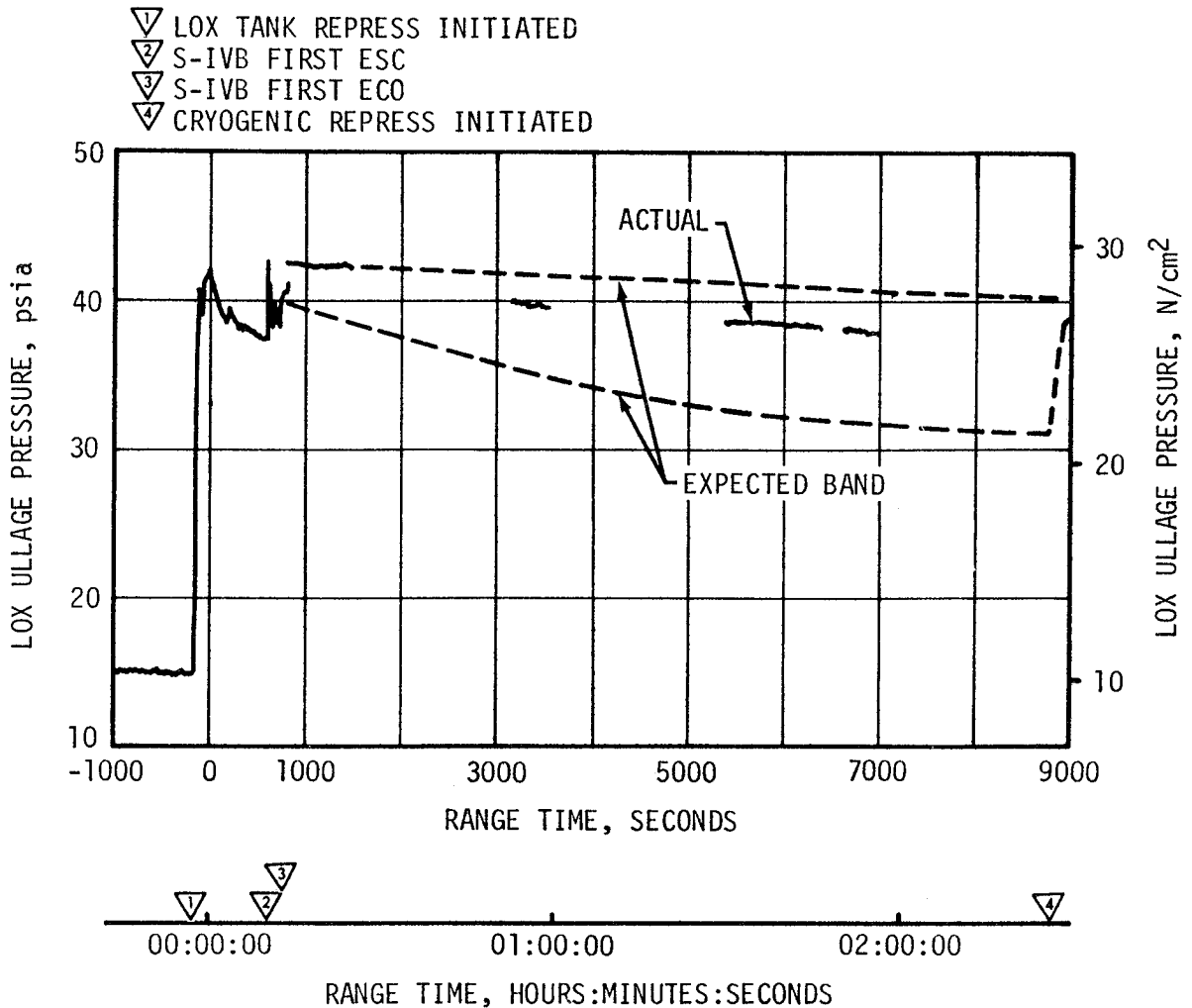


Figure 7-12. S-IVB LOX Tank Ullage Pressure - First Burn and Parking Orbit

During boost there was a normal rate of ullage pressure decay caused by an acceleration effect and ullage collapse. No makeup cycles occurred because of an inhibit until after Time Base 4 (T<sub>4</sub>). LOX tank ullage pressure was 37.1 psia just prior to ESC and was increasing at ESC due to a makeup cycle.

During first burn, three over-control cycles were initiated, exactly matching the predicted three cycles. The LOX tank pressurization flowrate variation was 0.25 to 0.33 lbm/s during under-control system operation. This variation is normal and is caused by temperature effects. Heat exchanger performance during first burn was satisfactory.

During orbital coast the LOX tank ullage pressure experienced a decay similar to, though less than, that experienced on the AS-506 and AS-507 flights. This decay was within the predicted band, and was not a problem.

Repressurization of the LOX tank prior to second burn was required and was satisfactorily accomplished by the burner. The tank ullage pressure was 40.0 psia at second ESC and satisfied the engine start requirements, as shown in Figure 7-13.

Pressurization system performance during second burn was satisfactory and had the same characteristics noted during first burn. There were no over-control cycles, as compared to a prediction of from zero to one. Flowrate varied between 0.33 and 0.39 lbm/s. Heat exchanger performance was satisfactory.

The LOX NPSP calculated at the interface was 25.6 psi at first burn ESC. The NPSP decreased after start and reached a minimum value of 23.9 psi at 1 second after ESC. This was 11.1 psi above the required NPSP at that time.

The LOX pump static interface pressure during first burn followed the cyclic trends of the LOX tank ullage pressure. The NPSP calculated at the engine interface was 22.9 psi at second burn ESC. At all times during second burn, NPSP was above the required level. Figures 7-14 and 7-15 summarize the LOX pump conditions for the first burn and second burn. The run requirements for first and second burn were satisfactorily met.

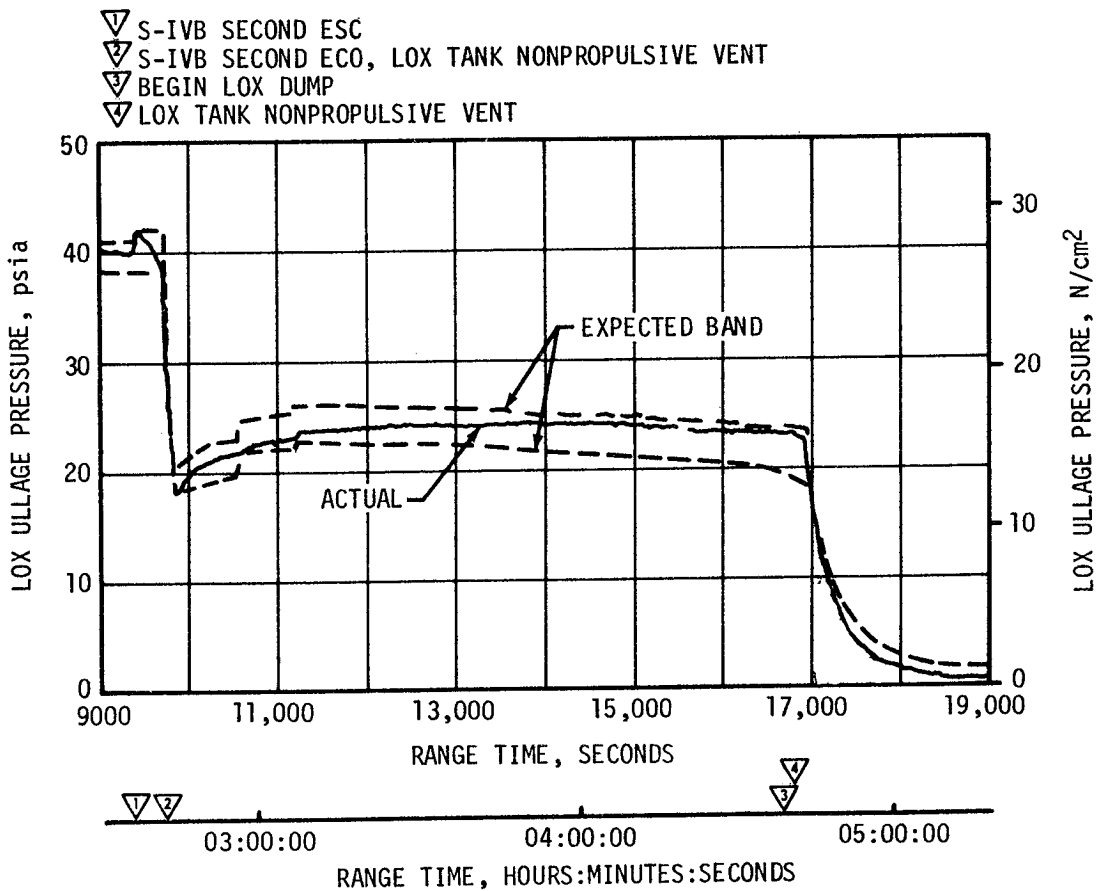


Figure 7-13. S-IVB LOX Tank Ullage Pressure - Second Burn and Translunar Coast

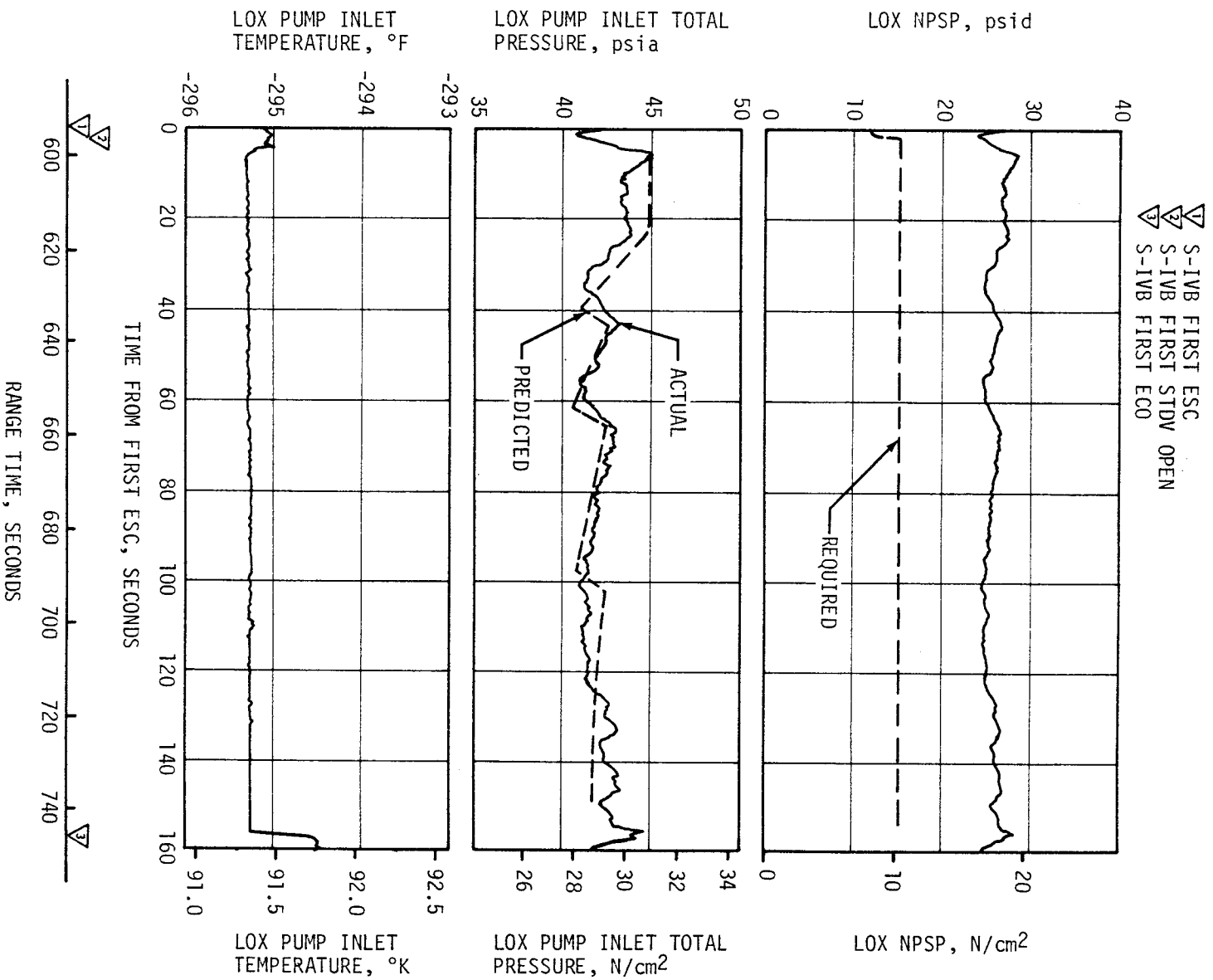


Figure 7-14. S-1VB LOX Pump Inlet Conditions - First Burn

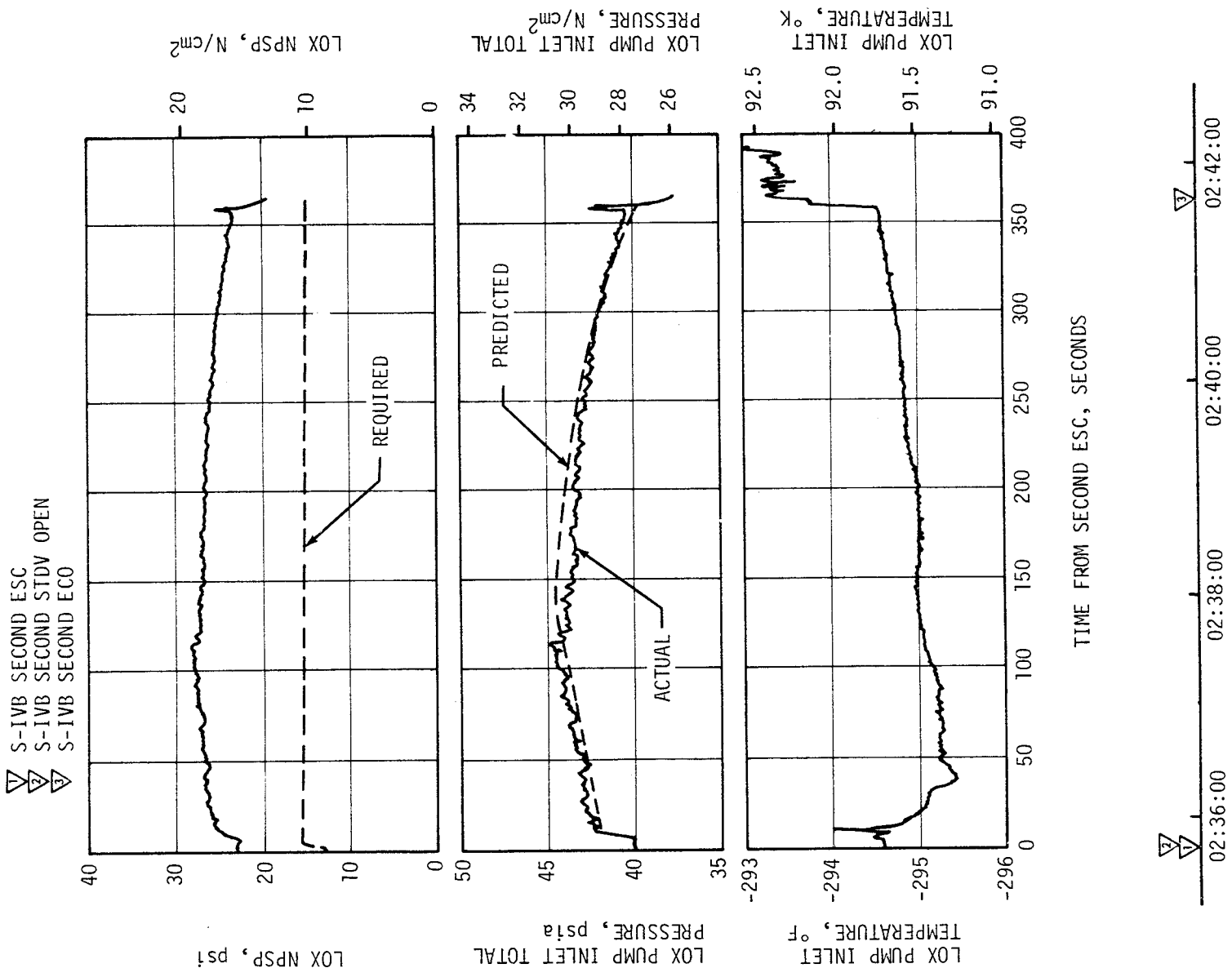


Figure 7-15. S-1VB LOX Pump Inlet Conditions - Second Burn

The cold helium supply was adequate to meet all flight requirements. At first burn ESC the cold helium spheres contained 381 lbm of helium. At the end of the second burn, the helium mass had decreased to 175 lbm. Figure 7-16 shows helium supply pressure history.

### 7.11 S-IVB PNEUMATIC CONTROL SYSTEM

The pneumatic control and purge system performed satisfactorily during all phases of the mission. Pneumatic regulator operation was nominal at all times. The LOX chilldown pump motor container purge pressure was lower than on previous flights. The low pressure was probably due to contamination of the sintered orifices that control the pressure. The lower pressure did not effect LOX chilldown pump performance.

### 7.12 S-IVB AUXILIARY PROPULSION SYSTEM

The APS demonstrated close to nominal performance throughout its flight and met control system demands out to propellant depletion at approximately 19.5 hours.

The APS propellant supply systems performed as expected during the flight. Propellant temperatures ranged from 71 to 96°F. The propellant usage, as shown in Table 7-4, approximated the nominal prediction out to 12 hours 47 minutes. At this time the APS yaw engines were erroneously fired as a result of the loss of the primary yaw gyro. When the backup yaw gyro took over, the yaw engine firing rate which had built up in magnitude and duration subsided to normal limit cycle pulsing operation. At 13 hours and 42 minutes the APS received an erroneous signal from the IU to return to the TD&E attitude. Following this unscheduled maneuver the APS maintained limit cycle operation until 19 hours and 9 minutes. At this time, more erroneous signals were received from the IU. At 70,150 seconds (19:29:10) a yaw engine in each module went on steady state and the pitch engines were fired in alternating series of pulses until propellant depletion. This APS activity was sufficient to cause a stage velocity change of 7 to 10 ft/s. All the erroneous firing signals received from the IU were after normal stage life time. For an additional discussion of the results of these erroneous firing signals see paragraph 10.4.4.

The APS propellant pressurization was satisfactory throughout the flight. However, Module 1 regulator outlet pressure started to increase at approximately 3 hours and by 7.5 hours the regulator outlet pressure had increased to 203 psia and then reached a maximum of 204.5 psia at 10 hours (Figure 7-17). Examination of the helium bottle temperature and regulator outlet pressure and the vehicle orientation indicates that solar heating was responsible for these pressure changes. A similar thermal effect on the regulator outlet pressure was experienced during the regulator qualification tests and also at approximately 5.5 hours after TLI on the AS-505 flight.

- ▽ S-IVB FIRST ECO
- ▽ START CRYOGENIC REPRESS
- ▽ S-IVB SECOND ESC
- ▽ S-IVB SECOND ECO
- ▽ START COLD HELIUM DUMP, 9716.0

- ▽ END COLD HELIUM DUMP, 10,597.0
- ▽ START COLD HELIUM DUMP, 13,359.4
- ▽ END COLD HELIUM DUMP, 14,196.6
- ▽ START COLD HELIUM DUMP, 16,884.8
- ▽ END COLD HELIUM DUMP, 18,684.4

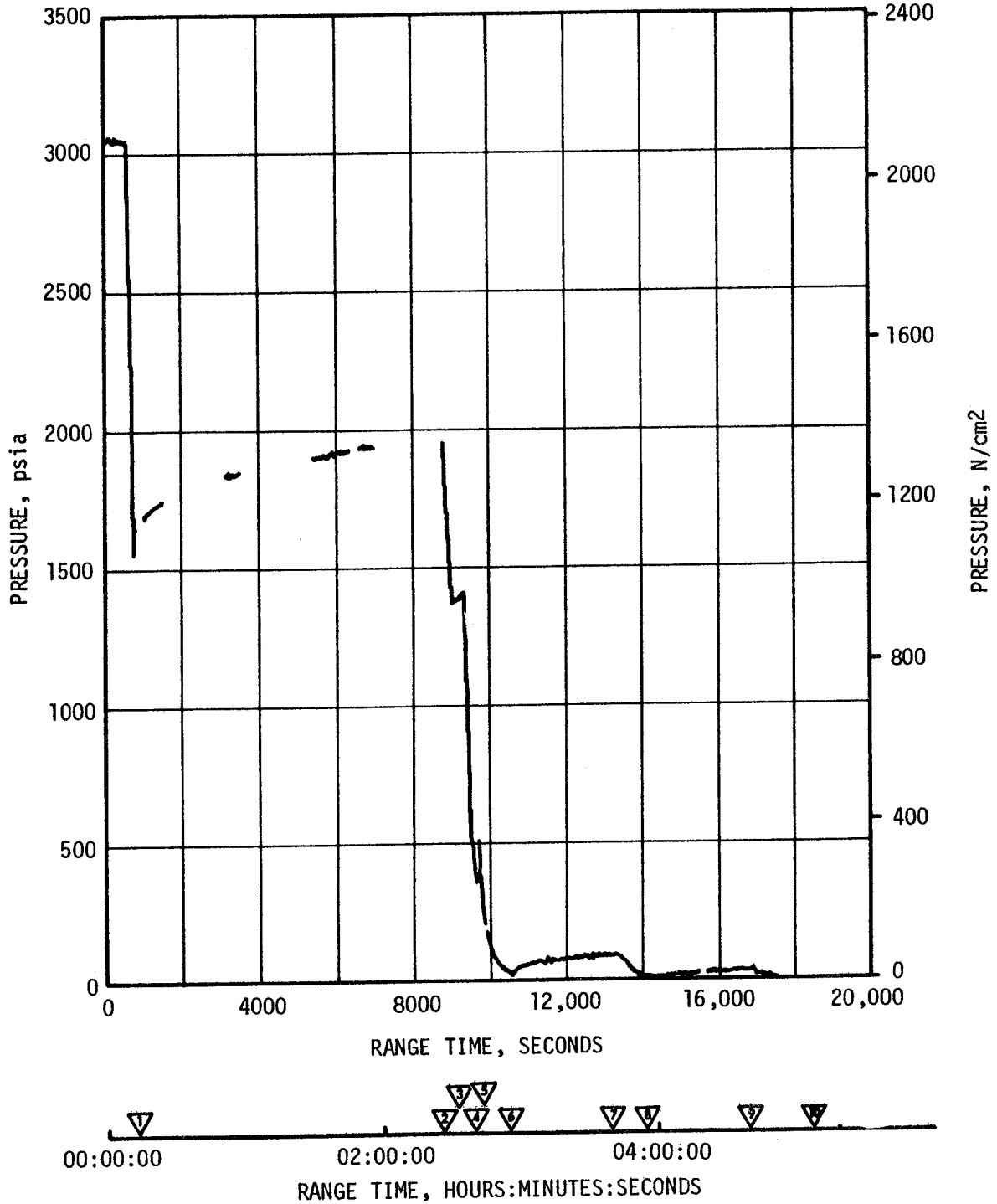


Figure 7-16. S-IVB Cold Helium Supply History

Table 7-4. S-IVB APS Propellant Consumption

TIME PERIOD	MODULE 1		MODULE 2	
	OXIDIZER, LBM	FUEL, LBM	OXIDIZER, LBM	FUEL, LBM
Initial Load	204.8	126.1	204.3	126.1
First Burn (Roll Control)	0.5	0.3	0.5	0.3
ECO to End of First APS Ullage Burn (86.7 sec)	12.9	10.2	12.9	10.2
End of First Ullage Burn to Start of Second Ullage Burn	13.8	8.2	3.5	2.6
Second Ullage Burn (76.7 sec)	11.5	9.1	11.7	9.2
Second Burn (Roll Control)	0.4	0.2	0.4	0.2
ECO to Start of Evasive Ullage Burn	16.0	10.1	14.4	9.0
Evasive Ullage Burn (80 sec)	11.9	9.4	11.9	9.4
From End of Evasive Ullage Burn to Start of Lunar Impact Ullage Burn at 6 Hours	8.1	5.1	12.0	7.5
Lunar Impact Ullage Burn (217 sec)	26.7	22.0	30.7	24.6
From End of Lunar Impact Burn to Loss of Yaw Gyro at Approx. 12 Hours 47 Minutes	17.9	11.2	18.1	11.3
Propellant Usage During Unstable Period During Loss of Yaw Gyro to Repeat of TD&E Maneuver at 13 Hours 42 Minutes	20.1	12.4	19.2	12.0
Propellant Usage From 13 Hours 42 Minutes to 19 Hours 9 Minutes	9.8	6.1	13.3	8.4
From 19 Hours 9 Minutes to Propellant Depletion	55.2	21.8	55.7	21.4
Note: The APS propellant consumption presented in this table was determined from helium bottle conditions (pressure, volume, temperature).				

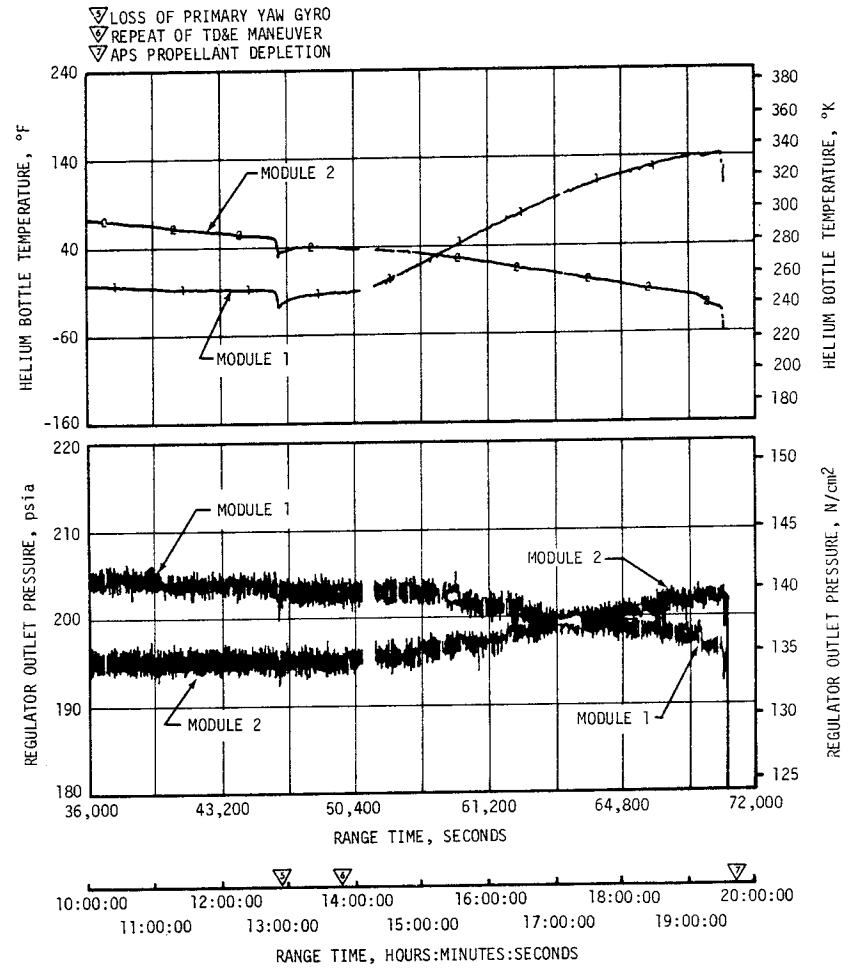
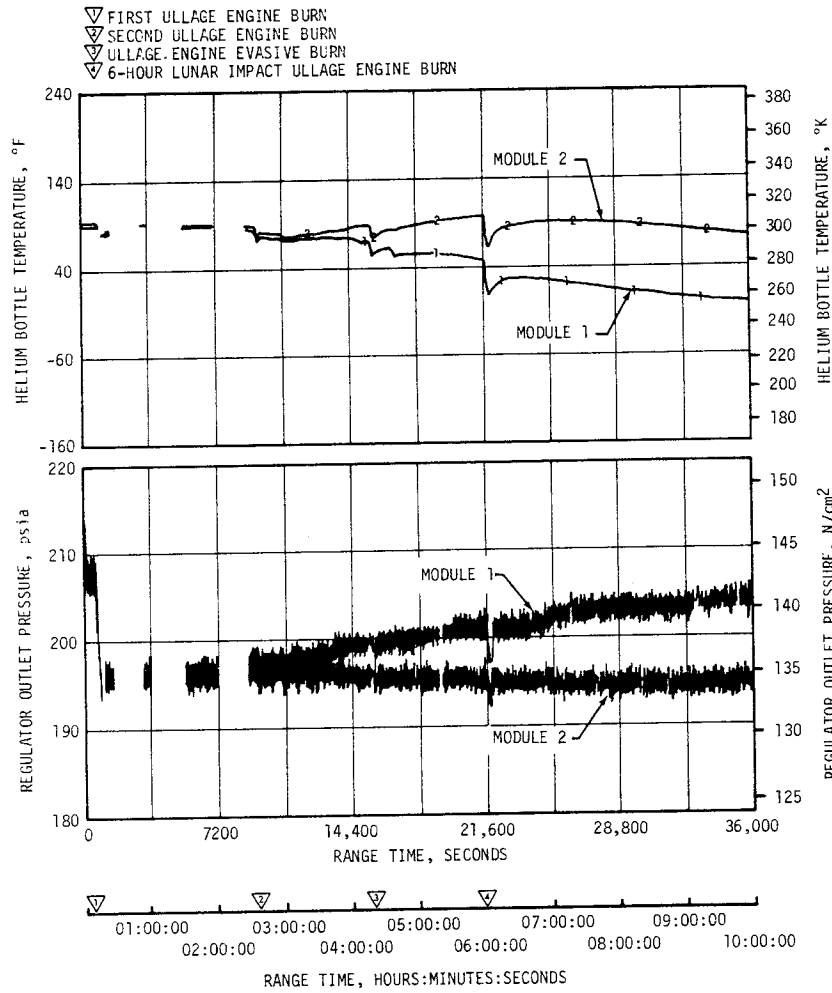


Figure 7-17. APS Helium Bottle Temperature and Regulator Outlet Pressure

Nominal primary regulator operation is  $196 \pm 3$  psig with a lockup of 203 psig. The higher regulator pressure of 204.5 psia observed during this flight does not present any system operation problems. A thermal analysis of the AS-508 flight indicated that the APS regulator temperature was maintained above  $-10^{\circ}\text{F}$  for approximately 6.5 hours beyond TLI.

The APS ullage pressures in the propellant ullage tanks ranged from 187 to 202 psia. The helium bottle temperatures ranged from  $-30$  to  $+140^{\circ}\text{F}$ .

The performance of the attitude control thrusters and the ullage thrusters was satisfactory throughout the mission. The thruster chamber pressures ranged from 95 to 102 psia. The ullage thrusters successfully completed the three sequenced burns of 86.7 seconds, 76.7 seconds and 80.0 seconds as well as the ground commanded 217 second lunar impact burn. The planned ullage burn at 9 hours, to impact the lunar target area, was not required.

### 7.13 S-IVB ORBITAL SAFING OPERATIONS

The S-IVB high pressure systems were safed following J-2 engine cutoff in order to demonstrate this capability. The thrust developed during the LOX dump was utilized to provide a velocity change for the lunar impact maneuver. The manner and sequence in which the safing was performed is presented in Figure 7-18.

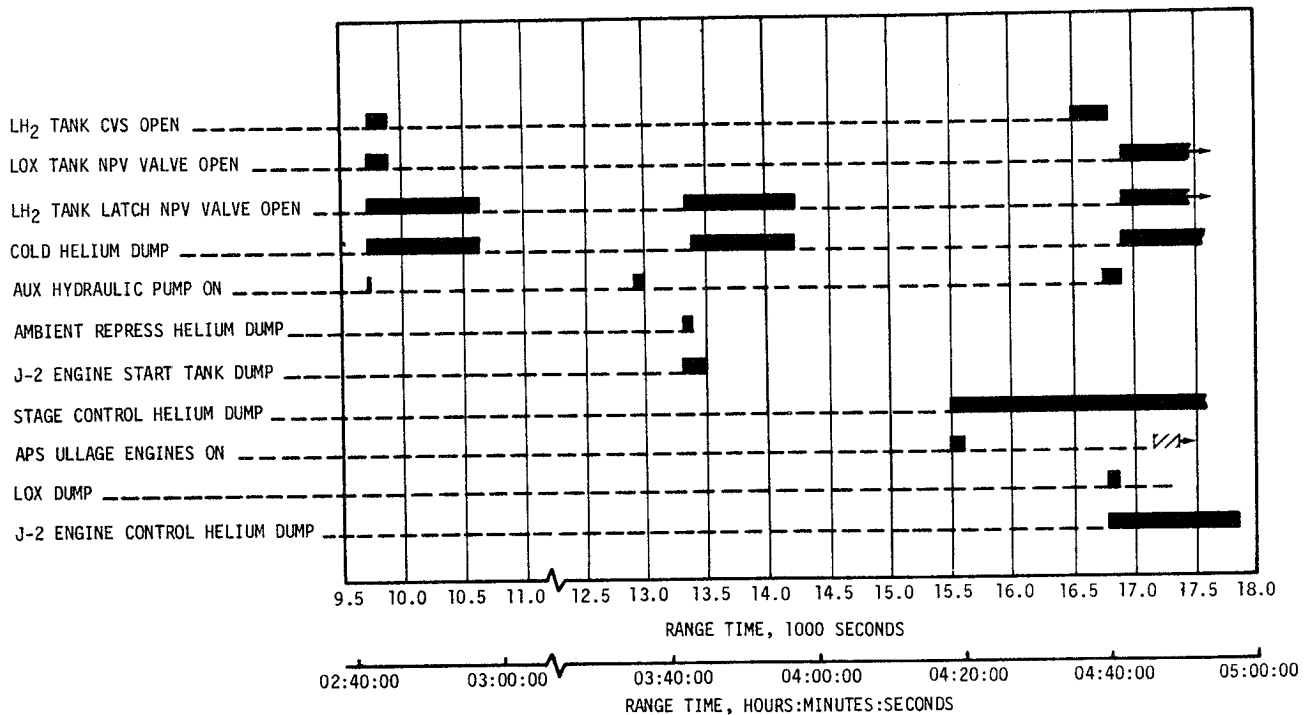


Figure 7-18. S-IVB LOX Dump and Orbital Safing Sequence

### 7.13.1 Fuel Tank Safing

The LH<sub>2</sub> tank was satisfactorily safed by accomplishing three programmed vents, as indicated in Figure 7-18, utilizing both the Nonpropulsive Vent (NPV) and CVS. The LH<sub>2</sub> tank ullage pressure during safing is shown in Figure 7-9. At second ECO, the LH<sub>2</sub> tank ullage pressure was 32.4 psia and after three vent cycles had decayed to approximately zero. The mass of GH<sub>2</sub> and LH<sub>2</sub> vented agrees with the 2510 lbm of liquid residual and pressurant in the tank at the end of powered flight.

### 7.13.2 LOX Tank Dump and Safing

Immediately following second burn cutoff, a programmed 150 second vent reduced LOX tank ullage pressure from 38.6 psia to 18.0 psia, as shown in Figure 7-13. Data levels were as expected with 73.6 lbm of helium and 128.9 lbm of GOX being vented overboard. As indicated in Figure 7-13, the ullage pressure then rose gradually due to self-pressurization, to 23.0 psia at the initiation of the TD&E maneuver.

The LOX tank dump was initiated at 16,759.4 seconds (04:39:19.4) and was satisfactorily accomplished. A steady-state liquid flow of 375 gpm was reached within 15 seconds. Gas ingestion did not occur during dump. The LOX residual at the start of dump was 3923 lbm. Calculations indicate that 2330 lbm of LOX was dumped. During dump, the ullage pressure decreased from 23.2 psia to 22.8 psia. LOX dump ended at 16,807.4 seconds (04:40:07.4) as scheduled by closure of the Main Oxidizer Valve (MOV). A steady-state LOX dump thrust of 760 lbf was obtained. The total impulse before MOV closure was 31,000 lbf-s, resulting in a calculated velocity change of 28.5 ft/s. Figure 7-19 shows the LOX dump thrust, LOX flowrate, oxidizer mass, and LOX ullage pressure during LOX dump. The predicted curves provided for the LOX flowrate and dump thrust correspond with the quantity of LOX dumped and the actual ullage pressure.

Seventy-two seconds following termination of LOX dump, the LOX NPV valve was opened and remained open for the duration of the mission. LOX tank ullage pressure decayed from 22.2 psia at 16,880 seconds (04:41:20) to zero pressure at approximately 31,000 seconds (08:36:40).

Sufficient impulse was derived from the LOX dump, LH<sub>2</sub> CVS operation, and APS ullage burn to achieve a successful lunar impact. For further discussion of the lunar impact refer to Section 4A.

### 7.13.3 Cold Helium Dump

A total of approximately 170 lbm of helium was dumped during the three programmed dumps, which occurred as shown in Figure 7-18.

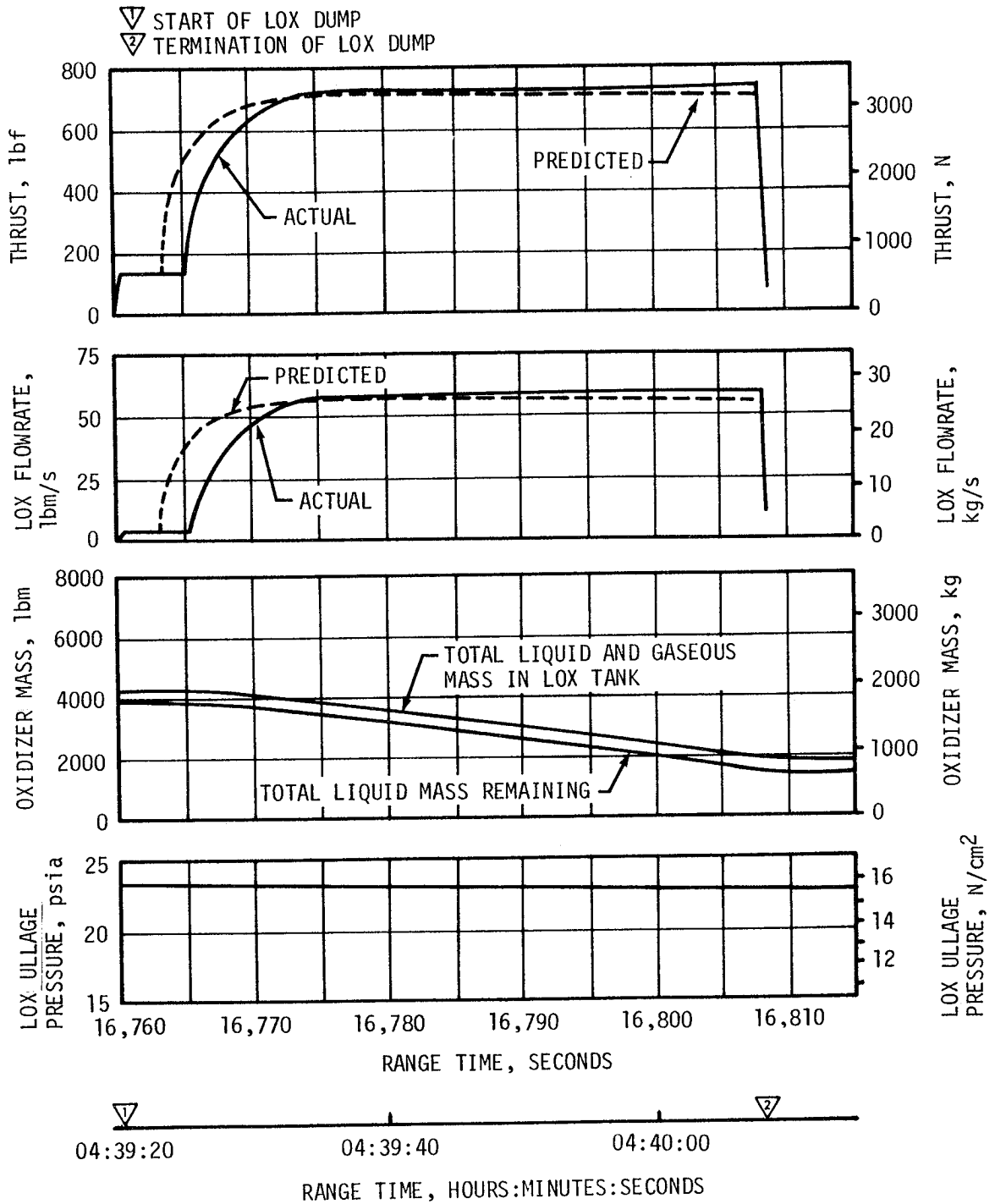


Figure 7-19. S-IVB LOX Dump Parameter Histories

#### 7.13.4 Ambient Helium Dump

Approximately 30.0 lbm of ambient helium in the LOX and LH<sub>2</sub> repressurization spheres was dumped via the fuel tank. The 62 second dump occurred at 13,298.4 seconds (03:41:38.4). The pressure decayed from 3000 to 380 psia.

#### 7.13.5 Stage Pneumatic Control Sphere Safing

The stage pneumatic control sphere was safed by initiating the J-2 engine pump and by flowing helium overboard through the pump seal cavities for 3600 seconds. This activity began at 15,480 seconds (04:18:00) and satisfactorily reduced the pressure in the sphere from 2870 to 1750 psia.

#### 7.13.6 Engine Start Tank Safing

The engine start tank was safed during a period of approximately 150 seconds beginning at 13,298.4 seconds (03:41:38.4). Safing was accomplished by opening the sphere vent valve. Pressure was decreased from 1250 to 10 psia with 4.20 lbm of hydrogen being vented.

#### 7.13.7 Engine Control Sphere Safing

The safing of the engine control sphere began at 16,760 seconds (04:39:20). The helium control solenoid was energized to vent helium through the engine purge system. The initial pressure in the sphere was 3080 psia, and it decayed to about 700 psia in 65 seconds. At this time gaseous helium from the ambient repressurization bottles began flowing to the engine control sphere. Helium from the control sphere and repressurization bottles continued to vent until 17,810 seconds (04:56:50). During this time, the pressure in the repressurization bottles had decayed from 700 to 150 psia. The control sphere pressure had decayed to 130 psia. Subsequent to the closing of the control solenoid, the control sphere repressurized to 170 psia without any noticeable decay in stage ambient repressurization bottle pressure. During the 1050 second safing period, a total of 11.01 lbm of helium was vented overboard.

#### 7.14 HYDRAULIC SYSTEM

The S-IVB hydraulic system performance was satisfactory during its complete mission (S-IC/S-II boost, first and seconds burns of S-IVB, and orbital coast).



## SECTION 8

### STRUCTURES

#### 8.1 SUMMARY

The structural loads experienced during the S-IC boost phase were well below design values. The maximum Q region bending moment was  $69 \times 10^6$  lbf-in. at the S-IC LOX tank which was 25 percent of design value. Thrust cutoff transients experienced by AS-508 were similar to those of previous flights. The maximum dynamic transient at the Instrument Unit (IU) resulting from S-IC Center Engine Cutoff (CECO) was  $\pm 0.20$  g longitudinal. At Outboard Engine Cutoff (OECO) a maximum dynamic longitudinal acceleration of  $\pm 0.28$  g and  $\pm 0.85$  g was experienced at the IU and Command Module (CM), respectively. The order of magnitude of the thrust cutoff responses are considered normal.

During S-IC stage boost phase, 4 to 5 hertz oscillations were detected beginning at 100 seconds. The maximum amplitude measured in the IU at 125 seconds was  $\pm 0.04$  g. Oscillations in the 4 to 5 hertz range have been observed on previous flights and are considered to be normal vehicle response to flight environment.

AS-508 experienced low frequency (14 to 16 hertz) POGO oscillations during S-II stage boost. Three distinct periods of structural/propulsion coupled oscillations exhibited peaks at 180, 250, and 330 seconds. The third period of oscillations resulted in LOX pump discharge pressure variations of sufficient magnitude to activate the center engine thrust OK pressure switches and shut down the engine 132 seconds early. All oscillations decayed to a normal level following CECO. Analysis of flight data indicates that no structural failure occurred as a result of the oscillations. Flight measurements also show that the oscillations were confined to the S-II stage and were not transmitted up the vehicle.

The structural loads experienced during the S-IVB stage burns were well below design values. During first burn the S-IVB experienced low amplitude, 18 to 20 hertz oscillations. The amplitudes measured on the gimbal block were comparable to previous flights and well within the expected range of values. Similarly, S-IVB second burn produced intermittent low amplitude oscillations in the 12 to 14 hertz frequency range which peaked near second burn cutoff.

Three vibration measurements were made on the S-IVB aft interstage. The maximum vibration levels measured occurred at liftoff and during the Mach 1 to Max Q flight period and were considered normal.

## 8.2 TOTAL VEHICLE STRUCTURES EVALUATION

### 8.2.1 Longitudinal Loads

The structural loads experienced during boost were well below design values with the exception of the S-II POGO phenomenon discussed in paragraph 8.2.3. The AS-508 vehicle liftoff occurred at a steady-state acceleration of 1.2 g. Maximum longitudinal dynamic response measured during thrust buildup and release was  $\pm 0.18$  g and  $\pm 0.40$  g at the IU and CM, respectively, as shown in Figure 8-1. Both values are lower than the respective values of  $\pm 0.25$  g and  $\pm 0.55$  g measured on AS-507.

The longitudinal loads experienced at the time of maximum bending moment (76 seconds) were as expected and are shown in Figure 8-2. The steady-state longitudinal acceleration for AS-508 was 1.9 g as compared to 2.03 g on AS-507.

Figure 8-2 also shows that the maximum longitudinal loads imposed on the S-IC stage thrust structure, fuel tank, and intertank occurred at CECO (135 seconds) at a longitudinal acceleration of 3.6 g. The maximum longitudinal loads imposed on all vehicle structure above the S-IC intertank occurred subsequent to OECO (164 seconds) at an acceleration of 3.8 g.

### 8.2.2 Bending Moments

The 1-2-1-1 engine start sequence (see paragraph 5.2) on AS-508 introduced lateral responses similar to those measured on AS-507. The maximum response level at the CM was approximately  $\pm 0.17$  g (0.118 Grms) as compared to the AS-507 maximum of approximately  $\pm 0.15$  g (0.104 Grms). The  $\pm 0.17$  g was 50 percent of the preflight predicted 3-sigma value of  $\pm 0.34$  g.

The inflight winds that existed during the maximum dynamic pressure phase of the flight peaked at 108.1 knots at 44,540 feet. As shown in Figure 8-3, the maximum bending moment imposed on the vehicle was  $69 \times 10^6$  lbf-in. at approximately 76 seconds. This moment loading was approximately 25 percent of design value.

### 8.2.3 Vehicle Dynamic Characteristics

8.2.3.1 Longitudinal Dynamic Characteristics. During S-IC stage boost phase, the significant vehicle response was the expected 4 to 5 hertz first longitudinal mode oscillations. These oscillations began at approximately 100 seconds and continued until CECO. Maximum amplitudes at the S-IC intertank sensor (A001-118) reached  $\pm 0.03$  g at 133 seconds and the IU sensor (A002-603) recorded  $\pm 0.04$  g at approximately 125 seconds (Figure 8-4).

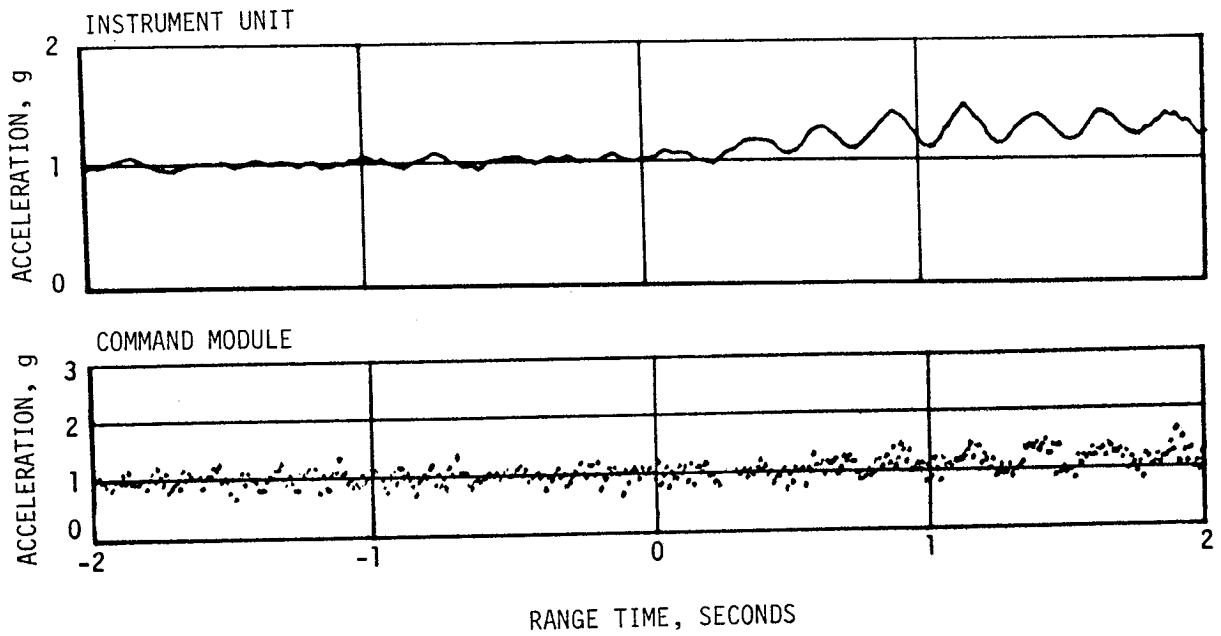


Figure 8-1. Longitudinal Acceleration at CM and IU During Thrust Buildup and Launch

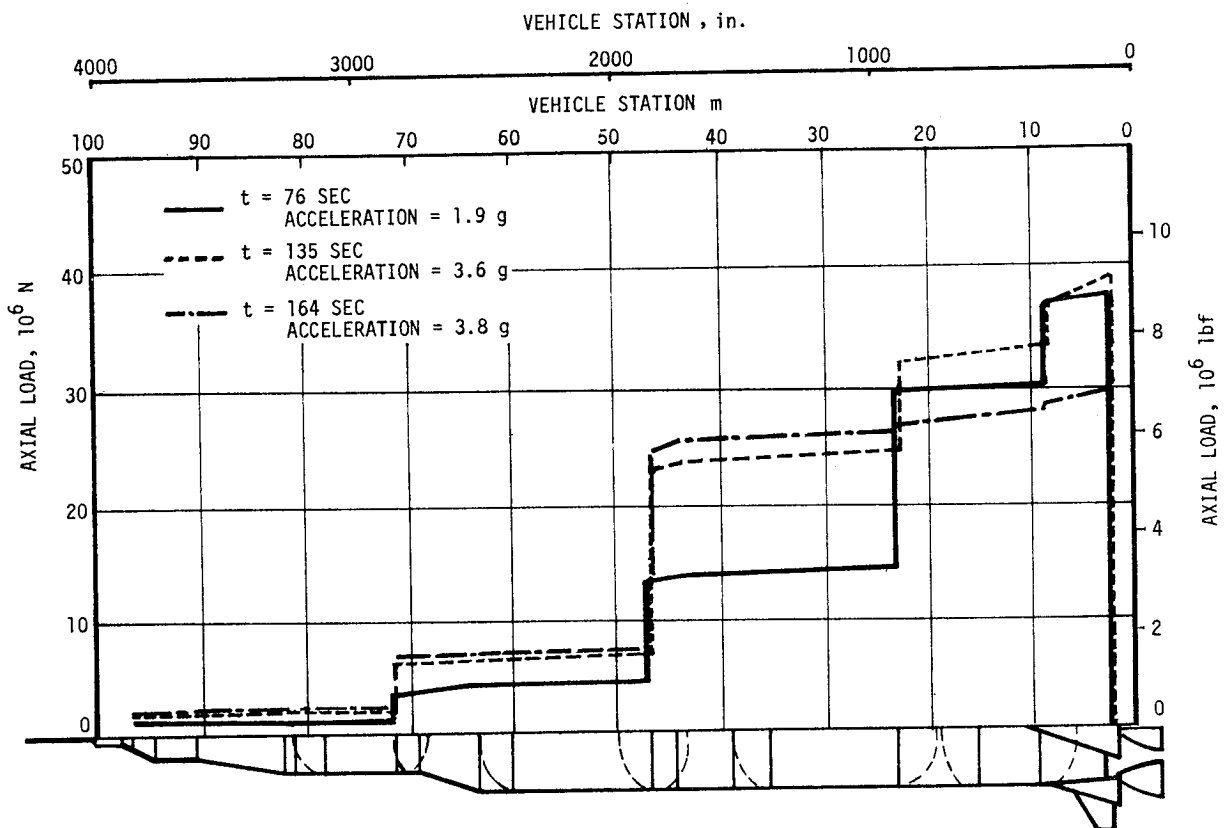


Figure 8-2. Longitudinal Load at Time of Maximum Bending Moment, CECO and OECO

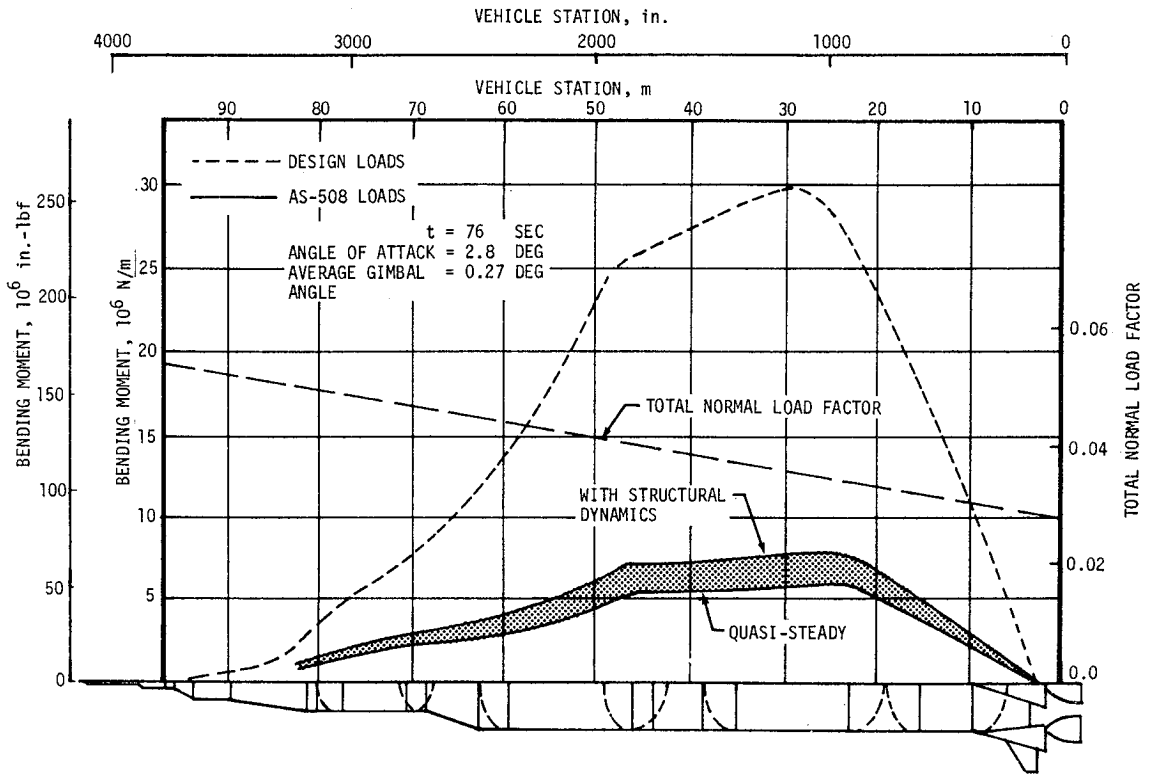


Figure 8-3. Maximum Bending Moment Near Max Q

This is appreciably less than the peak amplitude of  $\pm 0.07$  g measured on AS-507. Spectral analysis of chamber pressure measurements show no detectable buildup of structural/propulsion coupled oscillations. POGO did not occur during S-IC boost.

The AS-508 S-IC CECO and OECO transient responses shown in Figure 8-5 were similar to those of previous flights. The maximum dynamics at the IU resulting from CECO was  $\pm 0.20$  g. At OECO a maximum dynamic longitudinal acceleration of  $\pm 0.28$  g and  $\pm 0.85$  g was measured at the IU and CM, respectively.

AS-508 experienced low frequency (14 to 16 hertz) POGO oscillations during S-II stage boost. Three distinct periods of structural/propulsion coupled oscillations exhibited peaks at 180, 250, and 330 seconds. The third period of oscillations resulted in LOX pump discharge pressure variations of sufficient magnitude to activate the center engine thrust OK pressure switches and shut down the engine 132 seconds early. All oscillations decayed to a normal level following CECO.

Analysis shows that the vibration environment observed on AS-508 was similar to AS-507 during S-II stage burn prior to 327 seconds, see Figures 8-6 and 8-7. The oscillations are also apparent in the propulsion parameters as shown in Figures 8-8 and 8-9.

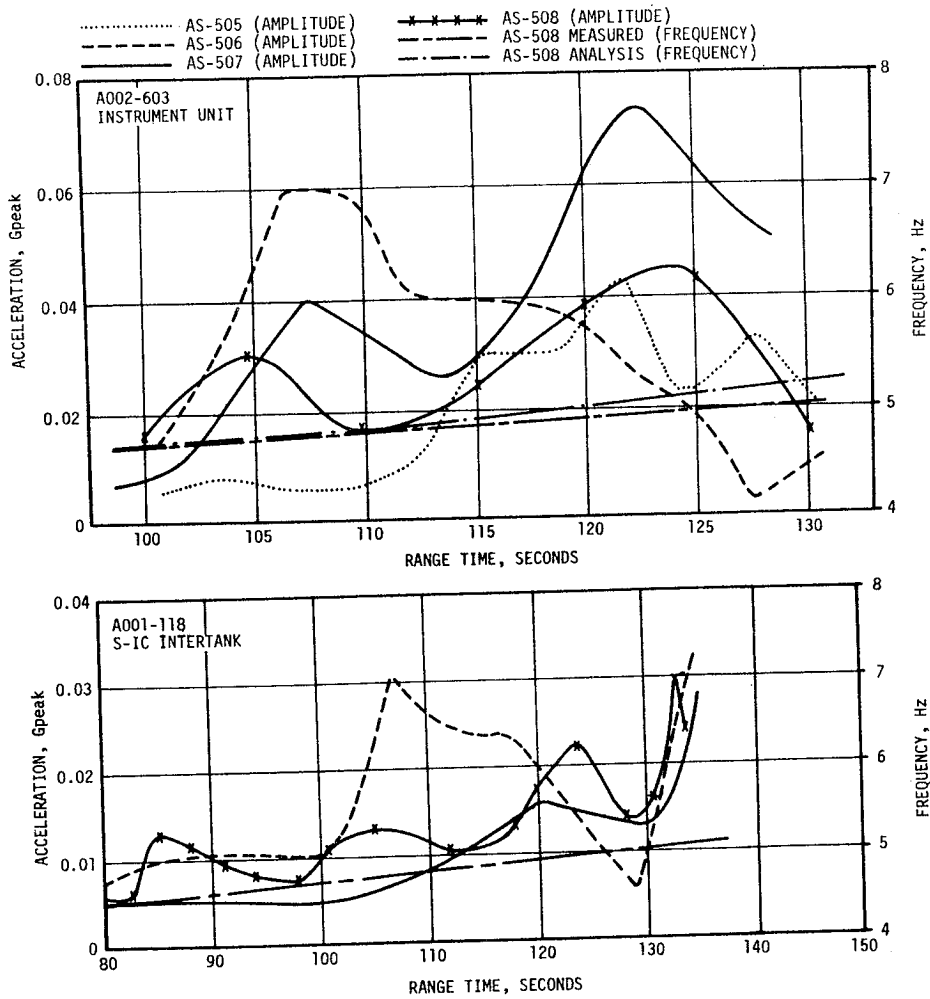


Figure 8-4. Comparison of Longitudinal Responses During S-IC Boost

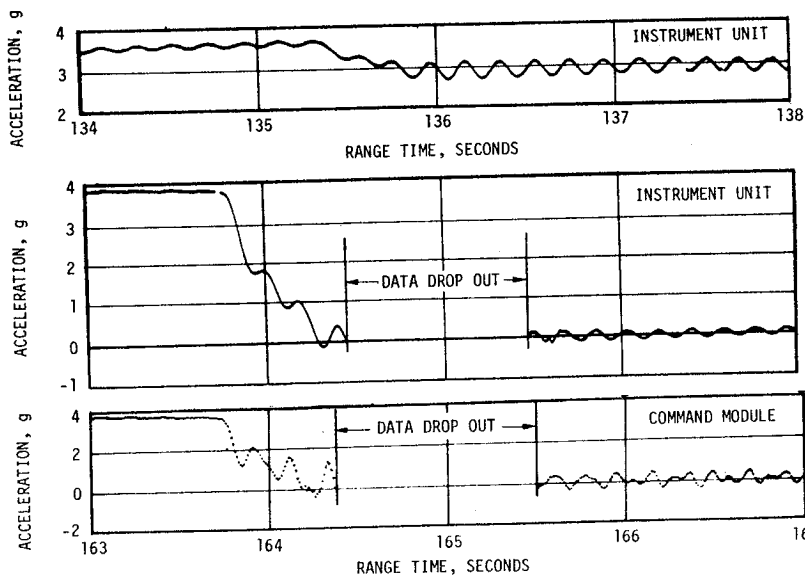


Figure 8-5. Longitudinal Acceleration at CM and IU at S-IC CECO and OECO

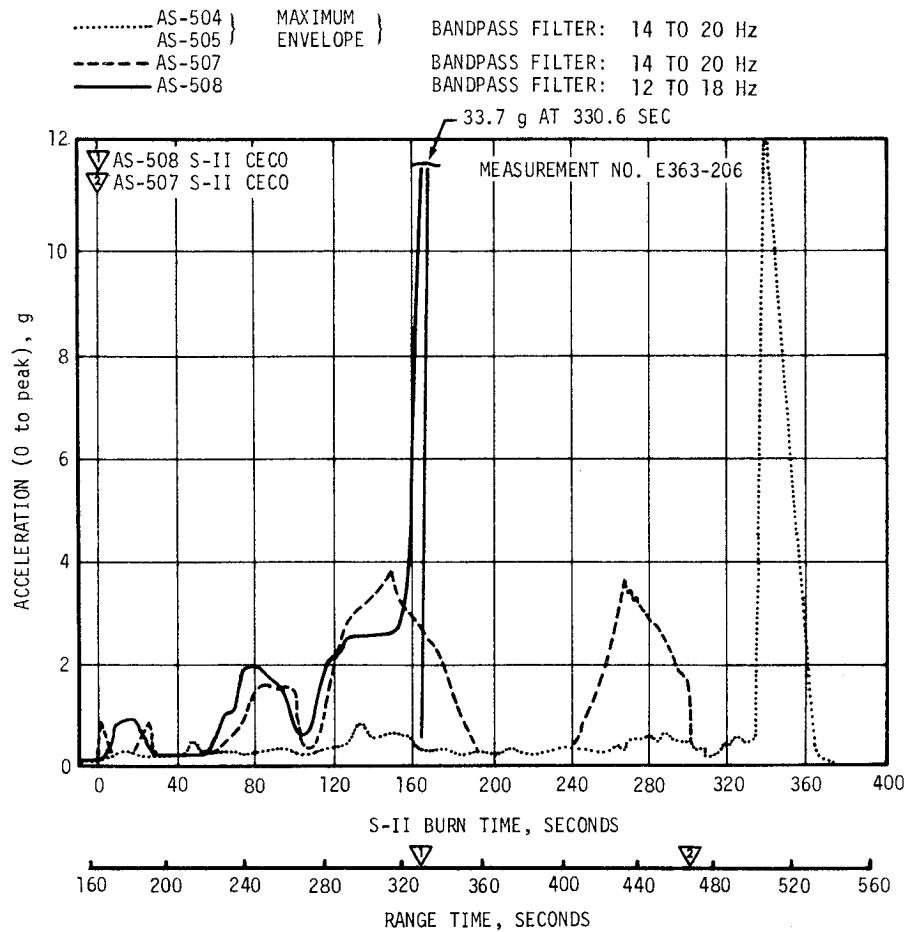


Figure 8-6. Comparison of S-II Engine No. 5 Thrust Pad Acceleration With Previous Flights

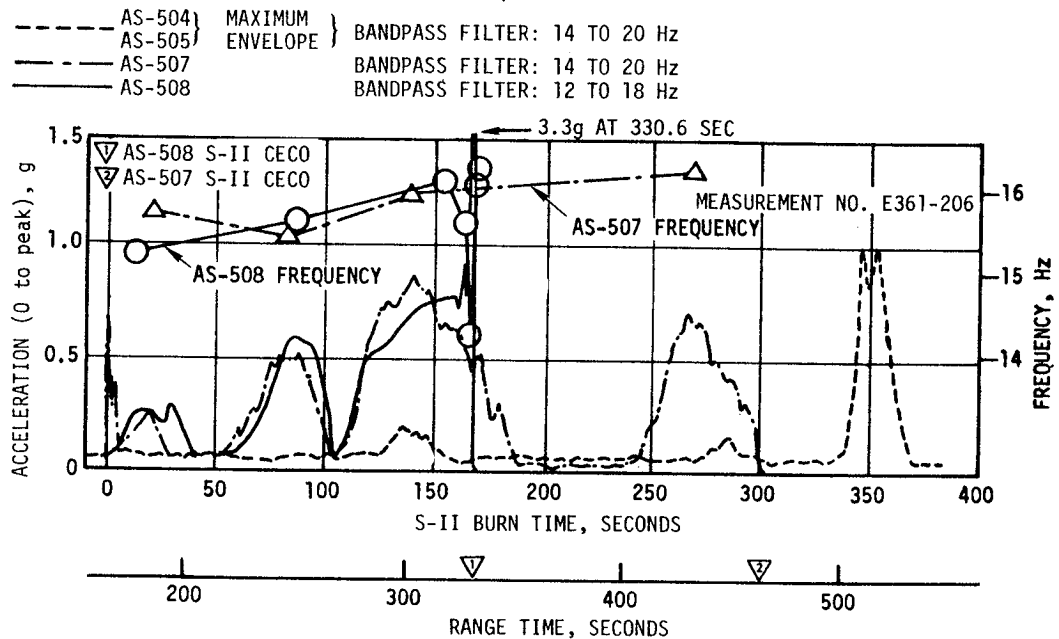


Figure 8-7. Comparison of S-II Engine No. 1 Thrust Pad Acceleration With Previous Flights

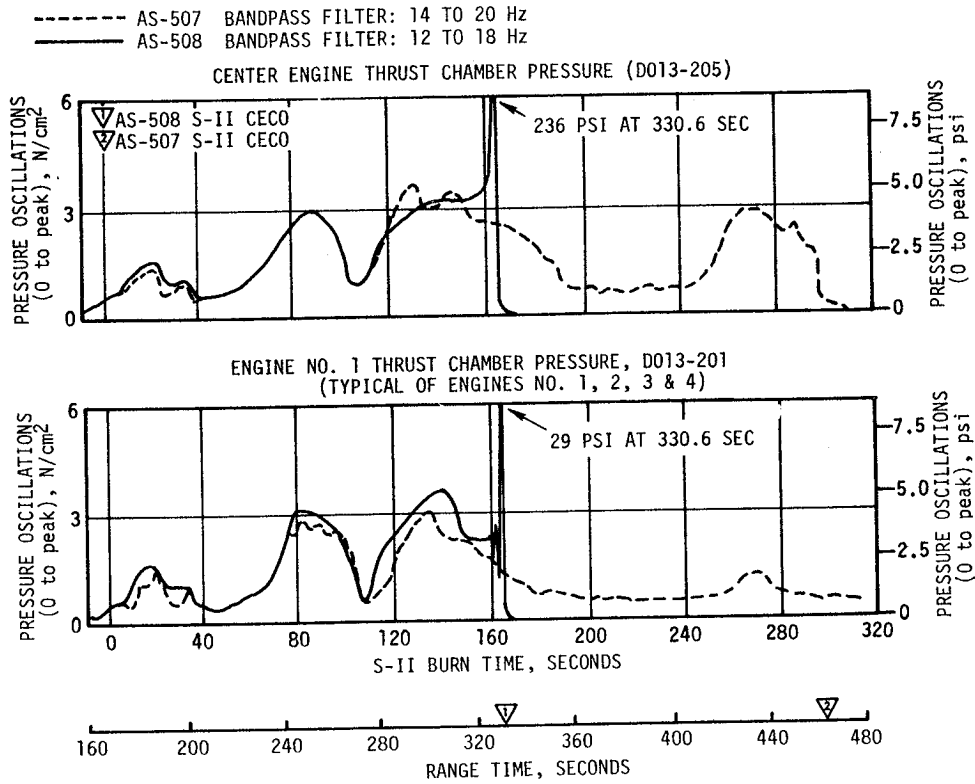


Figure 8-8. S-II Pre-CECO Thrust Chamber Pressure Characteristics

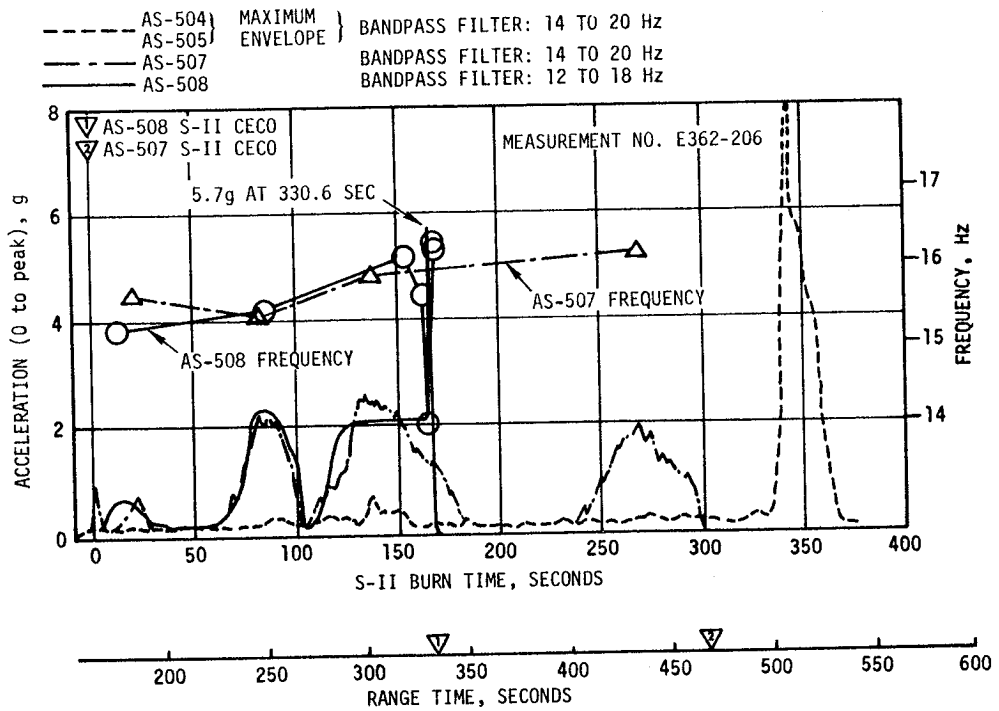


Figure 8-9. Comparison of S-II LOX Sump Acceleration With Previous Flights

Oscillations similar to those experienced on AS-507 had been expected on AS-508 because both configurations had similar dynamic response characteristics. However, at 327 seconds the center engine LOX inlet pressure dropped, indicating a growth of the cavitation field (see Figure 8-10). Oscillations started building up around the POGO loop following the pressure drop, as shown in Figure 8-11. By 329 seconds the inlet pressure amplitudes had exceeded  $\pm 20$  psi, and the pump was in deep cavitation. At this point, engine gain (ratio of engine thrust oscillations to LOX inlet pressure oscillations) had increased from 85 to 200 lb/psi, triggering a rapid divergence (see Figure 8-12).

At 330 seconds the crossbeam oscillations reached a peak amplitude of approximately  $\pm 33.7$  g. The 20 g peak accelerometer was saturated at this point so the acceleration levels are reconstructed values. Corresponding chamber pressure oscillations of approximately  $\pm 236$  psi (Figure 8-8) reflected LOX pump discharge oscillations of sufficient magnitude to trip the thrust OK pressure switches, and shut off the center engine. The crossbeam limit load was exceeded during peak oscillations, however, data show that no structural or engine failures occurred as a result of the oscillations.

The only significant difference between AS-507 and AS-508 that can be related to the divergent oscillations was an approximate 3 psi difference in Net Positive Suction Pressure (NPSP). This was due mostly to an approximate 3 psi reduction in LOX ullage pressure on AS-508 (see Figure 8-13), about 2 psi lower than predicted. The lower NPSP decreased the inboard line frequency (see Figure 8-14), which increased line gain by approximately 20 percent. The lower NPSP also reduced phase lag through the engines by 10 degrees. Both of these changes seen in the flight data are confirmed by ground test results.

The net effect of these two changes raised the inboard loop gain by 2 decibels. It also allowed the outboard loop to contribute half of the total forcing function out to 327 seconds. By comparison, the AS-507 outboard loop contribution dropped from 50 percent of the total to 20 percent between 300 and 310 seconds, as shown in Figure 8-15. At this time, the AS-507 oscillations started to decay.

The character of the changes indicate that the reduced ullage pressure contributed to making the AS-508 vehicle more unstable than AS-507 brought it to the point of cavitation, where divergent oscillations began. These oscillations then took over to force the system deeper into cavitation and thus to the  $\pm 33.7$  g level recorded on the crossbeam at CECO. The ullage pressure difference is considered to be only one of many S-II stage-to-stage minor variations that could contribute to the type of instability experienced on AS-508. Although slightly lower than predicted, the S-II LOX ullage pressure was well within the established limits prior to the time the large vibrations occurred.

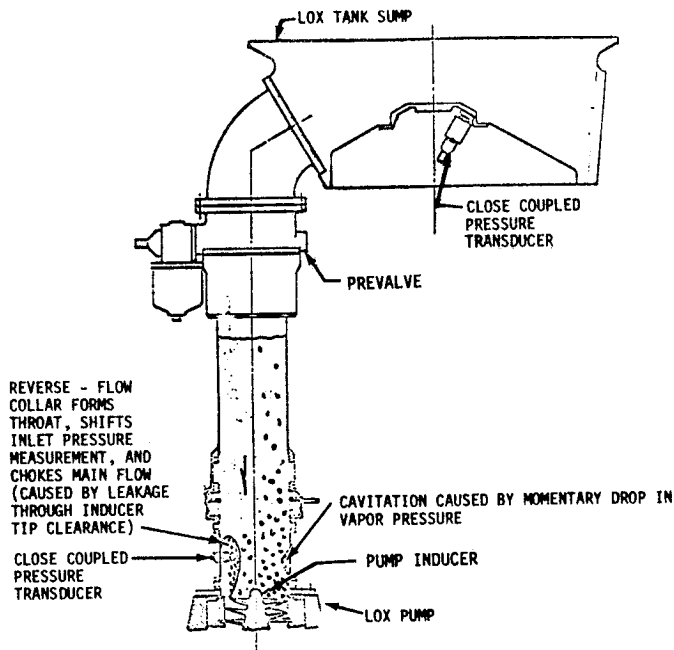


Figure 8-10. S-II Stage Center Engine LOX Feed System

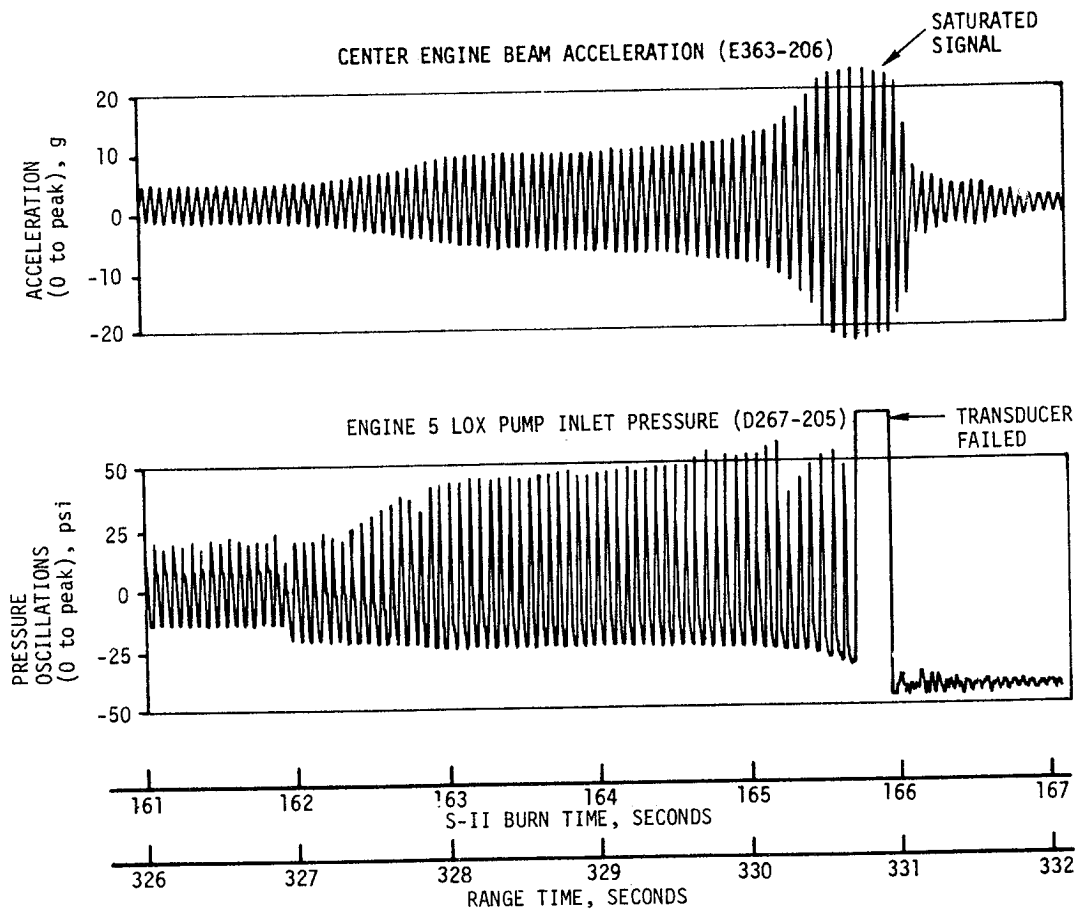


Figure 8-11. Center Engine LOX Pump Inlet Pressure Shift and Beam Vibration

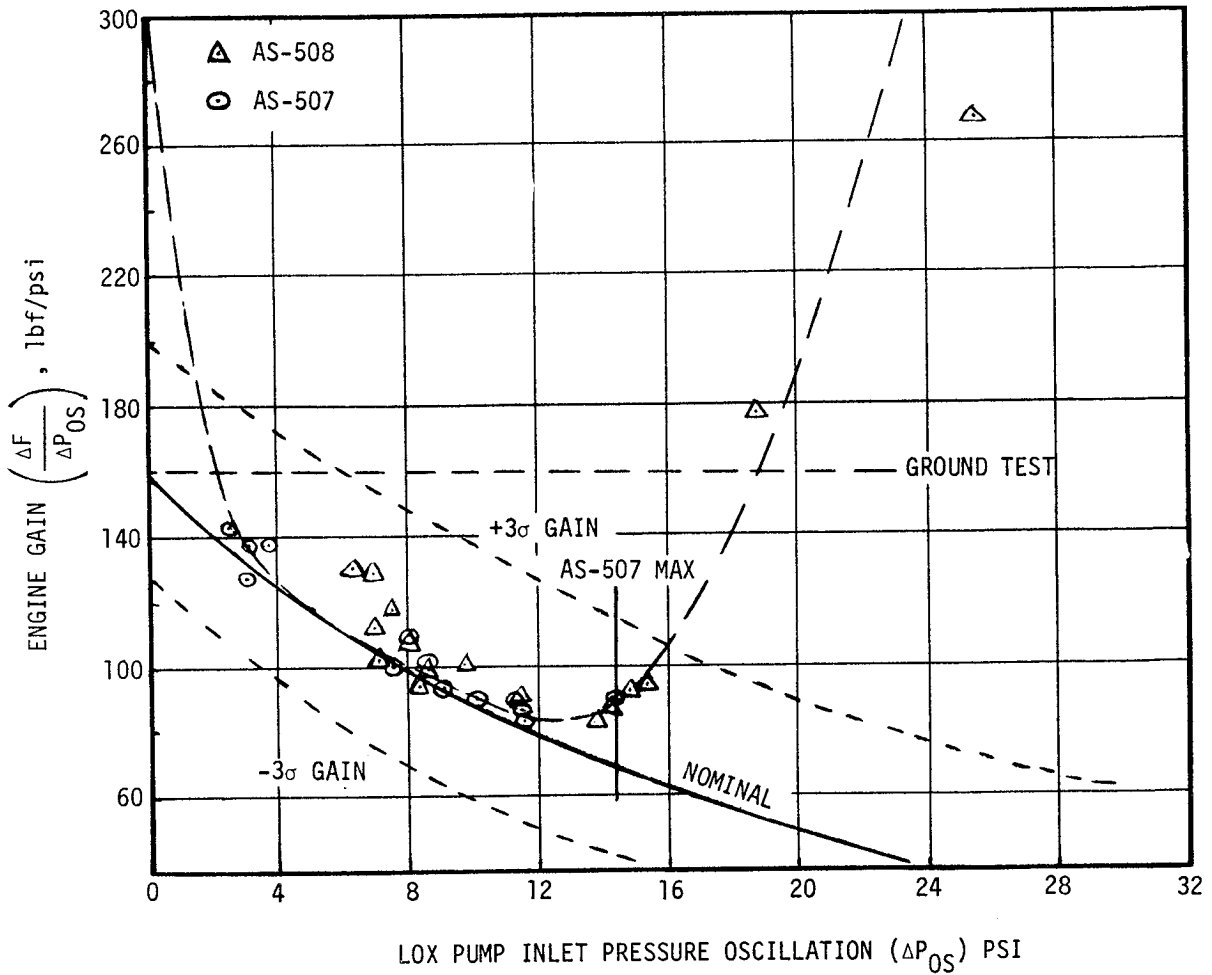


Figure 8-12. Center Engine Gain During S-II Oscillations

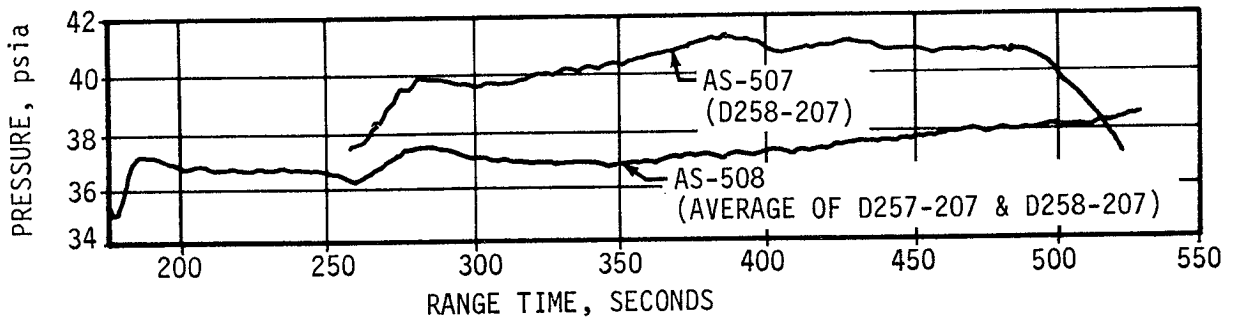


Figure 8-13. S-II LOX Ullage Pressure

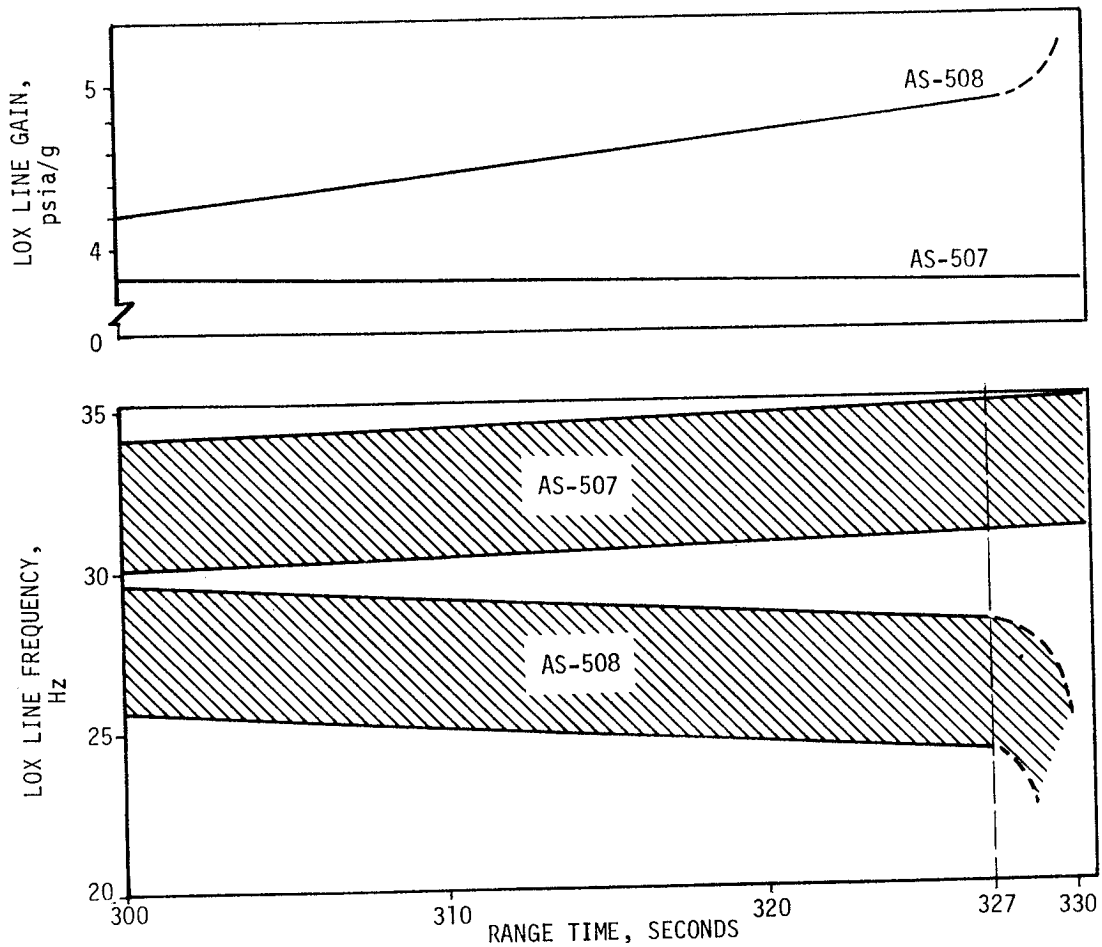


Figure 8-14. Comparison of AS-507/AS-508 S-II Engine No. 5 LOX Line Characteristics

- ▽ AS-508 CECO
- ▽ AS-507 CECO
- $\vec{F}$  = engine thrust vector
- $\vec{V}$  = thrust pad velocity vector

$$\text{PERCENT OUTBOARD} = \frac{4 \vec{F}_0 \cdot \vec{V}_0}{\vec{F}_I \cdot \vec{V}_I + 4 \vec{F}_0 \cdot \vec{V}_0}$$

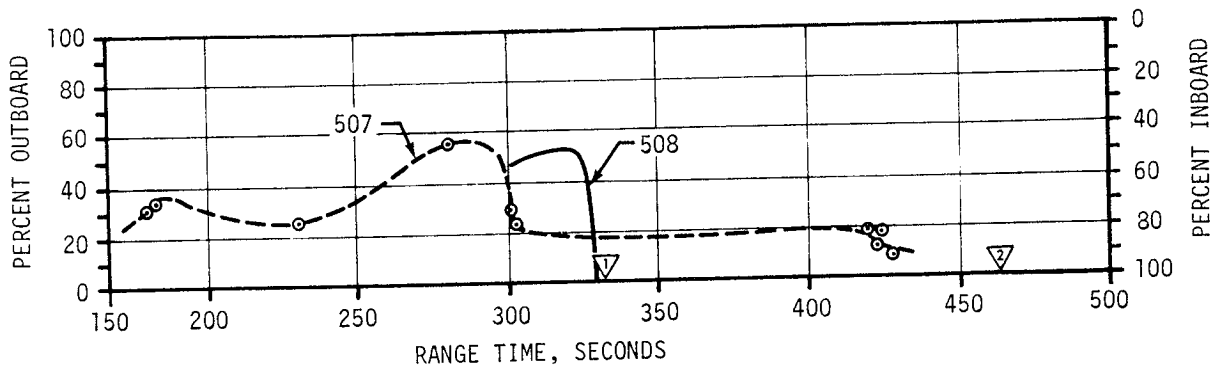


Figure 8-15. S-II Engine Inboard/Outboard Power Ratio

North American Rockwell (Space Division and Rocketdyne) does not agree that the reduced LOX tank ullage pressure made a significant contribution to the change in the dynamic response of the LOX feed system. They have offered the hypothesis that the generation of bubbles at the pump inlet is keyed to a specific vibration level on the center engine cross-beam. While such a phenomenon has been created in the laboratory at levels of vibration of one or two orders of magnitude higher than the 3 to 4 g observed just prior to the AS-508 instability, it is considered doubtful that this mechanism alone explains the difference in behavior between AS-507 and AS-508. A review of the crossbeam vibration levels shows that similar magnitudes were observed on AS-507 at the same time in flight and that similar levels had been reached and maintained for several seconds on AS-508 prior to the time that the gross instability occurred. As Rocketdyne contends, it is true that the small difference in NPSP would have a minor effect on the overall system stability; but, inasmuch as the system is marginally stable to begin with, only a minor change is necessary for the loop to become unstable. NAR has not proposed an explanation for the different behavior of AS-508 other than a random response to the vibration levels on the order of 3 to 4 g. In any case, the effect of the mechanism was to increase the compliance of the LOX feed system (lowering the inboard LOX line natural frequency) to where there was a high degree of coupling between the feed system and the crossbeam. The actual mechanism which caused the increase in compliance is not important to the solution of the problem, since the planned fix, installation of an 850 cu in. accumulator on the inboard LOX line, renders any typical variations in system compliance (an estimated 100 cu in. on AS-508) unimportant.

The response of the CM during the period of peak oscillation has been reviewed and is shown in Figure 8-16. The peak response is about  $\pm 0.12$  g and is associated with the transient of CECO. This level is very near the  $\pm 0.11$  g for the GECO transient on AS-507. The CM environment during S-II stage burn was no more severe than during prior low frequency oscillations resulting from S-II stage operation.

An accumulator is being installed on the center engine LOX line in AS-509 to "de-tune" or uncouple the structural and propulsion system elements and thereby suppress oscillation buildup. The accumulator system has already been tested during static firings on S-II-10 and S-II-12. Examination of possible attendant problems using a center engine LOX accumulator is continuing, along with an intense review of the characteristics of the low frequency oscillation phenomena.

The POGO Working Group also recommended the study of limit monitor systems which would provide for automatic engine shutdown if response levels exceed predetermined levels. The concept is such that a vibration detection system would monitor structural response and would initiate cutoff if vibrations approached a dangerous level. Of several proposed systems, the leading candidates are two systems based on; a G Limit Switch Accelerometer, and a Piezoelectric type Accelerometer. The only function of the vibration

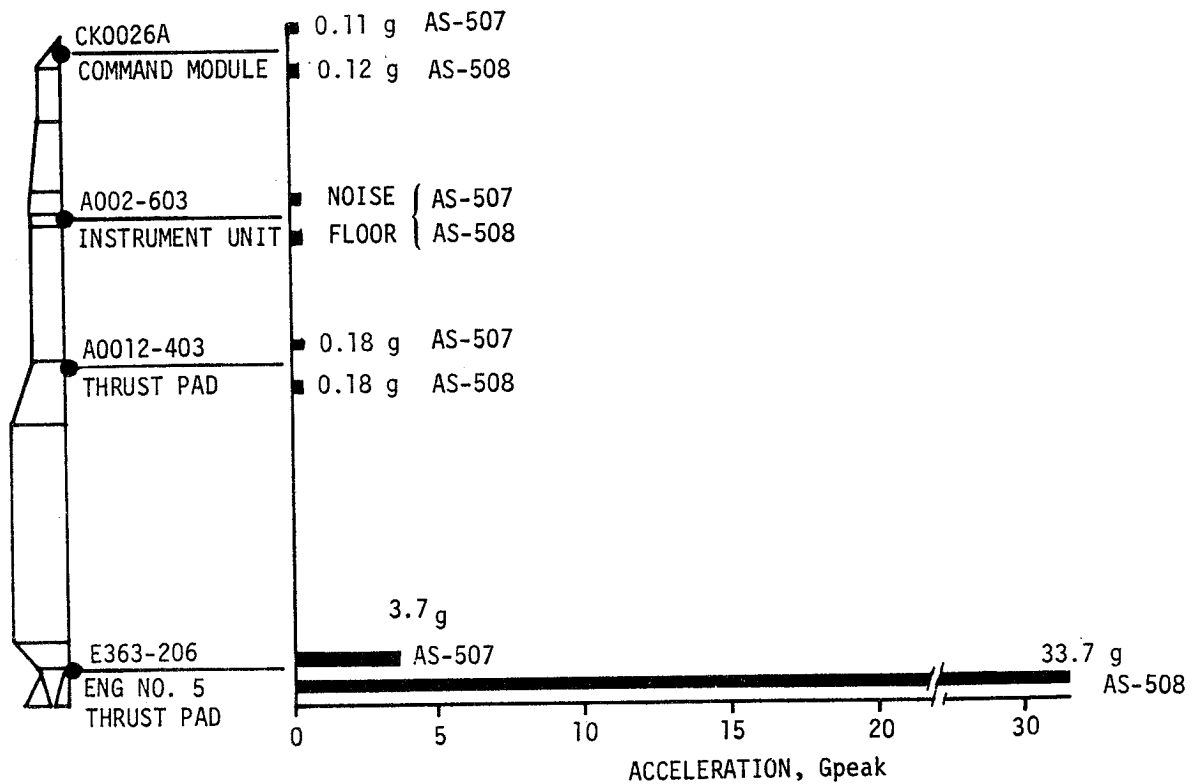


Figure 8-16. AS-508/AS-507 Longitudinal Acceleration Response Comparison During S-II Oscillations

detection system would be to preclude a Category 1 failure in the event that the accumulator system should perform in an unexpected manner.

Analysis of AS-507 and AS-508 flight data shows that oscillations of very low amplitude in a frequency band of 20 to 22.5 hertz are evident throughout S-II burn. The AS-508 peak oscillations ( $\pm 0.15$  g) were noted on engine No. 1 thrust pad between 548 and 558 seconds. The peak amplitude outside of this 10 second interval was approximately  $\pm 0.06$  g. A stability analysis shows a very weak 21 hertz instability at about the 30 inch LOX liquid level. The oscillations were confined to the aft section of the S-II stage and did not transmit up the vehicle.

Prior flights have noted the existence of 10 to 11 hertz low level oscillations just prior to OECO. This same phenomenon was noted on AS-508 with the amplitudes being higher than on AS-507. The peak response of  $\pm 0.27$  g recorded on the LOX sump was approximately double the  $\pm 0.12$  g level measured on AS-507 as noted in Figure 8-17. A stability analysis shows a weak 11 hertz instability late in the S-II burn.

Both the 11 and 21 hertz oscillations are confined to the outboard structural/propulsion coupled loop and are not harmonically coupled to each other. Neither of these responses are affected by the addition of the accumulator to the center engine LOX line. Evaluation of these two responses is continuing.

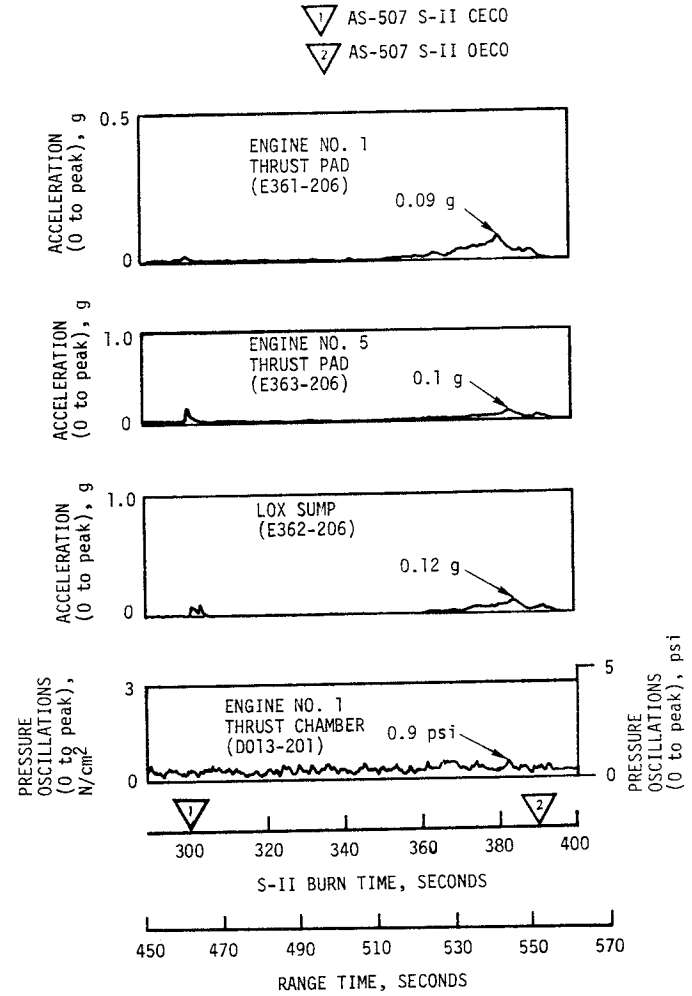
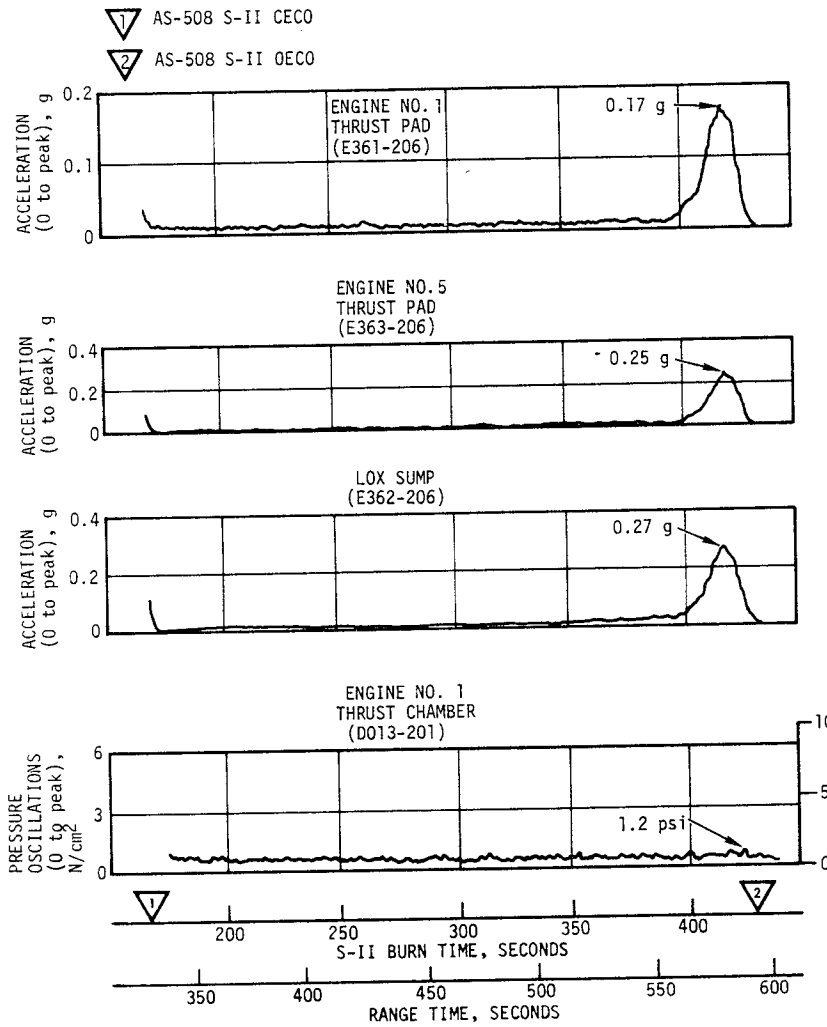


Figure 8-17. AS-508/AS-507 Acceleration and Pressure Characteristics From S-II CECO to OECO (8 to 14 Bandpass Filter)

During S-IVB first burn, low frequency (18 to 20 hertz) longitudinal oscillations similar to those observed on previous flights were again evident on AS-508. The AS-508 amplitudes ( $\pm 0.05$  g at gimbal block) were well below the maximum measured on AS-505 ( $\pm 0.30$  g) and within the expected range of values. Spectral analysis shows the structural mode frequency present in the LOX pump inlet and chamber pressures (Figure 8-18). However, there is no significant buildup in the chamber pressure at the structural frequency.

During S-IVB second burn, intermittent 12 to 14 hertz oscillations were measured beginning approximately 90 seconds prior to cutoff. The oscillations peaked approximately 10 seconds prior to cutoff with  $\pm 0.07$  g measured at the gimbal pad. This compares to  $\pm 0.12$  g on AS-507. Spectral analysis of the gimbal acceleration and chamber pressures reveal two closely spaced frequencies present in both measurements (Figure 8-19). The two frequencies have been identified as two coupled modes (longitudinal/pitch and longitudinal/yaw) with natural frequencies approximately 0.5 hertz apart. The coupling of these two modes produced the beating phenomenon observed in the data. This characteristic was observed on past S-IVB flights near second burn cutoff.

### 8.3 VIBRATION EVALUATION

One skin and two stringer vibration measurements were made on the S-IVB aft interstage during the AS-508 flight. Figure 8-20 shows that the vibration levels were slightly lower than measured on AS-507. The maximum levels occurred at liftoff and during the Mach 1 to Max Q flight period, as expected.

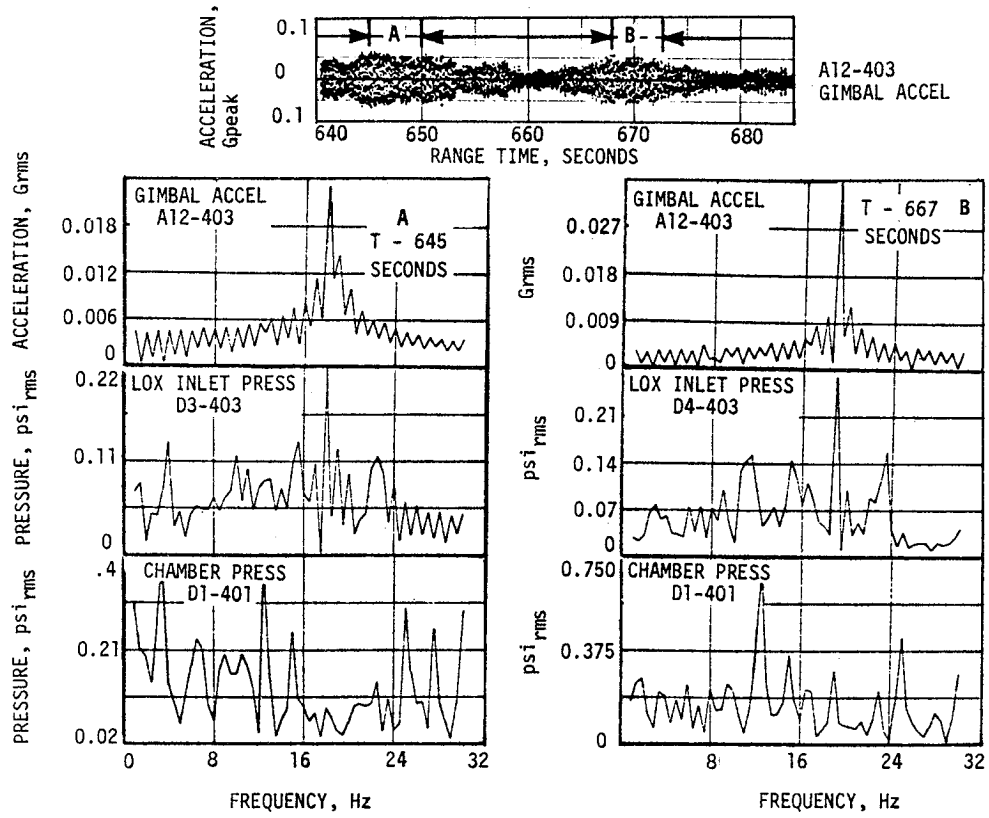


Figure 8-18. S-IVB First Burn Spectral Analyses

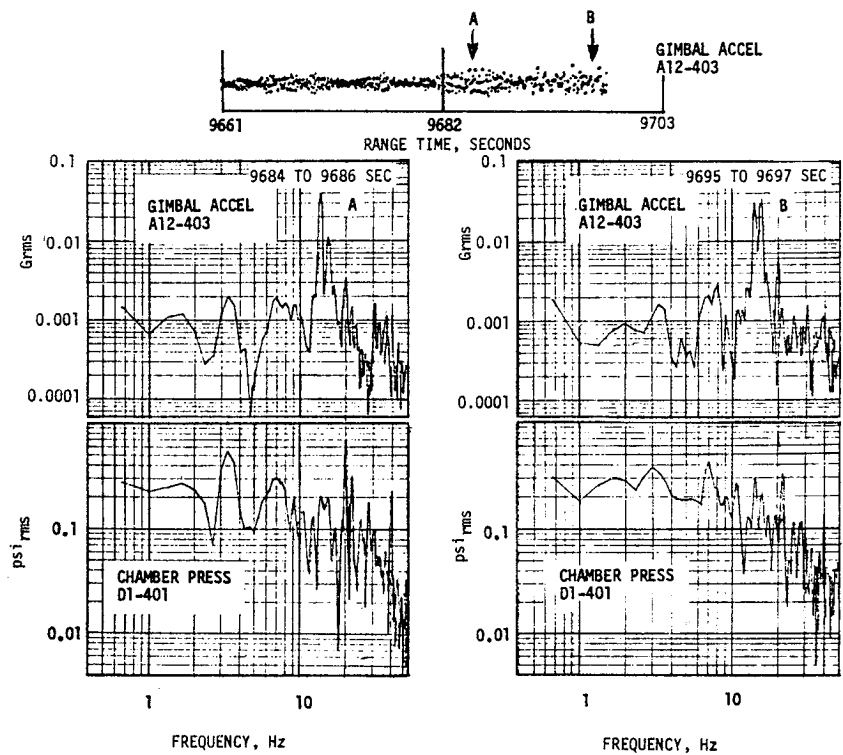


Figure 8-19. S-IVB Second Burn Spectral Analyses

81-8/71-8

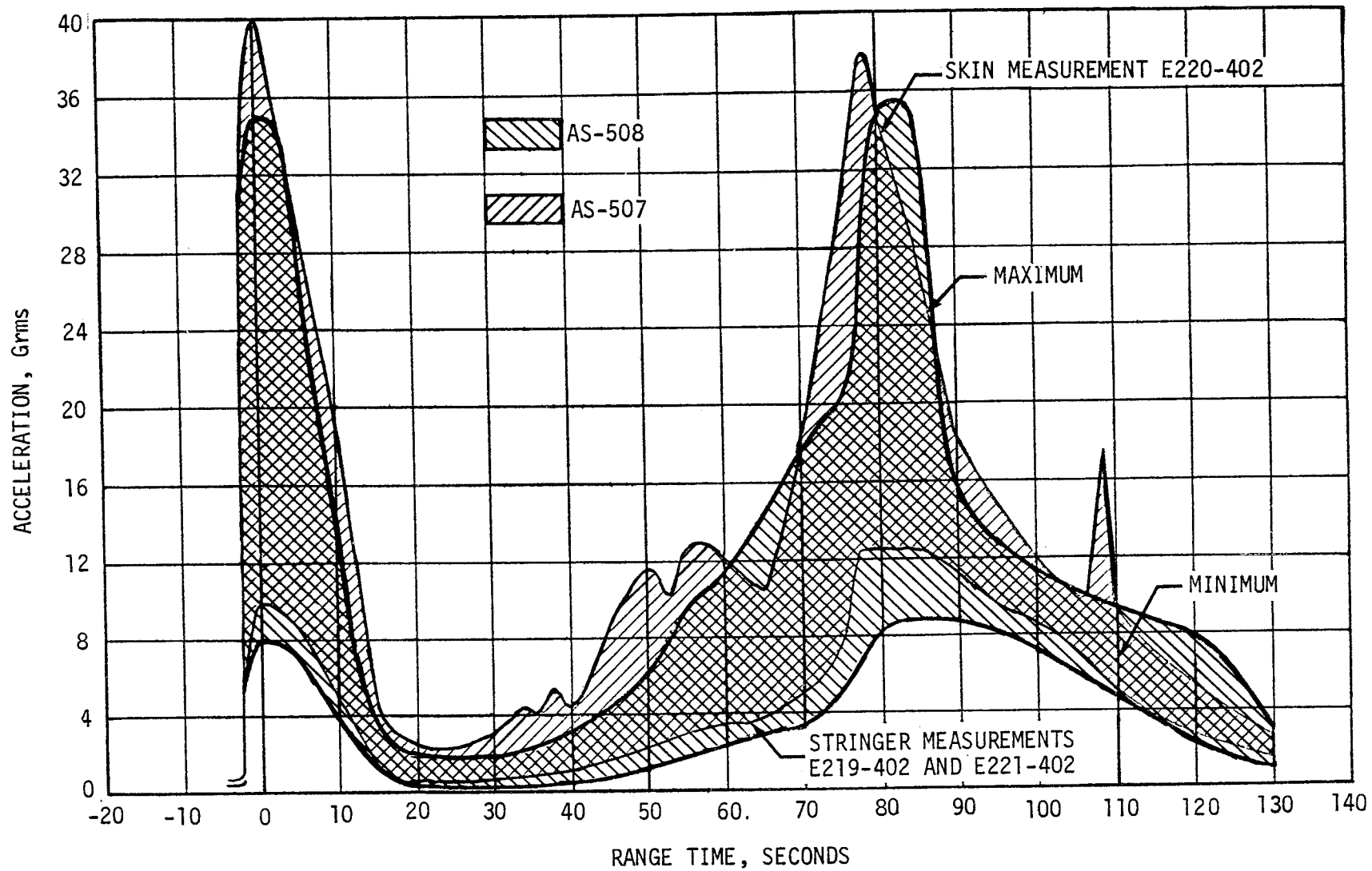


Figure 8-20. S-IVB Aft Interstage Skin and Stringer Vibration



## SECTION 9

### GUIDANCE AND NAVIGATION

#### 9.1 SUMMARY

##### 9.1.1 Performance of the Guidance and Navigation System as Implemented in the Flight Program

The guidance and navigation system performed satisfactorily throughout the mission. The parking orbit and Translunar Injection (TLI) parameters were within 3-sigma tolerances.

Guidance parameters were modified to compensate for the early S-II Center Engine Cutoff (CECO), and the S-IVB burn was lengthened to compensate for the additional gravity losses during S-II burn.

##### 9.1.2 Instrument Unit Components

The Launch Vehicle Digital Computer (LVDC), the Launch Vehicle Data Adapter (LVDA), and the ST-124M-3 inertial platform functioned satisfactorily. Crossrange velocity as measured by the inertial platform, exhibited a negative shift of approximately 0.65 m/s (2.13 ft/s) at approximately 3.4 seconds, introducing a 0.5 m/s (1.64 ft/s) velocity error. The velocity shift probably resulted from the accelerometer head momentarily contacting a mechanical stop due to the high vibration levels after liftoff. The effect on navigational accuracy was negligible. A similar crossrange velocity shift was exhibited on AS-506.

At 68,948 seconds (19:09:08), the LVDC exhibited a memory failure due to 6D10 battery depletion, and the flight program essentially ceased operation.

#### 9.2 GUIDANCE COMPARISONS

The postflight guidance error analysis was based on comparisons of the ST-124M-3 platform system measured velocities with the final postflight trajectory established from external tracking data (see paragraph 4.2). Velocity differences for boost-to-Earth Parking Orbit (EPO) are shown in Figure 9-1. A positive difference indicates trajectory data greater

than the platform measurement. The velocity differences at S-IVB first Engine Cutoff (ECO) were 1.27 m/s (4.17 ft/s), 3.64 m/s (11.94 ft/s), and -0.35 m/s (-1.15 ft/s), for vertical, crossrange, and downrange velocities, respectively. These differences are relatively small and well within the accuracy of the compared data and the preflight measured hardware errors. The 3.64 m/s (11.94 ft/s) difference in crossrange velocity includes an initial bias in the platform measured value of at least 0.5 m/s (1.64 ft/s), discussed in paragraph 9.4.2. Since the measured velocities were used to construct the postflight trajectory, the difference curve does not show the initial bias as such, however, the guidance velocities were constrained to tie in with tracking data after the vehicle reached sufficient altitude for the tracker to pick up track.

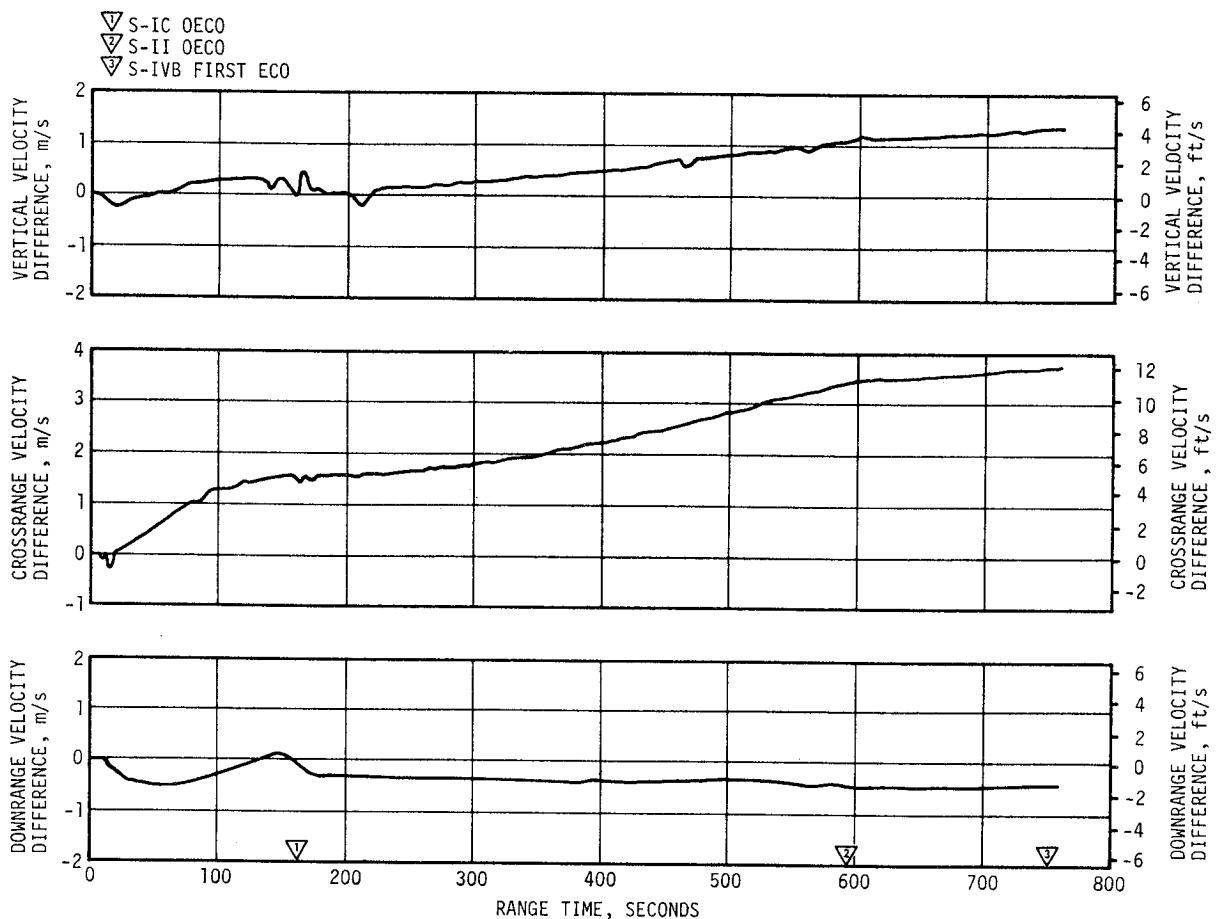


Figure 9-1. Trajectory and ST-124M-3 Platform Velocity Comparison Boost-to-EPO (Trajectory Minus Guidance)

The platform velocity comparisons for the S-IVB second burn are shown in Figure 9-2. Although the postflight trajectory during this period of flight was constructed using the measured velocities, the difference profiles are consistent with those for the boost-to-parking orbit trajectory. The vehicle was essentially flying along the platform vertical axis during the second burn phase. The differences shown could be caused by a relatively small platform misalignment due to a pitch gyro drift. The velocity difference curves for both burn phases have been simulated with a combination of hardware errors that are well within preflight measurements and/or 3-sigma hardware errors.

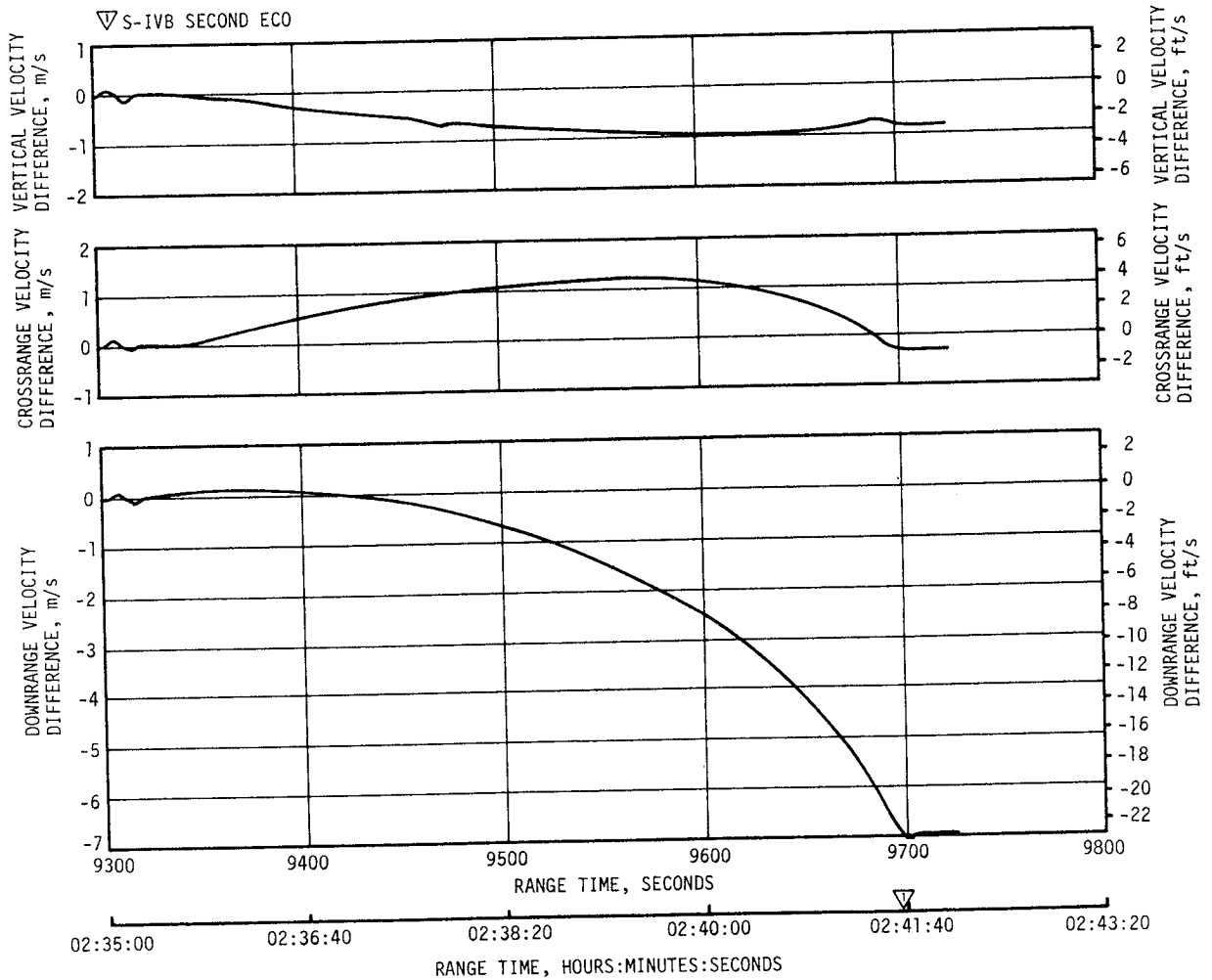


Figure 9-2. Trajectory and ST-124M-3 Platform Velocity Comparison Second S-IVB Burn

Platform velocity measurements at significant event times are shown in Table 9-1 along with corresponding values from both the postflight and Operational Trajectories (OT). The differences between the telemetered and postflight trajectory values reflect some combination of small guidance hardware errors and tracking errors. The differences between telemetered and OT values reflect differences between predicted and actual flight environment and vehicle performance. The values shown for the S-IVB second burn mode represent velocity change from Time Base 6 ( $T_6$ ) to TLI. The characteristic velocity determined from the platform velocities during the second burn was very close to nominal. LVDC characteristic velocity was 0.24 m/s (0.79 ft/s) higher than the postflight trajectory and 0.09 m/s (0.29 ft/s) lower than the OT. However, the LVDC velocity increase due to thrust decay after S-IVB cutoff was about 0.75 m/s (2.46 ft/s) higher than the OT.

Comparisons of navigation (PACSS 13 coordinate system) positions, velocities, and flight path angle are shown for significant flight event times in Table 9-2. The guidance (LVDC) and postflight trajectory values are in good agreement for the boost-to-parking orbit burn mode. Approximately 500 meters (1640 ft) of the crossrange position error may be attributed to the initial velocity bias. The total position and velocity differences are well within expected accuracy. The parking orbit trajectory was perturbed by a low vent thrust (the curve essentially follows the minimum predicted vent thrust) from time of orbital navigation (ECO +100 seconds) to approximately 2500 seconds (00:41:40) similar to AS-507 (see Figure 9-3). The state vector deviations at EPO together with low initial vent thrust caused oscillatory buildup in velocity component differences between the LVDC and postflight trajectory during parking orbit. At  $T_6$  the differences in geocentric radius and total velocity were -2847 meters (-9340 ft) and 2.24 m/s (7.35 ft/s), respectively. Table 9-3 presents the state vector differences at TLI between the LVDC and both the postflight trajectory and OT. The position component differences are large, but the velocities and geocentric radius are in good agreement.

### 9.3 NAVIGATION AND GUIDANCE SCHEME EVALUATION

The navigation and guidance functions were accomplished satisfactorily. The apparent crossrange velocity shift at liftoff, described in paragraph 9.4.2, had negligible effect on the overall navigational accuracy.

The Iterative Guidance Mode (IGM) phase times-to-go ( $T_{1I}$ ,  $T_{2I}$ , and  $T_{3I}$ ) and the performance indications ( $\tau_1$  and  $\tau_2$ ) were adjusted properly when the acceleration decreased at S-II CECO. The adaptability of the expanded IGM to an unexpected performance change was demonstrated by the modification of the guidance parameters independent of any engine-out discrete data. Had the flight program sensed no discretely indicating

Table 9-1. Inertial Platform Velocity Comparisons  
(PACSS 12 Coordinate System)

EVENT	DATA SOURCE	VELOCITY - M/S (FT/S)		
		VERTICAL ( $\dot{X}$ )	CROSSRANGE ( $\dot{Y}$ )	DOWN RANGE ( $\dot{Z}$ )
S-IC OECO	Guidance (LVDC)	2612.26 (8570.41)	12.20 (40.03)	2231.33 (7320.64)
	Postflight Trajectory	2612.13 (8569.97)	13.66 (44.82)	2230.59 (7318.20)
	Operational Trajectory	2604.90 (8559.87)	-1.83 (-5.99)	2242.12 (7356.05)
S-II OECO	Guidance (LVDC)	3645.04 (11,958.79)	-9.38 (-30.77)	6785.00 (22,260.50)
	Postflight Trajectory	3646.13 (11,962.36)	-6.01 (-19.72)	6784.55 (22,259.04)
	Operational Trajectory	3480.13 (11,417.73)	-2.96 (-9.72)	6810.35 (22,343.67)
S-IVB First Cutoff	Guidance (LVDC)	3374.44 (11,071.00)	3.95 (12.96)	7648.50 (25,093.50)
	Postflight Trajectory	3375.71 (11,075.15)	7.59 (24.90)	7648.15 (25,092.37)
	Operational Trajectory	3232.05 (10,603.84)	1.90 (6.22)	7610.45 (24,968.66)
Parking Orbit Insertion	Guidance (LVDC)	3373.75 (11,068.73)	3.95 (12.96)	7650.20 (25,099.08)
	Postflight Trajectory	3375.09 (11,073.13)	7.68 (25.19)	7649.79 (25,097.75)
	Operational Trajectory	3231.45 (10,601.86)	1.91 (6.26)	7611.89 (24,973.38)
S-IVB Second Cutoff*	Guidance (LVDC)	3145.35 (10,319.39)	167.78 (550.46)	-232.29 (-762.11)
	Postflight Trajectory	3144.60 (10,316.92)	167.41 (549.27)	-239.34 (-785.26)
	Operational Trajectory	3145.92 (10,321.28)	166.77 (547.15)	-236.51 (-775.96)
Translunar Injection*	Guidance (LVDC)	3149.35 (10,332.51)	168.10 (551.51)	-232.00 (-761.15)
	Postflight Trajectory	3148.60 (10,330.06)	167.79 (550.50)	-239.03 (-784.24)
	Operational Trajectory	3149.18 (10,331.95)	167.04 (548.04)	-236.26 (-775.14)

\*Values represent velocity change from Time Base 6.

Table 9-2. Guidance Comparisons (PACSS 13)

EVENT	DATA SOURCE	POSITIONS METERS (FT)				VELOCITIES M/S (FT/S)				FLIGHT PATH ANGLE (DEG)
		X <sub>s</sub>	Y <sub>s</sub>	Z <sub>s</sub>	R	X <sub>s</sub>	Y <sub>s</sub>	Z <sub>s</sub>	V <sub>s</sub>	γ
S-IC OEEO	Guidance	6,438,518 (21,123,746)	40,068 (131,456)	160,856 (527,742)	6,440,652 (21,130,747)	849.53 (2787.17)	132.51 (434.74)	2606.48 (8551.44)	2744.63 (9004.69)	19.4777
	Postflight Trajectory	6,438,480 (21,123,621)	40,213 (131,932)	160,822 (527,632)	6,440,613 (21,130,621)	849.43 (2786.85)	134.07 (439.85)	2605.74 (8549.03)	2743.98 (9002.55)	19.4799
	Operational Trajectory	6,437,615 (21,120,785)	39,559 (129,787)	160,819 (527,621)	6,439,745 (21,127,773)	837.84 (2748.81)	118.61 (389.15)	2606.32 (8550.93)	2740.25 (8990.31)	19.2487
S-II OEEO	Guidance	6,234,157 (20,453,272)	82,467 (270,561)	2,043,886 (6,705,662)	6,561,173 (21,526,157)	-2073.51 (-6802.85)	77.34 (253.74)	6572.71 (21,564.01)	6892.46 (22,613.06)	0.6508
	Postflight Trajectory	6,234,306 (20,453,761)	83,525 (274,032)	2,043,735 (6,705,167)	6,561,281 (21,526,511)	-2072.43 (-6799.31)	80.36 (263.65)	6572.30 (21,562.68)	6891.78 (22,610.82)	0.6571
	Operational Trajectory	6,278,758 (20,599,599)	79,949 (262,301)	1,897,926 (6,226,792)	6,559,826 (21,521,738)	-1932.96 (-6341.72)	88.00 (288.70)	6684.35 (21,930.27)	6958.78 (22,830.63)	0.6990
First S-IVB ECO	Guidance	5,784,653 (18,978,521)	94,118 (308,787)	3,099,452 (10,168,807)	6,563,359 (21,533,329)	-3680.79 (-12,076.08)	73.00 (239.50)	6866.95 (22,529.36)	7791.57 (25,562.89)	-0.0016
	Postflight Trajectory	5,784,978 (18,979,586)	95,665 (313,860)	3,099,286 (10,168,261)	6,563,588 (21,534,083)	-3679.50 (-12,071.86)	76.10 (249.69)	6866.74 (22,528.67)	7790.80 (25,560.38)	0.0038
	Operational Trajectory	5,884,096 (19,304,776)	92,064 (302,048)	2,906,360 (9,535,303)	6,563,382 (21,533,407)	-3451.37 (-11,323.38)	76.80 (251.97)	6984.89 (22,916.29)	7791.43 (25,562.45)	-0.0006
Parking Orbit Insertion	Guidance	5,747,430 (18,856,397)	94,843 (311,165)	3,167,921 (10,393,440)	6,563,358 (21,533,326)	-3762.80 (-12,345.14)	71.87 (235.79)	6824.46 (22,389.96)	7793.40 (25,568.90)	-0.0003
	Postflight Trajectory	5,747,768 (18,857,508)	96,420 (316,338)	3,167,747 (10,392,870)	6,563,593 (21,534,099)	-3761.42 (-12,340.63)	74.97 (245.96)	6824.19 (22,389.09)	7792.53 (25,566.05)	0.0053
	Operational Trajectory	5,849,162 (19,190,164)	92,826 (304,548)	2,976,017 (9,763,834)	6,563,382 (21,533,407)	-3534.69 (-11,596.76)	75.63 (248.14)	6944.85 (22,784.93)	7792.99 (25,567.55)	0.0000
Time Base 6	Guidance	-5,481,236 (-17,983,058)	-103,293 (-338,888)	-3,619,347 (-11,874,499)	6,569,196 (21,552,480)	4291.66 (14,080.25)	-114.43 (-375.43)	-6503.00 (-21,335.30)	7792.34 (25,565.42)	0.0278
	Postflight Trajectory	-5,465,307 (-17,930,796)	-105,283 (-345,418)	-3,638,169 (-11,936,250)	6,566,349 (21,543,139)	4318.34 (14,167.78)	-116.95 (-383.70)	-6487.97 (-21,285.98)	7794.58 (25,572.76)	0.0175
	Operational Trajectory	-5,484,533 (-17,993,875)	-103,217 (-338,638)	-3,612,411 (-11,851,743)	6,568,126 (21,548,968)	4284.43 (14,056.52)	-115.04 (-377.41)	-6508.93 (-21,354.74)	7793.31 (25,568.60)	0.0299
Second S-IVB ECO	Guidance	1,209,140 (3,966,993)	-120,274 (-394,601)	-6,591,207 (-21,624,696)	6,702,276 (21,989,093)	10,819.55 (35,497.21)	215.77 (707.91)	624.17 (2047.80)	10,839.68 (35,563.25)	7.0703
	Postflight Trajectory	1,238,978 (4,064,888)	-122,694 (-402,538)	-6,584,901 (-21,604,005)	6,701,570 (21,986,777)	10,817.69 (35,491.11)	216.48 (710.23)	652.14 (2139.56)	10,839.49 (35,562.64)	7.1822
	Operational Trajectory	1,245,288 (4,085,590)	-120,094 (-394,010)	-6,588,245 (-21,614,978)	6,705,978 (22,001,240)	10,814.79 (35,481.60)	215.15 (705.89)	653.27 (2143.26)	10,836.64 (35,553.28)	7.2237
Translunar Injection	Guidance	1,317,280 (4,321,784)	-118,110 (-387,501)	-6,584,528 (-21,602,781)	6,716,039 (22,034,249)	10,806.88 (35,455.64)	217.62 (713.98)	711.54 (2334.45)	10,832.46 (35,539.57)	7.5229
	Postflight Trajectory	1,347,108 (4,419,645)	-120,517 (-395,398)	-6,577,940 (-21,581,169)	6,715,543 (22,032,623)	10,804.62 (35,448.23)	218.43 (716.63)	739.47 (2426.07)	10,832.10 (35,538.38)	7.6347
	Operational Trajectory	1,353,383 (4,440,233)	-117,932 (-386,917)	-6,581,275 (-21,592,111)	6,720,025 (22,047,327)	10,800.92 (35,436.10)	216.96 (711.82)	740.40 (2429.14)	10,828.44 (35,536.39)	7.6758

Table 9-3. State Vector Differences at Translunar Injection

PARAMETER	OPERATIONAL TRAJECTORY MINUS LVDC	POSTFLIGHT TRAJECTORY MINUS LVDC
$\Delta X_S$ , meters (ft)	36,103 (118,448)	29,928 (98,189)
$\Delta Y_S$ , meters (ft)	178 (584)	-2407 (-7897)
$\Delta Z_S$ , meters (ft)	3253 (10,672)	6588 (21,614)
$\Delta R$ , meters (ft)	3986 (13,077)	496 (1627)
$\dot{\Delta X}_S$ , m/s (ft/s)	-5.96 (-19.55)	-2.26 (-7.41)
$\dot{\Delta Y}_S$ , m/s (ft/s)	-0.66 (-2.16)	0.81 (2.66)
$\dot{\Delta Z}_S$ , m/s (ft/s)	28.86 (94.68)	27.93 (91.63)
$\Delta V_S$ , m/s (ft/s)	-4.02 (-13.19)	-0.36 (-1.18)

the cutoff of an engine, the guidance reaction would have been the same; the discrete is now employed only for setting a mode code bit for telemetry. In the version of IGM used last on AS-505, the reaction to a thrust-loss was initiated by sensing the engine-out discrete and sampling acceleration for three computation cycles to determine the validity of the discrete. With recognition of the discrete, the result is a slower reaction to thrust loss which perturbs the guidance outputs longer than in the expanded IGM.

The pitch and yaw guidance commands showing the reactions to the S-II CECO as well as the balance of first burn are shown in Figure 9-4. The second burn pitch and yaw guidance commands are shown in Figure 9-5.

Although the vehicle was inserted into parking orbit 44 seconds late, it was farther down range than predicted and, therefore, nearer the point at which  $T_6$  should begin. This difference in range angle caused

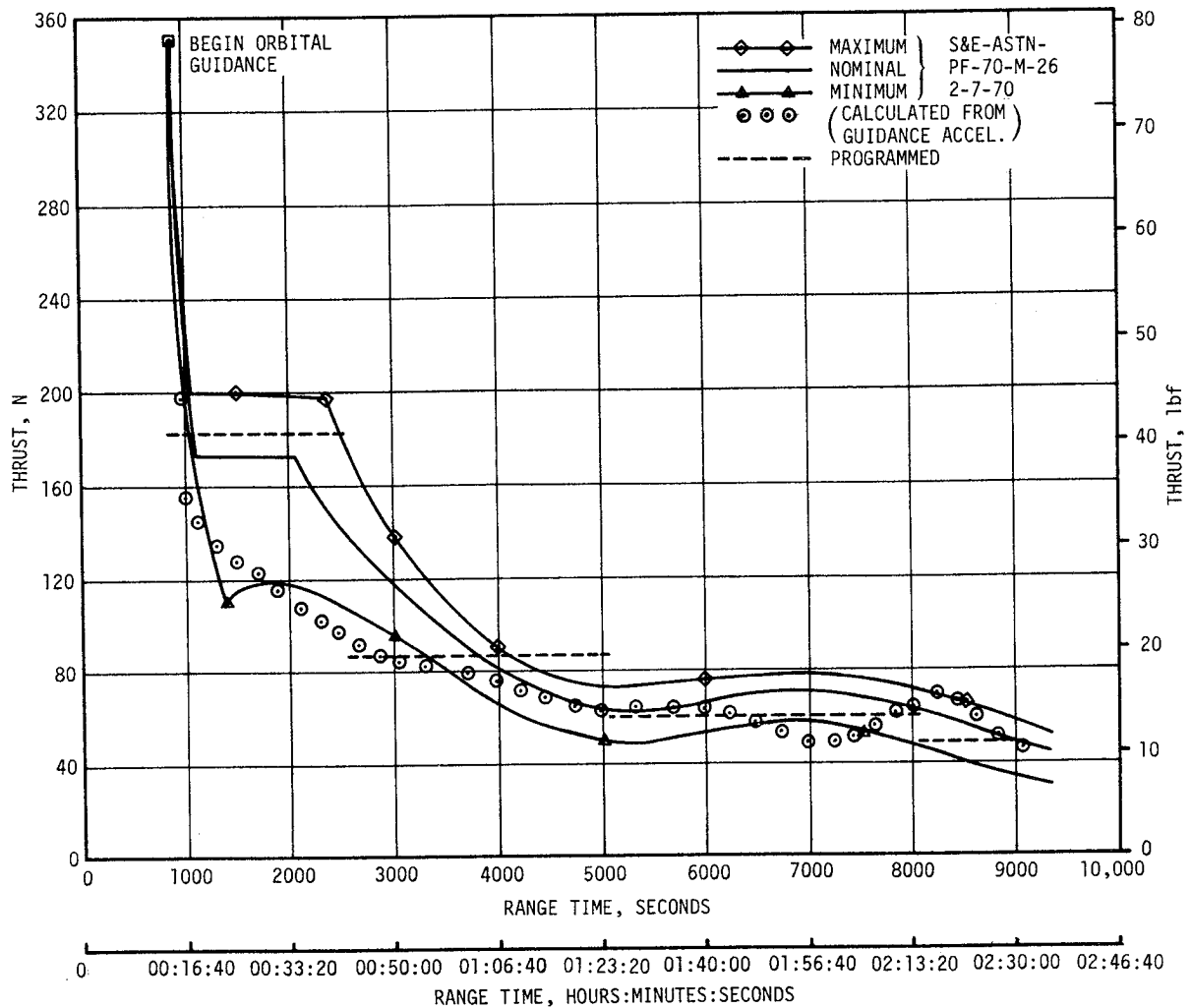


Figure 9-3. LH<sub>2</sub> Continuous Vent Thrust During Parking Orbit

the time from  $T_5$  to  $T_6$  to be 25.9 seconds less than predicted. The close agreement between achieved and targeted TLI parameters, as shown in Table 9-4, is indicative of satisfactory  $T_6$  initiation.

All orbital guidance functions were accomplished satisfactorily. At 49,353 seconds (13:42:33), an unplanned Transposition, Docking and Ejection (TD&E) maneuver was performed as discussed in paragraph 10.4.4. This maneuver was verified by postflight simulation. The inertial attitude acquired was quite different than that at the actual TD&E maneuver performed because the vehicle radius vector from earth was in a different direction relative to the inertial coordinate frame. From this occurrence at 49,353 seconds (13:42:33) until the program ceased functioning at 68,948 seconds (19:09:08), the vehicle attitude remained inertially fixed.

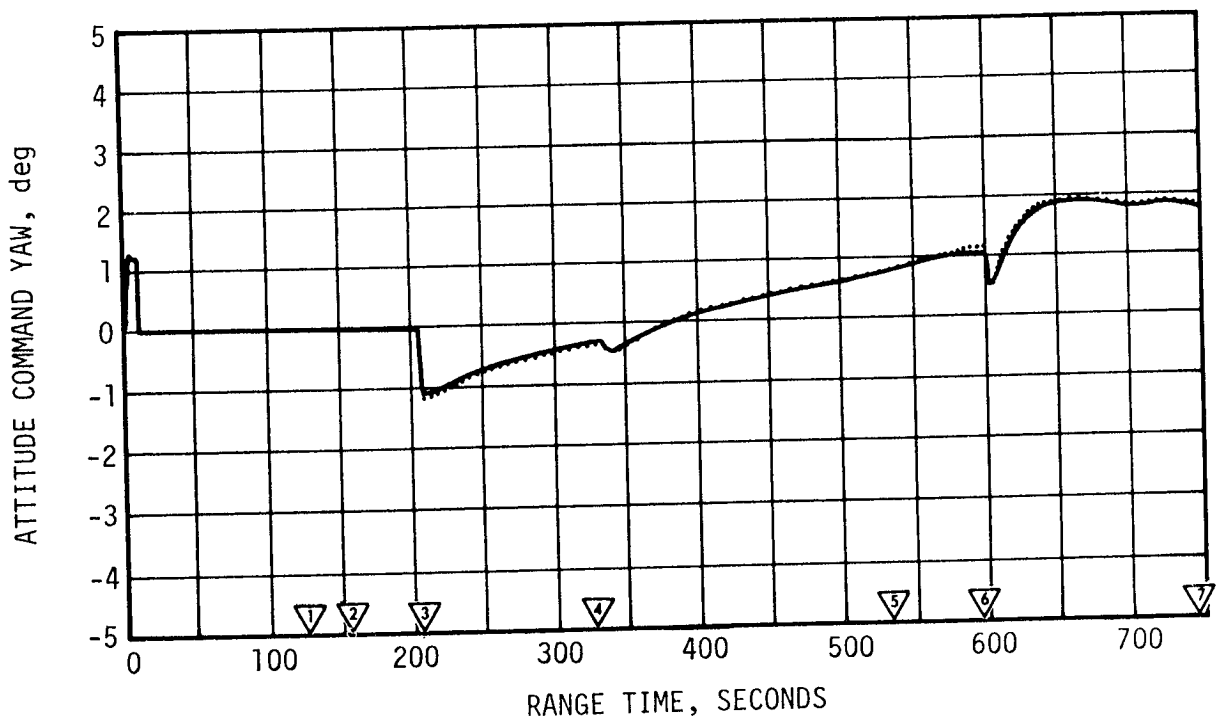
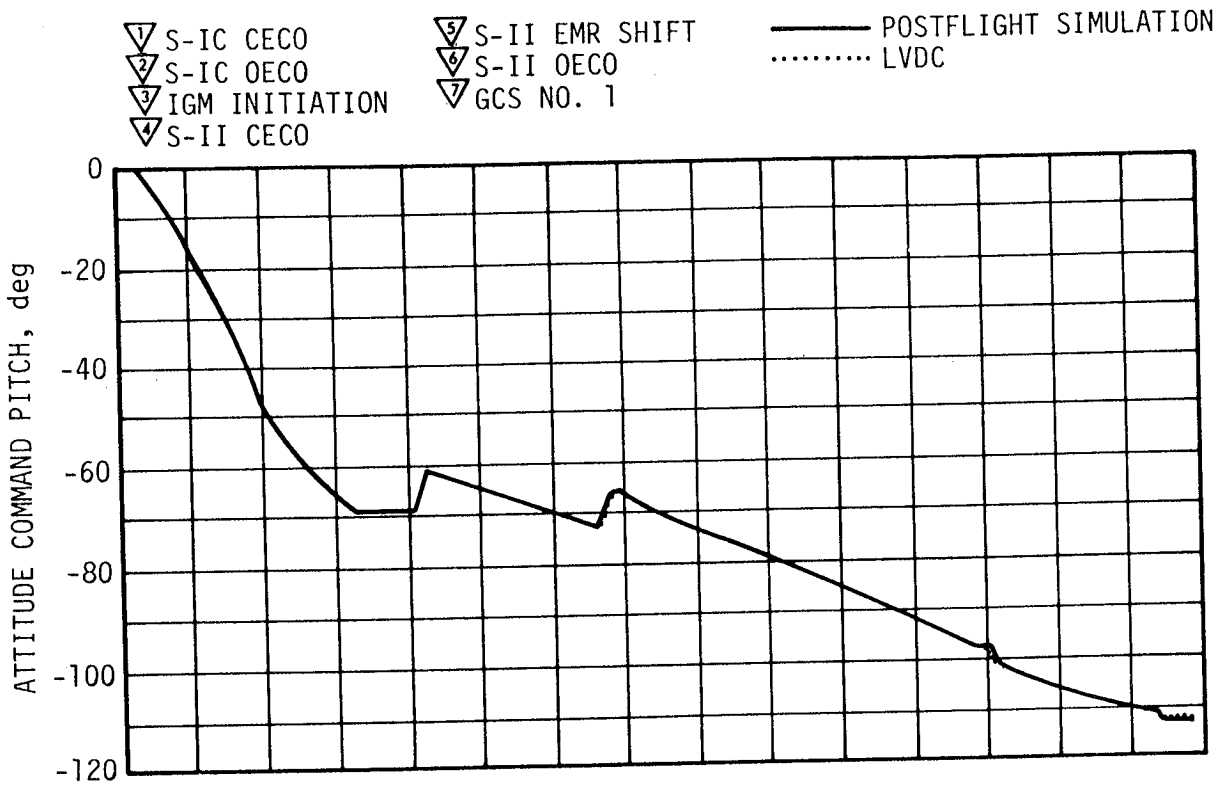


Figure 9-4. Attitude Commands During Boost to EPO

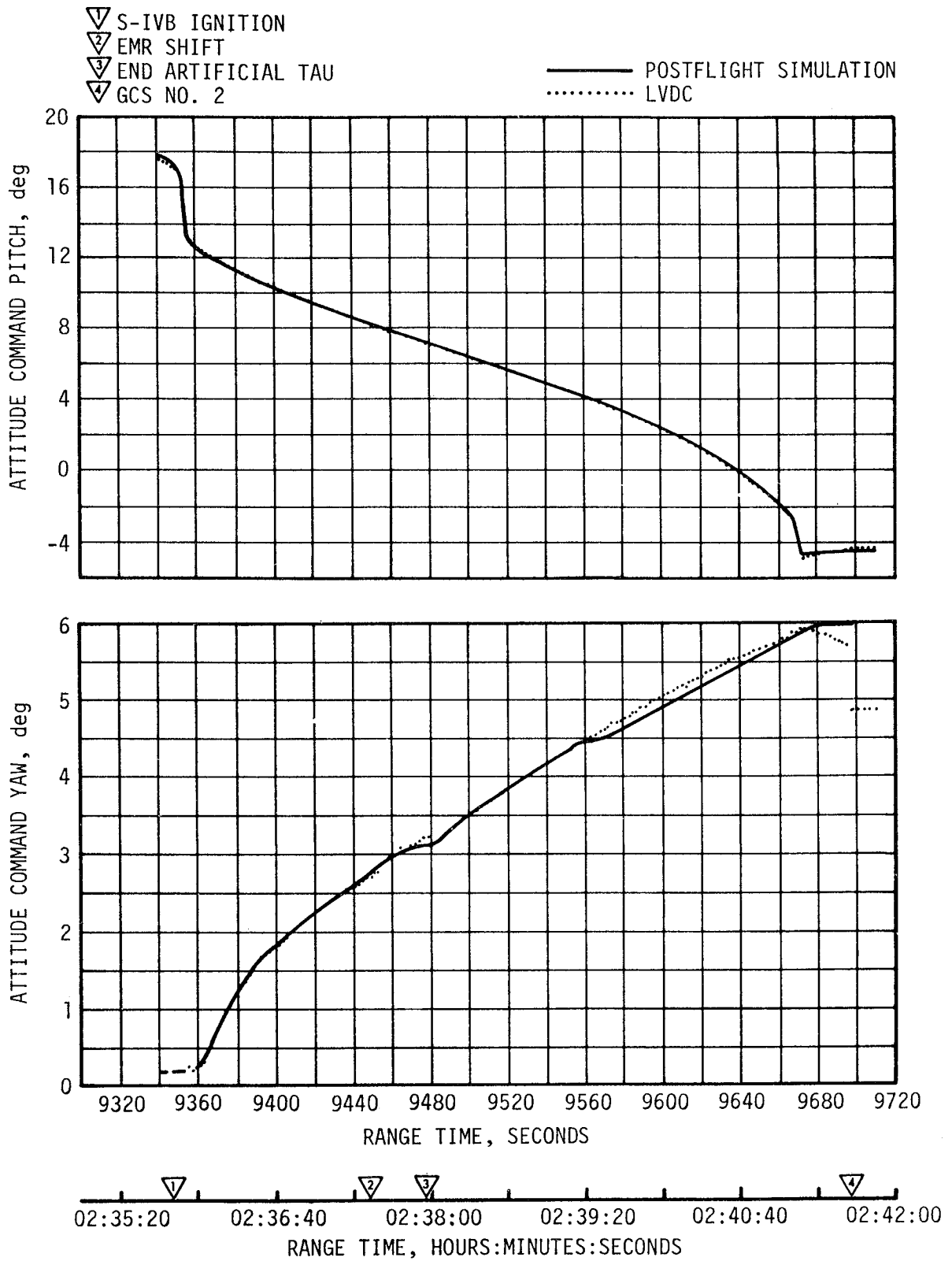


Figure 9-5. Attitude Commands During S-IVB Second Burn

Table 9-4. AS-508 Guidance System Accuracy

EVENT	PARAMETER	TARGETED*	GUIDANCE ACHIEVED**	GUIDANCE ACHIEVED MINUS TARGETED
GRR	Firing Azimuth (deg)	72.04392	-	-
	Flight Azimuth (deg)	72.04344	-	-
Insertion	Inclination (deg)	32.53843	32.53842	-0.00001
	Descending Node (deg)	123.1270	123.1268	-0.0002
	Radius (m)	6,563,366	6,563,358	-8
	Velocity (m/s)	7793.043	7793.043	0.0
	Path Angle (deg)	0.0	-0.0004959	-0.0004959
Injection	Inclination (deg)	31.82763	31.82876	0.00113
	Descending Node (deg)	123.0412	123.0406	-0.0006
	Twice Specific Orbital Energy (m <sup>2</sup> /s <sup>2</sup> )	-1,363,732	-1,363,732	0.0
	Eccentricity	0.977440	0.977421	-0.000019
	Argument of Perigee (deg)	-147.4838	-147.4877	-0.0039
<p>*Obtained from LVDC Boost Initialization and Restart Telemetry.  **Determined from Navigator State Vector for an Unbiased Cutoff.</p>				

The orbital insertion parameters after S-IVB first burn are shown in Table 9-5. The TLI parameters after S-IVB second burn are shown in Table 9-6. The difference between the LVDC and OT total energy ( $C_3$ ) is due essentially to a 0.75 m/s (2.46 ft/s) higher velocity gain, due to thrust decay, than that used to establish the OT. The postflight trajectory includes the measured thrust decay.

The active guidance phases start and stop times are shown in Table 9-7. The first phase of IGM guidance was nominal until S-II CECO. All IGM parameters adjusted correctly for the change in stage performance.

At 68,948 seconds (19:09:08) the LVDC lost its ability to access memory due to 6D10 battery depletion, and the program essentially ceased operation. This simultaneous inability to correctly access either memory module is discussed in paragraph 9.4.1.

#### 9.4 GUIDANCE SYSTEM COMPONENT EVALUATION

##### 9.4.1 LVDC and LVDA Performances

No LVDC or LVDA performance component malfunction was indicated prior to the LVDA power supply output decay. At 48,027 seconds (13:20:27), bit 8 of the Error Monitor Register was set. The cause has not been identified.

Table 9-5. Parking Orbit Insertion Parameters

PARAMETER	OPERATIONAL TRAJECTORY (OT)	POSTFLIGHT TRAJECTORY (OMPT)	GUIDANCE (LVDC)	OMPT MINUS OT	LVDC MINUS OT
Space-Fixed Velocity, m/s (ft/s)	7792.99 (25,567.55)	7792.53 (25,566.05)	7793.40 (25,568.90)	-0.46 (-1.50)	0.41 (1.35)
Geocentric Radius, meters (ft)	6,563,382 (21,533,407)	6,563,593 (21,534,099)	6,563,358 (21,533,326)	211 (692)	-24 (-81)
Flight Path Angle, deg	0.0000	0.0053	-0.0003	0.0053	-0.0003
Descending Node, deg	123.1253	123.0840	123.1247	-0.0429	-0.0006
Inclination, deg	32.5386	32.5247	32.5384	-0.0139	-0.0002
Eccentricity	0.000012	0.000135	0.000091	0.000123	0.000079

Table 9-6. Translunar Injection Parameters

PARAMETER	OPERATIONAL TRAJECTORY (OT)	POSTFLIGHT TRAJECTORY (OMPT)	GUIDANCE (LVDC)	OMPT MINUS OT	LVDC MINUS OT
Total Velocity, m/s (ft/s)	10,828.44 (35,526.39)	10,832.10 (35,538.38)	10,832.46 (35,539.57)	3.66 (11.99)	4.02 (13.18)
Geocentric Radius, meters (ft)	6,720,025 (22,047,327)	6,715,543 (22,032,623)	6,716,039 (22,034,249)	-4482 (-14,704)	-3986 (-13,078)
Descending Node, deg	123.0310	122.9970	123.0408	-0.0340	0.0098
Inclination, deg	31.8329	31.8170	31.8285	-0.0159	-0.0044
Eccentricity	0.9772165	0.9772267	0.9774900	0.0000102	0.0002735
Argument of Perigee, deg	212.5063	212.4406	212.5109	-0.0657	0.0046
$C_3$ , $m^2/s^2$ ( $ft^2/s^2$ )	-1,376,265 (-14,814,467)	-1,376,274 (-14,814,574)	-1,359,565 (-14,634,236)	-9 (-107)	16,700 (180,231)

Table 9-7. Start and Stop Times for IGM Guidance Commands

EVENT*	IGM PHASE (SEC)		ARTIFICIAL TAU (SEC)		STEERING MISALIGNMENT CORRECTION (SEC)		TERMINAL GUIDANCE (SEC)		CHI FREEZE (SEC)	
	START	STOP	START	STOP	START	STOP	START	STOP	START	STOP
First Phase IGM	204.5	534.7	-	-	223.9	-	-	-	-	-
Second Phase IGM	534.7	592.7	534.7	545.8	-	591.7	-	-	-	-
Third Phase IGM	592.7	743.2	600.2	611.2	607.4	742.4	716.9	743.2	743.2	763.2
Fourth Phase IGM	9352.4	9449.1	-	-	9363.0	-	-	-	-	-
Fifth Phase IGM	9449.1	9695.7	9449.1	9478.4	-	9695.0	9668.3	9695.7	9695.7	9846.6

\*All times are for the start of the computation cycle in which the event occurred.

No degradation of performance was observed. The first indication of LVDC degradation was the first of a series of intermittent B memory failures at 68,856 seconds (19:07:36). At 68,877 seconds (19:07:57) the first of a series of A memory failures was telemetered. Both A and B memory failures continued for approximately 91 seconds before the simultaneous A and B memory failures at 68,948 seconds (19:09:08).

The only indication of the simultaneous memory failures was telemetered via the LVDA Data Output Multiplexer (DOM) output of the interrupt storage register, which was the last LVDC or LVDA data telemetered. The only interrupt set was the simultaneous memory failure interrupt. The execution of only the interrupt storage register read command indicates that the LVDC program entered the interrupt processor program module and then ceased to function before responding to the interrupt.

At the time of the simultaneous memory failures, the LVDA power supply outputs to the LVDC were as follows:

<u>Supply</u>	<u>Output; Volts</u>
+20	+15.9
+12	+ 9.2
+ 6	+ 5.92
- 3	- 3.06

The LVDC temperatures were as follows:

<u>Measurement</u>	<u>Function Monitored</u>	<u>Temperature °F</u>	
		<u>Indicated</u>	<u>Redline</u>
C53-603	Buffer Oscillator	125.2	143.6 Max
C54-603	Memory	110.3	116.6 Max

Two error monitor register bit 3 indications of triple modular redundant interface output latch logic signal disagreements occurred at 20,907 seconds (05:48:27) and 20,967 seconds (05:49:27). As in previous flights, these signal disagreements were associated with the digital command system operation. The indications were expected and are acceptable operation.

At approximately 42,100 seconds (11:41:40), error monitor register bit 5 was set, indicating the voltage of one of the input buses was below the minimum usable level. The 6D41 voltage went below 24 volts at 41,560 seconds (11:32:40). In addition to the continuous error monitor register bit 5 indications of low 6D41 voltage, error monitor register bit 8 indications were telemetered every computation cycle beginning at 48,027 seconds (13:20:27) and continuing for approximately 400 seconds.

These indicate logic signal disagreements at the data latch through which data are transferred between the LVDA and LVDC. Real time telemetry data for the entire period were not analyzed. No error time word was telemetered following the continuous error monitor register bit 5 indications of low input voltage conditions at 42,100 seconds (11:41:40). This may preclude any determination for the cause of the error monitor register bit 8 indications.

#### 9.4.2 ST-124M-3 Inertial Platform

The ST-124M-3 Stabilized Platform Subsystem (ST-124M-3 SPS) performed satisfactorily until loss of 6D10 battery power at approximately 66,000 seconds (18:20:00).

At approximately 3.4 seconds, during a period of high radially directed vibration, the crossrange velocity measurement exhibited a shift of 0.65 m/s (2.13 ft/s), resulting in a velocity error of approximately 0.5 m/s (1.64 ft/s) as shown in Figure 9-6. The shift is significant because of its similarity to the negative shift experienced shortly after the liftoff of AS-506. Contact of the oscillating accelerometer head with a mechanical stop has been postulated as the cause of the AS-506 negative shift. This can not be confirmed because the accelerometer head position was measured with a sampled measurement. A measurement change effective on AS-508 provided continuous measurement of the accelerometer head position via an FM/FM channel. The FM/FM data were telemetered via the DF-1 telemetry link on a 59-hertz response channel. Although the telemetry channel response was sufficient to accurately reproduce head deflections at frequencies up to 59 hertz, a signal conditioning dc amplifier within the measuring rack used to condition the measurement for the telemetry system attenuates all signals above 20 hertz. The raw telemetry data from the Y-accelerometer head position show a burst of oscillations between 2.0 and 3.0 seconds at frequencies ranging from 32 to 36 hertz. The maximum head deflection from the raw telemetry data measured +4.34 degrees. Taking into account the rolloff characteristics of the amplifier at 35 hertz, this becomes an actual head deflection of +5.95 degrees. Since the stops are specified to be 6 degrees (+0, -0.5), it is concluded that the probable cause of the velocity shift was the accelerometer head momentarily contacting the mechanical stops. Figure 9-7 is a reconstructed FM trace of the head deflection from 2.0 to 2.9 seconds. There are five points (3 positive and 2 negative) where the 5.5 degree points were exceeded. The observed maximum amplitude of the output count deviation was 41 counts (2.05 m/s [6.72 ft/s]) occurring at 2.52 seconds. Other output pulse count deviations shortly after this time exceeded 35 counts. The signs of the velocity deviations and the times of direction changes can not be determined because of the lack of telemetry of the other output pulse train from the crossrange accelerometer.

The crossrange accelerometer reasonableness test constant is 2 m/s (6.56 ft/s) during the first 10 seconds of flight. This would limit the acceptable velocity change over a nominal computation cycle length to 1.7 m/s (5.6 ft/s). The maximum crossrange velocity change, sampled by the LVDA, in the first 10 seconds of the AS-508 mission was -0.65 m/s (-2.13 ft/s).

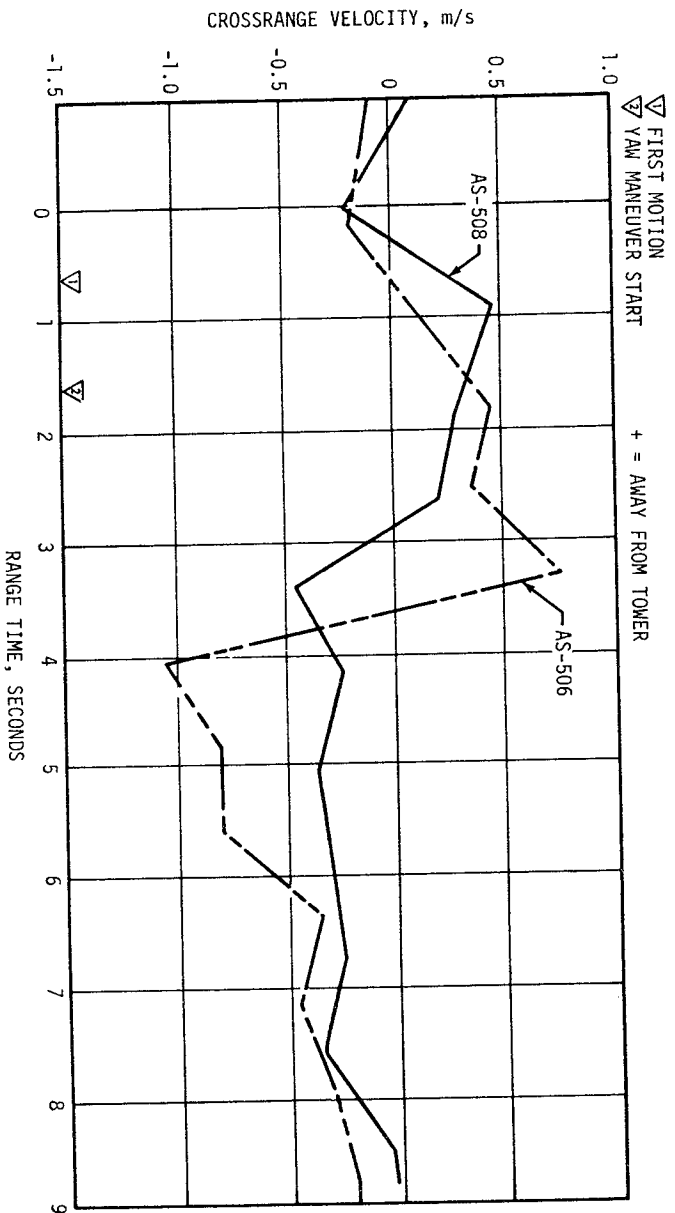


Figure 9-6. Crossrange Velocity Measured by the ST-124M-3 Inertial Platform

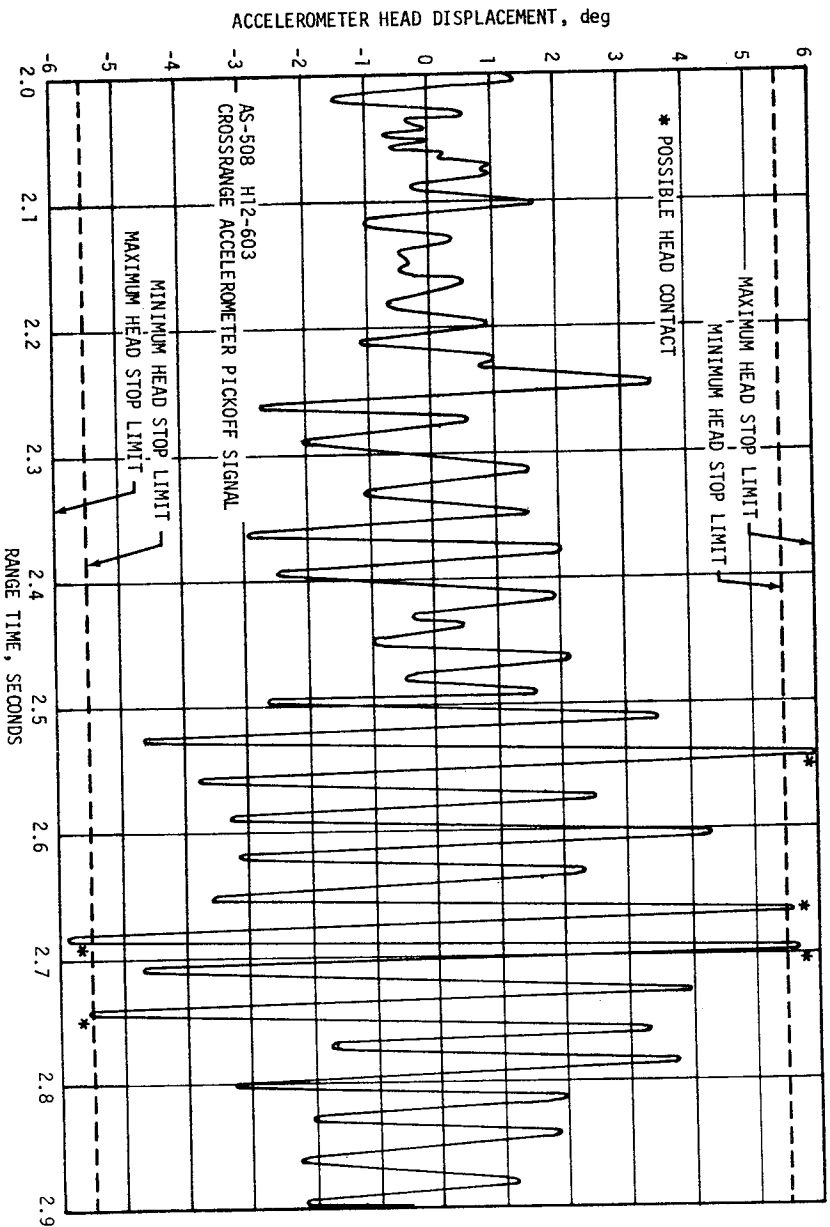


Figure 9-7. ST-124M-3 Accelerometer Pickoff

The presence of radially-directed vibration having significant energy at frequencies near 37 hertz (the resonant frequency of the accelerometer loop) is characteristic of the present Saturn V configuration during the first 10 seconds of flight. Nothing presently exists to preclude the occurrence of crossrange velocity shifts, such as those experienced on AS-506 and AS-508, during the early portions of future missions. The probability of any significant overall navigation accuracy degradation because of such a shift is negligibly small; the probability of permanent accelerometer impairment is practically nonexistent.

The performance of the stabilization gyro servo loops was nominal until loss of power at the end of the IU life. Telemetry data indicated typical gyro pickoff deflections during the vibration period around lift-off. Pickoff deflections noted at Command Service Module (CSM) separation were:

X gyro	1.6°P-P
Y gyro	0.32°P-P
Z gyro	1.36°P-P

At CSM docking the deflections on all three gyros were approximately 0.15°P-P.

Oscillations of 0.25°P-P at approximately 5 hertz were in evidence on the X gyro pickoff before and after S-IC CECO. Spurts of 2.5 hertz at 0.1°P-P were noted on the Y gyro pickoff prior to S-II CECO.

As the vehicle battery power decayed, the X and Z gyro servo loops started to oscillate, as expected, at 69,000 seconds (19:10:00). The Y gyro oscillations were less severe and came in spurts starting at approximately 69,900 seconds (19:25:00).

The inertial gimbal temperature (Figure 14-8) began decreasing shortly after liftoff as experienced on previous Saturn V flights. A low of 101.9°F was reached at approximately 17,000 seconds (04:43:20). After this time the temperature began increasing, but stayed within specified limits as did the three platform associated electronic boxes until loss of environmental cooling at approximately 50,000 seconds (13:53:20). At 67,000 seconds (18:36:20) all ST-124M-3 SPS box temperatures were still within specified limits but rising. Decaying IU battery power at this time caused additional data to be erroneous.

The gas bearing differential and internal ambient pressures remained within specified tolerances through 60,000 seconds (16:40:00). With loss of sphere pressure, these parameters decayed to 2.2 psid and 1.8 psia, respectively. See Figure 14-9.

### 9.4.3 Ladder Outputs

The ladder networks and converter amplifiers performed satisfactorily. At 68,948 seconds (19:09:08), the time of the LVDC memory failure, the ladder amplifiers for the pitch and yaw attitude error channel drifted to full scale positive values. Full scale at this time was approximately 11.8 degrees due to the decaying supply voltages. The roll ladder output did not drift, indicating that it was the last serviced by the minor loop. The flight control subsystem responded to the attitude error input by commanding pitch and yaw thruster firings to balance the attitude error signals, as discussed in paragraph 10.4.4.

### 9.4.4 Telemetry Outputs

Analysis of the LVDA telemetry buffer and flight control computer attitude error plots indicate symmetry between the buffer outputs and the ladder outputs. The LVDC power supply plots indicate satisfactory power supply performance. The H60-603 guidance computer telemetry was satisfactory.

### 9.4.5 Discrete Outputs

No valid discrete output register words (tags 043 and 052) were observed to indicate guidance failure.

### 9.4.6 Switch Selector Functions

Switch selector data indicate that the LVDA switch selector functions were performed satisfactorily. No error monitor words were observed that indicate disagreement in the triple modular redundant switch selector register positions or in the switch selector feedback circuits. No mode code 24 words or switch selector feedback words were observed that indicated a switch selector feedback was in error. In addition, no indications were observed to suggest that the B channel input gates to the switch selector register positions were selected.



## SECTION 10

### CONTROL AND SEPARATION

#### 10.1 SUMMARY

The AS-508 control system, which was essentially the same as that of AS-507, performed satisfactorily. The Flight Control Computer (FCC), Thrust Vector Control (TVC), and Auxiliary Propulsion System (APS) satisfied all requirements for vehicle attitude control during the flight. Bending and slosh dynamics were adequately stabilized. The prelaunch programmed yaw, roll, and pitch maneuvers were properly executed during S-IC boost.

During the maximum dynamic pressure region of flight, the launch vehicle experienced winds that were less than 95-percentile April winds. The maximum average pitch and yaw engine deflections were in the maximum dynamic pressure region.

S-IC/S-II first and second plane separations were accomplished with no significant attitude deviations. Related data indicate that the S-IC retromotors performed as expected. At Iterative Guidance Mode (IGM) initiation, a pitchup transient occurred similar to that seen on previous flights. The S-II retromotors and S-IVB ullage motors performed as expected and provided a normal S-II/S-IVB separation.

Satisfactory control of the vehicle was maintained during first and second S-IVB burns and during coast in Earth Parking Orbit (EPO). During the Command and Service Module (CSM) separation from the S-IVB/IU and during the Transposition, Docking and Ejection (TD&E) maneuver, the control system maintained the vehicle in a fixed inertial attitude to provide a stable docking platform. Following TD&E, S-IVB/IU attitude control was maintained during the evasive maneuver, the maneuver to lunar impact attitude, and the LOX dump and APS burns.

An unscheduled decrease in range rate of approximately 2 to 3 m/s (7 to 10 ft/s) was experienced for approximately 60 seconds beginning at 70,150 seconds (19:29:10). This unscheduled maneuver had no adverse effect on lunar targeting.

## 10.2 S-IC CONTROL SYSTEM EVALUATION

The AS-508 control system performed satisfactorily during S-IC powered flight. The vehicle flew through winds which were less than 95 percentile for April in the maximum dynamic pressure region of flight. Less than 10 percent of the available engine deflection was used throughout flight (based on average engine gimbal angle). The S-IC outboard engines canted as planned.

All dynamics were within vehicle capability. In the region of high dynamic pressure, the maximum angles-of-attack were -2.9 degrees in pitch and 1.4 degrees in yaw. The maximum average pitch and yaw engine deflections were 0.4 degree each and occurred in the maximum dynamic pressure region. Both deflections were due to wind shears. The absence of any divergent bending or slosh frequencies in vehicle motion indicates that bending and slosh dynamics were adequately stabilized.

Vehicle attitude errors required to trim out the effects of thrust imbalance, thrust misalignment and control system misalignments were within predicted envelopes. Vehicle dynamics prior to S-IC/S-II first plane separation were within staging requirements.

Maximum control parameters during S-IC burn are listed in Table 10-1. Pitch and yaw plane time histories are shown in Figure 10-1. Dynamics in the region between liftoff and 40 seconds result primarily from guidance commands. In the region between 40 and 110 seconds, maximum dynamics were caused by the pitch tilt program, wind magnitude, and wind shears. Dynamics from 110 seconds to separation were caused by high altitude winds, separated air flow aerodynamics, center engine shutdown and tilt arrest. The transient at Center Engine Cutoff (CECO) indicates that the center engine cant was 0.13 degree in pitch and 0.24 degree in yaw.

Table 10-1. Maximum Control Parameters During S-IC Flight

PARAMETER	PITCH PLANE		YAW PLANE		ROLL PLANE	
	AMPLITUDE	RANGE TIME (SEC)	AMPLITUDE	RANGE TIME (SEC)	AMPLITUDE	RANGE TIME (SEC)
Attitude Error, deg	1.32	90.7	1.07	11.5	-0.78	14.1
Angular Rate, deg/s	-0.92	92.0	0.44	5.5	1.6	14.8
Average Gimbal Angle, deg	0.36	14.0	0.36	11.3		
Angle-of-Attack, deg	-2.88	69.9	1.44	82.1		
Angle-of-Attack Dynamic Pressure Product, deg-N/cm <sup>2</sup> (deg-lbf/ft <sup>2</sup> )	7.83 (1635.34)	75.4	4.47 (933.58)	82.1		
Normal Acceleration m/s <sup>2</sup> (ft/s <sup>2</sup> )	-0.48 (-1.57)	88.9	0.57 (1.87)	88.0		

The attitude errors between liftoff and 20 seconds indicate that the equivalent thrust vector misalignments prior to outboard engine cant were -0.08, -0.15, and -0.02 degree in pitch, yaw, and roll, respectively. These errors are required to trim out the effects of thrust imbalance, offset Center of Gravity (CG), thrust vector misalignment and control system misalignments. The equivalent thrust vector misalignments after outboard engine cant were -0.03, -0.11, and 0.0 degree in pitch, yaw, and roll, respectively. The predicted and measured misalignments, slow release forces, winds, and the thrust-to-weight ratio at liftoff are shown in Table 10-2. Pitch and yaw plane angles-of-attack are shown in Figure 10-2.

Figure 10-1. Pitch and Yaw Plane Dynamics During S-IC Burn

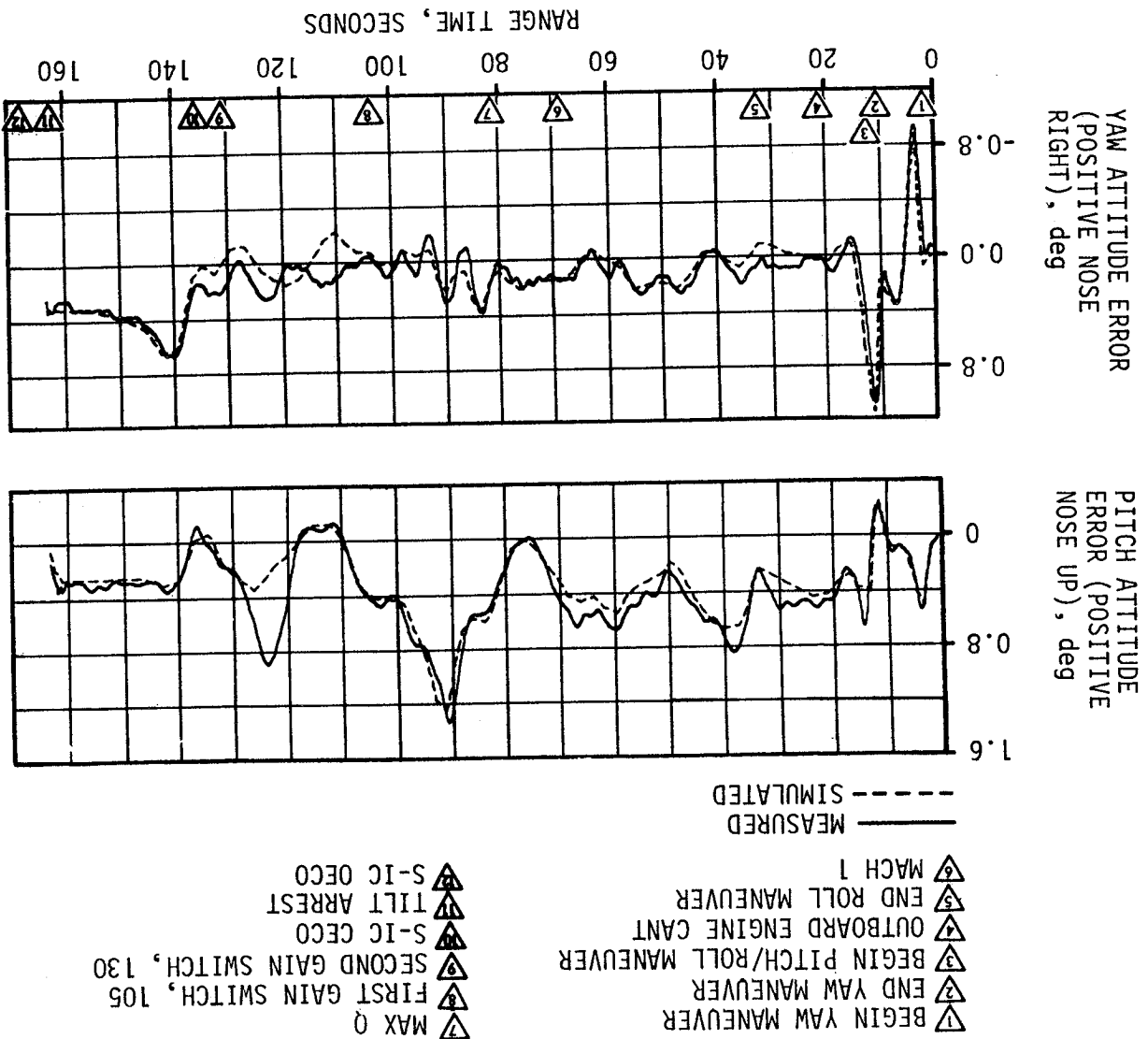


Table 10-2. AS-508 Liftoff Misalignment Summary

PARAMETER	PREFLIGHT PREDICTED			LAUNCH		
	PITCH	YAW	ROLL	PITCH	YAW	ROLL
Thrust Misalignment, deg*	±0.34	±0.34	±0.34	-0.08	-0.15	-0.02
Center Engine Cant, deg*	-	-	-	0.13	0.24	-
Vehicle Stacking and Pad Misalignment, deg	±0.29	±0.29	0.0	0.03	-0.04	-0.03
Attitude Error at Holddown Arm Release, deg	0.0	0.0	0.0	-0.04	-0.06	0.06
Peak Soft Release Force Per Rod, N (lbf)	415,900 (93,300)			**		
Wind	14.4 m/s (28.0 knots) at 18.3 meters (60 feet)			6.3 m/s (12.2 knots) at 18.3 meters (60 feet)		
Thrust to Weight Ratio	1.178			1.199		

\*Thrust misalignment of 0.34 degree encompasses the center engine cant. A positive polarity was used to determine minimum fin tip/umbilical tower clearance. A negative polarity was used to determine vehicle/GSE clearances.  
 \*\*Data not available.

### 10.3 S-II CONTROL SYSTEM EVALUATION

The S-II stage attitude control system performance was satisfactory. Analysis of the magnitude of modal components in the engine deflections revealed that vehicle structural bending and propellant sloshing had negligible effect on control system performance. The maximum control parameter values for the S-II burn period are shown in Table 10-3. The maximum values of pitch and yaw control parameters occurred in response to initiation of Phase I IGM. The maximum values of roll control parameters occurred in response to S-IC/S-II separation disturbances. The control responses were within expectations.

Between the events of S-IC Outboard Engine Cutoff (OECO) and initiation of IGM, the attitude commands were held constant. Significant events which occurred during that interval were S-IC/S-II separation, S-II stage J-2 engine start, second plane separation and Launch Escape Tower (LET) jettison. The attitude control dynamics throughout this interval indicated stable control, as shown in Figure 10-3. Steady-state attitudes were achieved within 20 seconds after S-IC/S-II separation.

At IGM initiation, the vehicle was commanded to pitch up and then down. The transient amplitudes experienced were similar to those of previous flights. At the premature S-II CECO, the Instrument Unit (IU) detected an engine out condition and issued compensating attitude commands. These commands were similar to those issued under normal CECO conditions; however, the amplitudes were larger to correct for deviations from the prescribed trajectory. In the pitch axis, an attitude error of -1.9 degrees and a rate of +1.2 deg/s were introduced by the guidance response

Figure 10-2. Angle-of-Attack During S-IC Burn

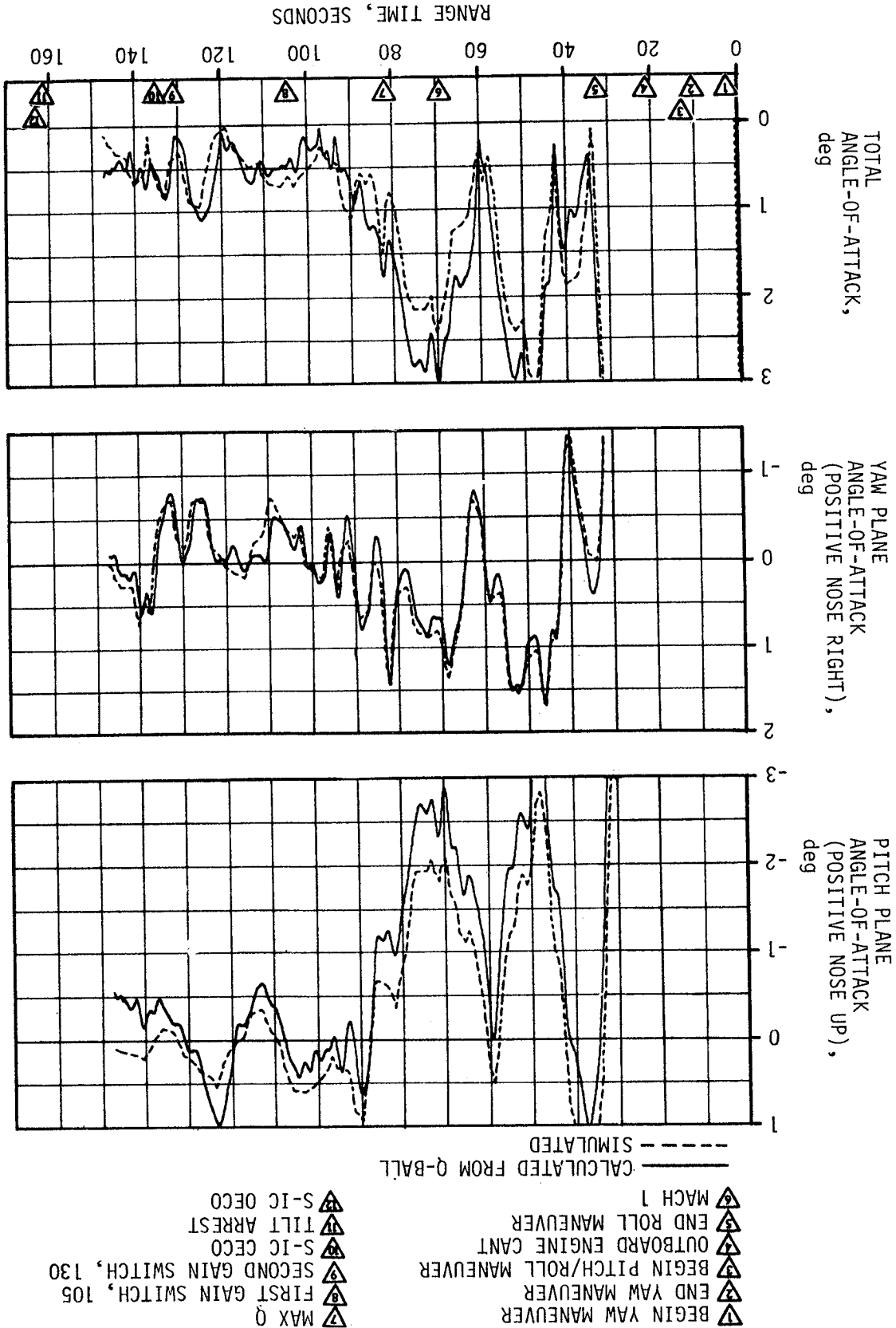


Table 10-3. Maximum Control Parameters During S-II Burn

PARAMETER	PITCH PLANE		YAW PLANE		ROLL PLANE	
	AMPLITUDE	RANGE TIME (SEC)	AMPLITUDE	RANGE TIME (SEC)	AMPLITUDE	RANGE TIME (SEC)
Attitude Error, deg	-1.9	210	0.7	208.0	-0.6	165.0
Angular Rate, deg/s	1.2	211	-0.3	209.0	0.9	165.5
Average Gimbal Angle, deg	-0.9	208	0.5	202.5	-0.6	165.5

- ▽ S-IC/S-II SEPARATION COMMAND
- ▽ S-II SECOND PLANE SEPARATION COMMAND
- ▽ IGM PHASE 1 INITIATED
- ▽ S-II CECO
- ▽ IGM PHASE 2 INITIATED, S-II LOW EMR SHIFT
- ▽ S-II OECS

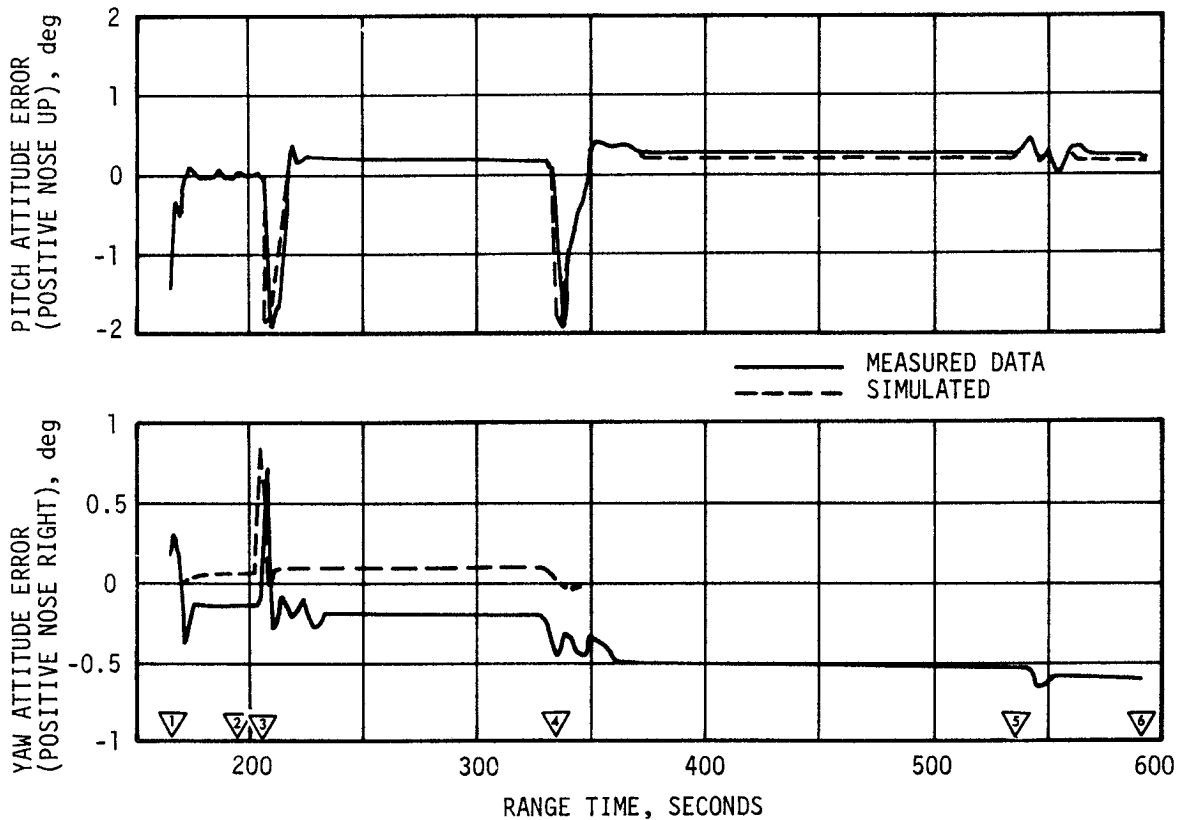


Figure 10-3. Pitch and Yaw Plane Attitude Errors During S-II Burn

to the decrease in thrust. The flight control computer issued a  $\pm 0.3$  degree, one-cycle command to the actuators. In yaw, a constant offset of 0.2 degree of all engines existed throughout the remaining burn. This offset is attributed to a combination of vehicle CG offset and imbalanced thrust from control engines.

Figure 10-3 compares flight and simulation data. These data agree in the regions of greatest control system activity. Uncertainties in engine location, thrust vector alignments, and engine thrust buildup characteristics account for the main differences in data.

#### 10.4 S-IVB CONTROL SYSTEM EVALUATION

The S-IVB TVC system provided satisfactory pitch and yaw control during first powered flight. The APS provided satisfactory roll control during first and second burns.

During S-IVB first and second burns, control system transients were experienced at S-II/S-IVB separation, guidance initiation, Engine Mixture Ratio (EMR) shift, terminal guidance mode, and J-2 engine cutoff. These transients were expected and were well within the capabilities of the control system.

#### 10.4.1 Control System Evaluation During First Burn

The S-IVB first burn pitch and yaw attitude errors are presented in Figure 10-4. The significant events related to control system operation are indicated in the figure. The maximum attitude errors and rates occurred at IGM initiation. A summary of the first burn maximum values of critical flight control parameters is presented in Table 10-4.

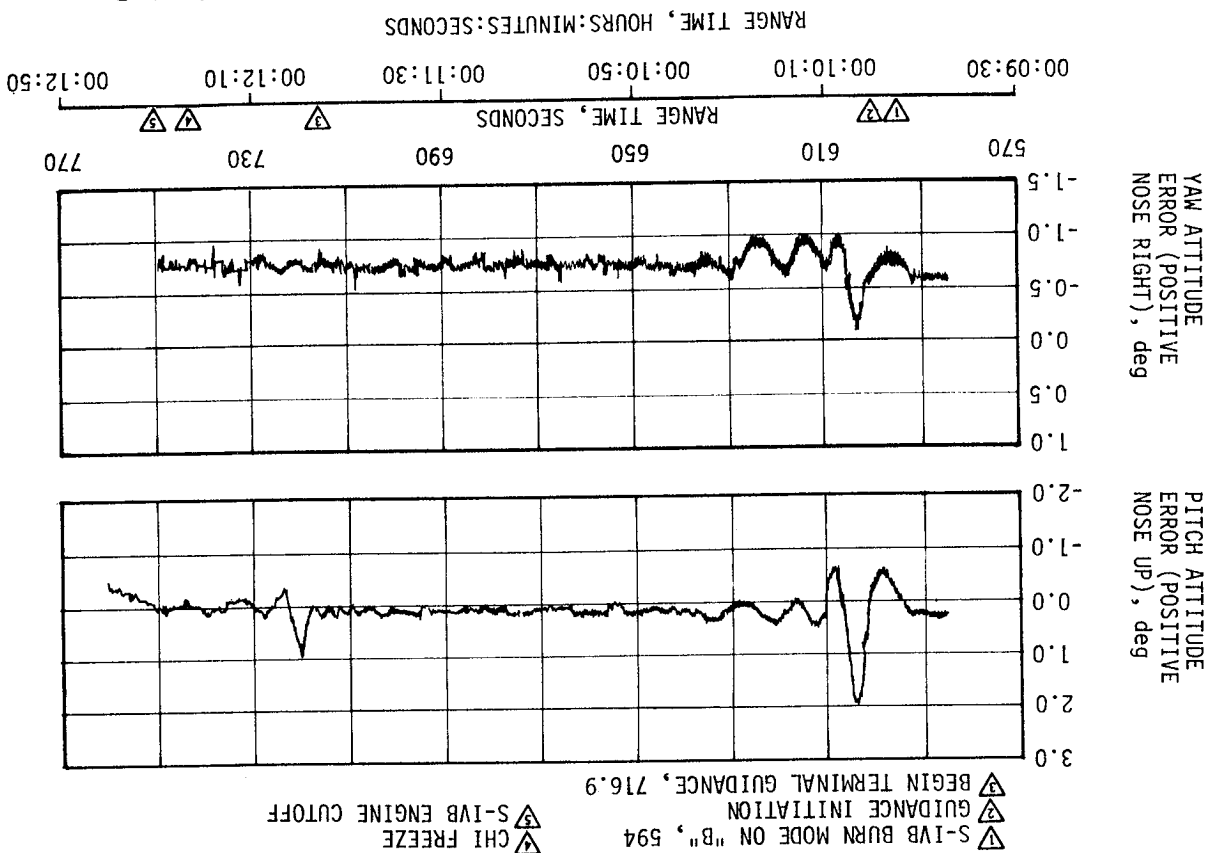


Figure 10-4. Pitch and Yaw Attitude Errors During S-IVB First Burn

Table 10-4. Maximum Control Parameters During S-IVB First Burn

PARAMETER	PITCH PLANE		YAW PLANE		ROLL PLANE	
	AMPLITUDE	RANGE TIME (SEC)	AMPLITUDE	RANGE TIME (SEC)	AMPLITUDE	RANGE TIME (SEC)
Attitude Error, deg	1.92	603.9	-1.08	614.0	-1.10	621.1
Angular Rate, deg/s	-1.30	605.4	-0.35	604.3	-0.63	594.1
Average Gimbal Angle, deg	1.31	603.5	-0.77	606.0	--	--

The pitch and yaw effective thrust vector misalignments during first burn were +0.20 and -0.29 degree, respectively. As experienced on previous flights, a steady-state roll torque of 15.0 N-m (11.0 lbf-ft) counterclockwise looking forward, required roll APS firings during first burn. The steady-state roll torque experienced on previous flights has ranged between 61.4 N-m (45.3 lbf-ft) counterclockwise and 54.2 N-m (40.0 lbf-ft) clockwise.

Propellant sloshing during first burn was observed on data obtained from the Propellant Utilization (PU) sensors. The propellant slosh did not have any noticeable effect on the operation of the attitude control system.

#### 10.4.2 Control System Evaluation During Parking Orbit

The APS provided satisfactory orientation and stabilization during parking orbit. Following S-IVB first cutoff, the vehicle was maneuvered to the in-plane local horizontal and the orbital pitch rate was established. The pitch attitude error for this maneuver is shown in Figure 10-5.

#### 10.4.3 Control System Evaluation During Second Burn

The S-IVB second burn pitch and yaw attitude errors are presented in Figure 10-6. The significant events are indicated in this figure. The maximum attitude errors and rates occurred at guidance initiation. A summary of the second burn maximum values of critical flight control parameters is presented in Table 10-5.

The pitch and yaw effective thrust vector misalignments during second burn were approximately +0.25 and -0.29 degree, respectively. The steady-state roll torque during second burn ranged from 11.3 N-m (8.4 lbf-ft), counterclockwise looking forward, at the low EMR to 12.9 N-m (9.5 lbf-ft) at the 5.0:1.0 EMR.

Figure 10-6. Pitch and Yaw Attitude Errors During S-IVB Second Burn

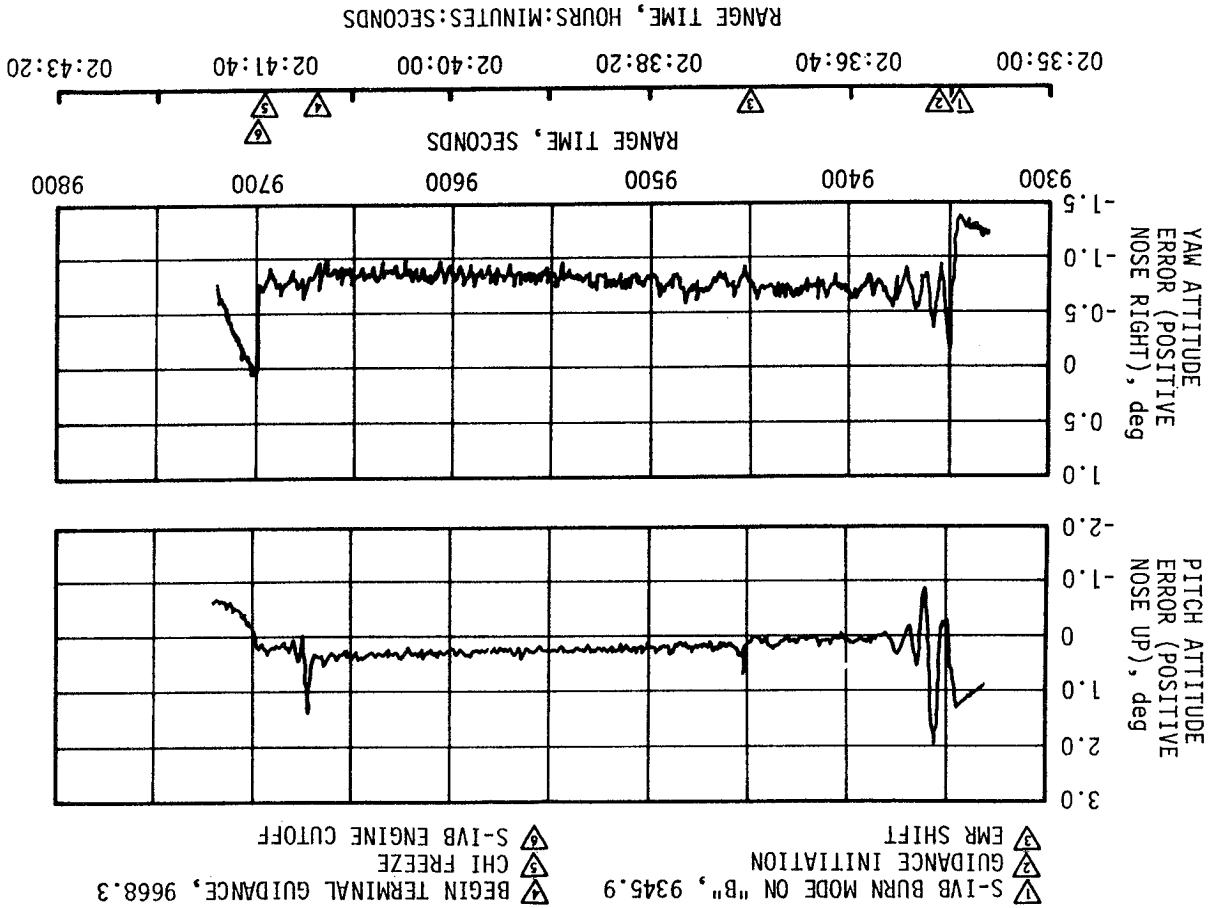


Figure 10-5. Pitch Attitude Error During Parking Orbit

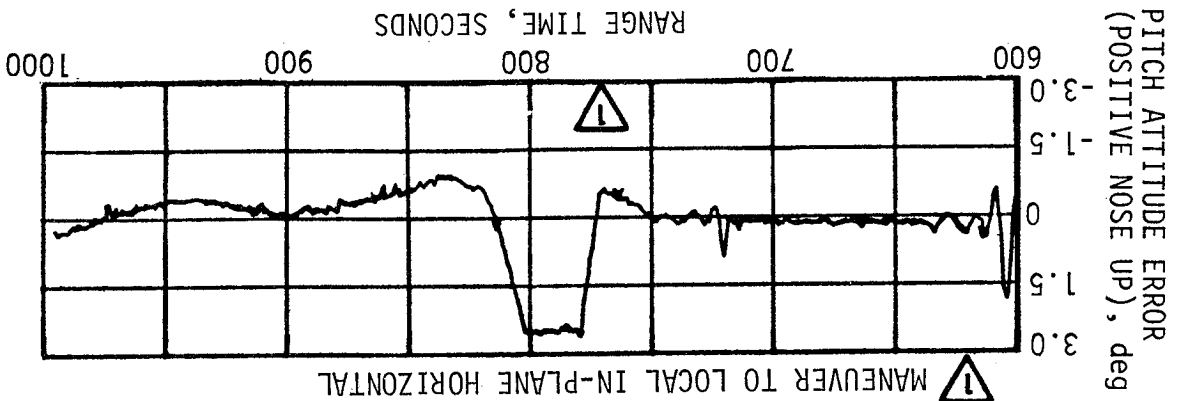


Table 10-5. Maximum Control Parameters During S-IVB Second Burn

PARAMETER	PITCH PLANE		YAW PLANE		ROLL PLANE	
	AMPLITUDE	RANGE TIME (SEC)	AMPLITUDE	RANGE TIME (SEC)	AMPLITUDE	RANGE TIME (SEC)
Attitude Error, deg	1.99	9356.5	-1.36	9346.0	-1.17	9496.6
Angular Rate, deg/s	-1.38	9357.5	0.41	9348.9	0.11	9350.8
Average Gimbal Angle, deg	1.30	9357.1	-1.07	9346.3	--	--

Propellant sloshing during second burn was observed on data obtained from the PU sensors. LOX sloshing can be observed on pitch attitude control parameters during the first 10 seconds of S-IVB second burn; however, the LOX sloshing had no noticeable effect on the operation of the attitude control system.

#### 10.4.4 Control System Evaluation After S-IVB Second Burn

The APS provided satisfactory orientation and stabilization from Translunar Injection (TLI) through the APS ullage burn for lunar target impact. Each of the planned maneuvers was performed satisfactorily. Several events that occurred beyond the normal lifetime of the IU are explained below because of their possible effect on future S-IVB lunar impacts.

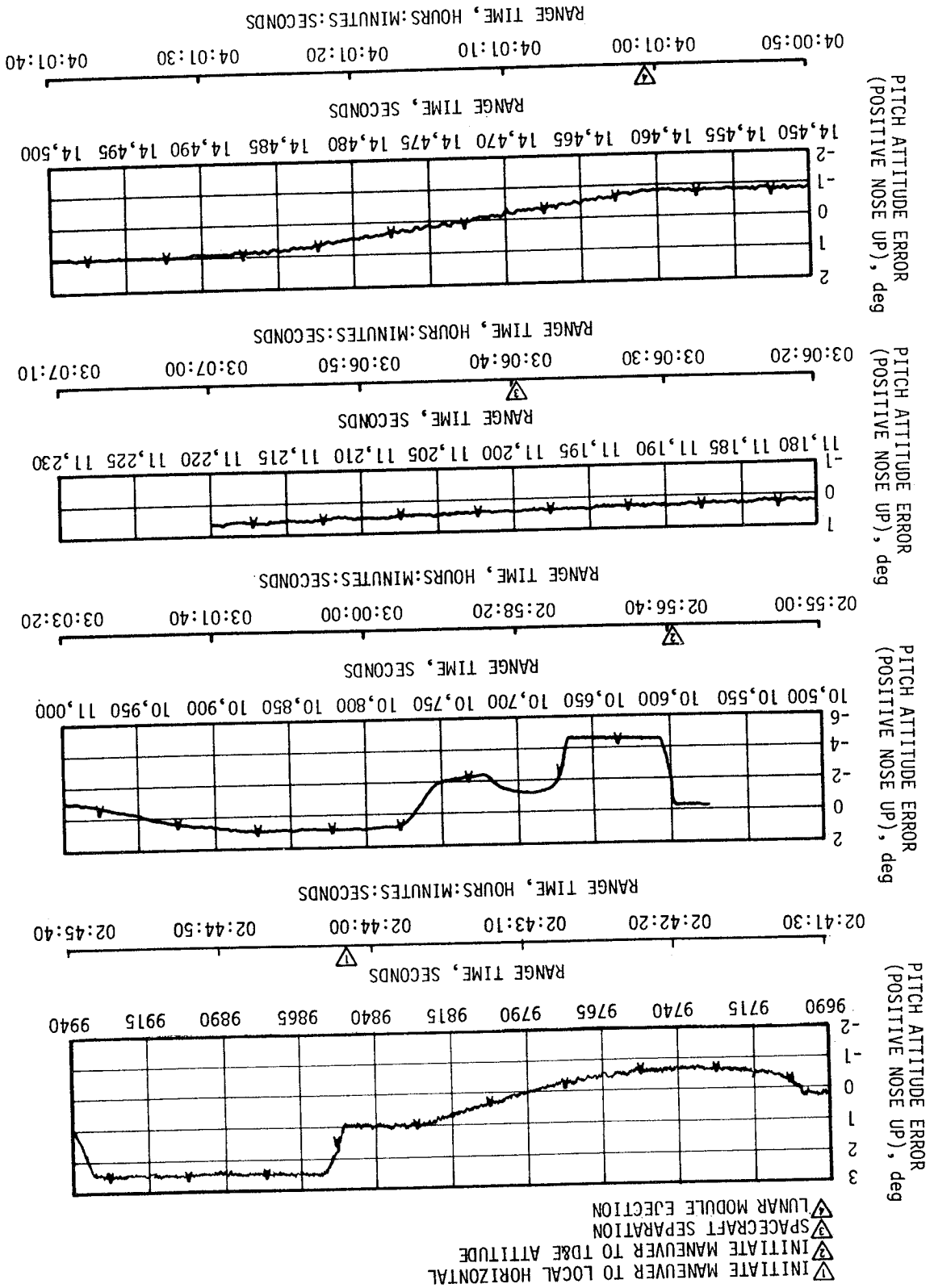
The pitch attitude error for significant events during translunar coast is shown in Figure 10-7. Significant events related to attitude control system operation during coast are noted.

Following S-IVB second cutoff, the vehicle was maneuvered to the in-plane local horizontal at 9848 seconds (02:44:08) (through approximately -27 degrees in pitch and -4 degrees in yaw) and an orbital pitch rate established. At 10,598 seconds (02:56:38), the vehicle was commanded to maneuver to the separation TD&E attitude (through approximately 120, -40, and -180 degrees in pitch, yaw, and roll, respectively).

Spacecraft separation which occurred at 11,198.9 seconds (03:06:38.9) appeared normal, as indicated by the relatively small disturbances induced on the S-IVB. Pitch attitude error data for spacecraft docking was not available for analysis; however, the APS control engine burn history indicated that larger than normal disturbances were experienced at spacecraft docking which occurred at 11,948.8 seconds (03:19:08.8).

At 14,940 seconds (04:09:00), a maneuver was initiated to the evasive ullage burn attitude. This involved maneuvering from the TD&E yaw attitude of -40.3 degrees to +40.0 degrees. At 15,481 seconds (04:18:01), the APS ullage engines were commanded on for 80 seconds to provide the necessary separation distance between the S-IVB and the CSM.

Figure 10-7. Pitch Attitude Error During Translunar Coast (Sheet 1 of 2)



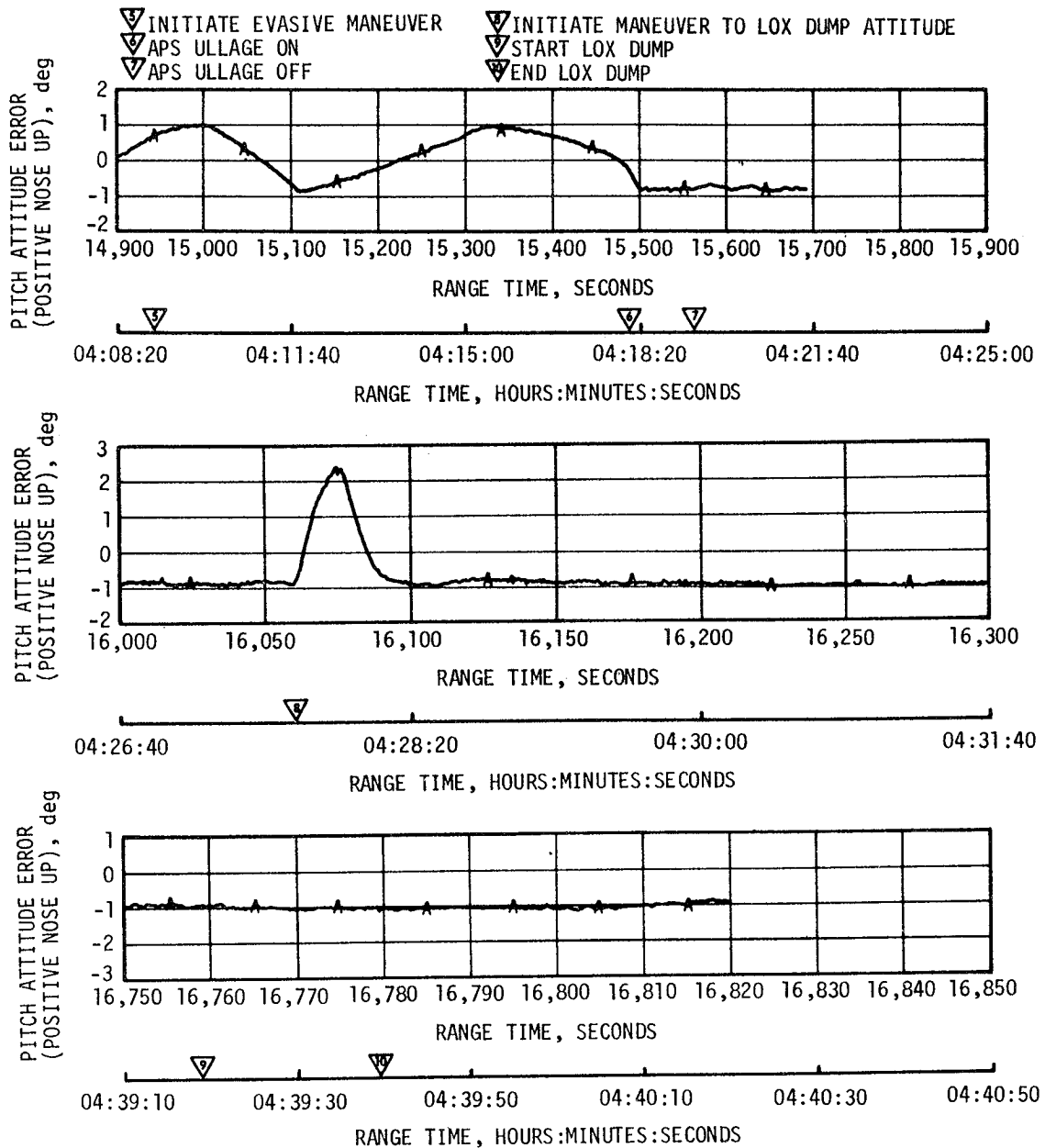


Figure 10-7. Pitch Attitude Error During Translunar Coast (Sheet 2 of 2)

The maneuver to LOX dump attitude was performed at 16,060 seconds (04:27:40). This was a two-axis maneuver with pitch commanded from 176.7 to 183.0 degrees and yaw from 40.0 to -5.4 degrees referenced to the in-plane local horizontal. LOX dump occurred at 16,759.4 seconds (04:39:19.4) and lasted for 48 seconds.

At 20,887 seconds (05:48:07), a ground command was sent to perform a maneuver to the desired attitude for the APS ullage burn for lunar target impact. The vehicle was commanded to pitch -1 degree and yaw -3 degrees. At 21,600 seconds (06:00:00), the APS ullage engines were commanded on for 217 seconds to provide  $\Delta V$  for lunar target impact.

Auxiliary Propulsion System propellant consumption for attitude control and propellant settling prior to the APS burn for lunar target impact was larger than the mean consumption predicted for module 1, and the same as the mean predicted for module 2. The total propellant (fuel and oxidizer) used was 57.9 kilograms (127.7 lbm) and 52.5 kilograms (115.7 lbm) for modules 1 and 2, respectively. This was 39 and 35 percent of the total available in each module (approximately 149.7 kilograms [330 lbm]). APS propellant consumption is tabulated in Section 7, Table 7-4.

At approximately 46,050 seconds (12:47:30), the yaw attitude error started to diverge and was followed by an oscillatory motion with increasing amplitude until the attitude error limited at  $\pm 2.5$  degrees. The frequency of this oscillation was approximately 0.077 hertz. This control system instability was indicative of loss of rate feedback in the control system loop. Examination of the active rate gyro during this interval indicated that the yaw rate gyro was not sensing the vehicle oscillations in order to provide rate damping in the control system. As a result, instability occurred until the vehicle angular rate increased to a sufficient amplitude (difference between the active and reference rate gyro greater than 1.65 deg/s) to initiate an automatic switchover from the active to the spare rate gyro. Switchover to the spare rate gyro was observed at 46,233 seconds (12:50:33) after which the control system oscillations were rapidly damped, as shown in Figure 10-8. The loss of the active yaw rate gyro was caused by a loss of power from the 6D40 battery.

At approximately 49,353 seconds (13:42:33), the TD&E maneuver was performed for a second time. The maneuver was not planned, but apparently occurred due to inherent characteristics of the Launch Vehicle Digital Computer (LVDC) located in the IU. A counter in the LVDC overflows at approximately 32,768 seconds in Time Base 8 ( $T_8$ ) (48,247.4 seconds [13:24:07.4]), after which the counter reverts to counting backwards. Certain functions such as normal switch selector commands are inhibited from occurring again; however, the TD&E maneuver was mechanized such that at the appropriate time in the reverse count it would be initiated a second time. The maneuver was verified through evaluation of the control system attitude errors, angular rates, and APS engine firings. This TD&E maneuver did not degrade Command and Communication System (CCS) tracking or the lunar impact attitude.

Loss of attitude control was experienced at approximately 68,950 seconds (19:09:10) with the pitch and yaw attitude errors diverging to a maximum value of approximately 11.8 degrees, as explained in paragraph 10.5. As a result of the large attitude errors, the APS control engines fired to establish pitch and yaw body rates of approximately -2 deg/s. These rates were maintained to offset the constant attitude error signals. Figure 10-9 shows the pitch and yaw attitude control system responses for this time period.

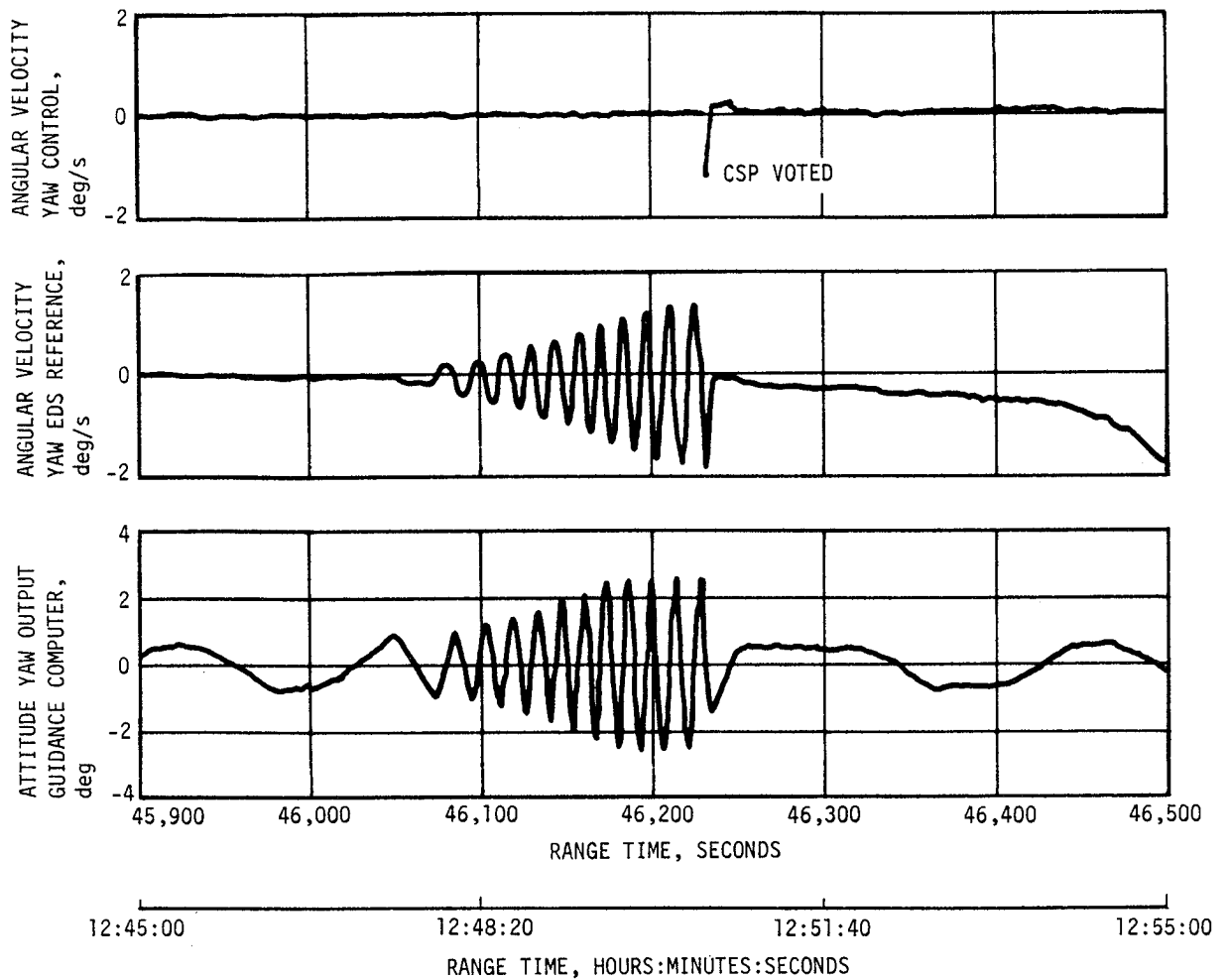
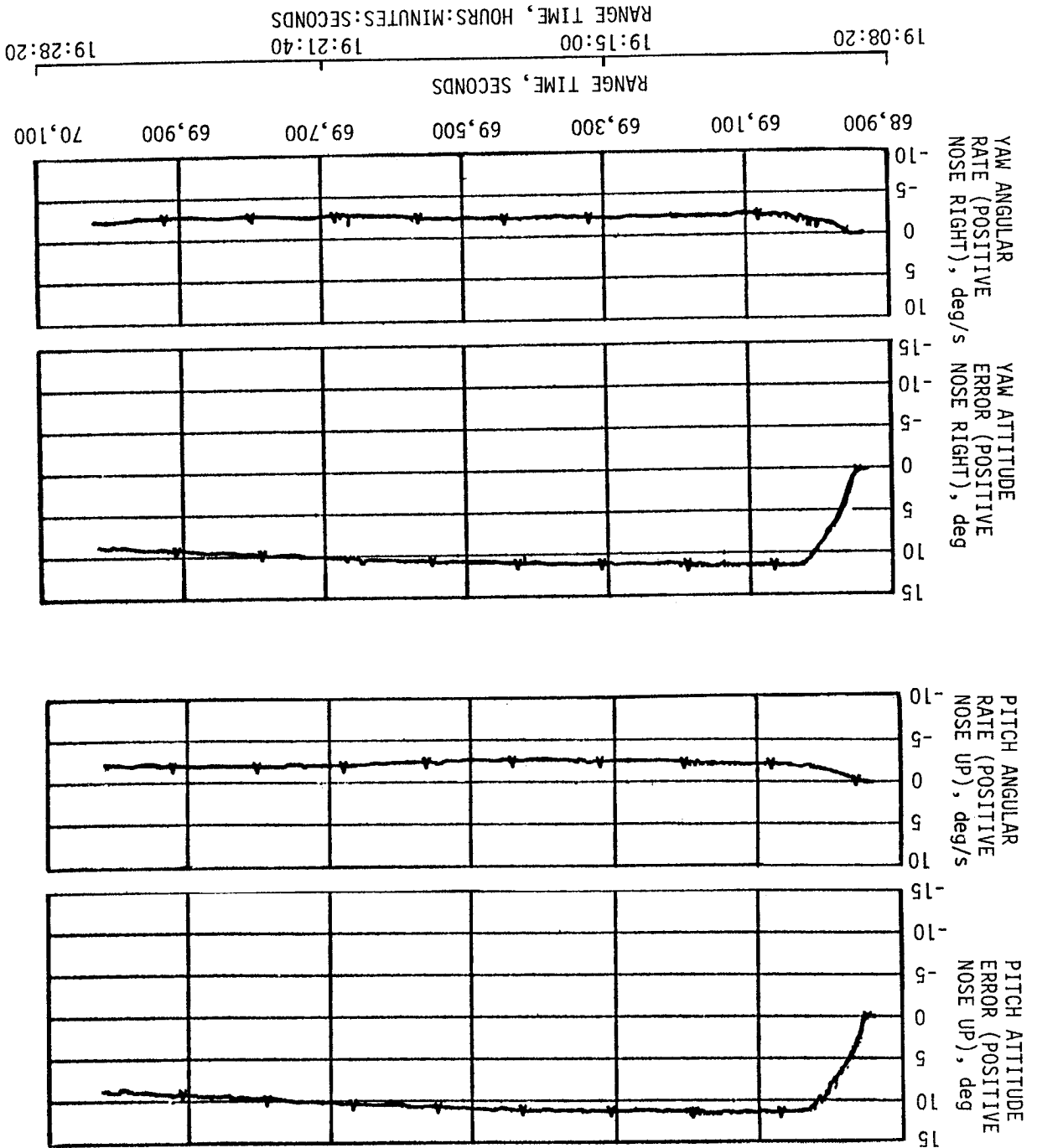


Figure 10-8. Yaw Rate Gyro Switch

At approximately 70,150 seconds (19:29:10) the yaw control rate gyro signal indicated that a failure occurred resulting in loss of rate feedback in the control system, caused by insufficient electrical power in the 6D10 battery. Loss of the yaw rate feedback, combined with the large attitude error signal, caused two yaw ( $I_{II}$  and  $III_{II}$ ) control engines to come full on in order to establish the necessary rate to offset the attitude error signal. With loss of the yaw rate feedback, the control system could not correct for the rate imparted to the vehicle by the yaw control engines and commanded the yaw engines to remain full on. After approximately 86 seconds, module 1 fuel depleted at 70,235 seconds (19:30:35). Fuel normally depletes first since the oxidizer to fuel loading ratio is approximately 1.64 (near that of the attitude control engine operating ratio), but the APS ullage engines operate at an oxidizer to fuel ratio of 1.27. Following fuel depletion, the oxidizer will provide a thrust of approximately 44.48 Newtons (10 lbf) (normal thrust is 654.8 Newtons [147.2 lbf]). Module 2 fuel depleted at 70,256.5 seconds (19:30:56.5), approximately 21.5 seconds after module 1 fuel depleted.

Figure 10-9. Pitch and Yaw Control System Response to Loss of Attitude Reference



Because only one yaw engine was burning for 21.5 seconds, a significant amount of roll torque was applied to the vehicle causing the roll rate to increase to approximately 27 deg/s. Roll rate feedback was lost shortly after the yaw rate feedback, and therefore was not present to prevent a large roll rate. Module 1 and module 2 oxidizer depletion times were 70,276 seconds (19:31:16) and 70,294 seconds (19:31:34), respectively. It is quite possible that the full on yaw/roll APS control engines provided significant translational  $\Delta V$ , which changed the lunar impact point. A complete evaluation of the potential  $\Delta V$  contribution of the attitude control engines is presently being performed.

#### 10.5 INSTRUMENT UNIT CONTROL COMPONENTS EVALUATION

The Flight Program Minor Loop implemented all guidance commands, providing satisfactory attitude error outputs through the Launch Vehicle Data Adapter (LVDA) to the FCC. No valid Minor Loop Error Telemetry occurred during the mission.

The yaw command rate gyro input to the control computer ceased to operate because of insufficient battery voltage. The yaw channel of the control system began oscillating with no rate input at 46,050 seconds (12:47:30), as indicated by yaw attitude error and yaw reference rate gyro telemetry.

At approximately 46,233 seconds (12:50:33), the Control Signal Processor (CSP) sensed a sufficient voltage difference (7.4 volts) between the command channel and reference channels to select the properly functioning spare gyro channel. Upon switching to the spare rate channel, the control system ceased oscillation, as shown in Figure 10-8.

At 68,948 seconds (19:09:08), the LVDC lost its ability to access memory, due to 6D10 battery depletion, and the flight program essentially ceased operation. Because of the cessation of Minor Loop output to the LVDA digital-to-analog converter (ladder register), the ladder amplifiers for the pitch and yaw attitude error channel drifted to full scale positive values. (Full scale at this time was approximately 11.8 degrees because of the decaying supply voltages.) The roll ladder amplifier did not drift, indicating that it was the last serviced by the Minor Loop. The Flight Control Subsystem responded to the attitude error input by commanding sufficient pitch and yaw thruster firings to cause rates which balanced the attitude error signals. The resulting rates were approximately -2 deg/s about the pitch and yaw axes, as shown in Figure 10-9.

This condition persisted until the 6D10 battery depleted to the extent that a yaw comparator relay relaxed, allowing the rate input to the FCC to switch to the command gyro which had no output. The spare yaw rate gyro had been in use because of the previous depletion of the 6D40 battery which powered the command yaw gyro. The FCC reacted to the sudden loss of the yaw rate input by firing the APS yaw thrusters continuously to depletion. Enough coupling occurred to cause perturbation of the pitch

rate gyro which, along with the FCC, was powered by the depleting 6D30 battery. The subsequent oscillating pitch rate signal caused alternate firings of the pitch thrusters. These conditions prevailed until oxidizer depletion at 70,294 seconds (19:31:34).

The APS thrust imparted a rotational velocity of approximately 12 deg/s to the vehicle and changed the translational velocity by approximately 2.5 m/s (8.2 ft/s). Simulations verify the capability of the APS to change the translational velocity by this amount.

The observed sequence of events was dictated largely by the sequence of battery depletion. Had a different battery load allocation been implemented, then the pitch channel may have been firing continuously with the yaw channel oscillating. The translational and rotational velocity changes would then be quite different because pitch impulse is one-half that of the yaw channel.

A different battery depletion sequence would also cause the loss of a different set of LVDA power supplies at the depletion of the second battery, possibly causing different attitude error output.

The final velocity change, due to uncontrolled APS thrusting, can be eliminated by deactivating the FCC at the end of the IU mission. The feasibility and means of best accomplishing this are presently being evaluated.

## 10.6 SEPARATION

S-IC/S-II separation and associated sequencing was accomplished as planned. Dynamic conditions at separation fell within estimated end conditions, and well within the staging limits. The AS-508 measured longitudinal acceleration of the S-IC dropped stage was similar to previous vehicles. Pitch and yaw gyro data showed no disturbances, indicating a clean severance of the stages.

The AS-508 flight was not instrumented for monitoring second plane separation. To give an indication of the dynamics of second plane separation, based on available flight data, the dynamics of both the second stage and the separating interstage were calculated. The calculated dynamics of separation show no significant differences from previous flights.

The S-II retromotors and the S-IVB ullage motors performed satisfactorily and provided a normal S-II/S-IVB separation. Dynamic conditions were within staging limits with separation conditions similar to those observed on previous flights.

Separation of the CSM from the LV occurred as planned. There were no large control disturbances noted during the separation. The attitude of the LV was adequately maintained during the docking of the CSM with the Lunar Module (LM). The CSM/LM then successfully spring ejected from the LV. There were no significant control disturbances during the ejection.

SECTION 11  
ELECTRICAL NETWORKS  
AND  
EMERGENCY DETECTION SYSTEM

11.1 SUMMARY

The AS-508 launch vehicle electrical systems and Emergency Detection System (EDS) performed satisfactorily throughout the required period of flight. Operation of the batteries, power supplies, inverters, Exploding Bridge Wire (EBW) firing units and switch selectors was normal.

AS-508 was the first flight that significant data were available to battery depletion.

11.2 S-IC STAGE ELECTRICAL SYSTEM

The S-IC stage electrical system performance was satisfactory. Battery voltages remained well within performance limits of 26.5 to 32.0 vdc during powered flight. The battery currents were within predicted limits and below the maximum limit of 64 amperes for each battery. Battery power consumption was well within the rated capacity of each battery, as shown in Table 11-1.

Table 11-1. S-IC Stage Battery Power Consumption

BATTERY	BUS DESIGNATION	RATED CAPACITY (AMP-MIN)	POWER CONSUMPTION*	
			AMP-MIN	PERCENT OF CAPACITY
Operational	1D10	640	28.1	4.4
Instrumentation	1D20	640	86.1	13.5
*Battery power consumptions were calculated from power transfer until S-IC/S-II separation.				

The two measuring power supplies remained well within the  $5 \pm 0.05$  vdc design requirement.

All switch selector channels functioned properly, and all outputs were issued within required time limits in response to Instrument Unit (IU) commands.

The separation and retromotor EBW firing units were armed and triggered as programmed. Charging times and voltage limits were within predictions.

The command destruct EBW firing units were in the required state-of-readiness if vehicle destruct had been necessary.

### 11.3 S-II STAGE ELECTRICAL SYSTEM

The S-II stage electrical system performed satisfactorily. Battery voltages remained within specified limits throughout the prelaunch and flight periods. Bus currents also remained within required and predicted limits. Main bus current averaged 38 amperes during S-IC boost and varied from 49 to 57 amperes during S-II boost. Instrumentation bus current averaged 22 amperes during S-IC and S-II boost. Recirculation bus current averaged 97 amperes during S-IC boost. Ignition bus current averaged 29 amperes during the S-II ignition sequence. Battery power consumption was well within the rated capacity of each battery, as shown in Table 11-2.

The five temperature bridge power supplies, the three instrumentation power supplies, and the five LH<sub>2</sub> inverters all performed within acceptable limits.

All switch selector channels functioned properly, and all outputs were issued within required time limits in response to the IU commands.

Table 11-2. S-II Stage Battery Power Consumption

BATTERY	BUS DESIGNATION	RATED CAPACITY (AMP-HR)	POWER CONSUMPTION*		TEMPERATURE (°F)	
			AMP-HR	PERCENT OF CAPACITY	MAX	MIN
Main	2D11	35	8.50	24.3	98.0	87.0
Instrumentation	2D21	35	4.94	14.1	83.5	80.0
Recirculation No. 1	2D51	30	5.74	19.1	85.5	79.5
Recirculation No. 2	2D51 and 2D61	30	5.78	19.3	88.5	82.5

\*Battery power consumptions were calculated from power transfer until S-II/S-IVB separation.

Performance of the EBW circuitry for the separation system was satisfactory. Firing units charge and discharge responses were within predicted time and voltage limits. The command destruct EBW firing units were in the required state-of-readiness if vehicle destruct had been necessary.

#### 11.4 S-IVB STAGE ELECTRICAL SYSTEM

The S-IVB stage electrical system performed satisfactorily. The battery voltages, currents, and temperature remained within normal range beyond the required battery lifetime. Forward No. 2 battery depleted at 31,400 seconds (08:43:20) after supplying 122.9 percent of the rated capacity. Battery voltage and current plots are shown in Figures 11-1 through 11-4. Battery power consumption and capacity for each battery are shown in Table 11-3.

The three 5-vdc and seven 20-vdc excitation modules all performed within acceptable limits. The LOX and LH<sub>2</sub> chilldown inverters performed satisfactorily and fulfilled load requirements.

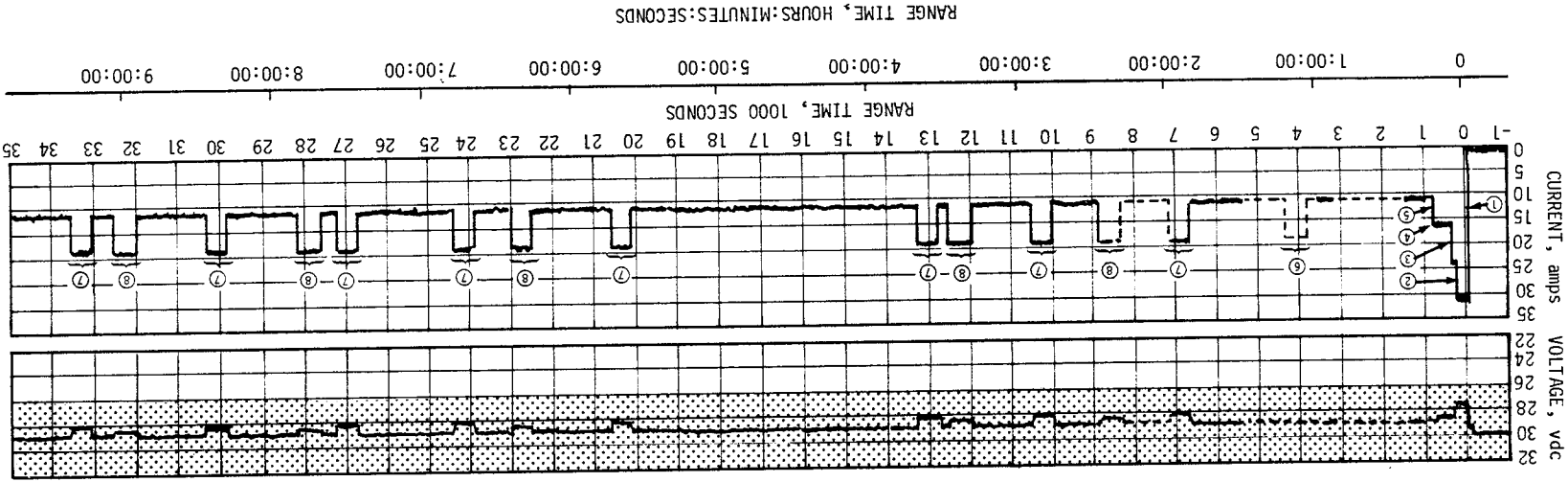
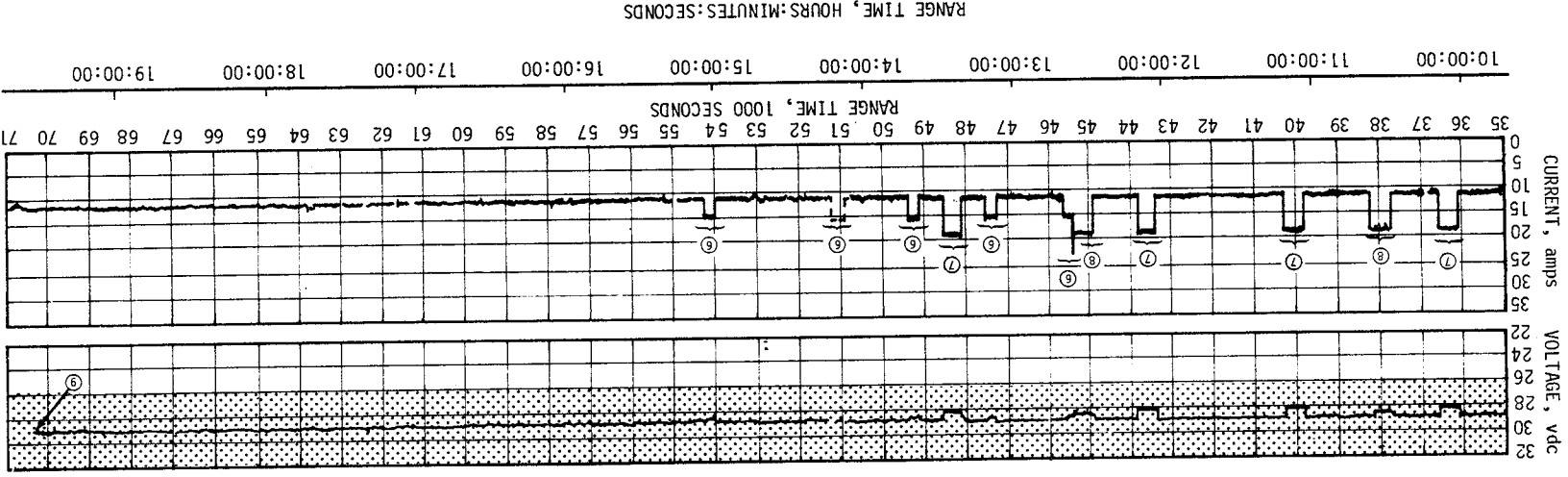
All switch selector channels functioned properly, and all outputs were issued within required time limits in response to IU commands.

Performance of the EBW circuitry for the separation system was satisfactory. Firing units charge and discharge responses were within

Table 11-3. S-IVB Stage Battery Power Consumption

BATTERY	RATED CAPACITY (AMP-HR)	POWER CONSUMPTION	
		AMP-HR*	PERCENT OF CAPACITY
Forward No. 1	300.0	234.79	78.3
Forward No. 2	24.75	30.42**	122.9
Aft No. 1	300.0	205.32	68.4
Aft No. 2	75.0	33.30	44.4
<p>* Actual usage to 70,380 seconds (19:33:00) is based on flight data.</p> <p>** The battery voltage fell below the minimum operating limit of 24.5 volts at 31,400 seconds (08:43:20). Calculation of actual power consumption was terminated at this time.</p>			

Figure 11-1. S-IVB Stage Forward No. 1 Battery Voltage and Current



- ① TRANSFER TO INTERNAL POWER
- ② FORWARD NO. 1 BATTERY HEATER OFF
- ③ FORWARD NO. 2 BATTERY HEATER OFF
- ④ RANGE SAFETY NO. 1 OFF
- ⑤ SSB DISABLE
- ⑥ FORWARD NO. 2 BATTERY HEATER CYCLE
- ⑦ FORWARD NO. 1 BATTERY UNIT 2 HEATER CYCLE
- ⑧ FORWARD NO. 1 BATTERY HEATER CYCLE
- ⑨ 301 MULTIPLEXER WENT OUT OF SYNC (IU)
- ACTUAL
- - - PREDICTED
- ⋯ ACCEPTABLE LIMITS

- ① TRANSFER TO INTERNAL POWER
- ② RANGE SAFETY NO. 2 OFF
- ③ PU INVERTER POWER OFF
- ④ PU INVERTER POWER ON
- ⑤ PU 4.5 TO 1 ON
- ⑥ PU PROGRAM MIXTURE RATIO OFF
- ⑦ FORWARD NO. 2 BATTERY DEPLETION

······ ACCEPTABLE LIMITS  
 - - - - PREDICTED  
 ———— ACTUAL

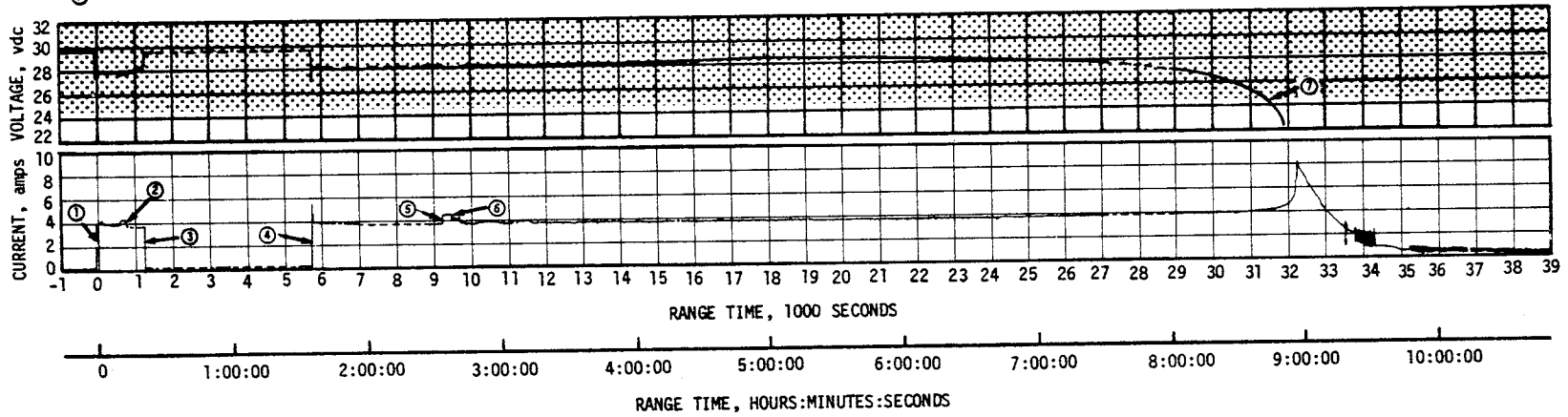


Figure 11-2. S-IVB Stage Forward No. 2 Battery Voltage and Current

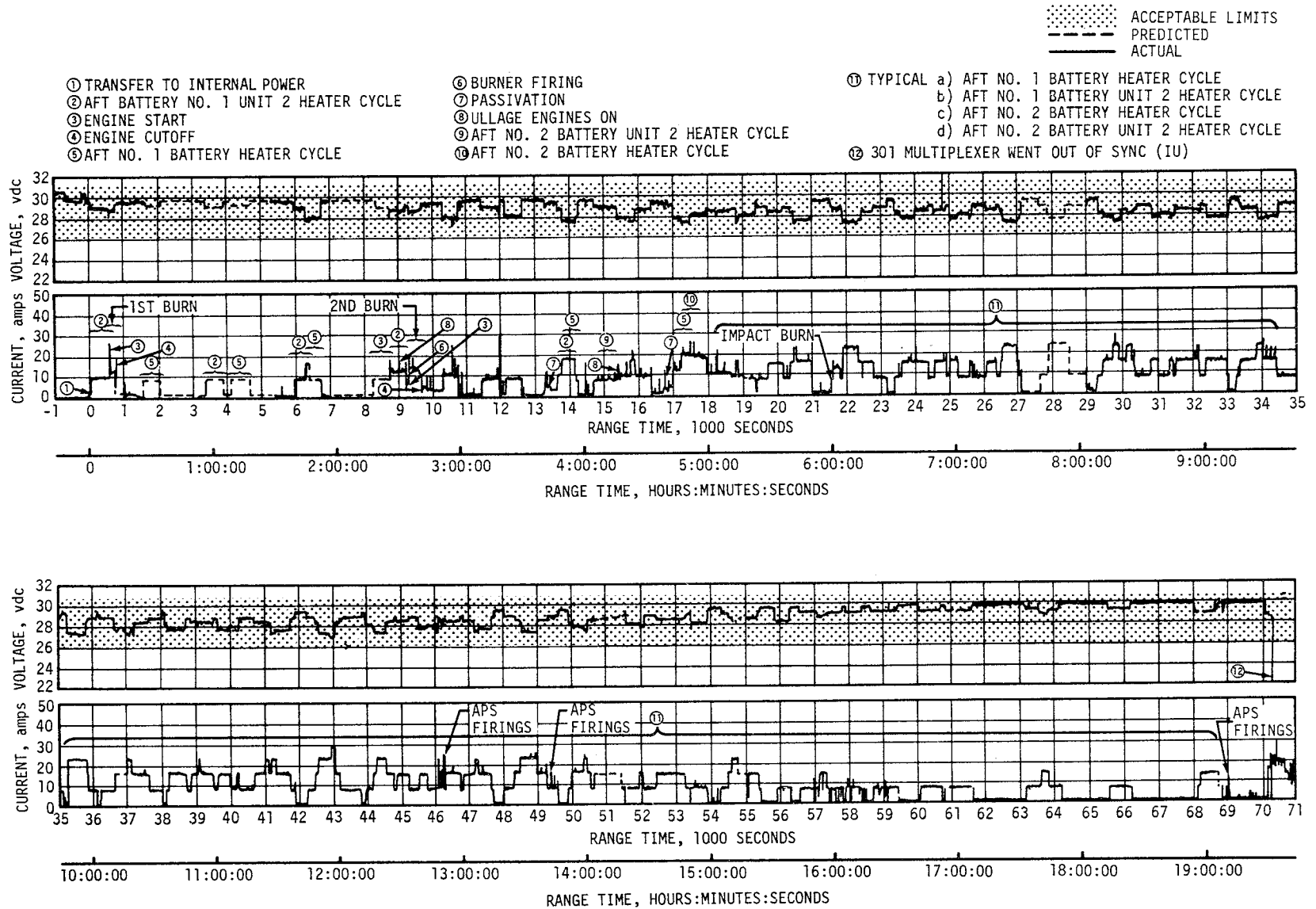


Figure 11-3. S-IVB Stage Aft No. 1 Battery Voltage and Current

- ① TRANSFER TO INTERNAL POWER
- ② LOX AND LH<sub>2</sub> CHILLDOWN PUMPS OFF
- ③ ENGINE START
- ④ AUX HYDRAULIC PUMP OFF
- ⑤ AUX HYDRAULIC PUMP CYCLE

- ⑥ AUX HYDRAULIC PUMP ON
- ⑦ LOX AND LH<sub>2</sub> CHILLDOWN PUMPS ON
- ⑧ AFT NO. 2 BATTERY HEATER CYCLE (NOT DATA)
- ⑨ NO LOAD - LIMITS DO NOT APPLY
- ⑩ 301 MULTIPLEXER WENT OUT OF SYNC (IU)

..... ACCEPTABLE LIMITS  
 - - - - - PREDICTED  
 \_\_\_\_\_ ACTUAL

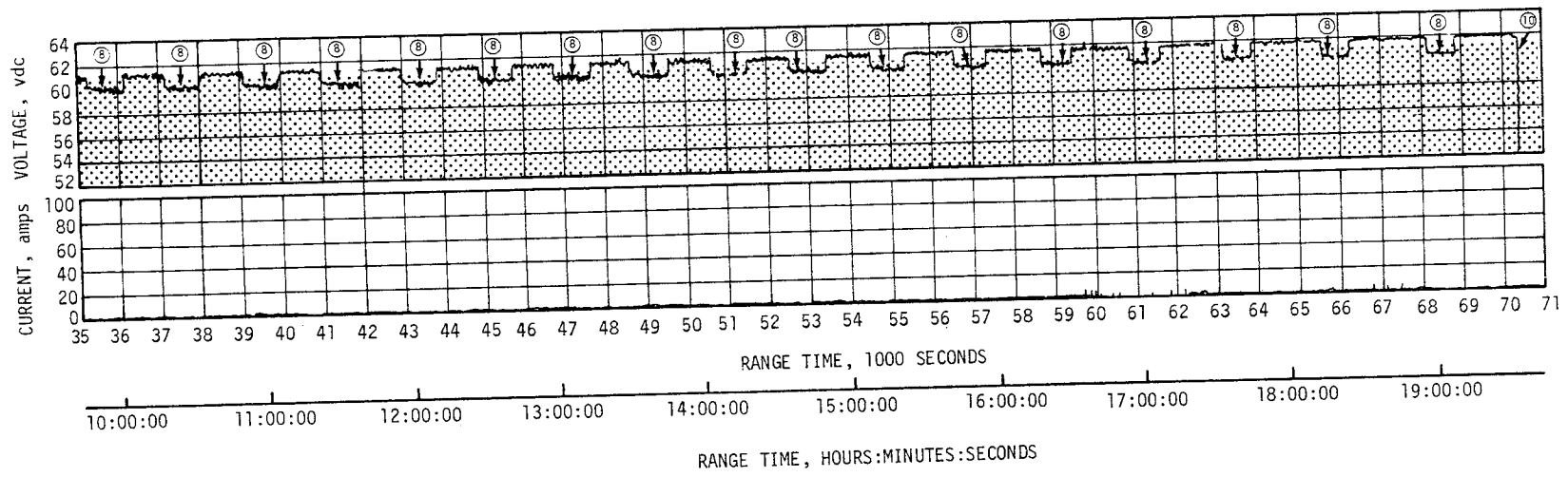
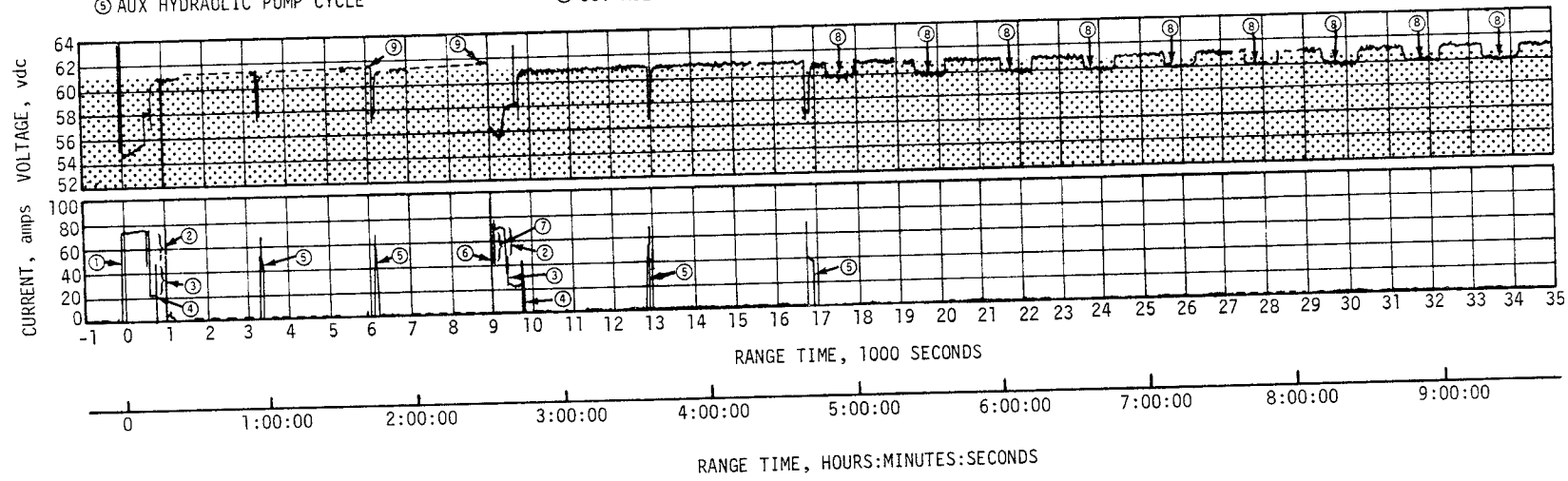


Figure 11-4. S-IVB Stage Aft No. 2 Battery Voltage and Current

predicted time and voltage limits. The command destruct firing units were in the required state-of-readiness if vehicle destruct had been necessary.

### 11.5 INSTRUMENT UNIT ELECTRICAL SYSTEM

Battery 6D20 was added to the IU electrical system on the AS-508 vehicle to provide power for operating the Command and Communication System (CCS) transponder and power amplifier until S-IVB/IU lunar impact.

The IU electrical system functioned normally. All battery voltages and temperatures increased gradually from liftoff as expected. Batteries 6D10, 6D30, and 6D40 remained within normal range beyond their expected lifetime. Batteries 6D10, 6D30 and 6D40 depleted after supplying 106.3, 107.4 and 108.0 percent, respectively, of their rated capacity. AS-508 was the first flight that significant data were available to battery depletion. The performance of guidance, navigation, and control systems was affected by battery depletion, as discussed in Sections 9 and 10. The 6D20 battery operated satisfactorily throughout flight. The CCS which was powered by battery 6D20 was operating when the S-IVB/IU impacted the lunar surface. Battery power consumption, capacity, and lifetime for each battery are shown in Table 11-4. Battery voltages, currents and temperatures are shown in Figure 11-5 through 11-8.

The 56-vdc power supply maintained an output voltage of 55.8 to 56.6 vdc, well within the required tolerance of  $56 \pm 2.5$  vdc.

Table 11-4. IU Battery Power Consumption

BATTERY	RATED CAPACITY (AMP-HR)	POWER CONSUMPTION		BATTERY LIFETIME (HOURS)
		AMP-HR	PERCENT OF CAPACITY	
6D10	350	372	106.3	18.4*
6D20	350	322**	92.0**	**
6D30	350	376	107.4	19.1*
6D40	350	378	108.0	11.3*

\* Actual battery life was assumed to end when bus voltage fell below the nominal limit of  $28 \pm 2$  volts.

\*\* The CCS transponder, powered by the 6D20 battery, was operating at S-IVB/IU lunar impact which occurred at 280,601 seconds (77:56:41). Power consumption until S-IVB/IU lunar impact was calculated based on nominal operation.

4

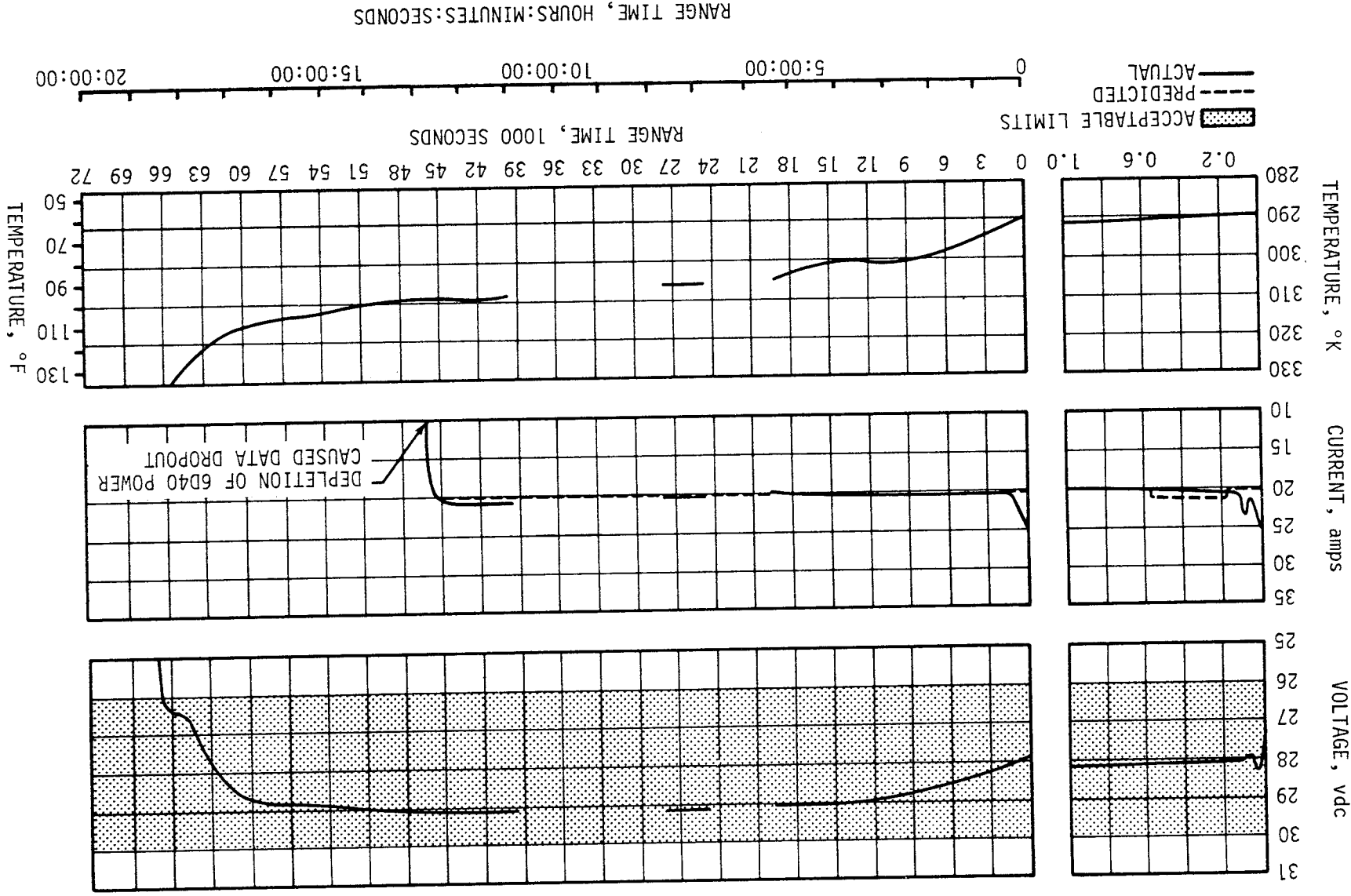


Figure 11-5. IU Battery 6D10 Voltage, Current and Temperature

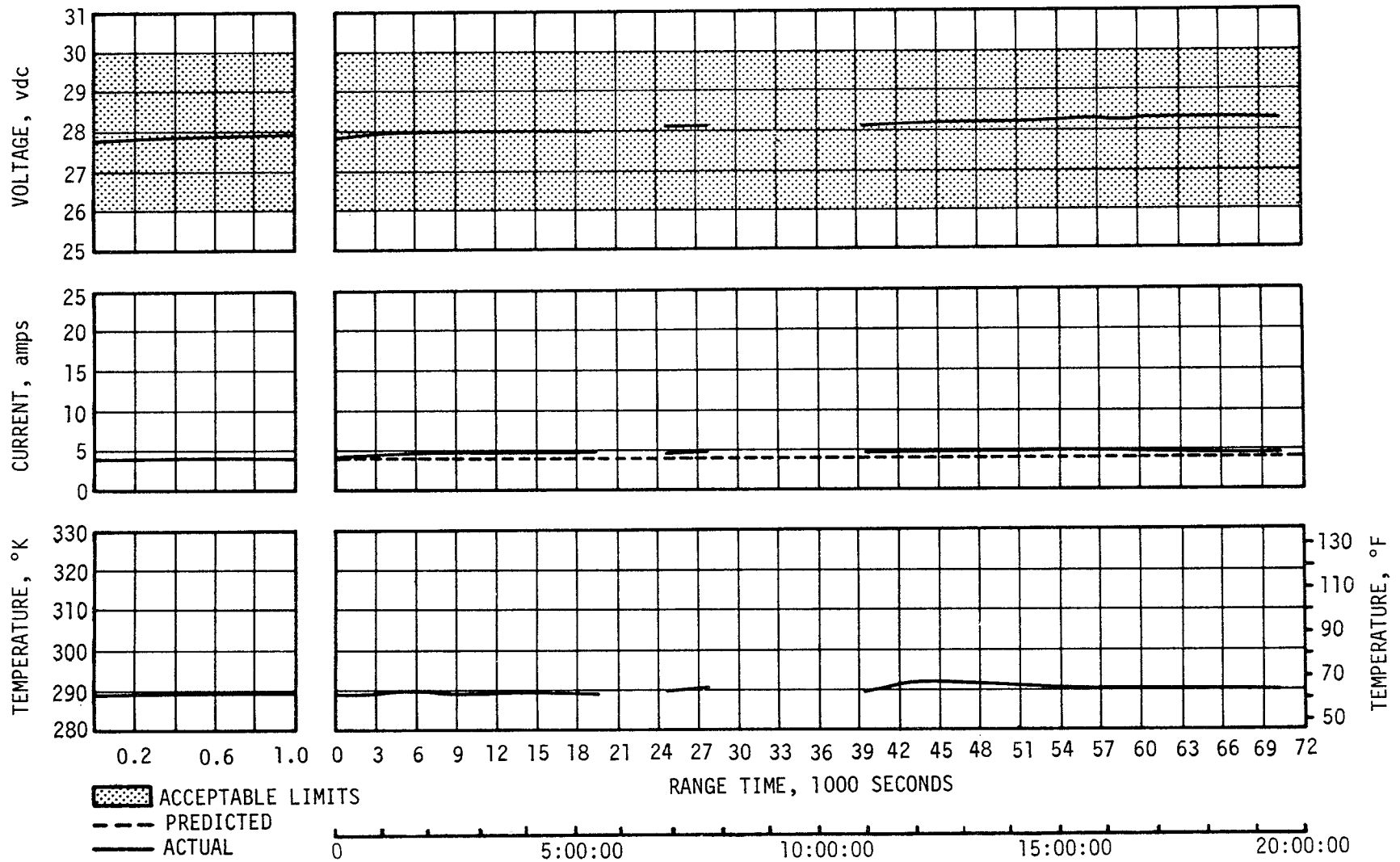


Figure 11-6. IU Battery 6D20 Voltage, Current and Temperature

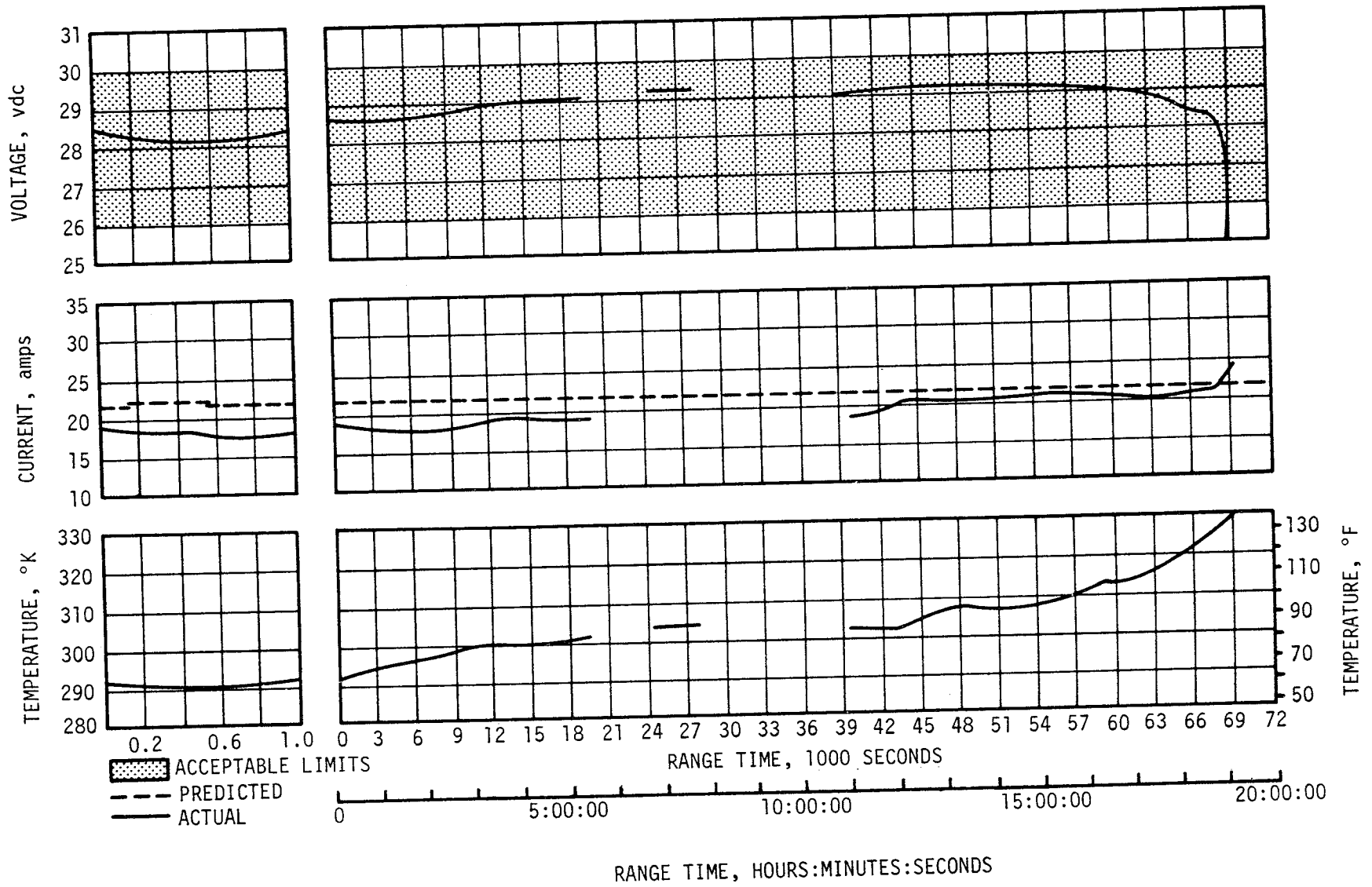


Figure 11-7. IU Battery 6D30 Voltage, Current and Temperature

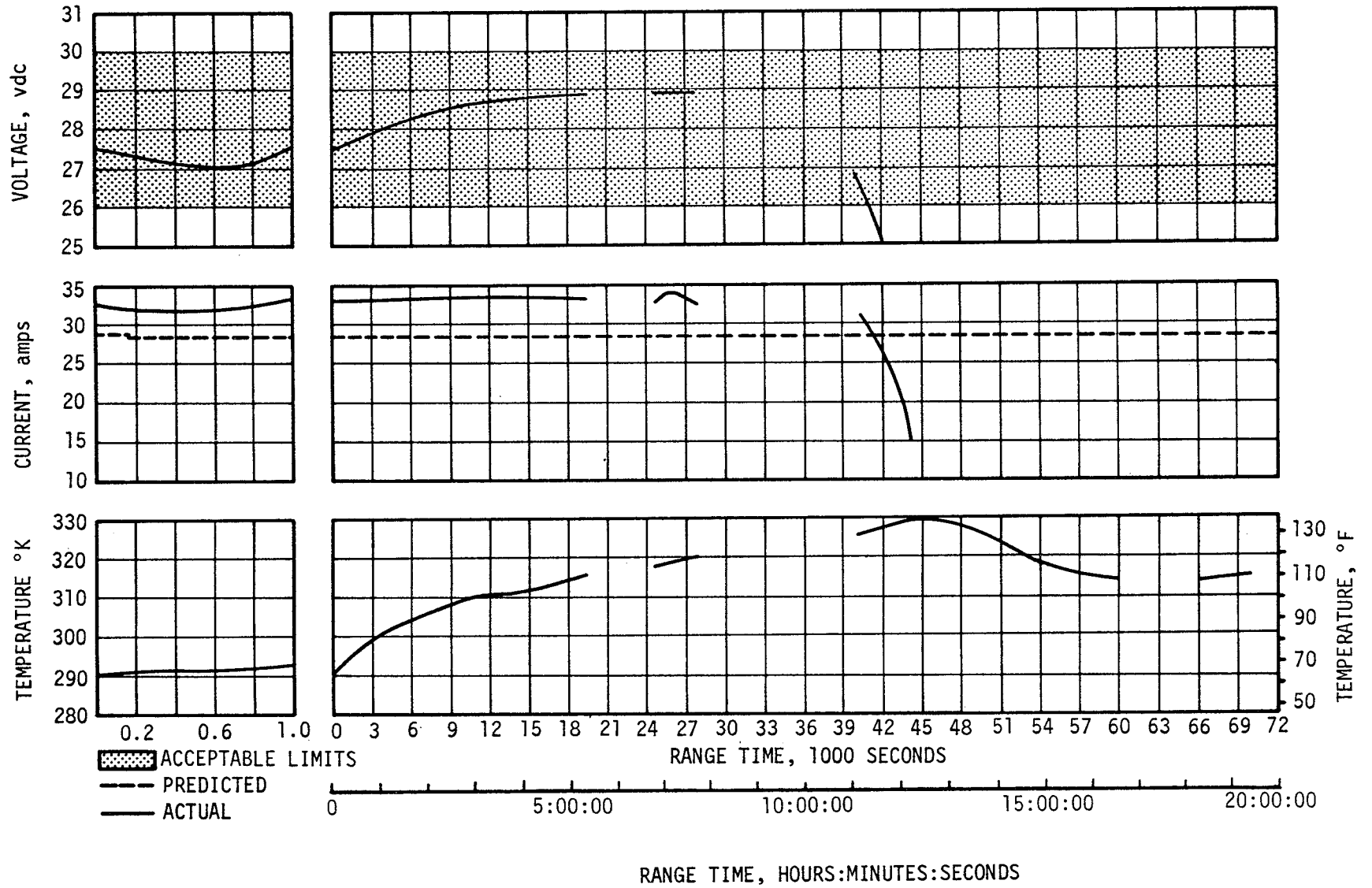


Figure 11-8. IU Battery 6D40 Voltage, Current and Temperature

The 5-vdc measuring power supply performed normally, maintaining a constant voltage within specified tolerances.

The switch selector, electrical distributors, and network cabling performed normally.

#### 11.6 SATURN V EMERGENCY DETECTION SYSTEM (EDS)

The performance of the AS-508 was normal and no abort limits were exceeded. EDS related events and discrete indications occurred as expected. S-II and S-IVB stage tank ullage pressures remained within the abort limits and displays to the crew were normal. The performance of all thrust OK pressure switches and associated voting logic, which monitor engine status, was normal insofar as EDS operation was concerned. However, variations in the LOX pump discharge pressure tripped the S-II stage center engine thrust OK pressure switches causing early shutdown of the S-II stage center engine. This problem is discussed in detail in paragraphs 6.3 and 8.2.

The dynamic pressure at maximum angle-of-attack as sensed by the Q-ball mounted atop the escape tower was 0.65 psid at 75 seconds. This pressure was only 20.3 percent of the EDS abort limit of 3.2 psid. As noted in section 10, none of the rate gyros gave any indication of angular overrate in the pitch, yaw or roll axis. The maximum angular rates were well below the abort limits.



## SECTION 12

### VEHICLE PRESSURE AND ACOUSTIC ENVIRONMENT

#### 12.1 SUMMARY

The S-IC base heat shield was instrumented with two differential pressure measurements. The AS-508 flight data show good agreement with data from previous flights.

In general, the S-II heat shield forward face and thrust cone static pressures agree favorably with previous flights. The heat shield aft face pressure was somewhat higher than seen on previous flights but was consistent with the outboard engines being gimballed more inboard on the AS-508 flight.

Acoustical measurements were made at 12 locations on the S-IVB interstage and aft skirt. Generally, AS-508 acoustic flight data agree favorably with data from previous flights. The six measurements located near vehicle position IV experienced a data dropout at liftoff.

#### 12.2 BASE PRESSURES

##### 12.2.1 S-IC Base Pressures

The S-IC base heat shield was instrumented with two differential (internal minus external) pressure measurements. The AS-508 flight data, Figure 12-1, show good agreement with data from previous flights. A maximum differential pressure of 0.18 psid occurred at an altitude of approximately 4 n mi.

The S-II stage base heat shield forward face pressure was below the data band of previous flights, prior to interstage separation, as shown in Figure 12-2. However, a measurement bias is suspected as the cause because of the inconsistency of this measurement with the values indicated by the thrust cone and heat shield aft face pressure sensors prior to J-2 engine ignition (see Figures 12-3 and 12-4). A bias of this magnitude is caused by ambient condition changes and transducer calibration inaccuracies. This measurement bias is not considered to be a problem.

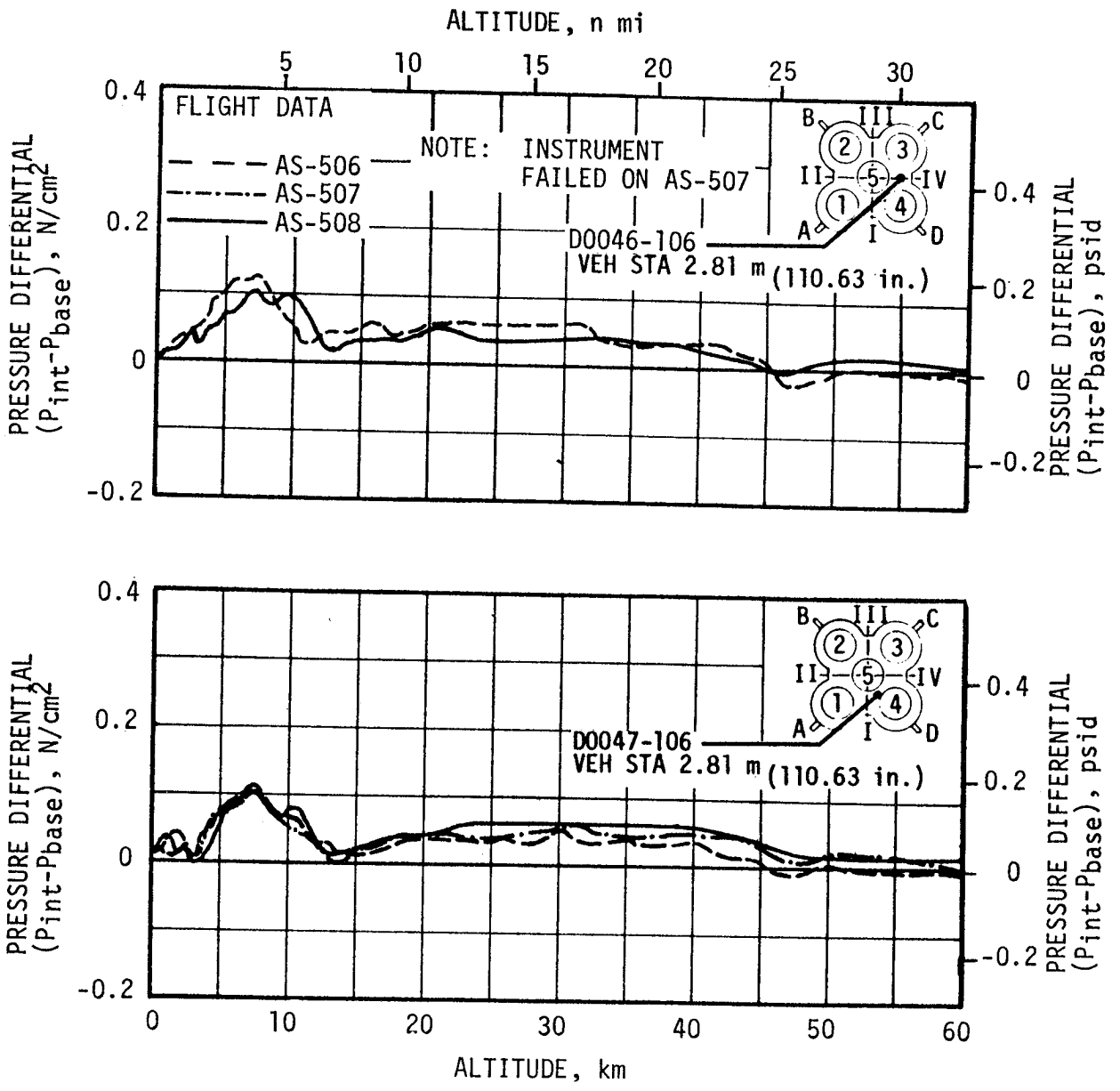


Figure 12-1. S-IC Base Heat Shield Differential Pressure

The AS-508 thrust cone pressure, prior to interstage separation, shows good agreement with data from previous flights as shown in Figure 12-3. After interstage separation the indicated pressure was higher than seen on any previous flights, but was still within acceptable limits. The postflight analytical values of heat shield forward face and thrust cone region pressures were obtained from analytical values of the heat shield aft face pressures using correlations derived from AS-501 through AS-507 flight data.

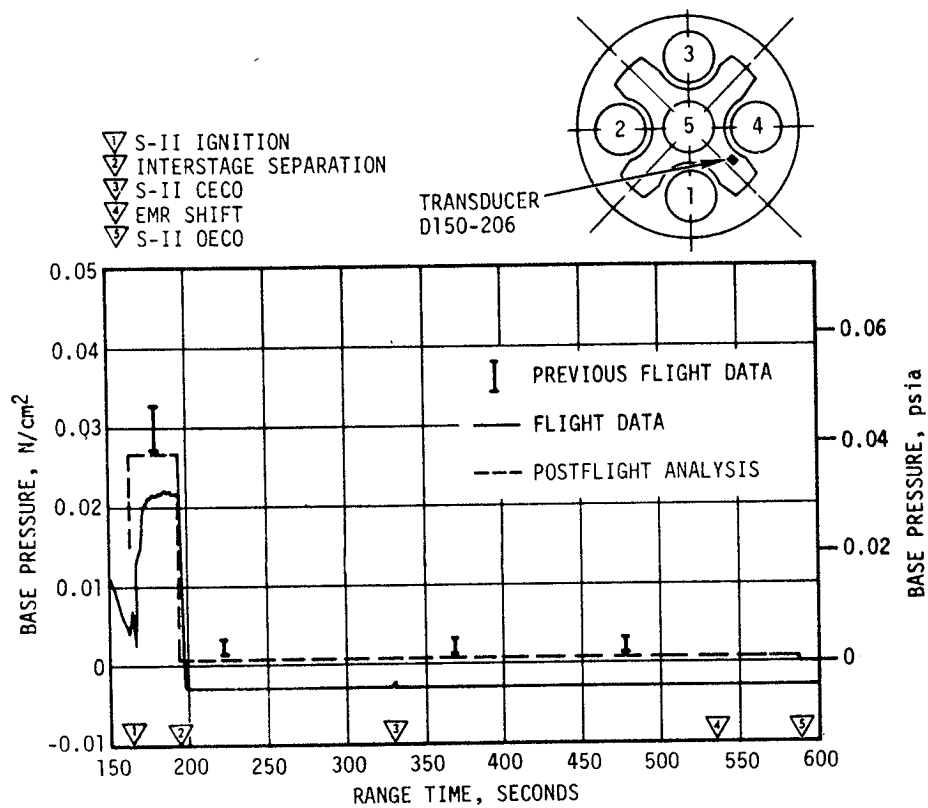


Figure 12-2. S-II Base Heat Shield Forward Face Pressure

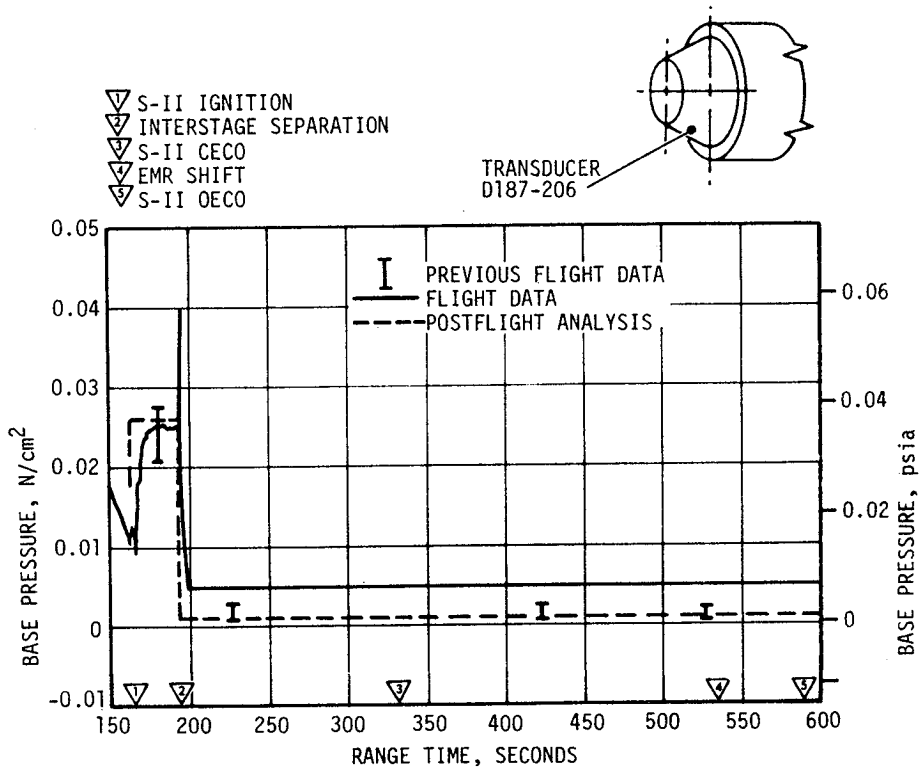


Figure 12-3. S-II Thrust Cone Pressure

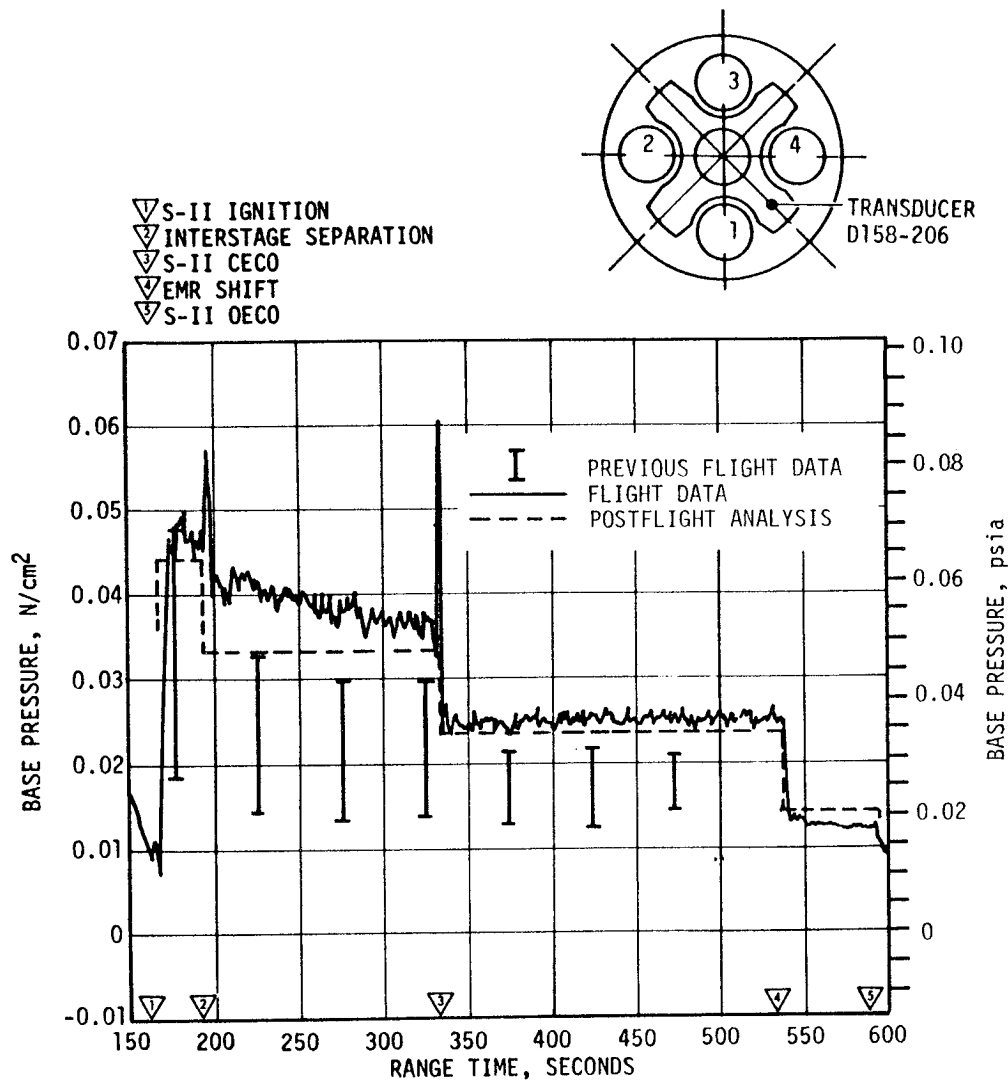


Figure 12-4. S-II Heat Shield Aft Face Pressure

The heat shield aft face pressures observed on AS-508 were, in general, higher than those measured on previous flights. Prior to interstage separation, the heat shield aft face pressure data was equal to the maximum pressure recorded at this pressure transducer location during the previous flights, as shown in Figure 12-4. After interstage separation the pressure was approximately 0.01 psia above pressures noted during previous flights. This higher flight pressure is consistent with the nominal AS-508 steady-state J-2 engine deflection patterns which show that the engines were gimballed further inboard on AS-508 than on previous flights. After Center Engine Cutoff (CECO), the pressure dropped 0.02 psia and remained constant until Engine Mixture Ratio (EMR) shift. This expected CECO pressure drop was not recorded by transducer D158-206 on previous flights; however, it was clearly indicated by all other aft face pressure measurements of previous flights.

## SECTION 13

### VEHICLE THERMAL ENVIRONMENT

#### 13.1 SUMMARY

The AS-508 S-IC base region thermal environments exhibited trends similar to those seen on previous flights with magnitudes, in general, lower than those seen on AS-507.

The base thermal environments on the S-II stage were similar to those measured on previous flights and were well below design limits. Both the total heating rate measurement and the recovery temperature probe for the base heat shield indicated higher magnitudes than those seen on AS-507. This could be expected since the outboard engines were gimballed further inboard than on AS-507.

Aerodynamic heating environments and S-IVB base thermal environments were not measured on AS-508.

#### 13.2 S-IC BASE HEATING

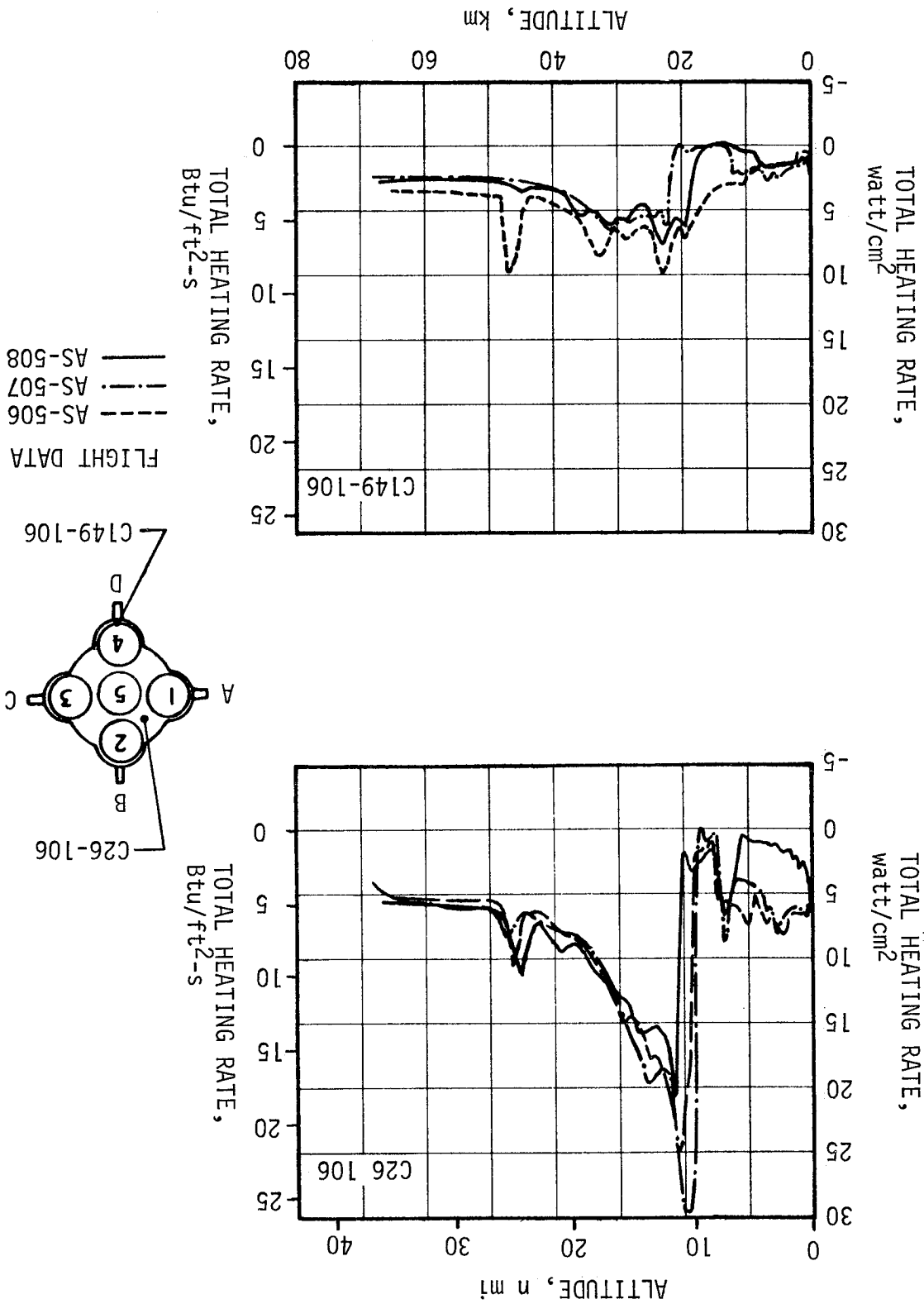
Thermal environments in the base region of the S-IC stage were recorded by two total calorimeters and two gas temperature probes which were located on the base heat shield. Data from these instruments are compared with AS-506 and AS-507 flight data and are presented in Figures 13-1 and 13-2. The AS-508 S-IC base heat shield thermal environments exhibit similar trends and are less severe than those measured on previous flights. The maximum recorded total heating rate, 18 Btu/ft<sup>2</sup>-s, occurred at approximately 11 n mi. The maximum recorded gas temperature, 1628°F occurred at approximately 12 n mi. In general, Center Engine Cutoff (CECO) on AS-508 produced a spike in the thermal environment data with a magnitude and duration similar to previous flight data.

Ambient gas temperatures under the engine cocoons (measurements C242-101 through C242-105) were within the band of previous flight data and within the predicted band. These temperatures are shown in Figure 13-3.

#### 13.3 S-II BASE HEATING

Figure 13-4 presents the AS-508 total heating rate throughout S-II burn as recorded by transducer C722-206 on the aft face of the base heat shield. The postflight analytical curve for this transducer and the previous flights data band are also shown for comparison. The analytical heat rate represents the theoretical response of the transducer to the total

Figure 13-1. S-IC Base Heat Shield Total Heating Rate



The postflight analytical values of heat shield aft face pressures are evaluated using a semi-empirical correlation between heat shield aft face static pressures and heating rates. This correlation is based on 1/25 scale model hot flow test results and AS-501 through AS-507 flight data. The effects of the S-IC/S-II stage interstage separation, CECO, and EMR shift are included in the analysis.

## 12.3 ACOUSTIC ENVIRONMENT

### 12.3.1 External Acoustics

AS-508 external fluctuating pressures were measured at 12 vehicle stations located on the S-IVB interstage and S-IVB aft skirt. Figure 12-5 shows the instrument numbers and locations of the 12 pressure transducers. Six instruments, B0033-402 through B0038-404, indicated data dropouts at around liftoff. These instruments are located near vehicle Position IV; the remaining instruments, located on or near vehicle Position III, show no data dropouts during this time period. The data dropouts lasted approximately 6 seconds and did not appear to be a direct result of the AS-508 external acoustic environment at liftoff. The cause of the dropouts has not been determined.

The vehicle overall sound pressure levels at liftoff are shown in Figure 12-6. AS-508 liftoff data show good agreement with previously measured data.

Figure 12-7 presents overall fluctuating pressure/time histories for S-IC boost. AS-507 flight data and Saturn V 4 percent scale model test data are included for comparison. AS-508 overall time histories were generally comparable to AS-507 data. Similar trends were evident in the two sets of data and agreement was good during periods of peak noise. The differences in fluctuating pressure between AS-507 and AS-508 during periods of low aerodynamic noise are believed to be caused by the difference in calibration levels of the two flights. AS-508 data are believed to be more accurate. However, it should be noted that the temperature limit of the transducers appears to have been exceeded after 100 seconds due to aerodynamic heating. Effects of the heating on the validity of the data beyond 100 seconds are not known.

The Saturn V 4 percent scale model test data (Mach = 0.6 to 1.45) show good agreement with data from 10 of the 12 flight instruments. Lower fluctuating pressure levels during flight were shown by instruments B0031-402 and B0032-402 which were located just aft of the S-IVB auxiliary propulsion system on Position III. Power spectra at or near maximum aerodynamic noise generally show good agreement with respect to shape and decibel level between AS-507 and AS-508 flights (see Figure 12-8).

INSTRUMENT NUMBER	VEHICLE STA. METERS (IN.)	INSTRUMENT NUMBER	VEHICLE STA. METERS (IN.)
B0028-402	64.72 (2548)	B0034-402	64.87 (2554)
B0029-402	65.38 (2574)	B0035-402	65.76 (2589)
B0030-402	65.76 (2589)	B0036-402	69.24 (2726)
B0031-402	68.86 (2711)	B0037-404	70.38 (2771)
B0032-402	69.42 (2733)	B0038-404	70.71 (2784)
B0033-402	64.24 (2529)	B0039-404	70.71 (2784)

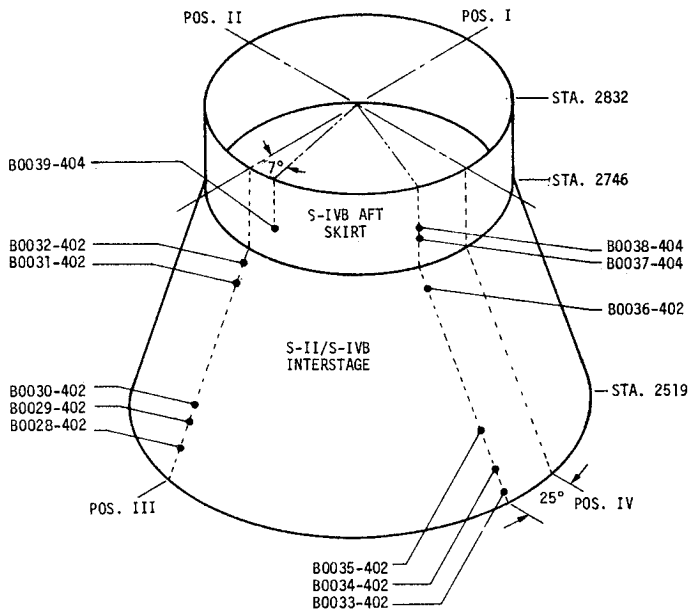


Figure 12-5. AS-508 Acoustic Instrumentation

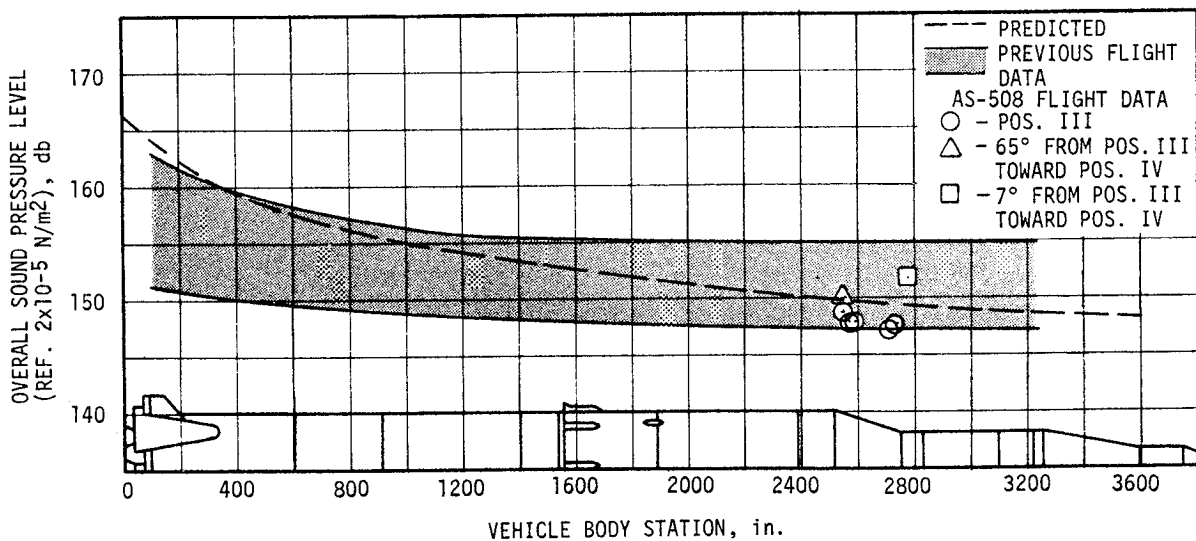


Figure 12-6. External Overall Sound Pressure Level At Liftoff

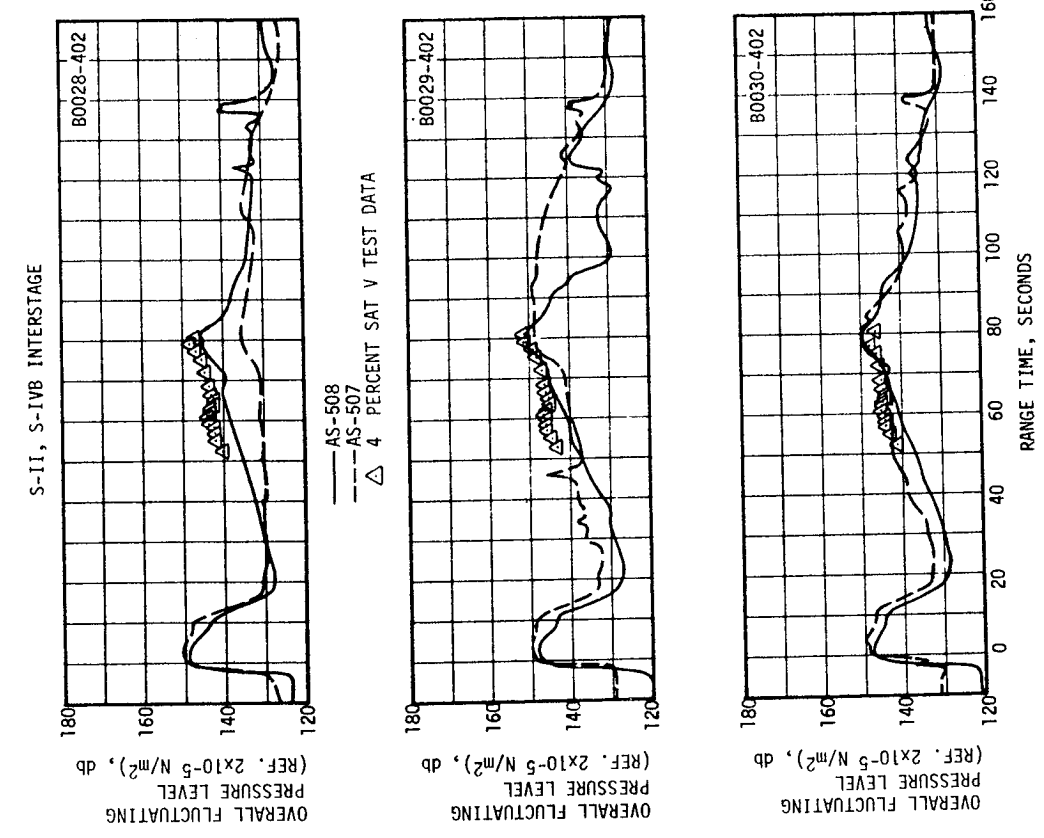
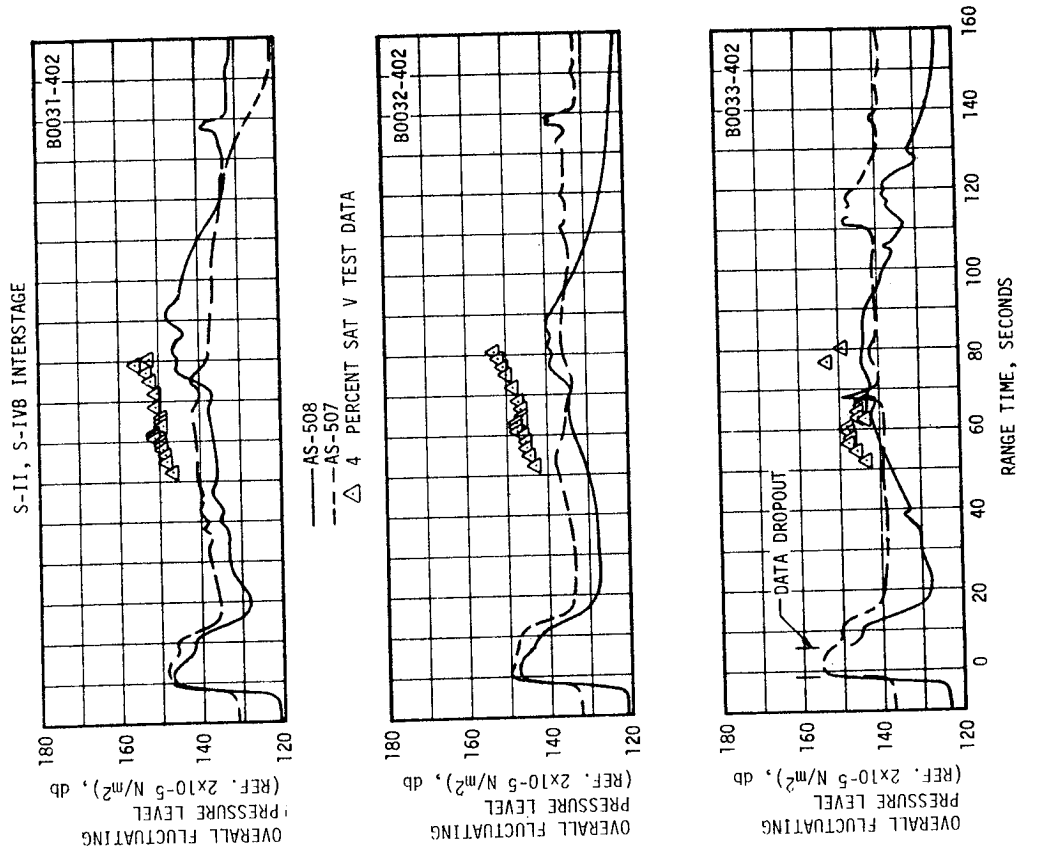


Figure 12-7. Vehicle External Overall Fluctuating Pressure Level (Sheet 1 of 2)

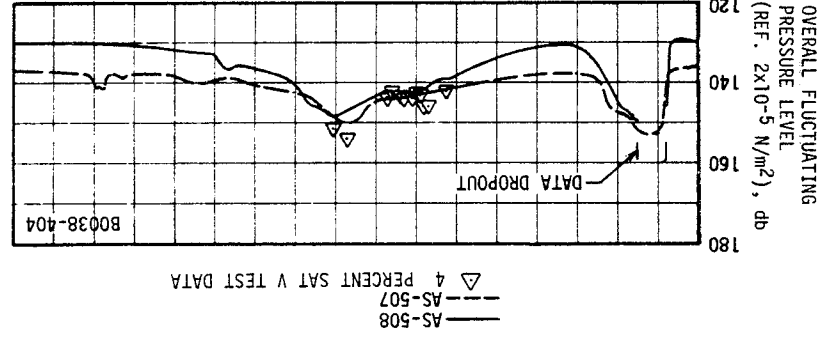
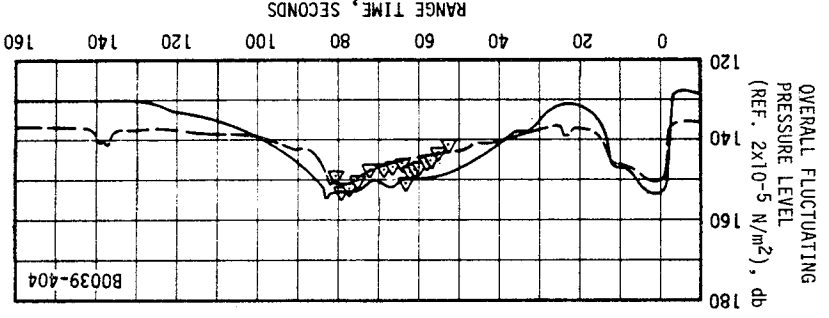
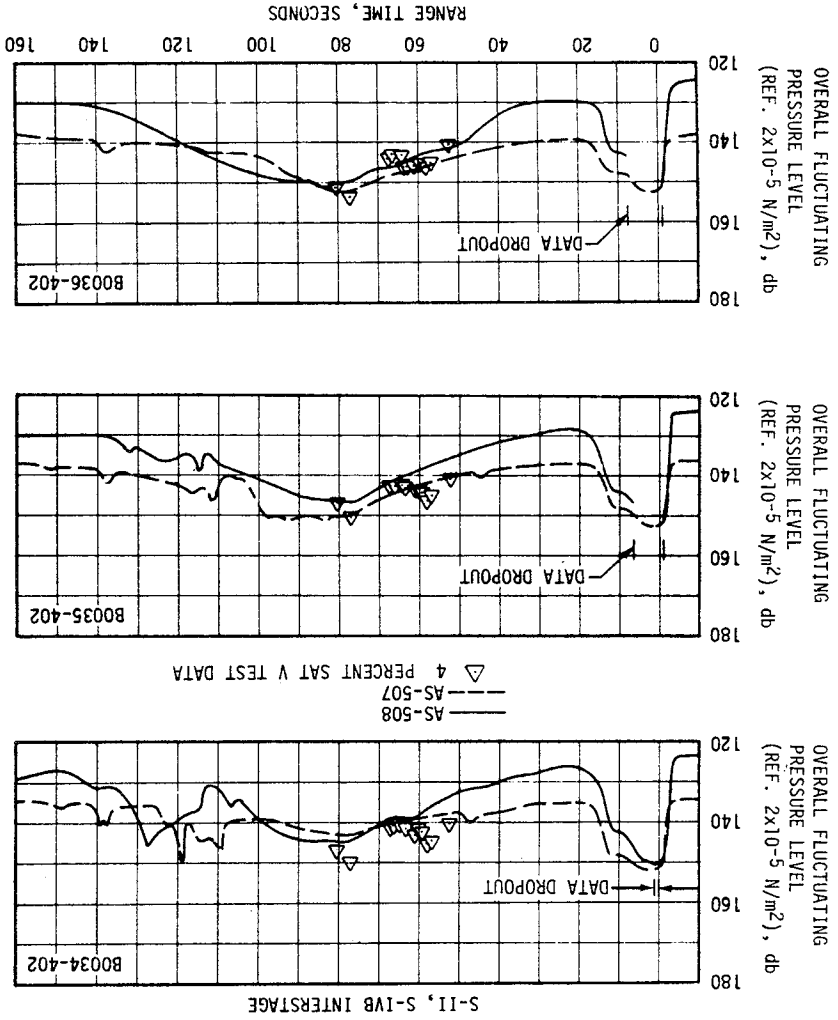


Figure 12-7. Vehicle External Overall Fluctuating Pressure Level (Sheet 2 of 2)

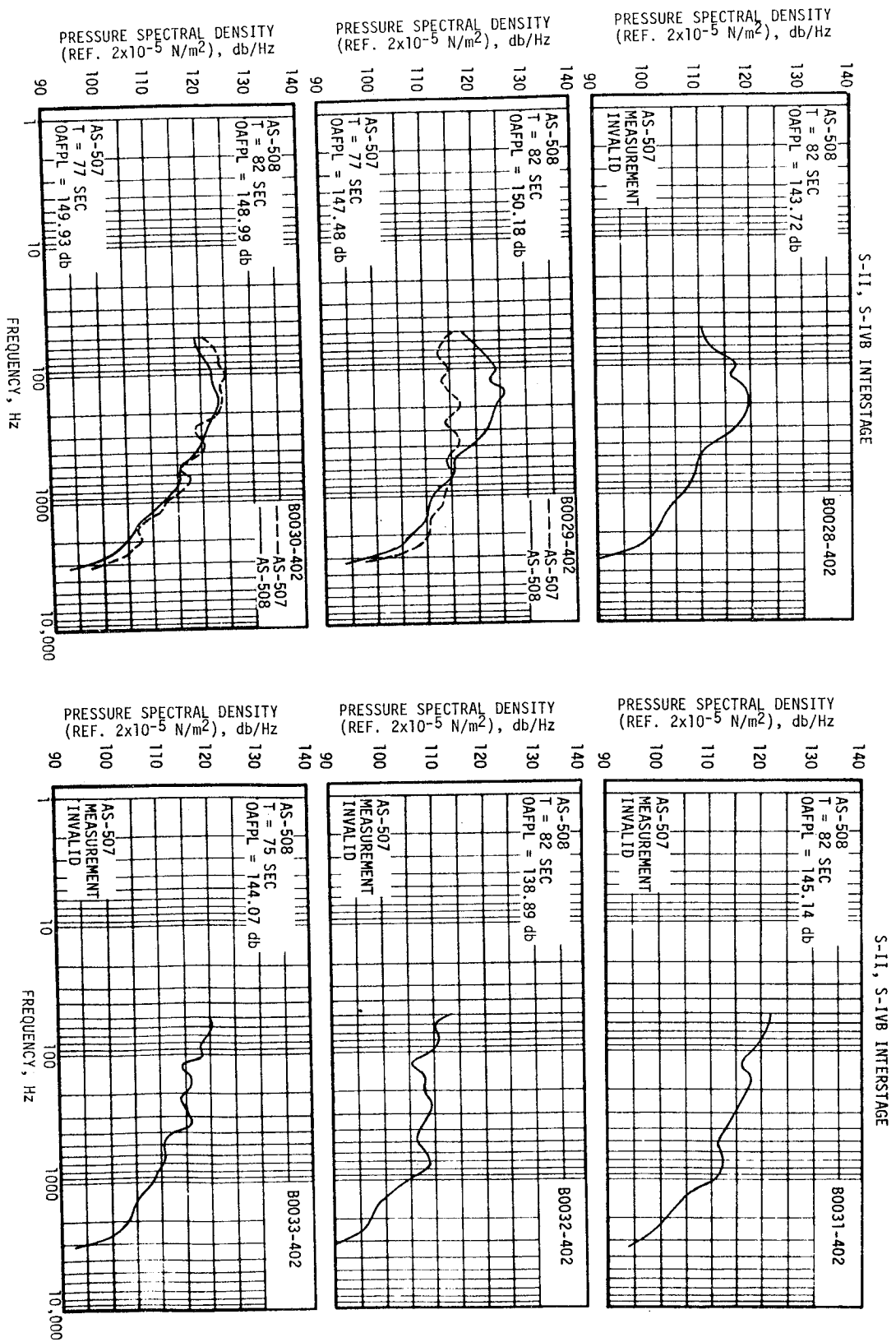


Figure 12-8. Vehicle External Fluctuating Pressure Spectral Densities (Sheet 1 of 2)

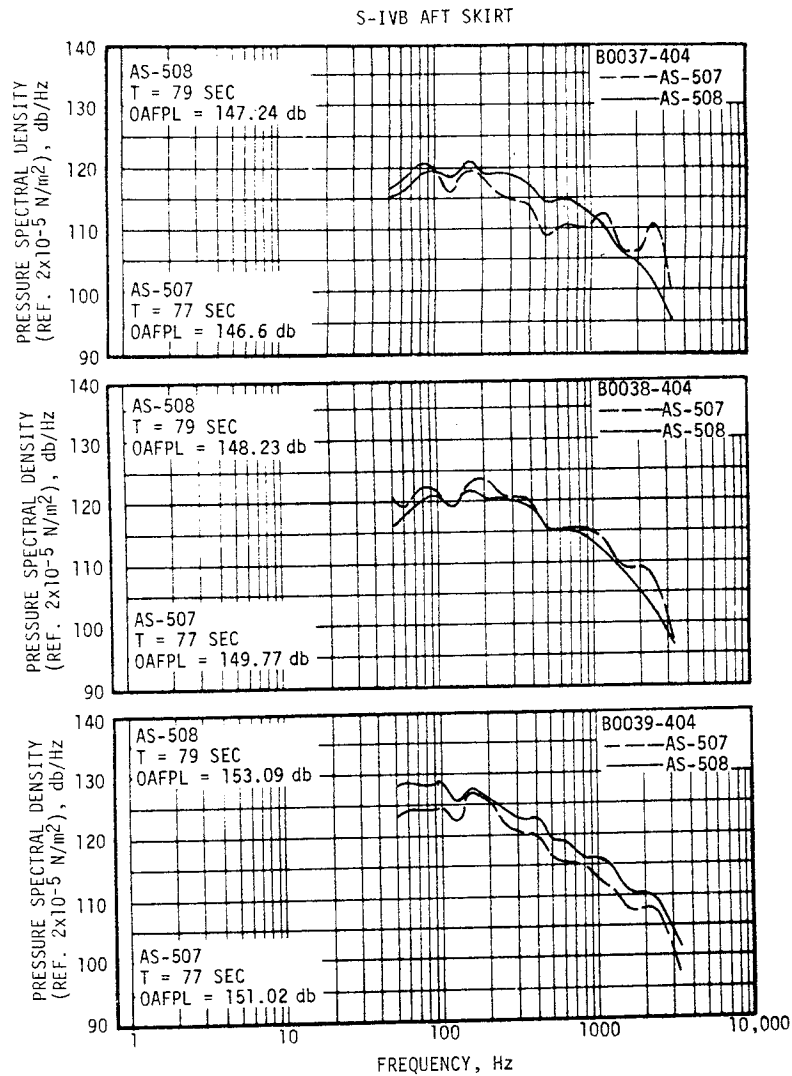
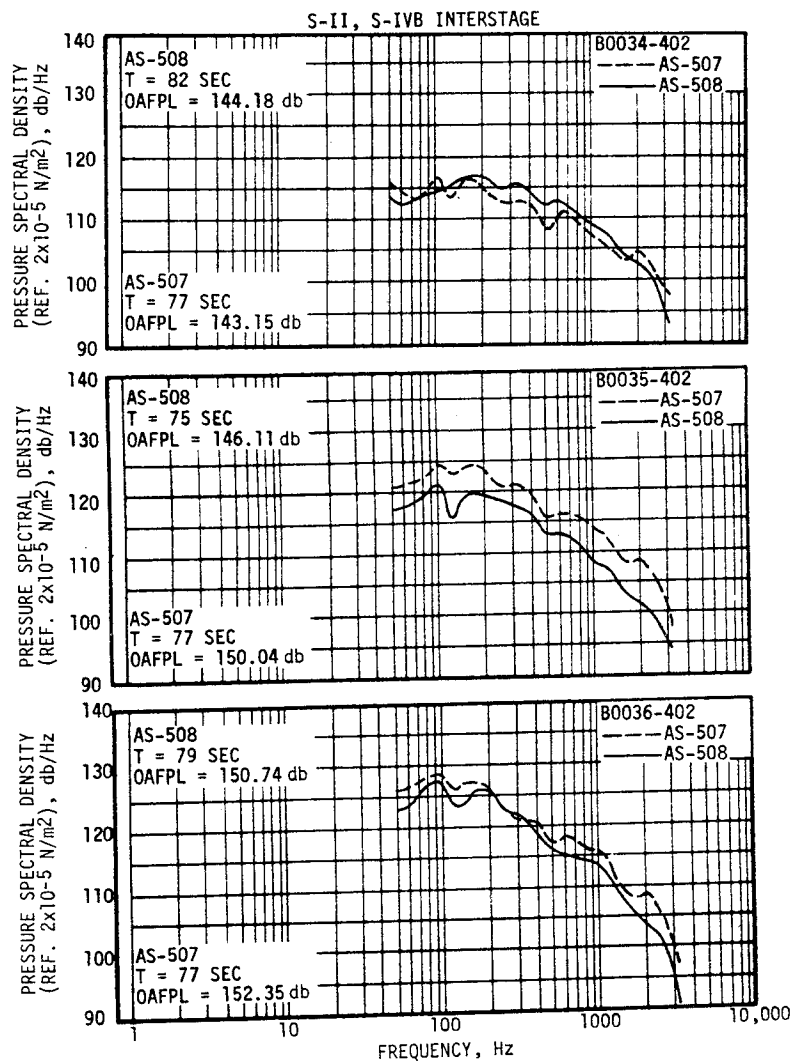


Figure 12-8. Vehicle External Fluctuating Pressure Spectral Densities (Sheet 2 of 2)

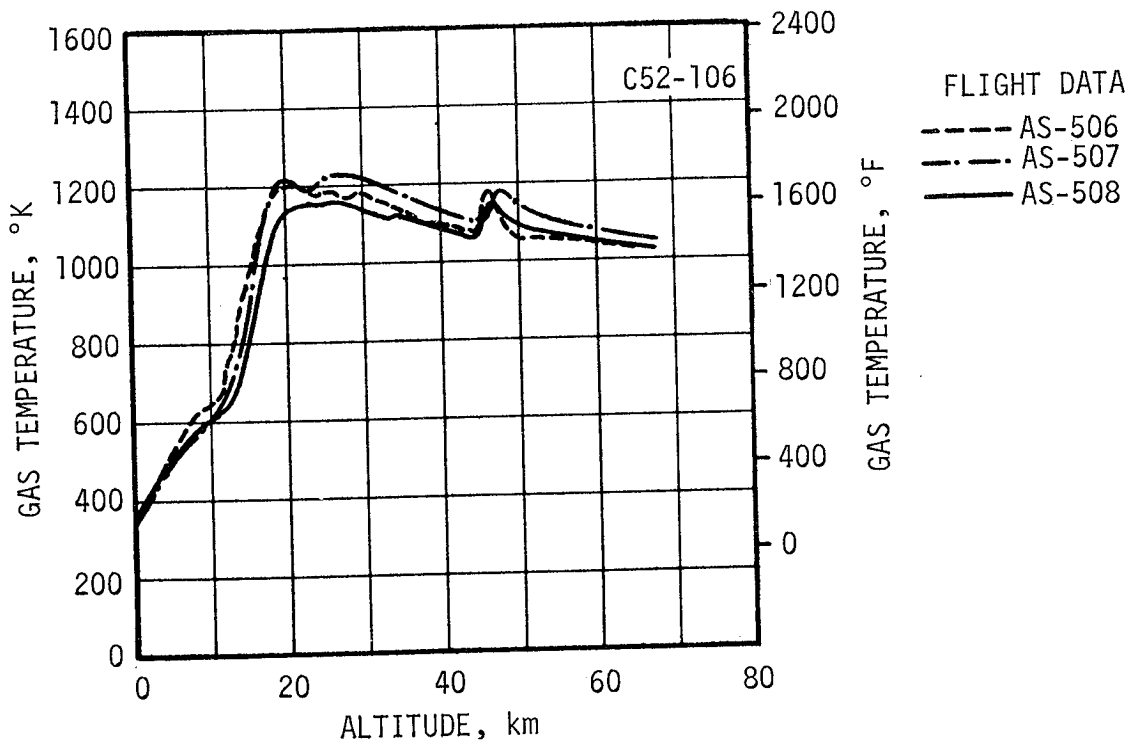
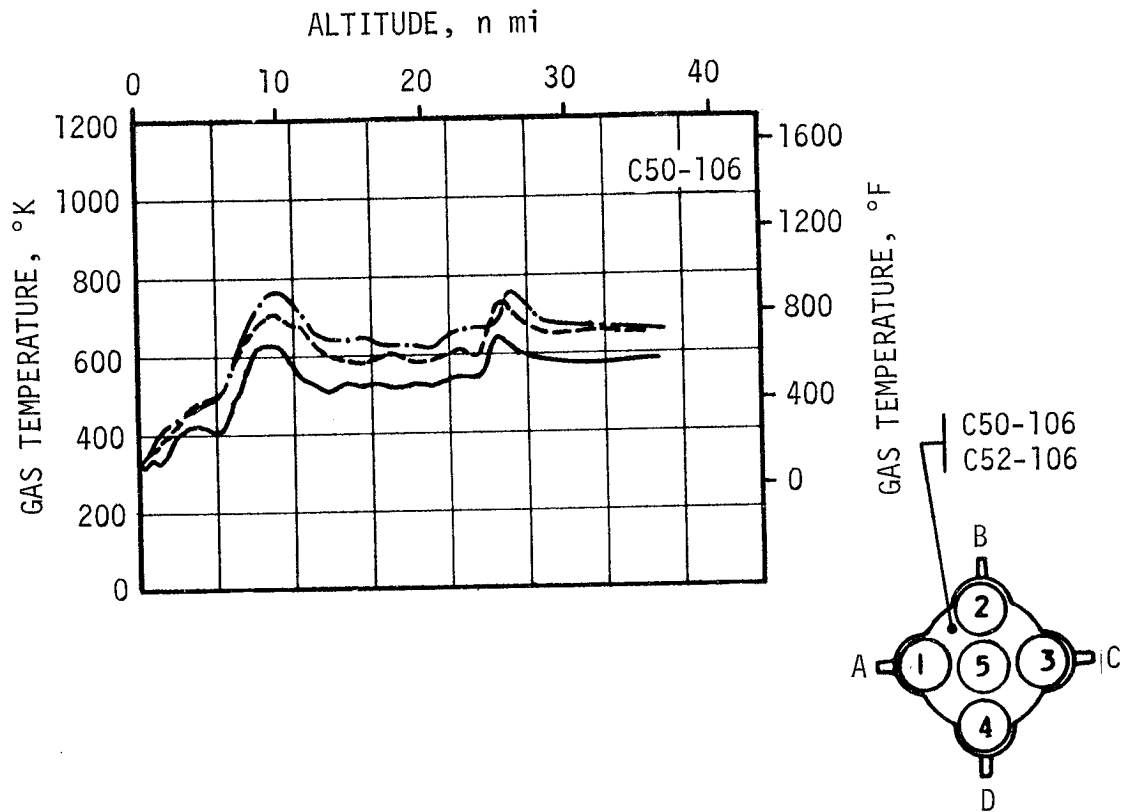


Figure 13-2. S-IC Base Gas Temperature

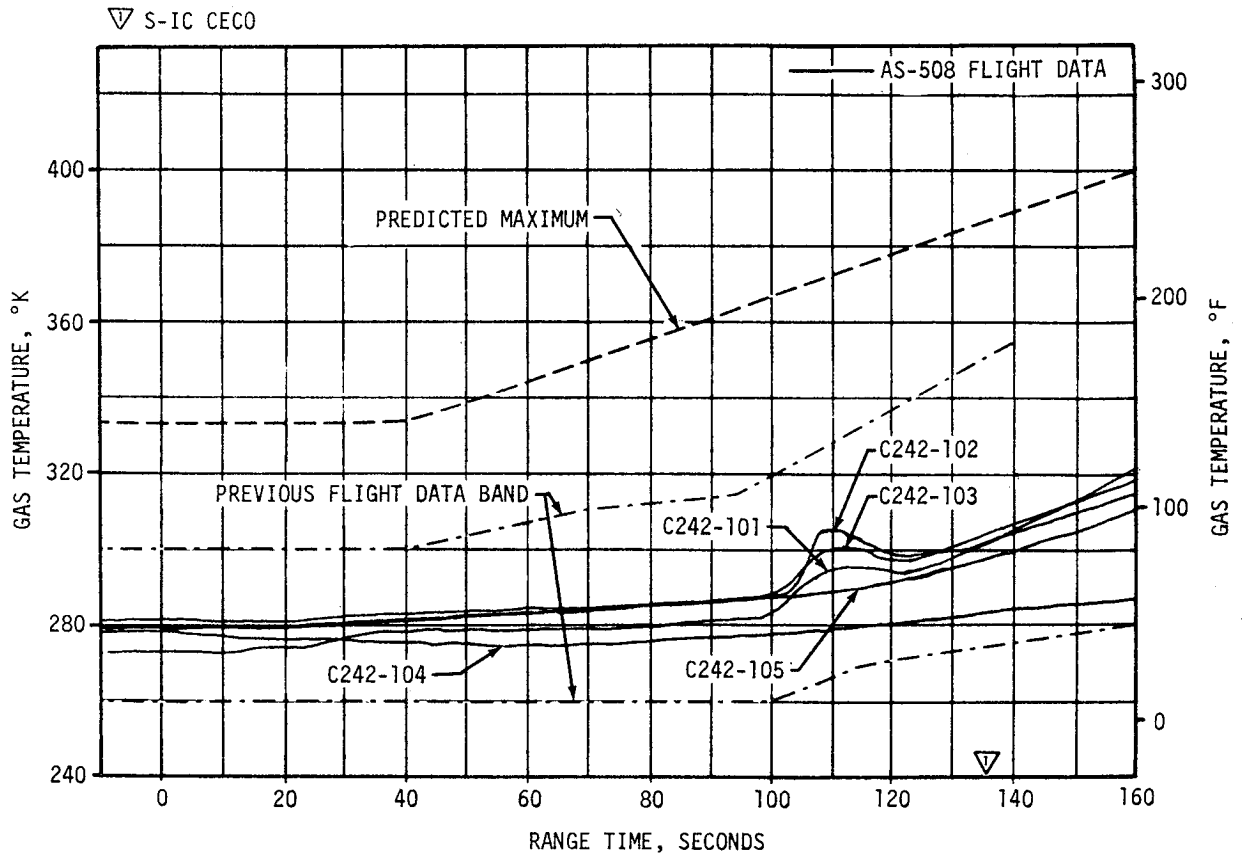


Figure 13-3. S-IC Ambient Gas Temperature Under Engine Cocoon

thermal environment reflected by thermal math models. Key flight parameters relating to engine performance, engine position and reference temperatures are used in the postflight analysis. The math models are based on both theoretical and empirical postulates. The AS-508 heating rate was within the previous flights data band up to approximately 450 seconds, at which time the AS-508 heating rate exceeded the previously measured values. The AS-508 flight heating rate was expected to be higher throughout S-II burn because the outboard J-2 engines were gimballed further inboard for nominal steady state flight. Figure 13-4 also shows that the heating rate increased through S-II boost up to Engine Mixture Ratio (EMR) shift.

Figure 13-5 shows the AS-508 flight data and postflight analysis of the heat shield recovery temperature transducer C731-206. The analytical temperature curve represents a calculated transducer reading based on math models using key flight parameters. The gas recovery temperature is an analytically derived value computed from the flight measurement data. The measured flight temperature was higher than that recorded during previous flights. Note that the flight values are the probe temperatures and not the gas recovery temperatures. The temperature data show that



the analyzed gas recovery temperature was 1180°F prior to CECO, 1420°F after CECO, and 1230°F after EMR shift. This is approximately 100°F, 170°F, and 160°F higher than the corresponding AS-507 values. The increased gas recovery temperature is consistent with the AS-508 steady state J-2 engine deflection pattern which indicates that the engines were gimballed more inboard than during the AS-507 flight. Flight data at 175 seconds are considered invalid, because a considerable increase in heat transfer coefficient or gas recovery temperature would be required to produce the indicated temperature. Transducer C722-206, located in the same quadrant, did not reflect increases in the heat transfer coefficient or recovery temperature.

Figure 13-6 shows the AS-508 flight data and postflight analysis of the heat shield aft radiation heat rate. The analytical radiation heat rate represents the heat rate at the transducer location and is derived from a math model. The model uses flight parameters such as engine performance and position to calculate the incident radiation. AS-508 flight data compare favorably with previous flight data, noting the effects of early S-II CECO on the heating rate trends.

There were no structural temperature measurements on the base heat shield and only three thrust cone forward surface temperature measurements in the base region. A maximum postflight predicted temperature was determined for the aft surface of the heat shield using predicted base heating rates for the AS-508 flight. This postflight predicted temperature was 1057°F which compared favorably with previous flights; being well within the maximum design temperatures of 1460°F for no engine out and 1550°F for one control engine out. The maximum measured temperature on the thrust cone was 10°F. The measured temperatures were well below design values and in good agreement with postflight predictions.

#### 13.4 VEHICLE AEROHEATING THERMAL ENVIRONMENT

Aerodynamic heating environments were not measured on the AS-508 vehicle. Due to the similarity in the trajectory, the aerodynamic heating environments are believed to be approximately the same as previous flight environments. Flow separation on the AS-508 vehicle, as observed from ground optical data, occurred at approximately 116 seconds. The forward point of flow separation versus range time is presented in Figure 13-7. The effects of CECO on the forward point of flow separation during the AS-508 flight were similar to previous flights. It should be noted that at higher altitudes the measured location of the forward point of flow separation is questionable due to loss of resolution in the ground optical data.

- ▽ S-II IGNITION
- ▽ INTERSTAGE SEPARATION
- ▽ S-II CECCO
- ▽ EMR SHIFT
- ▽ S-II DECO

TRANSDUCER  
C692-206

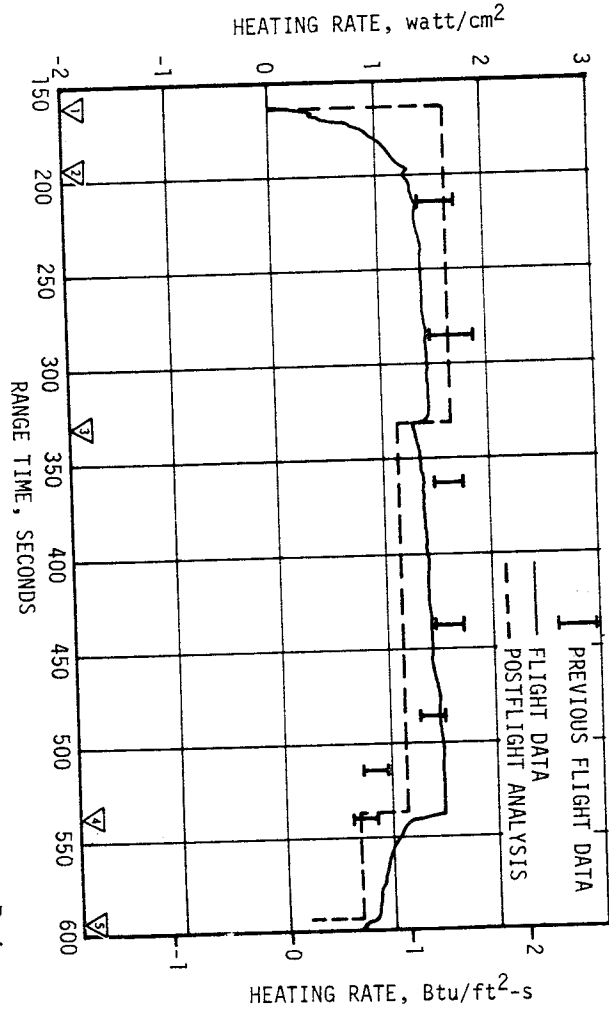
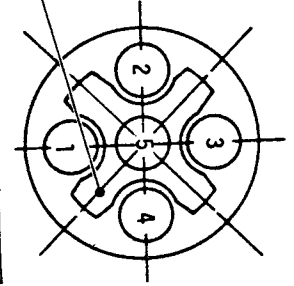


Figure 13-6. S-II Heat Shield Aft Radiation Heat Rate

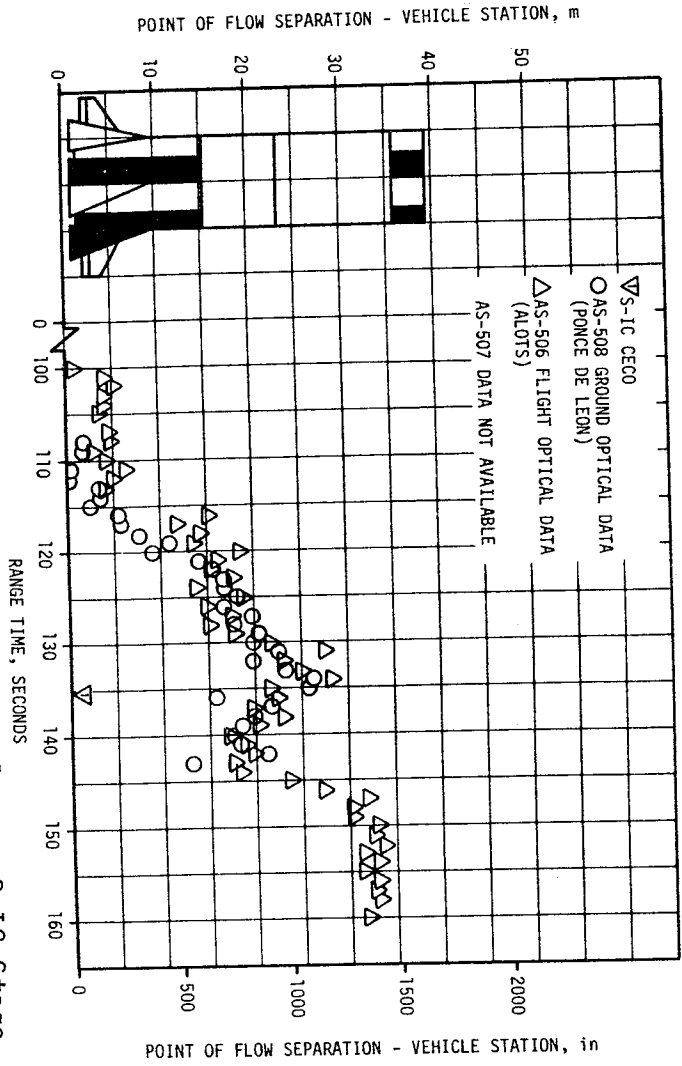


Figure 13-7. Forward Location of Separated Flow on S-IC Stage



## SECTION 14

### ENVIRONMENTAL CONTROL SYSTEMS

#### 14.1 SUMMARY

The S-IC stage forward compartment ambient temperatures were maintained above the minimum performance limit during the AS-508 countdown. The S-IC stage aft compartment environmental conditioning system performed satisfactorily except that the temperature in the vicinity of battery 12K10 dropped below battery qualification limits during LOX loading. However, the temperature was within limits at liftoff.

The S-II thermal control and compartment conditioning system apparently performed satisfactorily since the ambient temperatures external to the containers were normal and there were no problems with the equipment in the containers.

The Instrument Unit (IU) Environmental Control System (ECS) performed satisfactorily for the duration of its mission. Coolant temperatures, pressures, and flowrates were continuously maintained within the required limits.

#### 14.2 S-IC ENVIRONMENTAL CONTROL

The S-IC stage forward skirt ECS has three phases of operation during prelaunch operations. When onboard electrical systems are energized, but prior to cryogenic loading, conditioned air is used to maintain the desired environment. When cryogenic loading begins warmed GN<sub>2</sub> is substituted for the conditioned air. The third phase uses a warmer GN<sub>2</sub> flow to offset the cooling effects caused by S-II stage J-2 engine thrust chamber chilldown. All three phases functioned satisfactorily as evidenced by ambient temperature readings. Measurement C206-120 recorded a -87°F during the S-II stage J-2 engine thrust chamber chilldown sequence. This was above the allowable limit of -90°F.

The S-IC stage thrust structure compartment ECS had ECP-579 incorporated. This ECP reorificed the distribution manifold and the main compartment vents to keep the ambient temperature near battery 12K10 within the batteries qualification limits of 80 ±15°F. However, after start of LOX loading the ambient temperature near this battery decreased to a low of 61°F indicating that the ECP fix was not successful (see Figure 14-1).

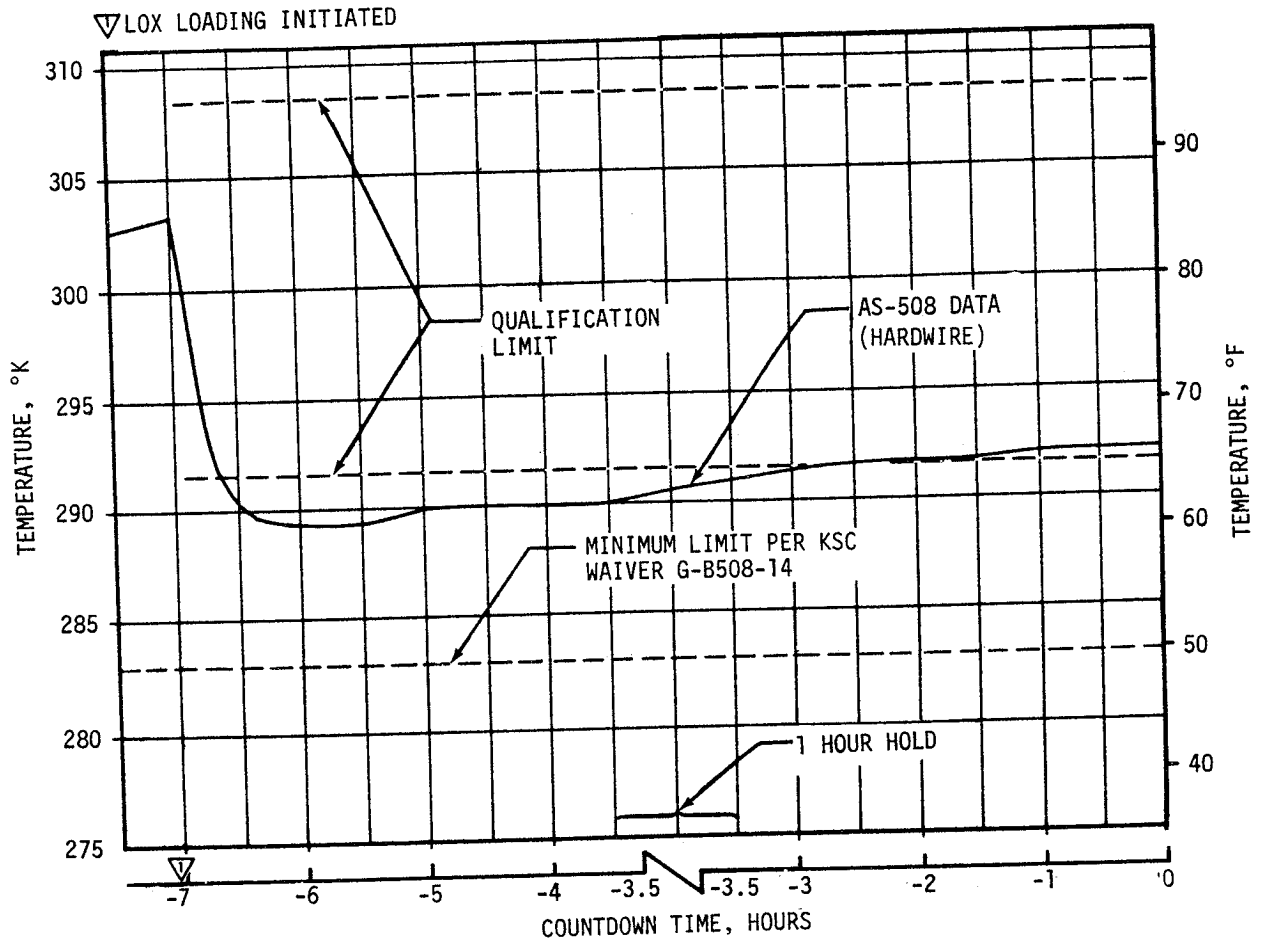


Figure 14-1. S-IC Aft Compartment Temperature Near Battery 12K10

However, KSC waiver G-B508-14 lowered the acceptable temperature limit to 50°F. All other ambient temperature measurements in this area were normal and ranged from 75.0°F at C107-115 to 55.2°F at C203-115.

### 14.3 S-II ENVIRONMENTAL CONTROL

The engine compartment conditioning system maintained the ambient temperature and thrust cone surface temperatures within design ranges throughout the launch countdown. The system also maintained an inert atmosphere within the compartment as evidenced by the absence of H<sub>2</sub> or O<sub>2</sub> indications on the hazardous gas monitor.

No equipment container temperature measurements were taken. However, since the ambient measurements external to the containers were satisfactory and there were no problems with the equipment in the containers, it is assumed that the thermal control system performed adequately.

## 14.4 IU ENVIRONMENTAL CONTROL

### 14.4.1 Thermal Conditioning System

Performance of the IU Thermal Conditioning System (TCS) was satisfactory throughout its flight. The temperature of the Methanol/Water (M/W) coolant supplied to the coldplates and internally cooled components was continuously maintained within the required 45 to 68°F temperature band.

Figure 14-2 shows TCS temperature control parameters over the total time span for which data were received. Sublimator cooling was nominal as evidenced by normal coolant temperature cycling through 46,100 seconds (12:48:20). The last cooling cycle started at about 48,180 seconds (13:23:00).

Sublimator performance during ascent is shown in Figure 14-3. The water valve opened at approximately 183 seconds, allowing water to flow to the sublimator. Full cooling from the sublimator was not evidenced until approximately 520 seconds at which time the coolant temperature at the temperature control point began to decrease rapidly. The low cooling rate during the first 300 seconds after the water valve opened is typical of a slow starting sublimator. At the first thermal switch sampling, at

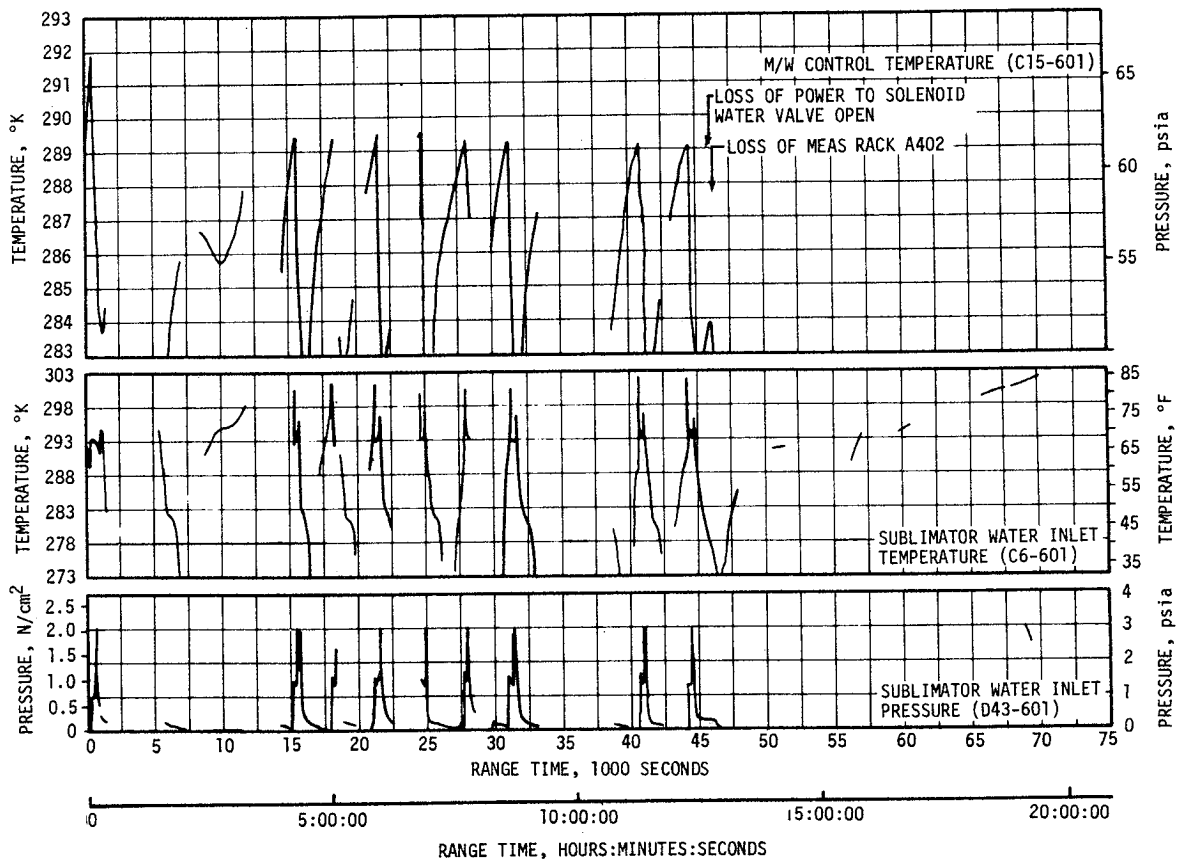


Figure 14-2. IU TCS Coolant Control Parameters

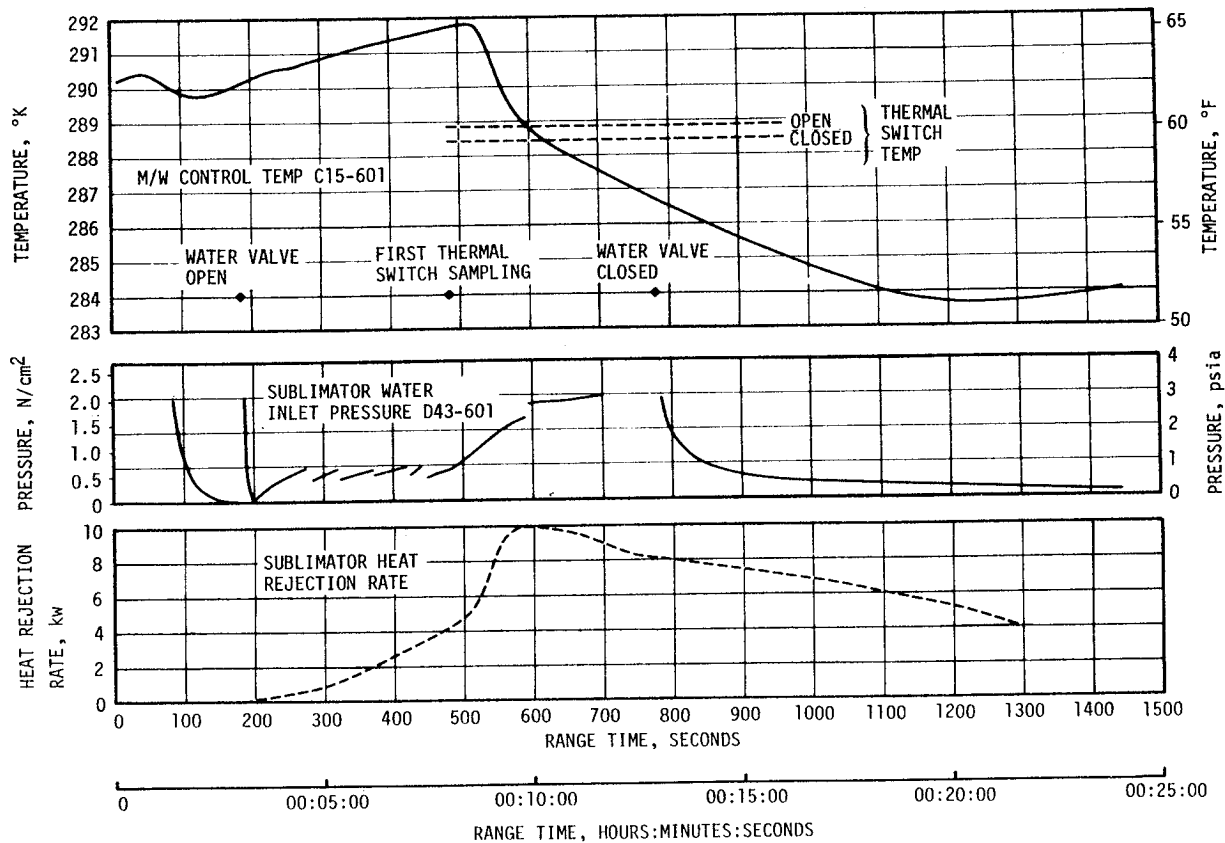


Figure 14-3. IU Sublimator Performance During Ascent

approximately 483 seconds, the coolant temperature was still above the water valve actuation point and the valve remained open. The second thermal switch sampling occurred at approximately 781 seconds and the water valve was closed.

Hydraulic performance of the TCS was as expected throughout the flight. System flowrates and pressures are shown in Figure 14-4. Note the decay in pump outlet pressure (and hence fluid flowrate) beginning at about 40,000 seconds (11:06:40). This corresponds with the decrease in pump voltage as battery output power became depleted.

The TCS GN<sub>2</sub> sphere pressure decay which is indicative of GN<sub>2</sub> usage rate was within the expected range (see Figure 14-5).

All component temperatures remained within their expected ranges throughout the primary mission (see Figure 14-6) and continued under ECS control until loss of power. The Launch Vehicle Data Adapter (LVDA) and Launch Vehicle Digital Computer (LVDC) began heating from internal power dissipation after the coolant pump stopped circulating M/W. The IU exterior about position III was in the shade and the Flight Control Computer (FCC), panel 16, began a cooling trend at about 50,000 seconds

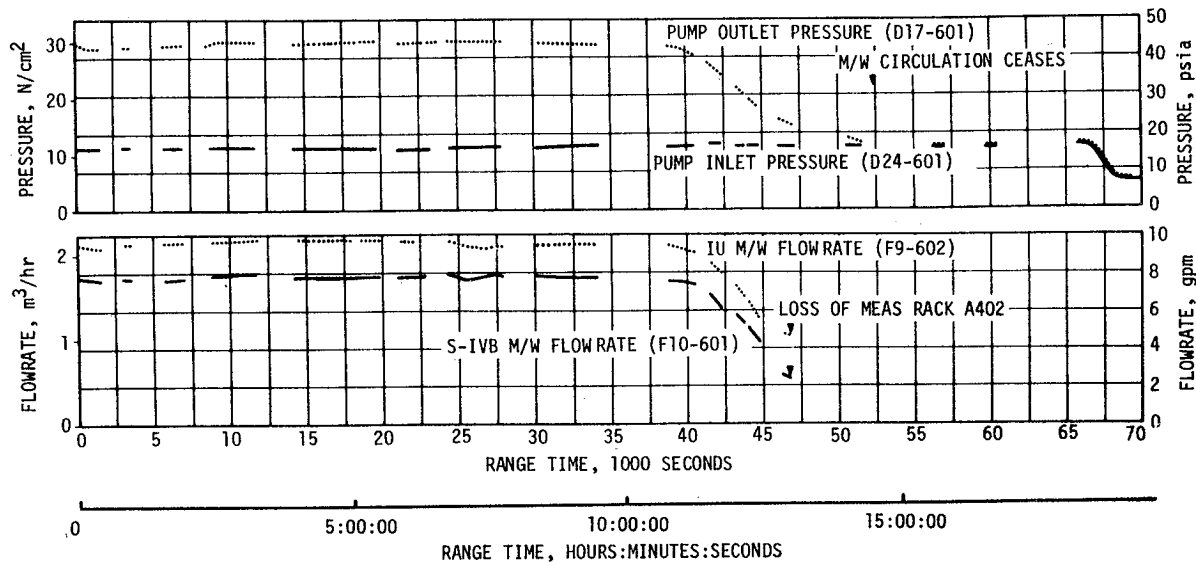


Figure 14-4. IU TCS Hydraulic Performance

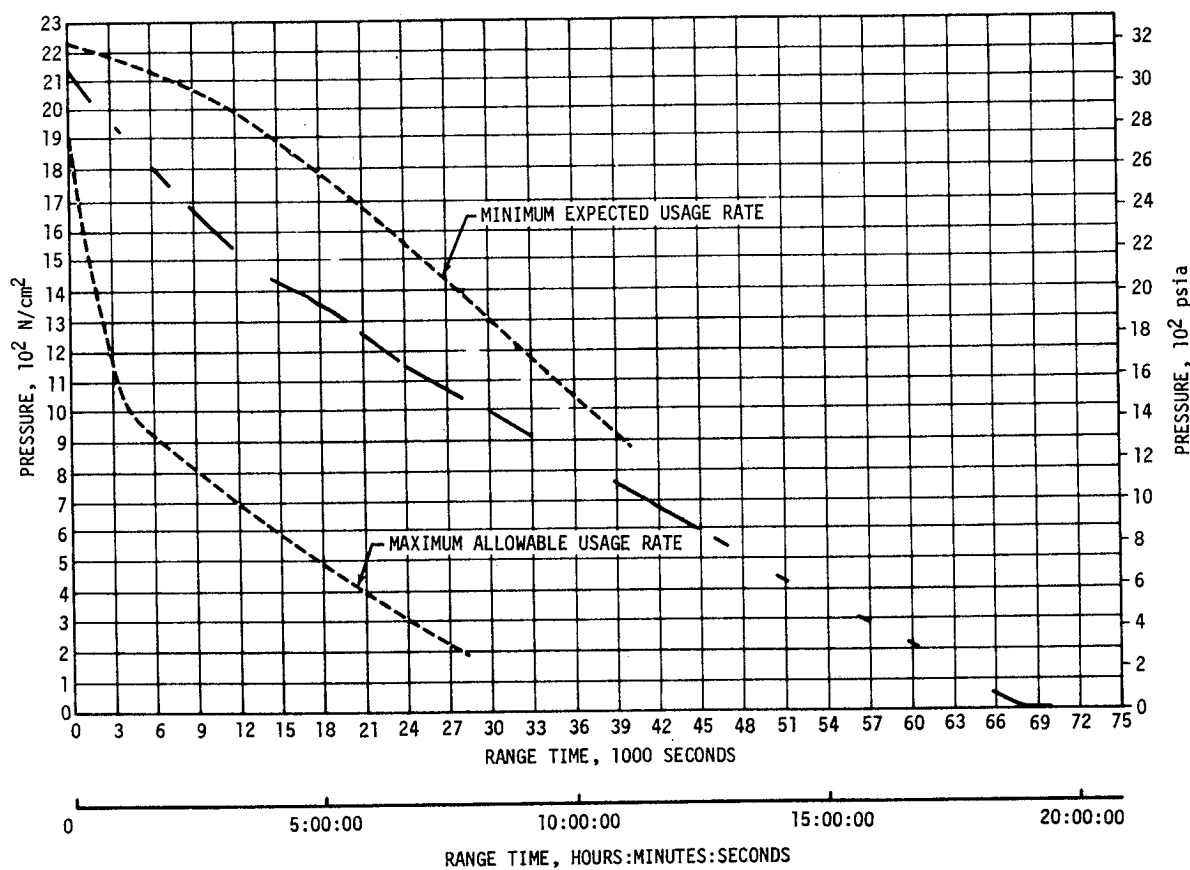


Figure 14-5. IU TCS GN<sub>2</sub> Sphere Pressure (D025-601)

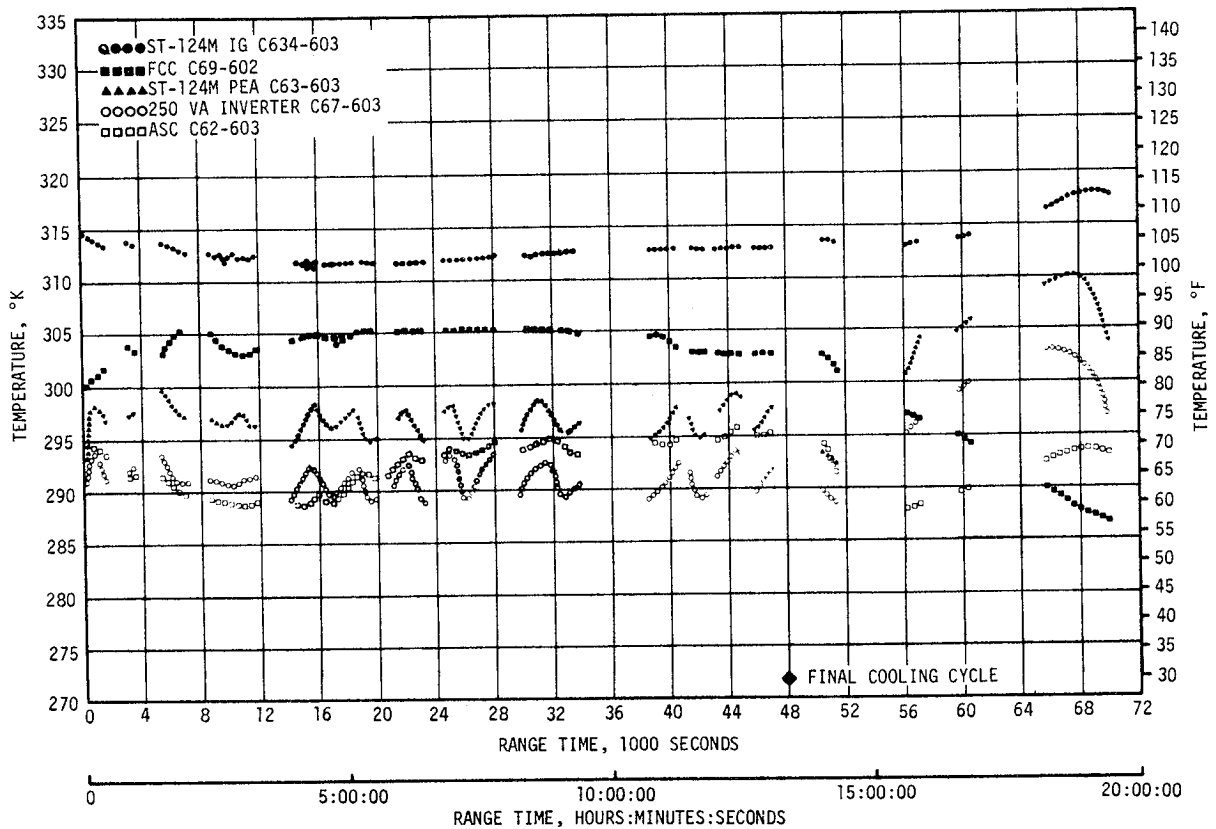
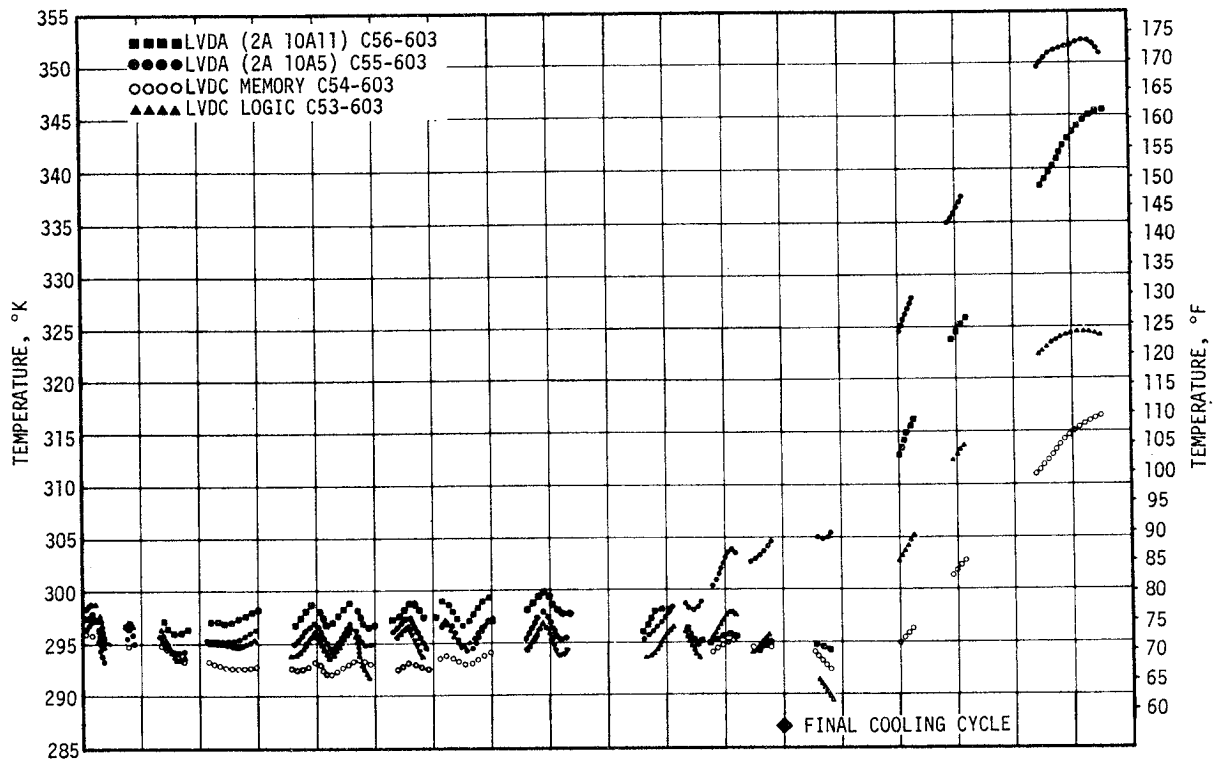


Figure 14-6. Selected IU Component Temperatures

(13:53:20) due to heat loss to the IU structure (see Figure 14-6). The entire IU interior was shaded after 50,400 seconds (14:00:00) upon return to the Transposition, Docking and Ejection (TD&E) attitude.

The thermal radiation shrouds added on AS-508 were effective in shielding the components from solar heating. This is illustrated by the AS-507 and AS-508 comparisons in Figure 14-7. The platform on panel 21 and the Accelerometer Signal Conditioner (ASC), Platform Electronics Assembly (PEA), AC Power Supply (ACS) on panel 20, which showed strong solar heating effect after 15,000 seconds (04:10:00) on AS-507, were also in line with the direct solar rays on AS-508 during TD&E attitude (14,500 to 14,900 seconds [04:01:40 to 04:08:20]), and LOX dump attitude (16,200 to 17,000 seconds [04:30:00 to 04:43:20]) through lunar impact attitude (ending at 43,850 seconds [12:10:50]).

#### 14.4.2 ST-124M-3 Gas Bearing System

The Gas Bearing System (GBS) performance was satisfactory throughout the mission. Figure 14-8 shows platform pressure differential and internal ambient pressure. The GBS GN<sub>2</sub> supply sphere pressure decay was within the expected range as shown in Figure 14-9.

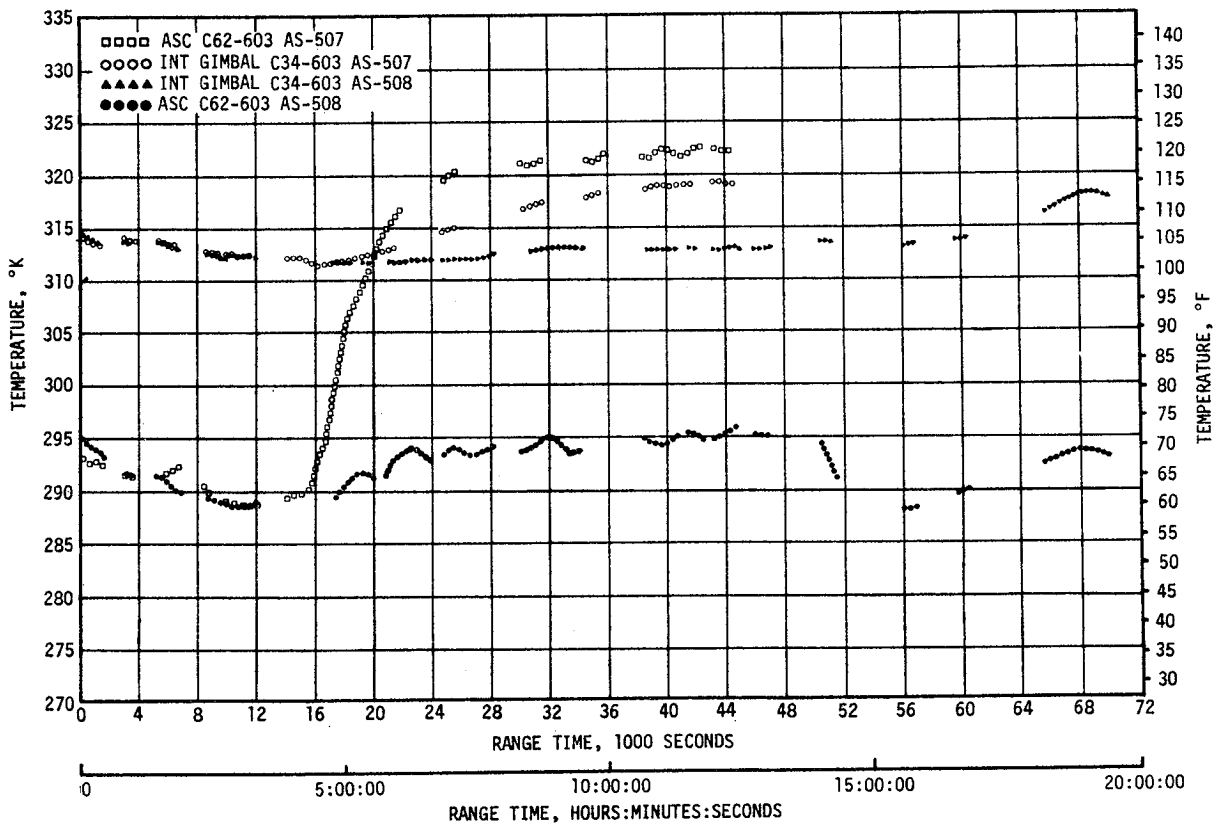


Figure 14-7. Comparison of AS-507 and AS-508 IU Temperatures

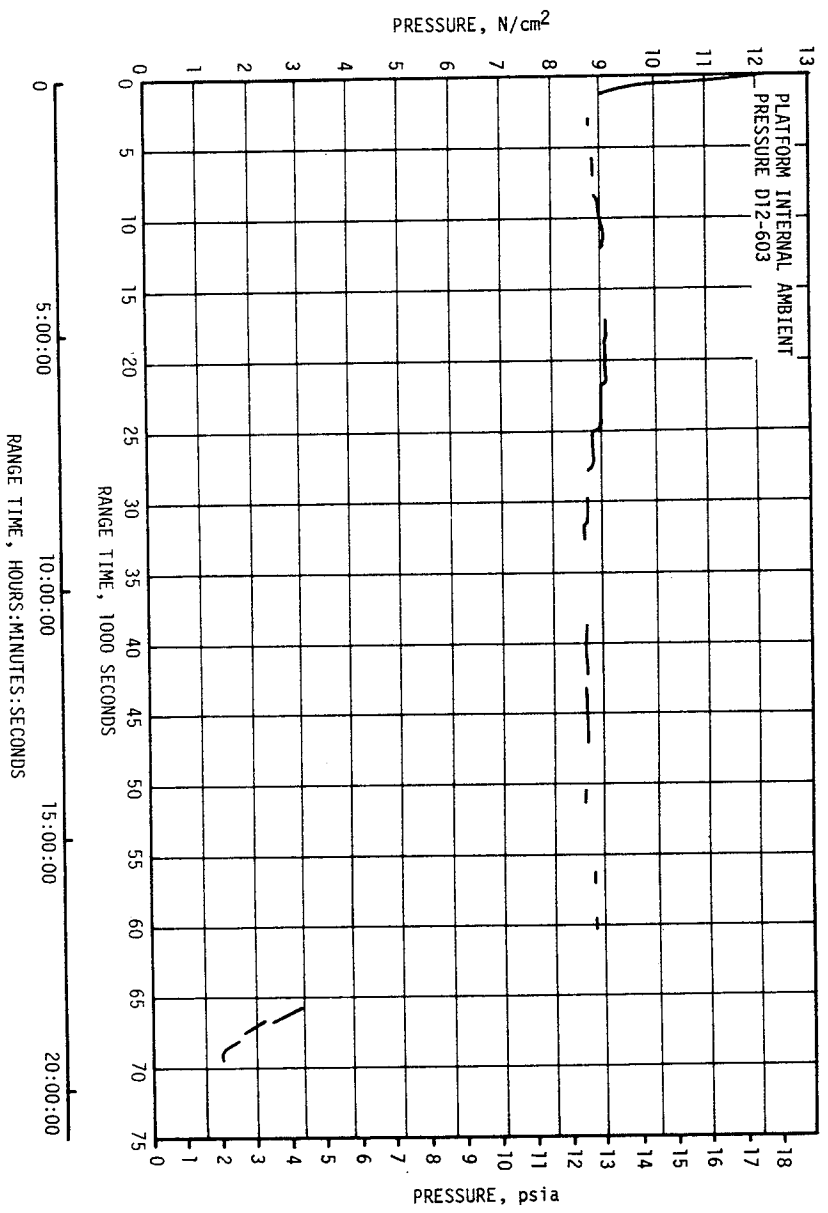
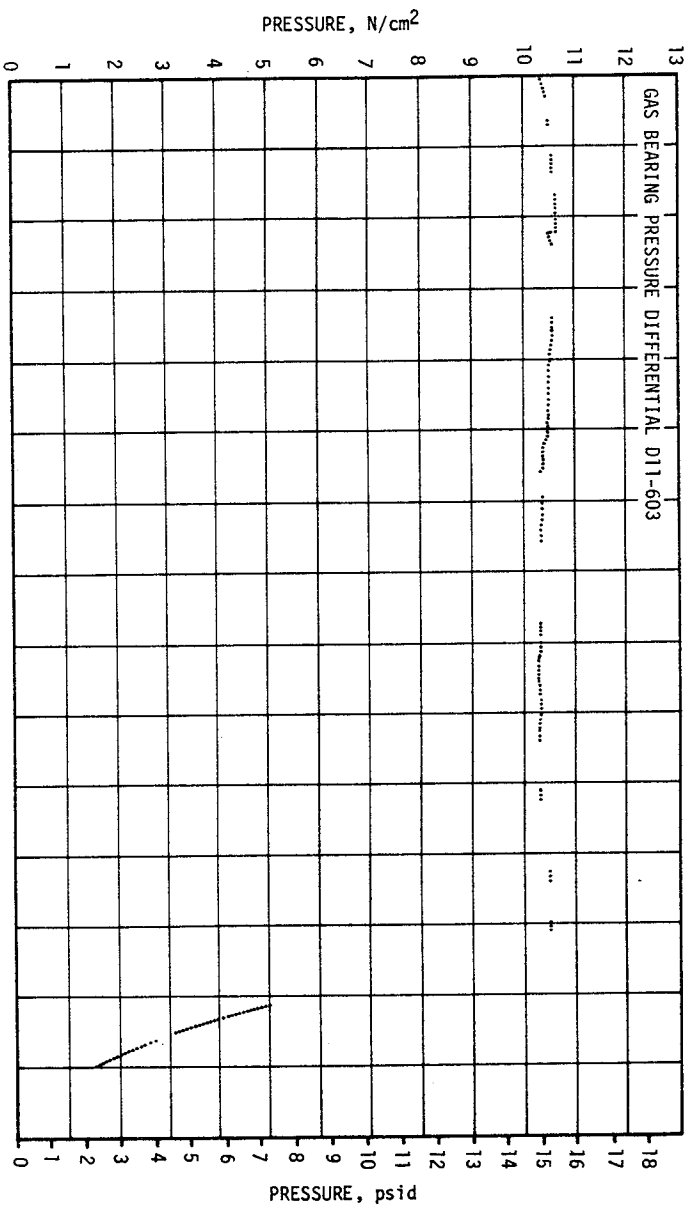


Figure 14-8. IU Inertial Platform GN<sub>2</sub> Pressures

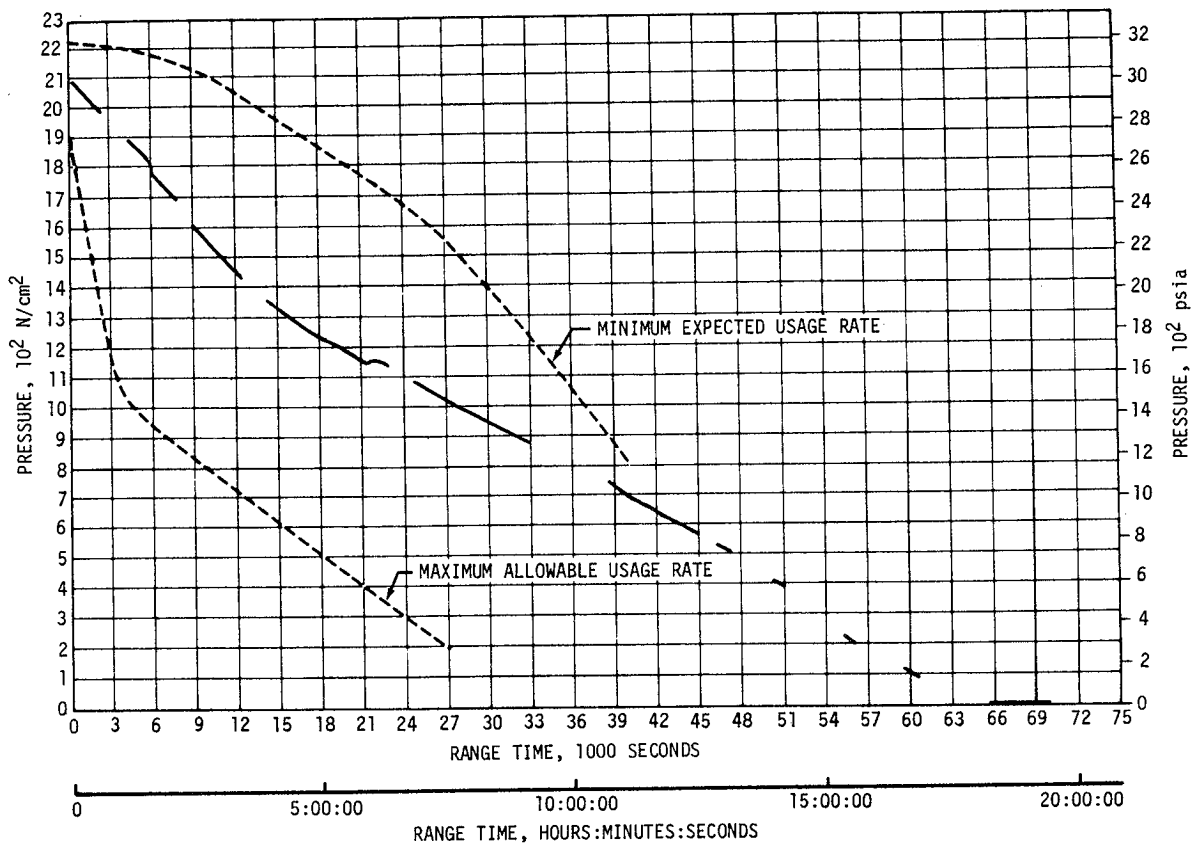


Figure 14-9. IU GBS GN<sub>2</sub> Sphere Pressure (D010-603)

## SECTION 15

### DATA SYSTEMS

#### 15.1 SUMMARY

All data systems performed satisfactorily throughout the flight. Flight measurements from onboard telemetry were 99.9 percent reliable, matching the high performance of AS-506 and AS-507.

Telemetry performance was normal. Radiofrequency (RF) propagation was generally good, though the usual problems due to flame effects and staging were experienced. Usable VHF data were received to 14,280 seconds (03:58:00). The Secure Range Safety Command Systems (SRSCS) on the S-IC, S-II, and S-IVB stages were ready to perform their functions properly, on command, if flight conditions during launch phase had required destruct. The system properly safed the S-IVB on a command transmitted from Bermuda (BDA) at 760.0 seconds. The performance of the Command and Communications System (CCS) was excellent. The only significant problem encountered during the flight was signal interference between the Instrument Unit (IU) CCS and the Lunar Module (LM) Unified S-Band (USB) system during translunar coast. This problem was caused by the necessity to apply power to the LM early. Usable CCS telemetry data were received to 70,380 seconds (19:33:00). Ascension (ACN), Goddard Experimental Test Center (ETC 3), Goldstone (GDS), Hawaii (HAW), Madrid (MAD) and Merritt Island Launch Area (MILA) were receiving CCS signal carrier at S-IVB/IU lunar impact at 280,601 seconds (77:56:41). Good tracking data were received from the C-Band radar, with Carnarvon (CRO) indicating final Loss of Signal (LOS) at 44,220 seconds (12:17:00).

The 67 ground engineering cameras provided good data during the launch.

#### 15.2 VEHICLE MEASUREMENTS EVALUATION

The AS-508 launch vehicle had 1385 measurements scheduled for flight; six measurements were waived prior to start of the automatic countdown sequence leaving 1379 measurements active for flight. Of the waived measurements, five provided valid data during the flight. A summary of measurement reliability is presented in Table 15-1 for the total vehicle and for each stage. Measurement reliability was 99.9 percent. This reliability is the same as on AS-506 and AS-507, when the highest reliability for any Saturn V flight was attained.

The waived measurements, totally failed measurements, partially failed measurements and questionable measurements are listed by stage in Tables 15-2, 15-3, and 15-4. None of the listed failures had any significant impact on postflight evaluation.

### 15.3 AIRBORNE VHF TELEMETRY SYSTEMS EVALUATION

Performance of the nine VHF telemetry links was generally satisfactory with only minor exceptions. A brief summary of these links is shown in Table 15-5.

All inflight calibrations occurred as programmed and were within specifications.

Data degradation and dropouts were experienced at various times during boost, as on previous flights, due to the attenuation of RF signals. Signal attenuation was caused by main flame effects, S-IC/S-II staging, S-II ignition and S-II second-plane separation. Magnitude of these effects was comparable to that experienced on previous flights. S-IC main flame effects caused a temporary loss of VHF telemetry data on the S-IC stage. At S-IC/S-II staging, signal strength on all VHF telemetry links dropped below threshold for approximately 1.0 second. Signal degradation due to S-II ignition and S-II flame effects was sufficient to cause temporary loss of VHF telemetry data on the S-IC and S-II stages. S-II VHF data were lost during S-II second-plane separation. In addition, there were intervals during the launch phase where some data were so degraded as to be unusable. Loss of these data, however, posed no problem since losses were of such short duration as to have little or no impact on flight analysis.

The performance of the S-IVB and IU VHF telemetry systems was normal during earth orbit, S-IVB second burn and final coast. Usable VHF telemetry data were received to 14,280 seconds (03:58:00). A summary of available VHF telemetry coverage showing Acquisition of Signal (AOS) and LOS for each station is shown in Figure 15-1.

### 15.4 C-BAND RADAR SYSTEM EVALUATION

The C-Band radar operated satisfactorily during flight, although several ground stations experienced some of the usual tracking problems.

As on previous flights, MILA experienced phase front disturbances during launch (erroneous pointing information caused by a sudden antenna null or a distorted beacon return). However, the AS-508 disturbances were not as severe as experienced on previous flights and tracking continuity was maintained.

The BDA FPS-16 radar could not track from 342 to 348 seconds due to interference of the BDA FPQ-6 radar transmitting signal.

Table 15-1. AS-508 Measurement Summary

MEASUREMENT CATEGORY	S-IC STAGE	S-II STAGE	S-IVB STAGE	INSTRUMENT UNIT	TOTAL VEHICLE
Scheduled	288	579	290	228	1385
Waived	1	4	1	0	6
Failures	0	0	1	0	1
Partial Failures	3	2	6	0	11
Questionable	0	0	6	0	6
Reliability, Percent	100.0	100.0	99.7	100.0	99.9

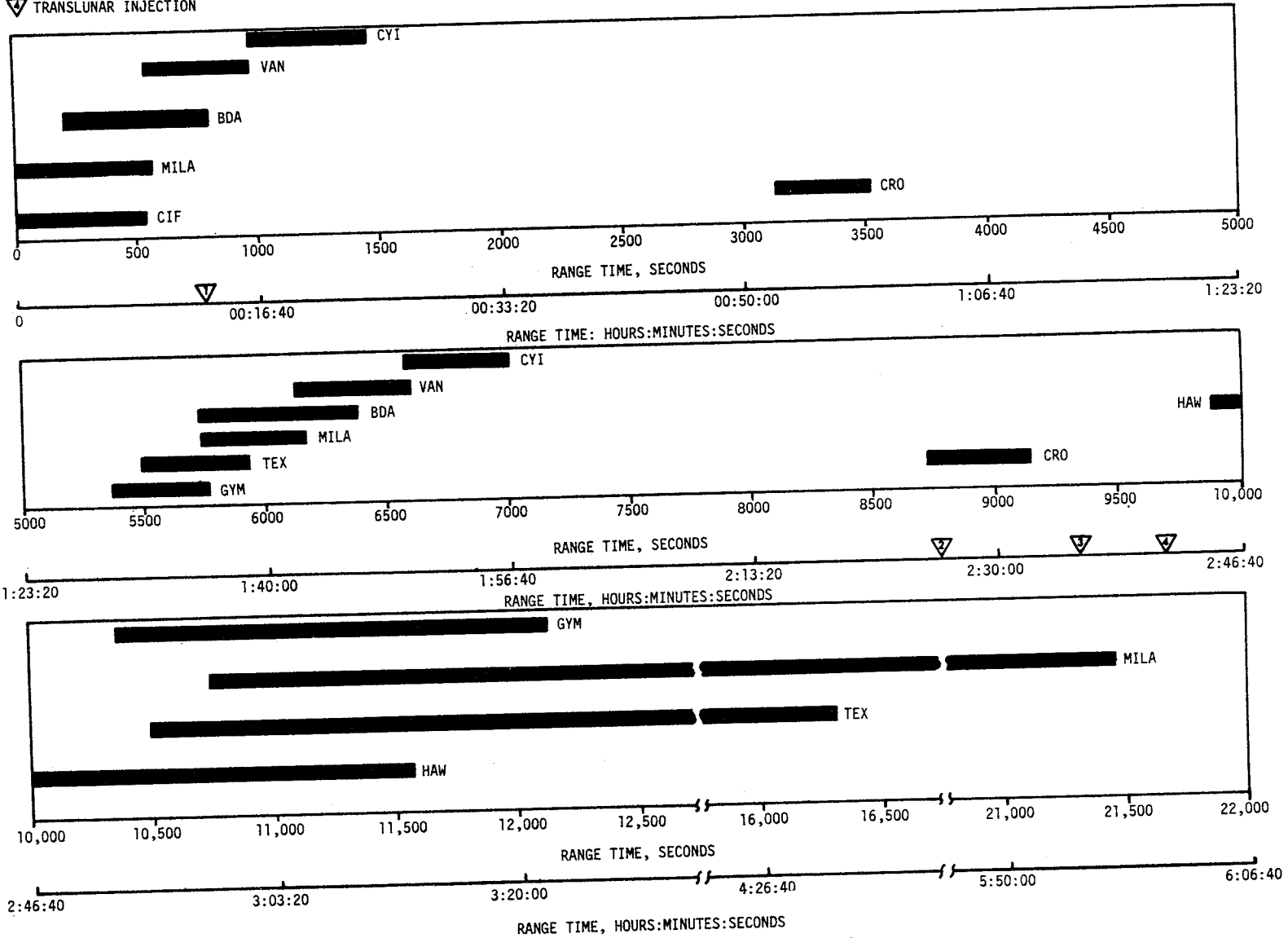
Table 15-2. AS-508 Flight Measurements Waived Prior to Flight

MEASUREMENT NUMBER	MEASUREMENT TITLE	NATURE OF FAILURE	REMARKS
S-IC STAGE			
D127-115	Pressure, LOX Suction Line, Engine No. 1	Output erratic during initial CDDT LOX loading and the latter portion of detanking.	Measurement provided valid data during flight. Waiver MICH-508-2.
S-II STAGE			
C604-218	LH <sub>2</sub> Tank Ullage Temperature	Erratic under cryogenic conditions.	Measurement provided valid data during flight.
D010-202	E2 LOX Turbine Outlet Pressure	Failed to meet calibration requirements for 'RACS HIGH MODE'. 'RUN MODE' was satisfactory.	Relay failure; measurement provided valid data during flight.
D267-201	E1 LOX Pump Inlet Pressure	Did not meet the ±4 percent full scale accuracy at ambient.	Torque shift; measurement provided valid data during flight.
D267-205	E5 LOX Pump Inlet Pressure	Did not meet the ±4 percent full scale accuracy at ambient.	Torque shift; measurement provided valid data until S-II CECCO when the over-pressure range of the transducer was exceeded.
S-IVB STAGE			
F0004-424	Flow Rate - Oxidizer Circulation Pump	Pickup coil malfunction.	Data was low with a high noise level.

Table 15-3. AS-508 Measurement Malfunctions

MEASUREMENT NUMBER	MEASUREMENT TITLE	NATURE OF FAILURE	TIME OF FAILURE (RANGE TIME)	DURATION SATISFACTORY OPERATION	REMARKS
TOTAL MEASUREMENT FAILURES, S-IVB STAGE					
F0005-404	Flow Rate - LH <sub>2</sub> Circulation Pump	Data erratic at 40 seconds, off scale low at 100 seconds.	40 seconds	-300 to +40 seconds	Caused by signal discontinuity in frequency converter.
PARTIAL MEASUREMENT FAILURES, S-IC STAGE					
A001-118	Acceleration, Longitudinal	Data noisy	4 to 12 seconds	152 seconds	Probable transducer failure
C003-104	Temperature, Turbine Manifold	Measurement failed off scale high	58 seconds	58 seconds	
K047-115	Thrust OK Pressure Switch No. 3 Engine No. 5	Switch cycled off one time	12 seconds	163.9 seconds	
PARTIAL MEASUREMENT FAILURES, S-II STAGE					
C003-201	E1 Fuel Turbine Inlet Temperature	Failed off scale high at 506 seconds	506 seconds	0 to 506 seconds	Failure probably caused by an open circuit in the transducer lower leg circuit
C648-219	H <sub>2</sub> Pressure Regulator Out Temperature	Failed off scale low at 390 seconds	390 seconds	0 to 390 seconds	Failure was probably caused by an open circuit in the transducer high side circuit
PARTIAL MEASUREMENT FAILURES, S-IVB STAGE					
C0007-401	Temperature - Engine Control Helium	Data dropped 90°F and became erratic between -23 seconds and liftoff	-23 seconds	Prior to -23 seconds and after liftoff to end of data	Caused by high resistance short circuit in probe
C0138-403	Temperature - Accumulator GN <sub>2</sub>	Data was erratic to off scale high during periods of vibration such as during auxiliary hydraulic pump operation	Slow variations observed during CDDT	During quiescent periods (low or no vibration)	Caused by a fractured sensor element
C0257-409	Temperature - Fuel Tank Continuous Vent 2	Data was 25°F lower than C0256-409 during the orbital period	3150 seconds	0 to 3150 seconds; 7000 to 8900 seconds; trend from 8900 to 9700 seconds to end of data	Distortion of probe, due to decrease in electrical insulation across sensor element or change in bridge resistance
D0218-408	Pressure - Differential LH <sub>2</sub> Chilldown Pump	Data indicates an accumulation of a 2.2 psi increase between 800 and 8920 seconds	800 seconds	0 to 800 seconds	Possible improper temperature compensator resistor in transducer
D0225-403	Pressure - Cold Helium Control Valve Inlet	Data was approximately 200 psi low during S-IVB first burn	600 seconds	Prior to 600 seconds and during S-IVB second burn	Caused by a negative shift in the amplifier zero balance circuit
D0256-403	Pressure - Ambient Helium Pneumatic Sphere	Data decreased 1.1 percent from -20 to -18 minutes; drifted slowly lower to 7.1 percent of full scale at 30,000 seconds	Drifting began prior to liftoff	Data is usable after compensation for drift	Probably moisture in connector caused a low impedance to ground

- ▽ PARKING ORBIT INSERTION
- ▽ BEGIN S-IVB RESTART PREPARATIONS
- ▽ S-IVB SECOND IGNITION
- ▽ TRANSLUNAR INJECTION



15-5

Figure 15-1. VHF Telemetry Coverage Summary

Table 15-4. AS-508 Questionable Flight Measurements

MEASUREMENT NUMBER	MEASUREMENT TITLE	REASON QUESTIONED	REMARKS
S-IVB STAGE			
B0033-402	Acoustic - Station 2529, Between 98-99 Ext.	Measurement indicated unexplained data dropouts during the early portion of the boost phase. 	Cause of data dropouts are undetermined. 
B0034-402	Acoustic - Station 2554, Between 98-99 Ext.		
B0035-402	Acoustic - Station 2589, Between 98-99 Ext.		
B0036-402	Acoustic - Station 2726, Between 98-99 Ext.		
B0037-404	Acoustic - Station 2771.5, Between 98-99 Ext.		
B0038-404	Acoustic - Station 2784, Between 98-99 Ext.		

The only problems reported during earth orbit were side lobe tracking and dropouts when attempting to track through the zenith. CRO's first attempt to acquire the vehicle at 3162 seconds resulted in tracking on a side lobe. The main lobe was acquired at 3246 seconds and no other problems were experienced during the remainder of the pass. Both the FPQ-6 and FPS-16 radars at BDA experienced dropouts when the vehicle passed directly over the stations. The resulting high azimuth rates exceeded the azimuth tracking rate capability of the antennas and respective dropouts of 30 and 29 seconds occurred.

During translunar coast, the BDA FPQ-6 radar experienced an unexpected signal fade, almost to the noise level, at a slant range of 16,000 miles. This signal fade appeared to be caused by a ground station problem, since the MILA TPQ-18 and BDA FPS-16 strip charts indicated a good signal level during this period of time. CRO indicated final LOS at 44,220 seconds (12:17:00).

A summary of available C-Band radar coverage showing AOS and LOS for each station is shown in Figure 15-2.

### 15.5 SECURE RANGE SAFETY COMMAND SYSTEMS EVALUATION

Telemetered data indicated that the command antennas, receivers/decoders, Exploding Bridge Wire (EBW) networks, and destruct controllers on each powered stage functioned properly during flight. They were in the required state-of-readiness if flight conditions during the launch had required

- ▽ PARKING ORBIT INSERTION
- ▽ BEGIN S-IVB RESTART PREPARATIONS
- ▽ S-IVB SECOND IGNITION
- ▽ TRANSLUNAR INJECTION

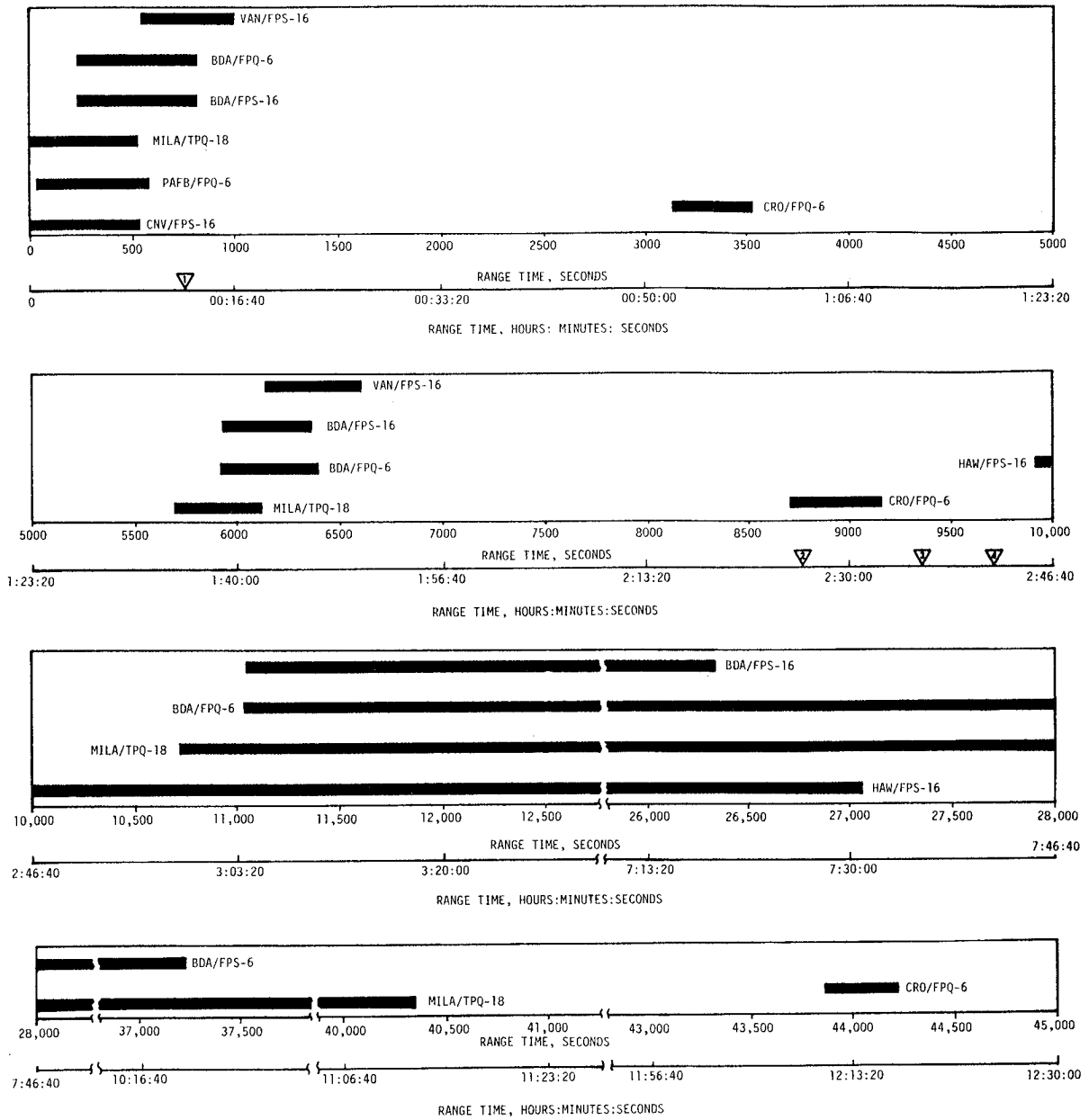


Figure 15-2. C-Band Radar Coverage Summary

vehicle destruct. Since no arm/cutoff or destruct commands were required, all data except receiver signal strength remained unchanged during the flight. At approximately 120 seconds, a momentary dropout occurred on the receiver signal strength measurements, as expected, when the command station switched transmitting antennas. Power to the S-IVB stage destruct system was cutoff at 760.0 seconds by ground command from BDA, thereby deactivating (safing) the system.

## 15.6 COMMAND AND COMMUNICATION SYSTEM EVALUATION

The performance of the CCS was excellent. No onboard equipment malfunctions occurred. The thermal shrouds designed to prevent the IU components, particularly the CCS cabling and components, from overheating apparently performed satisfactorily. The only significant problem encountered during the flight was signal interference between the IU CCS and the LM USB during translunar coast. This problem was caused by the necessity to apply power to the LM early. Application of power to the LM was not scheduled until after S-IVB/IU lunar impact.

The RF portion of the CCS performed satisfactorily during boost, earth orbit and Translunar Injection (TLI), with minor exceptions. Downlink data dropouts occurred during S-IC/S-II staging and at S-II second-plane separation, as on previous flights. Station handovers were accomplished with very little data loss. Performance during the second S-IVB burn could not be evaluated, since CCS ground station data were not available.

During translunar coast, the CCS RF performance was normal. The last CCS telemetry data were received at 70,380 seconds (19:33:00) due to 6D30 battery depletion. The CCS maintained two-way lock until S-IVB/IU lunar impact. The only dropouts (other than those at station handovers) occurred at Honeysuckle Creek (HSK) at 207,600 seconds (57:40:00) while the ground station crew attempted to find the best offset frequency for the uplink transmitter. An offset frequency was necessary to prevent interference with the LM USB system which uses the same nominal frequency. The frequency which provided the least interference was the CCS center frequency, 2101.8 megahertz, plus 57.4 kilohertz. ACN, ETC 3, GDS, HAW, MAD, and MILA indicated LOS at S-IVB/IU lunar impact at 280,601 seconds (77:56:41). A summary of CCS coverage giving AOS and LOS for each station is shown in Figure 15-3.

The command section of the CCS operated satisfactorily. All commands transmitted to the IU were accepted by the onboard equipment on the first attempt. No retransmission of commands was necessary as on most previous flights. The CCS command history is shown in Table 15-6.

## 15.7 GROUND ENGINEERING CAMERAS

In general, ground camera coverage was good. Sixty-seven items were received from KSC and evaluated. Two cameras had timing losses. As a result of these two failures, system efficiency was 97 percent. Only a few tracking items were included in the 67 items because of low cloud coverage.

Table 15-5. AS-508 Launch Vehicle Telemetry Links

LINK	FREQUENCY (MHz)	MODULATION	STAGE	FLIGHT PERIOD (RANGE TIME, SEC)	PERFORMANCE SUMMARY
AF-1	256.2	FM/FM	S-IC	0 to 414	Satisfactory
AP-1	244.3	PCM/FM	S-IC	0 to 414	Data Dropouts Range Time (sec)    Duration (sec) 135.2 (intermittent)    3.4 164.4    1.2 167.7    0.9
BF-1	241.5	FM/FM	S-II	0 to 640	Satisfactory
BF-2	234.0	FM/FM	S-II	0 to 640	Data Dropouts
BP-1	248.6	PCM/FM	S-II	0 to 640	Range Time (sec)    Duration (sec) 166.0    2.0 194.3    2.0
CP-1	258.5	PCM/FM	S-IVB	Flight Duration	Satisfactory
CS-1	253.8	SS/FM	S-IVB	0 to 780	Data Dropouts Range Time (sec)    Duration (sec) 164.4    1.0
DF-1	250.7	FM/FM	IU	Flight Duration	Satisfactory
DP-1	245.3	PCM/FM	II	Flight Duration	Data Dropouts
DP-1B (CCS)	2282.5	PCM/FM	IU	Flight Duration	Range Time (sec)    Duration (sec) 164.3 (VHF)    1.0 165.0 }    DP-1B    5.5 195.5 }    6.0

Table 15-6. Command and Communication System Commands History, AS-508

RANGE TIME		TRANSMITTING STATION	COMMAND	NUMBER OF WORDS		REMARKS
SECONDS	HRS:MIN:SECS			MODE	DATA	
11,022.0	03:03:42.0	GDS	LVDC Sector Dump for TLI State Vector	1	2	Accepted
14,940.3	04:09:00.3	GDS	Evasive Maneuver Attitude	1	0	Accepted
15,479.2	04:17:59.2	GDS	Initiate Timebase 8	1	0	Accepted
20,887.4	05:48:07.4	GDS	Lunar Impact Attitude Correction	1	6	Accepted
20,949.3	05:49:09.3	GDS	Single Word Dump for Lunar Impact Correction Command	6	18	Accepted

- ▲ PARKING ORBIT INSERTION
- ▲ BEGIN S-1VB RESTART PREPARATIONS
- ▲ S-1VB SECOND IGNITION
- ▲ S-1VB LUNAR INJECTION
- ▲ S-1VB/IU LUNAR IMPACT

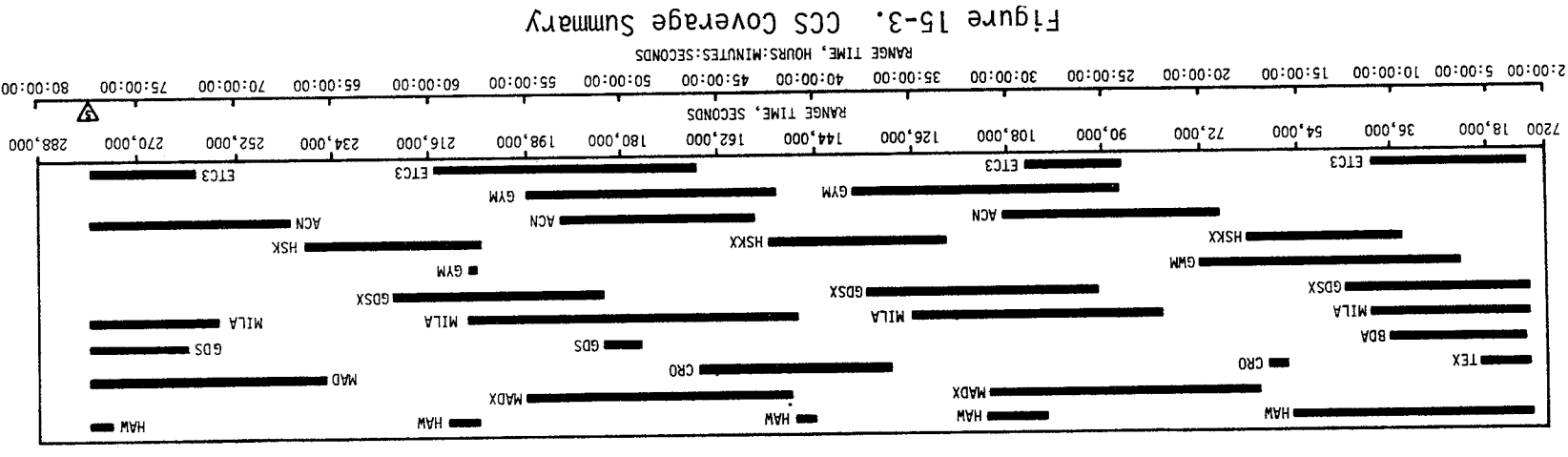
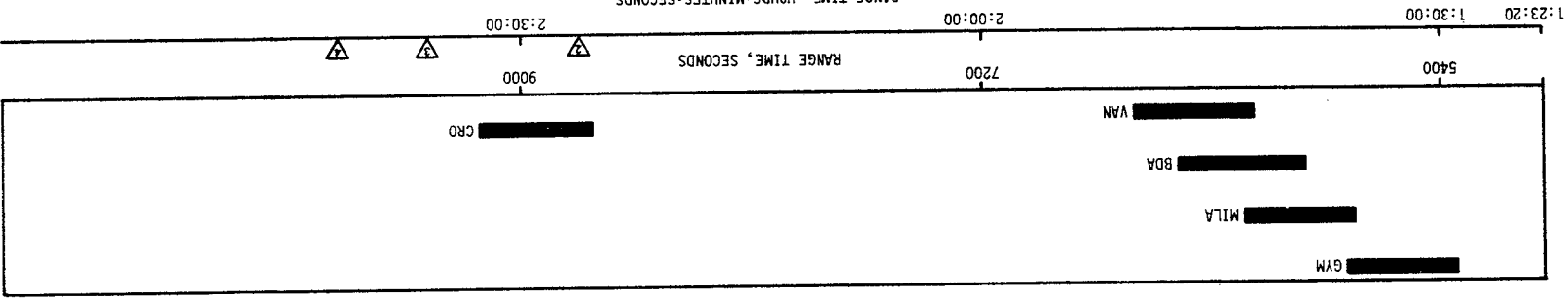
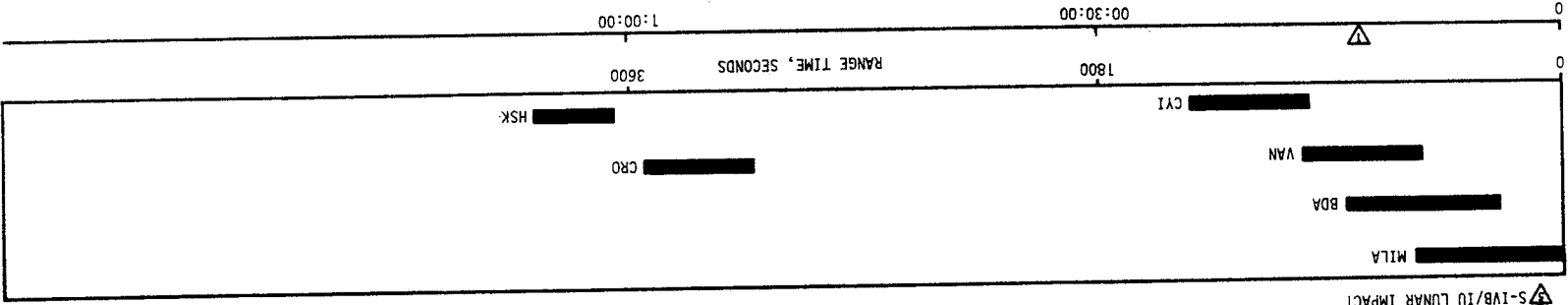


Figure 15-3. CCS Coverage Summary

## SECTION 16

### MASS CHARACTERISTICS

#### 16.1 SUMMARY

Total vehicle mass, determined from postflight analysis, was within 1.30 percent of prediction from ground ignition through S-IVB stage final shut-down. Despite an early S-II stage Center Engine Cutoff (CECO), the small variation indicates that hardware weights, propellant loads and propellant utilization during powered flight were close to predicted values.

#### 16.2 MASS EVALUATION

Postflight mass characteristics are compared with final predicted mass characteristics (MSFC Memorandum S&E-ASTN-SAE-70-4) and the final operational trajectory (MSFC Memorandum S&E-AERO-FMT-4-70).

The postflight mass characteristics were determined from an analysis of all available actual and reconstructed data from S-IC ignition through S-IVB second burn cutoff. Dry weights of the launch vehicle are based on actual stage weighings and evaluation of the weight and balance log books (MSFC Form 998). Propellant loading and utilization was evaluated from propulsion system performance reconstructions. Spacecraft data were obtained from the Manned Spacecraft Center (MSC).

Differences in dry weights of the inert stages and the loaded spacecraft were all within 0.45 percent of predicted, which was well within acceptable limits.

During S-IC burn phase, the total vehicle mass was lower than predicted by 4013 lbm (0.05 percent) at ignition, and by 3278 lbm (0.17 percent) at S-IC/S-II separation. These differences are attributed to S-IC stage dry weight and propellant loading which were less than that predicted. S-IC burn phase total vehicle mass is shown in Tables 16-1 and 16-2.

During S-II burn phase, the total vehicle mass was greater than predicted by 1449 lbm (0.10 percent) at ignition, and by 1338 lbm (0.29 percent) at S-II/S-IVB separation. These differences are due primarily to S-II and S-IVB stage propellant loading which was higher than predicted. Total vehicle mass for the S-II burn phase is shown in Tables 16-3 and 16-4.

Total vehicle mass during both S-IVB burn phases, as shown in Tables 16-5 through 16-8, was within 1.30 percent of the predicted values. A difference of 752 lbm (0.2 percent) from predicted at first burn ignition was due largely to a greater than predicted propellant loading. The difference at completion of second burn was -1123 lbm (0.79 percent) and resulted directly from an early S-II stage CECO. Total vehicle mass at spacecraft separation was 861 lbm (2.23 percent) lower than predicted.

A summary of mass utilization and loss, both actual and predicted, from S-IC stage ignition through spacecraft separation is presented in Table 16-9. A comparison of actual and predicted mass, center of gravity, and moment of inertia is shown in Table 16-10.

Table 16-1. Total Vehicle Mass, S-IC Burn Phase (Kilograms)

EVENTS	GROUND IGNITION		HOLDDOWN ARM RELEASE		CENTER ENGINE CUTOFF		OUTBOARD ENGINE CUTOFF		S-IC/S-II SEPARATION	
	PRED	ACT	PRED	ACT	PRED	ACT	PRED	ACT	PRED	ACT
RANGE TIME--SEC	-6.70	-6.70	0.30	0.30	135.27	135.18	164.00	163.60	164.80	164.40
DRY STAGE	130634.	130588.	130634.	130588.	130634.	130588.	130634.	130588.	130634.	130588.
LOX IN TANK	1478704.	1477908.	1447978.	1446402.	209086.	206172.	1001.	914.	889.	874.
LOX BELOW TANK	21100.	21094.	21859.	21854.	21843.	21837.	16871.	16740.	14819.	14482.
LOX ULLAGE GAS	189.	191.	210.	227.	2590.	2785.	3118.	3412.	3124.	3420.
FUEL IN TANK	646575.	644951.	636465.	634622.	100340.	96934.	8537.	6548.	7459.	5425.
FUEL BELOW TANK	4313.	4313.	5996.	5996.	5996.	5996.	5958.	5958.	5958.	5958.
FUEL ULLAGE GAS	34.	32.	34.	36.	210.	216.	242.	250.	243.	251.
N2 PURGE GAS	36.	36.	36.	36.	19.	19.	19.	19.	19.	19.
HELIUM IN BOTTLE	288.	288.	288.	285.	112.	104.	80.	70.	79.	69.
FROST	635.	635.	635.	635.	340.	340.	340.	340.	340.	340.
RETROCKET PROP	1026.	1026.	1026.	1026.	1026.	1026.	1026.	1026.	1026.	1026.
OTHER	239.	239.	239.	239.	239.	239.	239.	239.	239.	239.
TOTAL STAGE	2283779.	2281306.	2245406.	2241950.	472440.	466262.	168071.	166110.	164836.	162697.
TOTAL S-IC/S-II IS	5199.	5195.	5199.	5195.	5199.	5195.	5199.	5195.	5166.	5162.
TOTAL S-II STAGE	487816.	487944.	487616.	487944.	487395.	487722.	487395.	487722.	487395.	487722.
TOT S-II/S-IVB IS	3674.	3665.	3674.	3665.	3674.	3665.	3674.	3665.	3674.	3665.
TOTAL S-IVB STAGE	118714.	118985.	118714.	118985.	118623.	118894.	118623.	118894.	118623.	118894.
TOTAL INSTRU UNIT	2033.	2042.	2033.	2042.	2033.	2042.	2033.	2042.	2033.	2042.
TOTAL SPACECRAFT	49939.	49997.	49939.	49997.	49939.	49997.	49939.	49997.	49939.	49997.
TOTAL UPPERSTAGE	667177.	667830.	667177.	667830.	666865.	667517.	666865.	667517.	666832.	667484.
TOTAL VEHICLE	2950956.	2949136.	2912583.	2909780.	1139305.	1133780.	834937.	833628.	831668.	830181.

Table 16-2. Total Vehicle Mass, S-IC Burn Phase (Pounds)

EVENTS	GROUND IGNITION		HOLDDOWN ARM RELEASE		CENTER ENGINE CUTOFF		OUTBOARD ENGINE CUTOFF		S-IC/S-II SEPARATION	
	PRED	ACT	PRED	ACT	PRED	ACT	PRED	ACT	PRED	ACT
RANGE TIME--SEC	-6.70	-6.70	0.30	0.30	135.27	135.18	164.00	163.60	164.80	164.40
DRY STAGE	288000.	287899.	288000.	287899.	288000.	287899.	288000.	287899.	288000.	287899.
LOX IN TANK	3259985.	3258229.	3192246.	3188772.	460956.	454531.	2207.	2015.	1961.	1927.
LOX BELOW TANK	46518.	46505.	48193.	48180.	48156.	48144.	37196.	36906.	32672.	31927.
LOX ULLAGE GAS	418.	422.	463.	500.	5710.	6139.	6875.	7524.	6888.	7539.
FUEL IN TANK	1425454.	1421874.	1403166.	1399102.	221213.	213704.	18821.	14436.	16446.	11961.
FUEL BELOW TANK	9509.	9510.	13219.	13220.	13219.	13220.	13136.	13137.	13136.	13137.
FUEL ULLAGE GAS	76.	71.	76.	79.	464.	477.	535.	553.	537.	554.
N2 PURGE GAS	80.	80.	80.	80.	43.	43.	43.	43.	43.	43.
HELIUM IN BOTTLE	636.	636.	636.	628.	248.	230.	177.	154.	176.	153.
FROST	1400.	1400.	1400.	1400.	750.	750.	750.	750.	750.	750.
RETROCKET PROP	2264.	2264.	2264.	2264.	2264.	2264.	2264.	2264.	2264.	2264.
OTHER	528.	528.	528.	528.	528.	528.	528.	528.	528.	528.
TOTAL STAGE	5034871.	5029420.	4950274.	4942654.	1041553.	1027932.	370535.	366210.	363403.	358685.
TOTAL S-IC/S-II IS	11464.	11454.	11464.	11454.	11464.	11454.	11464.	11454.	11391.	11381.
TOTAL S-II STAGE	1075010.	1075733.	1075010.	1075733.	1074522.	1075245.	1074522.	1075245.	1074522.	1075245.
TOT S-II/S-IVB IS	8100.	8081.	8100.	8081.	8100.	8081.	8100.	8081.	8100.	8081.
TOTAL S-IVB STAGE	261721.	262317.	261721.	262317.	261521.	262117.	261521.	262117.	261521.	262117.
TOTAL INSTRU UNIT	4482.	4502.	4482.	4502.	4482.	4502.	4482.	4502.	4482.	4502.
TOTAL SPACECRAFT	110097.	110226.	110097.	110226.	110097.	110226.	110097.	110226.	110097.	110226.
TOTAL UPPERSTAGE	1470874.	1472313.	1470874.	1472313.	1470186.	1471625.	1470186.	1471625.	1470113.	1471552.
TOTAL VEHICLE	6505746.	6501733.	6421148.	6414967.	2511739.	2499557.	1840721.	1837835.	1833516.	1830238.

Table 16-3. Total Vehicle Mass, S-II Burn Phase (Kilograms)

EVENTS	S-IC IGNITION		S-II IGNITION		S-II MAINSTAGE		S-II ENGINE CUTOFF		S-II/S-IVB SEPARATION	
	PRED	ACT	PRED	ACT	PRED	ACT	PRED	ACT	PRED	ACT
RANGE TIME--SEC	-6.70	-6.70	166.40	166.00	168.40	168.00	558.11	592.64	559.10	592.70
S-IC/S-II SMALL IS	614.	612.	0.	0.	0.	0.				
S-IC/S-II LARGE IS	3968.	3972.	3968.	3972.	3968.	3972.				
S-IC/S-II PROPELLANT	616.	610.	312.	309.	0.	0.				
TOTAL S-IC/S-II IS	5199.	5195.	4281.	4281.	3968.	3972.				
DRY STAGE	35402.	35356.	35402.	35356.	35402.	35356.	35402.	35356.	35402.	35356.
LOX IN TANK	378549.	378802.	378549.	378802.	378082.	378335.	816.	815.	698.	697.
LOX BELOW TANK	737.	737.	737.	737.	800.	800.	787.	787.	787.	787.
LOX ULLAGE GAS	142.	169.	142.	169.	144.	171.	2357.	2543.	2364.	2550.
FUEL IN TANK	72347.	72438.	72341.	72432.	72128.	72218.	1916.	1932.	1863.	1879.
FUEL BELOW TANK	104.	104.	111.	111.	127.	127.	123.	123.	123.	123.
FUEL ULLAGE GAS	62.	66.	62.	66.	63.	66.	686.	805.	689.	808.
INSULATION PURGE GAS	17.	17.	0.	0.	0.	0.				
FROST	204.	204.	0.	0.	0.	0.				
START TANK	13.	13.	13.	13.	2.	2.	2.	2.	2.	2.
OTHER	34.	34.	34.	34.	34.	34.	34.	34.	34.	34.
TOTAL S-II STAGE	487616.	487944.	487395.	487722.	486785.	487113.	42127.	42400.	41967.	42239.
TOT S-II/S-IVB IS	3674.	3665.	3674.	3665.	3674.	3665.	3674.	3665.	3674.	3665.
TOTAL S-IVB STAGE	118714.	118985.	118623.	118894.	118623.	118894.	118623.	118894.	118621.	118892.
TOTAL IU	2033.	2042.	2033.	2042.	2033.	2042.	2033.	2042.	2033.	2042.
TOTAL SPACECRAFT	49939.	49997.	49939.	49997.	49939.	49997.	45855.	45919.	45855.	45919.
TOTAL UPPER STAGE	174360.	174690.	174270.	174599.	174270.	174599.	170186.	170521.	170184.	170519.
TOTAL VEHICLE	667177.	667830.	665946.	666603.	665024.	665685.	212314.	212921.	212151.	212758.

Table 16-4. Total Vehicle Mass, S-II Burn Phase (Pounds)

EVENTS	S-IC IGNITION		S-II IGNITION		S-II MAINSTAGE		S-II ENGINE CUTOFF		S-II/S-IVB SEPARATION	
	PRED	ACT	PRED	ACT	PRED	ACT	PRED	ACT	PRED	ACT
RANGE TIME--SEC	-6.70	-6.70	166.40	166.00	168.40	168.00	558.11	592.64	559.10	593.70
S-IC/S-II SMALL IS	1354.	1351.	0.	0.	0.	0.				
S-IC/S-II LARGE IS	8750.	8757.	8750.	8757.	8750.	8757.				
S-IC/S-II PROPELLANT	1360.	1346.	689.	682.	0.	0.				
TOTAL S-IC/S-II IS	11464.	11454.	9439.	9439.	8750.	8757.				
DRY STAGE	78050.	77947.	78050.	77947.	78050.	77947.	78050.	77947.	78050.	77947.
LOX IN TANK	834558.	835116.	834558.	835116.	833529.	834087.	1801.	1797.	1541.	1537.
LOX BELOW TANK	1625.	1625.	1625.	1625.	1764.	1764.	1736.	1736.	1736.	1736.
LOX ULLAGE GAS	314.	374.	314.	374.	318.	378.	5198.	5608.	5213.	5623.
FUEL IN TANK	159500.	159700.	159486.	159686.	159015.	159215.	4225.	4260.	4109.	4144.
FUEL BELOW TANK	231.	231.	245.	245.	282.	282.	272.	272.	272.	272.
FUEL ULLAGE GAS	138.	146.	138.	146.	139.	147.	1513.	1776.	1521.	1783.
INSULATION PURGE GAS	38.	38.	0.	0.	0.	0.				
FROST	450.	450.	0.	0.	0.	0.				
START TANK	30.	30.	30.	30.	5.	5.	5.	5.	5.	5.
OTHER	76.	76.	76.	76.	76.	76.	76.	76.	76.	76.
TOTAL S-II STAGE	1075010.	1075733.	1074522.	1075245.	1073179.	1073901.	92876.	93477.	92523.	92123.
TOT S-II/S-IVB IS	8100.	8081.	8100.	8081.	8100.	8081.	8100.	8081.	8100.	8081.
TOTAL S-IVB STAGE	261721.	262317.	261521.	262117.	261521.	262117.	261521.	262117.	261516.	262112.
TOTAL IU	4482.	4502.	4482.	4502.	4482.	4502.	4482.	4502.	4482.	4502.
TOTAL SPACECRAFT	110097.	110226.	110097.	110226.	110097.	110226.	101094.	101235.	101094.	101235.
TOTAL UPPER STAGE	384400.	385126.	384200.	384926.	384200.	384926.	375197.	375935.	375192.	375930.
TOTAL VEHICLE	1470874.	1472313.	1468161.	1469610.	1466128.	1467584.	468073.	469412.	467715.	469059.

Table 16-5. Total Vehicle Mass, S-IVB First Burn Phase (Kilograms)

EVENTS	S-IC IGNITION		S-IVB IGNITION		S-IVB MAINSTAGE		S-IVB ENGINE CUTOFF		S-IVB END DECAY	
	PRED	ACT	PRED	ACT	PRED	ACT	PRED	ACT	PRED	ACT
RANGE TIME--SEC	-6.70	-6.70	562.10	596.90	564.60	599.40	705.77	749.83	706.00	750.00
DRY STAGE	11362.	11383.	11339.	11360.	11339.	11360.	11278.	11299.	11278.	11299.
LOX IN TANK	86710.	86873.	86708.	86873.	86581.	86744.	61518.	60042.	61490.	60014.
LOX BELOW TANK	166.	166.	166.	166.	180.	180.	180.	180.	180.	180.
LOX ULLAGE GAS	17.	20.	20.	20.	23.	21.	105.	71.	105.	71.
FUEL IN TANK	19709.	19780.	19704.	19772.	19657.	19729.	14634.	14241.	14624.	14231.
FUEL BELOW TANK	21.	21.	26.	26.	26.	26.	26.	26.	26.	26.
FUEL ULLAGE GAS	20.	19.	20.	19.	20.	21.	64.	77.	64.	77.
ULLAGE ROCKET PROP	53.	53.	9.	8.						
APS PROPELLANT	285.	300.	285.	300.	285.	300.	283.	297.	283.	297.
HELIUM IN BOTTLES	201.	200.	201.	200.	200.	199.	179.	175.	179.	175.
FROST	136.	136.	45.	45.	45.	45.	45.	45.	45.	45.
START TANK GAS	2.	2.	2.	2.	0.	0.	3.	2.	3.	2.
OTHER	25.	25.	25.	25.	25.	25.	25.	25.	25.	25.
TOTAL S-IVB STAGE	118714.	118985.	118556.	118822.	118388.	118655.	88345.	86485.	88308.	86447.
TOTAL IU	2033.	2042.	2033.	2042.	2033.	2042.	2033.	2042.	2033.	2042.
TOTAL SPACECRAFT	45855.	45919.	45855.	45919.	45855.	45919.	45855.	45919.	45855.	45919.
TOTAL UPPERSTAGE	47888.	47961.	47888.	47961.	47888.	47961.	47888.	47961.	47888.	47961.
TOTAL VEHICLE	166603.	166946.	166445.	166784.	166276.	166616.	136234.	134446.	136197.	134408.

Table 16-6. Total Vehicle Mass, S-IVB First Burn Phase (Pounds)

EVENTS	S-IC IGNITION		S-IVB IGNITION		S-IVB MAINSTAGE		S-IVB ENGINE CUTOFF		S-IVB END DECAY	
	PRED	ACT	PRED	ACT	PRED	ACT	PRED	ACT	PRED	ACT
RANGE TIME--SEC	-6.70	-6.70	562.10	596.90	564.60	599.40	705.77	749.83	706.00	750.00
DRY STAGE	25050.	25097.	24999.	25046.	24999.	25046.	24864.	24911.	24864.	24911.
LOX IN TANK	191165.	191523.	191159.	191523.	190880.	191238.	135625.	132371.	135564.	132310.
LOX BELOW TANK	367.	367.	367.	367.	397.	397.	397.	397.	397.	397.
LOX ULLAGE GAS	39.	46.	46.	46.	52.	48.	233.	157.	233.	157.
FUEL IN TANK	43452.	43609.	43441.	43591.	43338.	43496.	32264.	31397.	32241.	31375.
FUEL BELOW TANK	48.	48.	58.	58.	58.	58.	58.	58.	58.	58.
FUEL ULLAGE GAS	45.	43.	45.	43.	46.	47.	143.	170.	143.	170.
ULLAGE ROCKET PROP	118.	118.	22.	19.						
APS PROPELLANT	630.	662.	630.	662.	630.	662.	626.	656.	626.	656.
HELIUM IN BOTTLES	445.	442.	444.	442.	443.	440.	396.	388.	396.	388.
FROST	300.	300.	100.	100.	100.	100.	100.	100.	100.	100.
START TANK GAS	5.	5.	5.	5.	1.	1.	7.	5.	7.	5.
OTHER	56.	57.	56.	57.	56.	57.	56.	57.	56.	57.
TOTAL S-IVB STAGE	261721.	262317.	261373.	261959.	261001.	261590.	194769.	190667.	194687.	190584.
TOTAL IU	4482.	4502.	4482.	4502.	4482.	4502.	4482.	4502.	4482.	4502.
TOTAL SPACECRAFT	101094.	101235.	101094.	101235.	101094.	101235.	101094.	101235.	101094.	101235.
TOTAL UPPERSTAGE	105576.	105737.	105576.	105737.	105576.	105737.	105576.	105737.	105576.	105737.
TOTAL VEHICLE	367297.	368054.	366949.	367696.	366577.	367327.	300345.	296404.	300263.	296321.

Table 16-7. Total Vehicle Mass, S-IVB Second Burn Phase (Kilograms)

EVENTS	S-IVB IGNITION		S-IVB MAINSTAGE		S-IVB ENGINE CUTOFF		S-IVB END DECAY		SPACECRAFT SEPARATION	
	PRED	ACT	PRED	ACT	PRED	ACT	PRED	ACT	PRED	ACT
RANGE TIME--SEC	9327.90	9346.40	9330.40	9348.90	9683.62	9697.17	9683.80	9697.40	14460.00	14460.80
DRY STAGE	11278.	11299.	11278.	11299.	11278.	11299.	11278.	11299.	11278.	11299.
LOX IN TANK	61388.	59945.	61269.	59824.	2093.	1694.	2065.	1667.	1992.	1612.
LOX BELOW TANK	166.	166.	180.	180.	180.	180.	180.	180.	166.	166.
LOX ULLAGE GAS	166.	136.	167.	136.	269.	204.	270.	204.	270.	104.
FUEL IN TANK	13509.	13294.	13463.	13251.	1020.	874.	1009.	864.	410.	703.
FUEL BELOW TANK	26.	26.	26.	26.	26.	26.	26.	26.	21.	21.
FUEL ULLAGE GAS	158.	151.	158.	152.	272.	248.	273.	248.	273.	136.
APS PROPELLANT	229.	246.	229.	246.	227.	241.	227.	241.	192.	238.
HELIUM IN BOTTLES	150.	164.	150.	164.	88.	107.	88.	107.	88.	13.
FROST	45.	45.	45.	45.	45.	45.	45.	45.	45.	45.
START TANK GAS	2.	2.	0.	0.	3.	2.	3.	2.	3.	2.
OTHER	25.	25.	25.	25.	25.	25.	25.	25.	25.	25.
TOTAL S-IVB STAGE	87148.	85505.	86993.	85352.	15532.	14949.	15492.	14912.	14768.	14369.
TOTAL IU	2033.	2042.	2033.	2042.	2033.	2042.	2033.	2042.	2033.	2042.
TOTAL SPACECRAFT	45855.	45919.	45855.	45919.	45855.	45919.	45855.	45919.	625.	625.
TOTAL UPPERSTAGE	47888.	47961.	47888.	47961.	47888.	47961.	47888.	47961.	2658.	2668.
TOTAL VEHICLE	135036.	133466.	134883.	133314.	63420.	62911.	63381.	62874.	17427.	17037.

Table 16-8. Total Vehicle Mass, S-IVB Second Burn Phase (Pounds)

EVENTS	S-IVB IGNITION		S-IVB MAINSTAGE		S-IVB ENGINE CUTOFF		S-IVB END DECAY		SPACECRAFT SEPARATION	
	PRED	ACT	PRED	ACT	PRED	ACT	PRED	ACT	PRED	ACT
RANGE TIME--SEC	9327.90	9346.40	9330.40	9348.90	9683.62	9697.17	9683.80	9697.40	14460.00	14460.80
DRY STAGE	24864.	24911.	24864.	24911.	24864.	24911.	24864.	24911.	24864.	24911.
LOX IN TANK	135339.	132158.	135077.	131890.	4616.	3735.	4553.	3677.	4393.	3556.
LOX BELOW TANK	367.	367.	397.	397.	397.	397.	397.	397.	367.	367.
LOX ULLAGE GAS	367.	301.	369.	302.	595.	450.	596.	450.	596.	230.
FUEL IN TANK	29784.	29309.	29681.	29214.	2250.	1929.	2225.	1905.	905.	1550.
FUEL BELOW TANK	58.	58.	58.	58.	58.	58.	58.	58.	48.	48.
FUEL ULLAGE GAS	349.	335.	350.	336.	601.	547.	603.	547.	603.	301.
APS PROPELLANT	505.	543.	505.	543.	501.	533.	501.	533.	424.	525.
HELIUM IN BOTTLES	332.	363.	332.	362.	196.	237.	195.	237.	195.	29.
FROST	100.	100.	100.	100.	100.	100.	100.	100.	100.	100.
START TANK GAS	5.	5.	1.	1.	7.	5.	7.	5.	7.	5.
OTHER	56.	57.	56.	57.	56.	57.	56.	57.	56.	57.
TOTAL S-IVB STAGE	192129.	188507.	191792.	188171.	34243.	32959.	34156.	32877.	32559.	31679.
TOTAL IU	4482.	4502.	4482.	4502.	4482.	4502.	4482.	4502.	4482.	4502.
TOTAL SPACECRAFT	101094.	101235.	101094.	101235.	101094.	101235.	101094.	101235.	1380.	1380.
TOTAL UPPERSTAGE	105576.	105737.	105576.	105737.	105576.	105737.	105576.	105737.	5862.	5882.
TOTAL VEHICLE	297704.	294244.	297368.	292908.	139819.	138696.	139733.	138614.	38422.	37561.

Table 16-9. Flight Sequence Mass Summary

MASS HISTORY	PREDICTED		ACTUAL	
	KG	LBM	KG	LBM
S-IC STAGE, TOTAL	2283778.	5034871.	2281305.	5029420.
S-IC/S-II IS, TOTAL	5199.	11464.	5195.	11454.
S-II STAGE, TOTAL	487616.	1075010.	487944.	1075733.
S-II/S-IVB IS, TOTAL	3674.	8100.	3665.	8081.
S-IVB STAGE, TOTAL	118714.	261721.	118984.	262317.
INSTRUMENT UNIT	2033.	4482.	2042.	4502.
SPACECRAFT, TOTAL	49939.	110097.	49997.	110226.
1ST FLT STG AT IGN THRUST BUILDUP	2950955. -38372.	6505746. -84597.	2949135. -39356.	6501733. -86766.
1ST FLT STG AT HDAR FROST	2912582. -294.	6421148. -650.	2909779. -294.	6414967. -650.
MAINSTAGE	-2076024.	-4576852.	-2074484.	-4573457.
N2 PURGE GAS	-16.	-37.	-16.	-37.
THRUST DECAY-IE	-808.	-1783.	-853.	-1881.
ENG EXPENDED PROP	-189.	-418.	-189.	-418.
S-II INSUL PURGE	-17.	-38.	-17.	-38.
S-II FROST	-204.	-450.	-204.	-450.
S-IVB FROST	-90.	-200.	-90.	-200.
THRUST DECAY-OE	0.	0.	0.	0.
1ST FLT STG AT OECO THRUST DECAY-OE	834936. -3235.	1840721. -7132.	833627. -3413.	1837835. -7524.
S-IC/S-II ULL RKT	-33.	-73.	-33.	-73.
1ST FLT STG AT SEP STG AT SEPARATION	831668. -164836.	1833516. -363403.	830181. -162697.	1830238. -358685.
S-IC/S-II SMALL IS	-614.	-1354.	-612.	-1351.
S-IC/S-II ULL RKT	-83.	-184.	-83.	-184.
2ND FLT STG AT SSC FUEL LEAD	666134. 0.	1468575. 0.	666788. 0.	1470017. 0.
S-IC/S-II ULL RKT	-187.	-414.	-184.	-407.
2ND FLT STG AT IGN THRUST BUILDUP	665946. -597.	1468161. -1318.	666603. -598.	1469610. -1319.
START TANK	-11.	-25.	-11.	-25.
S-IC/S-II ULL RKT	-312.	-689.	-309.	-682.
2ND FLT STG AT MS MAINSTAGE	665024. -444600.	1466128. -980176.	665684. -444655.	1467584. -980297.
LES	-4083.	-9003.	-4078.	-8991.
S-IC/S-II LARGE IS TD & ENG PROP	-3968. -57.	-8750. -126.	-3972. -57.	-8757. -126.
2ND FLT STG AT COS THRUST DECAY	212314. -160.	468073. -353.	212921. -160.	469412. -354.
S-IVB ULL RKT PROP	-2.	-5.	-2.	-5.
2ND FLT STG AT SEP STG AT SEPARATION	212151. -41967.	467715. -92523.	212758. -42239.	469053. -93123.
S-II/S-IVB IS DRY	-3193.	-7040.	-3183.	-7019.
S-II/S-IVB PROP	-480.	-1060.	-481.	-1062.
S-IVB AFT FRAME	-21.	-48.	-21.	-48.
S-IVB ULL RKT PROP	-1.	-3.	-1.	-3.
S-IVB DET PKG	-1.	-3.	-1.	-3.
3RD FLT STG AT SSC	166485.	367038.	166828.	367795.

Table 16-9. Flight Sequence Mass Summary (Continued)

MASS HISTORY	PREDICTED		ACTUAL	
	KG	LBM	KG	LBM
3RD FLT STG 1ST SSC	166485.	367038.	166828.	367795.
ULLAGE ROCKET PROP	-39.	-88.	-41.	-91.
FUEL LEAD	-0.	-1.	-3.	-8.
3RD FLT STG 1ST IGN	166445.	366949.	166784.	367696.
ULLAGE ROCKET PROP	-9.	-22.	-8.	-19.
START TANK	-1.	-4.	-1.	-4.
THRUST BUILDUP	-156.	-345.	-156.	-346.
3RD FLT STG 1ST MS	166276.	366577.	166616.	367327.
ULLAGE ROCKET CASE	-61.	-135.	-61.	-135.
MAINSTAGE	-29979.	-66093.	-32106.	-70782.
APS	-1.	-4.	-2.	-6.
3RD FLT STG 1ST COS	136234.	300345.	134446.	296404.
THRUST DECAY	-37.	-82.	-37.	-83.
3RD FLT STG 1ST ETD	136196.	300263.	134408.	296321.
ENGINE PROP	-18.	-40.	-18.	-40.
FUEL TANK LOSS	-1038.	-2289.	-847.	-1868.
LOX TANK LOSS	-31.	-69.	-5.	-12.
APS	-54.	-121.	-51.	-113.
START TANK	-0.	-2.	0.	0.
O2/H2 BURNER	-7.	-16.	-7.	-16.
3RD FLT STG 2ND SSC	135046.	297726.	133479.	294271.
FUEL LEAD	-9.	-22.	-12.	-27.
3RD FLT STG 2ND IGN	135036.	297704.	133466.	294244.
START TANK	-1.	-4.	-1.	-4.
THRUST BUILDUP	-150.	-332.	-150.	-332.
3RD FLT STG 2ND MS	134883.	297368.	133314.	293908.
MAINSTAGE	-71461.	-157545.	-70398.	-155202.
APS	-1.	-4.	-4.	-10.
3RD FLT STG 2ND COS	63420.	139819.	62911.	138696.
THRUST DECAY	-39.	-86.	-37.	-82.
3RD FLT STG 2ND ETD	63381.	139733.	62874.	138614.
JETTISON SLA	-1164.	-2567.	-1164.	-2567.
CSM	-28893.	-63699.	-28936.	-63795.
S-IVB STAGE LOSS	-388.	-857.	-282.	-623.
STRT TRANS/DOCK	32935.	72610.	32490.	71629.
CSM	28893.	63699.	28936.	63795.
END TRANS/DOCK	61828.	136309.	61427.	135424.
CSM	-28893.	-63699.	-28936.	-63795.
LM	-15171.	-33448.	-15192.	-33493.
S-IVB STAGE LOSS	-335.	-740.	-260.	-575.
LAU VEH AT S/C SEP	17427.	38422.	17037.	37561.
S/C NOT SEPARATED	-625.	-1380.	-625.	-1380.
IU	-2033.	-4482.	-2042.	-4502.
S-IVB STAGE	-14768.	-32559.	-14369.	-31679.

Table 16-10. Mass Characteristics Comparison

EVENT	MASS		LONGITUDINAL C.G. (X STA.)		RADIAL C.G.		ROLL MOMENT OF INERTIA		PITCH MOMENT OF INERTIA		YAW MOMENT OF INERTIA	
	KILO POUNDS	O/O DEV.	METERS INCHES	DELTA	METERS INCHES	DELTA	KG-M2 X10-6	O/O DEV.	KG-M2 X10-6	O/O DEV.	KG-M2 X10-6	O/O DEV.
S-IC STAGE DRY	PRED	130635. 288000.	9.326 367.2		0.0594 2.3409		2.510		16.537		16.463	
	ACTUAL	130589. 287899.	9.326 367.2	0.000 0.00	0.0594 2.3409	0.0000 0.0000	2.509	-0.03	16.531	-0.03	16.457	-0.03
S-IC/S-II INTER-STAGE, TOTAL	PRED	5200. 11464.	41.628 1638.9		0.1526 6.0108		0.132		0.079		0.079	
	ACTUAL	5195. 11454.	41.628 1638.9	0.000 0.00	0.1526 6.0108	0.0000 0.0000	0.132	-0.08	0.079	-0.08	0.079	-0.08
S-II STAGE, DRY	PRED	35403. 78050.	47.932 1887.1		0.1772 6.9778		0.575		2.004		2.017	
	ACTUAL	35356. 77947.	47.922 1886.7	-0.010 -0.39	0.1772 6.9778	0.0000 0.0000	0.575	-0.12	2.002	-0.12	2.014	-0.12
S-II/S-IVB INTER-STAGE, TOTAL	PRED	3674. 8100.	66.466 2616.8		0.0589 2.3194		0.065		0.044		0.045	
	ACTUAL	3665. 8081.	66.466 2616.8	0.000 0.00	0.0589 2.3194	0.0000 0.0000	0.065	-0.22	0.044	-0.22	0.044	-0.22
S-IVB STAGE, DRY	PRED	11362. 25050.	72.567 2857.0		0.2306 9.0801		0.082		0.300		0.300	
	ACTUAL	11384. 25097.	72.567 2857.0	0.000 0.00	0.2306 9.0801	0.0000 0.0000	0.082	0.19	0.301	0.19	0.301	0.19
VEHICLE INSTRUMENT UNIT	PRED	2033. 4482.	82.407 3244.4		0.4721 18.5884		0.019		0.010		0.009	
	ACTUAL	2042. 4502.	82.407 3244.4	0.000 0.00	0.4780 18.8215	0.0059 0.2330	0.019	0.45	0.010	0.45	0.009	0.45
SPACECRAFT, TOTAL	PRED	49939. 110097.	91.539 3603.9		0.1106 4.3566		0.092		1.594		1.597	
	ACTUAL	49998. 110226.	91.539 3603.9	0.000 0.00	0.1128 4.4418	0.0021 0.0852	0.091	-0.62	1.593	-0.05	1.596	-0.05

16-9

Table 16-10. Mass Characteristics Comparison (Continued)

EVENT	MASS		LONGITUDINAL C.G. (X STA.)		RADIAL C.G.		ROLL MOMENT OF INERTIA		PITCH MOMENT OF INERTIA		YAW MOMENT OF INERTIA	
	KILO POUNDS	O/O DEV.	METERS INCHES	DELTA	METERS INCHES	DELTA	KG-M2 X10-6	O/O DEV.	KG-M2 X10-6	O/O DEV.	KG-M2 X10-6	O/O DEV.
1ST FLIGHT STAGE AT IGNITION	PRED	2950957. 6505747.	30.338 1194.4		0.0039 0.1565		3.598		879.443		879.363	
	ACTUAL	2949136. 6501733.	30.366 1195.5	0.028 1.10	0.0042 0.1655	0.0002 0.0090	3.582	-0.43	879.541	0.01	879.461	0.01
1ST FLIGHT STAGE AT HOLDDOWN ARM RELEASE	PRED	2912584. 6421149.	30.285 1192.3		0.0042 0.1655		3.633		880.463		880.383	
	ACTUAL	2909780. 6414967.	30.312 1193.3	0.027 1.06	0.0042 0.1655	0.0000 0.0000	3.617	-0.42	880.506	0.00	880.426	0.00
1ST FLIGHT STAGE AT OUTBOARD ENGINE CUTOFF SIGNAL	PRED	834937. 1840721.	46.450 1828.7		0.0140 0.5515		3.618		442.126		442.050	
	ACTUAL	833628. 1837834.	46.566 1833.3	0.115 4.55	0.0144 0.5700	0.0004 0.0185	3.602	-0.43	439.100	-0.67	439.025	-0.67
1ST FLIGHT STAGE AT SEPARATION	PRED	831669. 1833516.	46.592 1834.3		0.0140 0.5515		3.616		437.783		437.707	
	ACTUAL	830181. 1830236.	46.717 1839.2	0.124 4.91	0.0144 0.5700	0.0004 0.0185	3.600	-0.43	434.443	-0.75	434.367	-0.75
2ND FLIGHT STAGE AT START SEQUENCE COMMAND	PRED	666135. 1468575.	55.778 2195.9		0.0177 0.7002		0.966		136.060		136.075	
	ACTUAL	666789. 1470017.	55.788 2196.3	0.010 0.39	0.0177 0.7000	-0.0000 -0.0002	0.966	0.02	136.254	0.14	136.268	0.14
2ND FLIGHT STAGE AT MAINSTAGE	PRED	665025. 1466128.	55.790 2196.4		0.0177 0.7002		0.954		135.941		135.956	
	ACTUAL	665685. 1467584.	55.800 2196.8	0.010 0.39	0.0177 0.7000	-0.0000 -0.0002	0.955	0.04	136.136	0.14	136.150	0.14
2ND FLIGHT STAGE AT CUTOFF SIGNAL	PRED	212315. 468073.	71.151 2801.2		0.0536 2.1103		0.852		44.524		44.538	
	ACTUAL	212922. 469411.	71.136 2800.6	-0.015 -0.59	0.0536 2.1103	0.0000 0.0000	0.852	0.03	44.692	0.38	44.705	0.37

16-10

Table 16-10. Mass Characteristics Comparison (Continued)

EVENT	MASS		LONGITUDINAL C.G. (X STA.)		RADIAL C.G.		ROLL MOMENT OF INERTIA		PITCH MOMENT OF INERTIA		YAW MOMENT OF INERTIA	
	KILO POUNDS	O/O DEV.	METERS INCHES	DELTA	METERS INCHES	DELTA	KG-M2 X10-6	O/O DEV.	KG-M2 X10-6	O/O DEV.	KG-M2 X10-6	O/O DEV.
2ND FLIGHT STAGE AT SEPARATION	PRED	212152. 467715.	71.171 2802.0		0.0536 2.1103		0.852		44.415		44.430	
	ACTUAL	212759. 469052.	71.155 2801.3	-0.016 -0.63	0.0536 2.1103	0.0000 0.0000	0.852	0.03	44.584	0.38	44.597	0.38
3RD FLIGHT STAGE AT 1ST START SEQUENCE COMMAND	PRED	166486. 367038.	77.150 3037.4		0.0374 1.4735		0.200		13.443		13.443	
	ACTUAL	166829. 367795.	77.152 3037.5	0.002 0.10	0.0373 1.4686	-0.0001 -0.0049	0.200	0.08	13.466	0.17	13.465	0.17
3RD FLIGHT STAGE AT 1ST IGNITION	PRED	166446. 366949.	77.150 3037.4		0.0374 1.4735		0.200		13.444		13.444	
	ACTUAL	166784. 367696.	77.152 3037.5	0.002 0.10	0.0373 1.4686	-0.0001 -0.0049	0.200	0.08	13.467	0.17	13.467	0.17
3RD FLIGHT STAGE AT 1ST MAINSTAGE	PRED	166277. 366577.	77.152 3037.4		0.0374 1.4735		0.200		13.442		13.442	
	ACTUAL	166617. 367327.	77.154 3037.5	0.002 0.10	0.0373 1.4686	-0.0001 -0.0049	0.200	0.08	13.465	0.17	13.464	0.17
3RD FLIGHT STAGE AT 1ST CUTOFF SIGNAL	PRED	136234. 300345.	78.041 3072.4		0.0455 1.7923		0.199		12.645		12.645	
	ACTUAL	134447. 296404.	78.120 3075.6	0.079 3.12	0.0459 1.8096	0.0004 0.0173	0.199	0.06	12.599	-0.35	12.599	-0.36
3RD FLIGHT STAGE AT 1ST END THRUST DECAY, START COAST	PRED	136197. 300263.	78.042 3072.5		0.0455 1.7923		0.199		12.644		12.644	
	ACTUAL	134409. 296321.	78.121 3075.6	0.079 3.12	0.0459 1.8096	0.0004 0.0173	0.199	0.06	12.598	-0.35	12.598	-0.35
3RD FLIGHT STAGE AT 2ND START SEQUENCE COMMAND	PRED	135046. 297726.	78.049 3072.8		0.0454 1.7887		0.198		12.641		12.641	
	ACTUAL	133479. 294271.	78.129 3075.9	0.079 3.14	0.0460 1.8146	0.0006 0.0259	0.199	0.15	12.595	-0.35	12.595	-0.35

16-11

Table 16-10. Mass Characteristics Comparison (Continued)

EVENT	MASS		LONGITUDINAL C.G. (X STA.)		RADIAL C.G.		ROLL MOMENT OF INERTIA		PITCH MOMENT OF INERTIA		YAW MOMENT OF INERTIA	
	KILO POUNDS	O/O DEV.	METERS INCHES	DELTA	METERS INCHES	DELTA	KG-M2 X10-6	O/O DEV.	KG-M2 X10-6	O/O DEV.	KG-M2 X10-6	O/O DEV.
3RD FLIGHT STAGE AT 2ND IGNITION	PRED	135037.	78.048		0.0454				12.643		12.643	
	ACTUAL	297704.	3072.7		1.7887		0.198		12.643		12.643	
3RD FLIGHT STAGE AT 2ND MAINSTAGE	PRED	133467.	78.128	0.079	0.0460	0.0006			12.597	-0.35	12.597	-0.36
	ACTUAL	294244.	3075.9	3.14	1.8146	0.0258	0.199	0.15	12.597	-0.35	12.597	-0.36
3RD FLIGHT STAGE AT 2ND CUTOFF SIGNAL	PRED	134884.	78.053		0.0456				5.360		5.360	
	ACTUAL	297368.	3072.9		1.7973		0.198		5.360		5.360	
3RD FLIGHT STAGE AT 2ND END THRUST DECAY	PRED	63421.	85.690		0.0948				5.174	-3.48	5.173	-3.48
	ACTUAL	139819.	3373.6		3.7355		0.197		5.174	-3.48	5.173	-3.48
CSM SEPARATED	PRED	62911.	85.886	0.195	0.0963	0.0014			5.164	-3.48	5.164	-3.48
	ACTUAL	138696.	3381.3	7.69	3.7918	0.0563	0.198	0.15	5.164	-3.48	5.164	-3.48
CSM DOCKED	PRED	63382.	85.699		0.0952				1.695		1.693	
	ACTUAL	139733.	3374.0		3.7492		0.197		1.695		1.693	
SPACECRAFT SEPARATED	PRED	62874.	85.895	0.196	0.0963	0.0010			0.620		0.617	
	ACTUAL	138614.	3381.7	7.72	3.7918	0.0426	0.198	0.15	0.620		0.617	
SPACECRAFT SEPARATED	PRED	32936.	78.776		0.0834				0.610	-1.59	0.606	-1.79
	ACTUAL	72610.	3101.4		3.2851		0.142	0.34	0.610	-1.59	0.606	-1.79
SPACECRAFT SEPARATED	PRED	32490.	78.952	0.175	0.0828	-0.0006			0.111		0.111	
	ACTUAL	71629.	3108.3	6.91	3.2600	-0.0251	0.142	0.34	0.111		0.111	
SPACECRAFT SEPARATED	PRED	61829.	85.204		0.1286				0.111		0.111	
	ACTUAL	136309.	3354.5		5.0637		0.188		0.111		0.111	
SPACECRAFT SEPARATED	PRED	61427.	85.364	0.160	0.1284	-0.0002			0.111		0.111	
	ACTUAL	135424.	3360.8	6.31	5.0558	-0.0078	0.189	0.19	0.111		0.111	
SPACECRAFT SEPARATED	PRED	17428.	73.658		0.1566				0.111		0.111	
	ACTUAL	38422.	2899.9		6.1682		0.111		0.111		0.111	
SPACECRAFT SEPARATED	PRED	17037.	73.758	0.099	0.1499	-0.0066			0.111		0.111	
	ACTUAL	37561.	2903.8	3.92	5.9053	-0.2628	0.111	0.21	0.111		0.111	

16-12

## SECTION 17

### SPACECRAFT SUMMARY

The Apollo 13 mission, planned as a lunar landing in the Fra Mauro area, was aborted because of the abrupt loss of service module cryogenic oxygen pressure at approximately 56 hours. After entering the lunar module and powering up the lunar module systems, the crew shut down all command and service module systems not required for the abort mission. A circumlunar profile was executed as the most efficient means of earth return, with the lunar module providing power and life support until transfer to the command module just prior to entry.

The space vehicle, with a crew of James A. Lovell, Mission Commander; Fred W. Haise, Jr., Lunar Module Pilot; and John L. Swigert, Jr., Command Module Pilot; was launched from Kennedy Space Center, Florida, at 2:13:00 P.M. Eastern Standard Time (19:13:00 GMT) April 11, 1970. Two days before launch, the Command Module Pilot, as a member of the Apollo 13 backup crew, was substituted for his prime crew counterpart, who was exposed and found susceptible to rubella (German measles). The only unexpected occurrence during launch was an early shutdown of the S-II center engine, with no appreciable effect on the flight. The activities during earth orbit checkout, translunar injection, and initial translunar coast were similar to those of Apollo 11 and 12. Soon after the spacecraft was ejected, the S-IVB was maneuvered using the auxiliary propulsion system to impact on the lunar surface and provide seismological data. The first midcourse correction inserted the spacecraft into a non-free-return trajectory.

At approximately 56 hours, the pressure in cryogenic oxygen tank 2 began to rise at an abnormally high rate, and soon thereafter, the tank abruptly lost pressure. The pressure in tank 1 also dropped but at a rate sufficient to maintain fuel cell 2 in operation for approximately 2 more hours. The loss of primary power in the command module required an immediate abort of the mission. The crew powered up the lunar module, and the first maneuver following the incident was made with the descent propulsion system to place the spacecraft once again on a free-return trajectory. A second maneuver performed with the descent engine 2 hours after passing pericynthian reduced the transearth transit time and moved the earth landing point from the Indian Ocean to the South Pacific. Two small transearth midcourse corrections were required prior to entry. After the service module was jettisoned, the crew observed and photographed the bay 4 area where the cryogenic tank anomaly had occurred, remarking

that the outer skin covering had been severely damaged and a large portion was missing. The lunar module was jettisoned 1 hour before entry, which was performed nominally using the primary guidance and navigation system. Landing occurred at 142:54:41 within sight of the recovery ship. The touchdown point was reported as 21 degrees 38 minutes 24 seconds south latitude and 165 degrees 21 minutes 42 seconds west longitude. The crew was retrieved and aboard the recovery ship within 45 minutes after landing.

For further details on the spacecraft performance, refer to the Apollo 13 Mission Report published by the NASA Manned Spacecraft Center at Houston, Texas.

## APPENDIX A

### ATMOSPHERE

#### A.1 SUMMARY

This appendix presents a summary of the atmospheric environment at launch time of the AS-508. The format of these data is similar to that presented on previous launches of Saturn vehicles to permit comparisons. Surface and upper levels winds, and thermodynamic data near launch time are given.

#### A.2 GENERAL ATMOSPHERIC CONDITIONS AT LAUNCH TIME

At launch time, a cold front extended from a low pressure cell in the North Atlantic, becoming stationary through northern Florida and along the Gulf Coast to a low pressure area located in southern Louisiana. See Figure A-1. The frontal intensity was weak in northern Florida but became stronger in the northwestern Gulf of Mexico-Louisiana area.

Surface winds in the Cape Kennedy area were light and variable, as shown in Table A-1. Generally, winds in the lower part of the troposphere were light, permitting the sea breeze to switch the surface wind to the east southeast by early afternoon.

Wind flow aloft is shown in Figure A-2 (500 millibar level). The maximum wind belt was located north of Florida giving less intense westerly wind flow over the Cape Kennedy, Florida area.

#### A.3 SURFACE OBSERVATIONS AT LAUNCH TIME

At launch time skies were overcast with 4/10 altocumulus at 5.8 kilometers (19,000 ft), and 10/10 thin cirrostratus with bases at an estimated 7.9 kilometers (26,000 ft). All surface observations at launch time are summarized in Table A-1. Solar radiation data are given in Table A-2.

#### A.4 UPPER AIR MEASUREMENTS

Data were used from four of the upper air wind systems to compile the final meteorological tape. Table A-3 summarizes the wind data systems used. Only the Rawinsonde and the Loki Dart meteorological rocket data were used in the upper level atmospheric thermodynamic analyses.

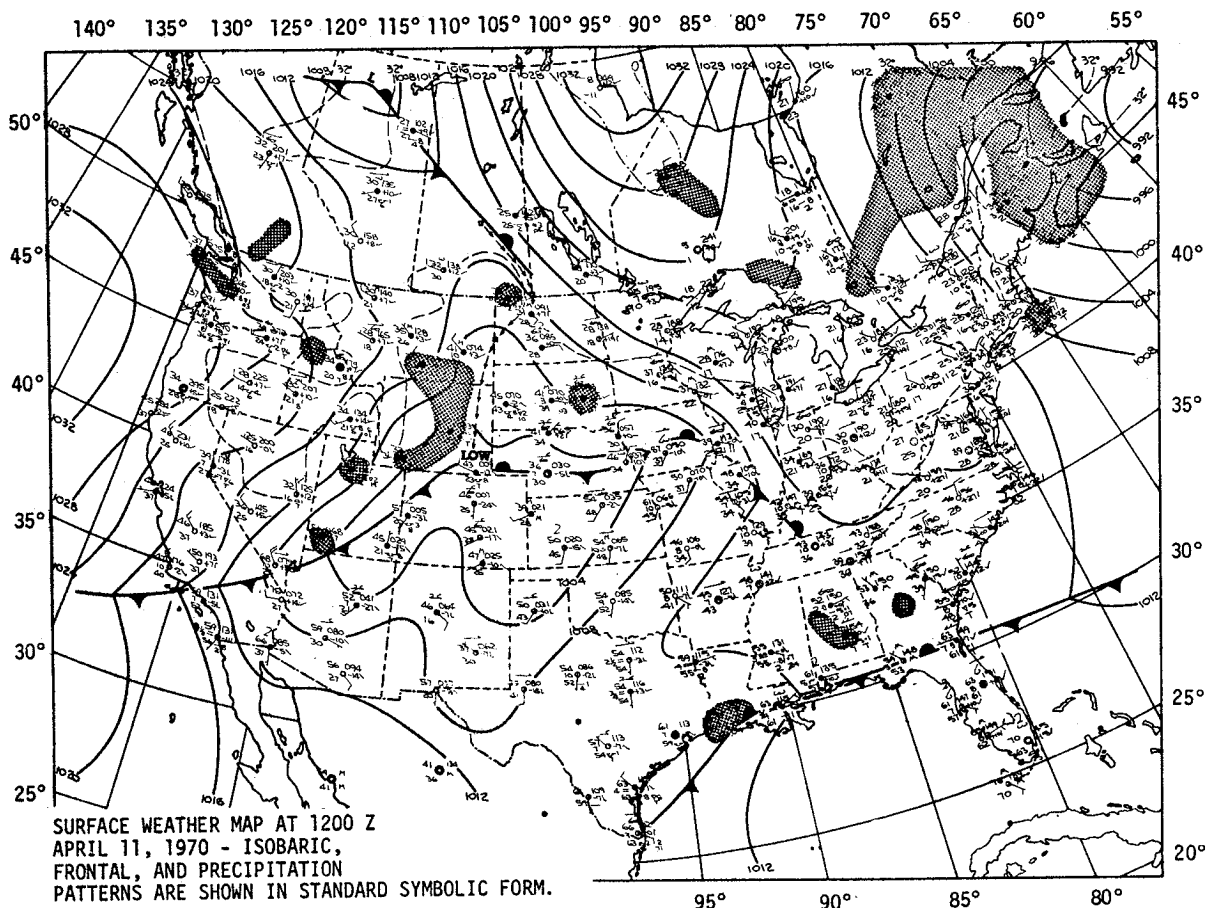
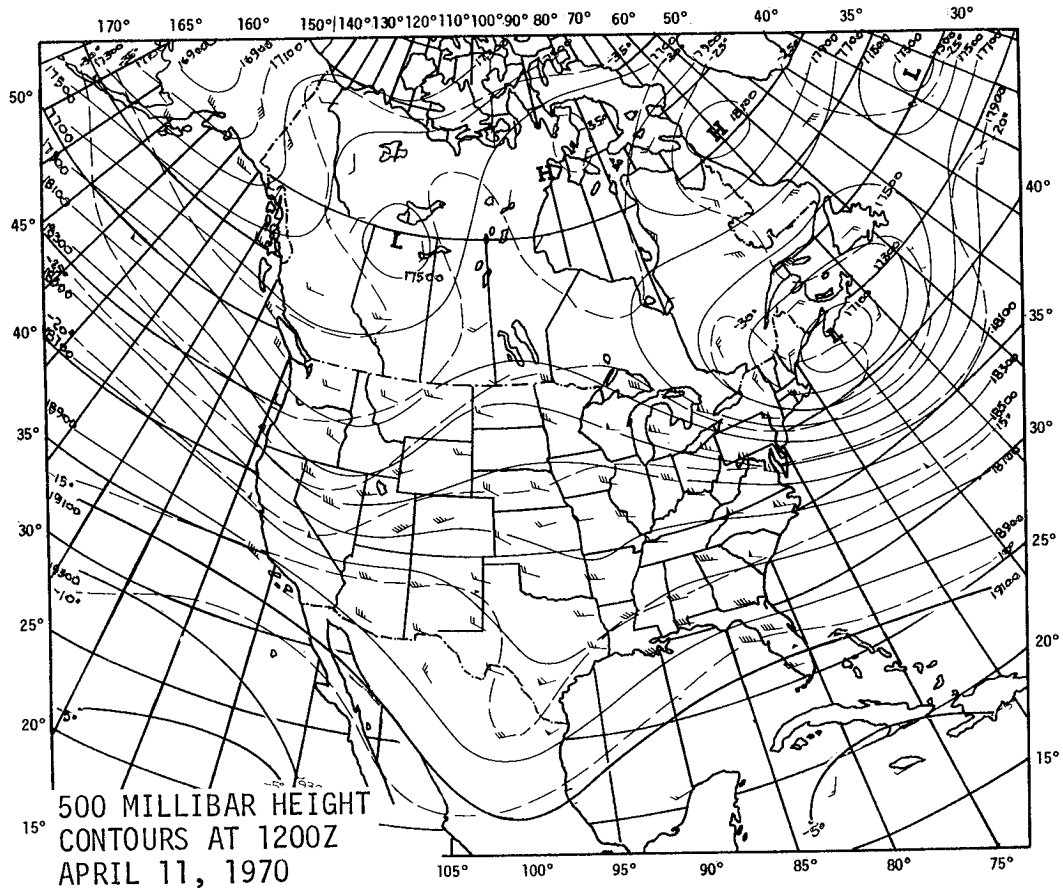


Figure A-1. Surface Weather Map Approximately 7 Hours Before Launch of AS-508

Table A-1. Surface Observations at AS-508 Launch Time

LOCATION	TIME AFTER T-0 (MIN)	PRES-SURE N/CM <sup>2</sup> (PSIA)	TEM-PERATURE °K (°F)	DEW POINT °K (°F)	VISI-BILITY KM (STAT MI)	AMOUNT (TENTHS)	SKY COVER TYPE	HEIGHT OF BASE METERS (FEET)	WIND	
									SPEED M/S (KNOTS)	DIR (DEG)
MILA (SSB) Kennedy Space Center, Florida	0	10.119 (14.68)	297.6 (76.0)	288.7 (60.0)	16 (10)	4	Alto-cumulus	5790 (19,000)	1.5 (3.0)	130
							Cirro-stratus	7925+ (26,000)+		
Cape Kennedy Rawinsonde Measurements	10	10.115 (14.67)	295.5 (72.1)	290.5 (63.3)	--	--	--	--	4.0 (7.8)	080
Pad 39A Lightpole SE 18.3 m (60.0 ft)*	0	--	--	--	--	--	--	--	6.3 (12.2)	105

\*Above natural grade.  
†Estimated.



CONTINUOUS LINES INDICATE HEIGHT CONTOURS IN FEET ABOVE SEA LEVEL.

DASHED LINES ARE ISOTHERMS IN DEGREES CENTIGRADE.

ARROWS SHOW WIND DIRECTION AND SPEED AT THE 500 MILLIBAR LEVEL.  
(ARROWS SAME AS ON SURFACE MAP).

Figure A-2. 500 Millibar Map Approximately 7 Hours  
Before Launch of AS-508

#### A.4.1 Wind Speed

The wind speed was 4.0 m/s (7.8 knots) at the surface, and increased to a peak of 55.6 m/s (108.1 knots) at 13.58 kilometers (44,540 ft). The winds began decreasing above this altitude, reaching a minimum of 1.0 m/s (1.9 knots) at 26.60 kilometers (87,270 ft) altitude. Above this altitude the wind speed continued to increase, as shown in Figure A-3.

Table A-2. Solar Radiation at AS-508 Launch Time, Launch Pad 39A

DATE	HOUR ENDING EST	TOTAL HORIZONTAL G-CAL/CM <sup>2</sup> MIN	NORMAL INCIDENT G-CAL/CM <sup>2</sup> MIN	DIFFUSE SKY G-CAL/CM <sup>2</sup> MIN
April 11, 1970	0500	0.00	0.00	0.00
	0600	0.00	0.00	0.00
	0700	0.02	0.01	0.02
	0800	0.14	0.03	0.13
	0900	0.21	0.00	0.21
	1000	0.51	0.21	0.36
	1100	1.01	0.85	0.30
	1200	1.20	0.91	0.37
	1300	1.25	0.71	0.59
	1400	0.85	0.27	0.61
	1500	0.63	0.20	0.47
	1600	0.52	0.15	0.42
	1700	0.42	0.23	0.31

Table A-3. Systems Used to Measure Upper Air Wind Data for AS-508

TYPE OF DATA	RELEASE TIME		PORTION OF DATA USED			
	TIME (UT)	TIME AFTER T-0 (MIN)	START		END	
			ALTITUDE M (FT)	TIME AFTER T-0 (MIN)	ALTITUDE M (FT)	TIME AFTER T-0 (MIN)
FPS-16 Jimsphere	1930	17	0	17	15,225 (49,950)	69
Rawinsonde	1923	10	15,250 (50,032)	60	24,750 (81,200)	91
Loki Dart	2058	105	61,750 (202,589)	105	25,000 (82,020)	131
Super Loki	2143	150	80,500 (264,104)	152	62,000 (203,410)	170

5

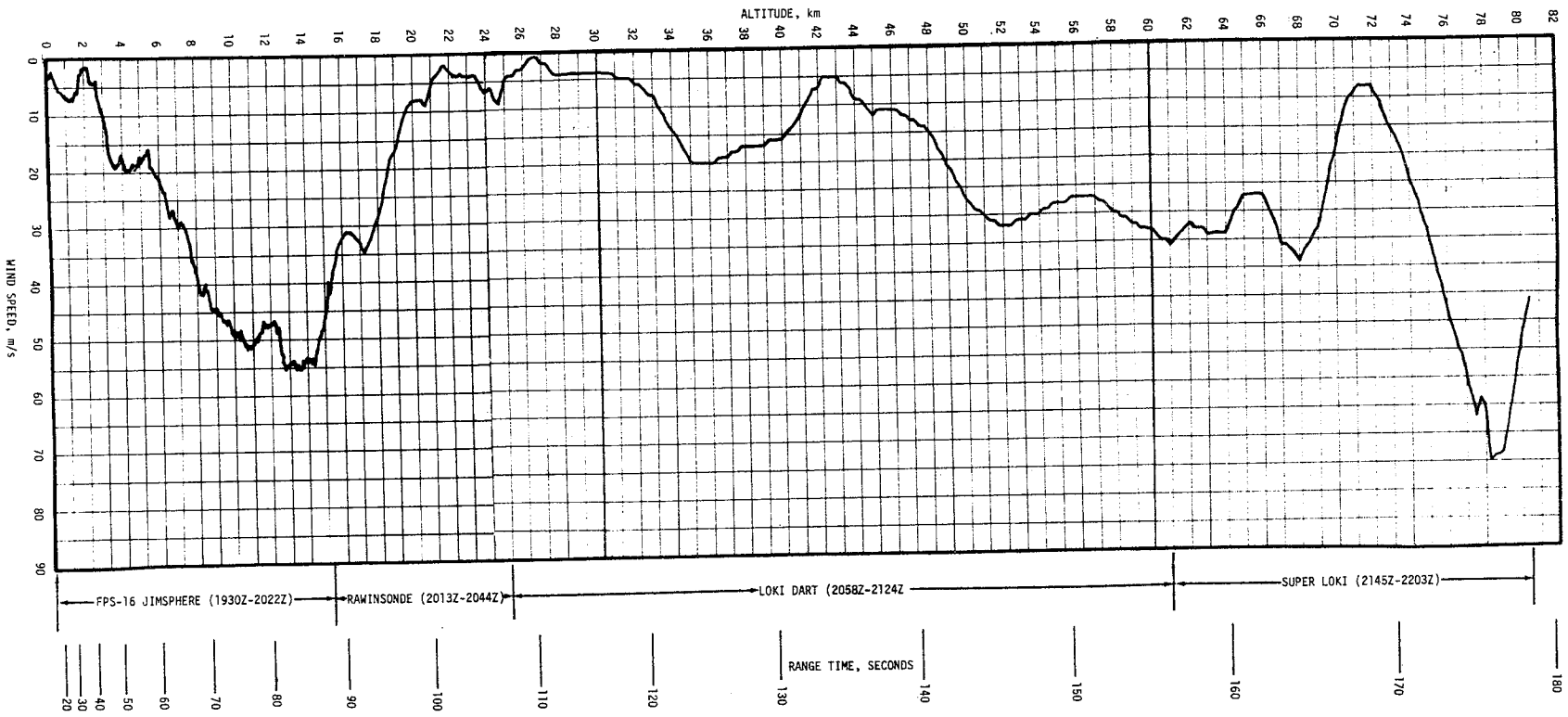


Figure A-3. Scalar Wind Speed at Launch Time of AS-508

#### A.4.2 Wind Direction

At launch time the surface wind direction was easterly and shifted clockwise to a westerly direction within the first 3 kilometers (9840 ft) of altitude. The wind direction stayed westerly with increasing altitude until the wind speed became light and variable above 18 kilometers (59,050 ft). Figure A-4 shows a complete wind direction versus altitude profile.

#### A.4.3 Pitch Wind Component

The pitch wind velocity component (component parallel to the horizontal projection of the flight path) at the surface was a head wind of 3.9 m/s (7.6 knots). The pitch component became a tail wind with altitude, resulting in a maximum tail wind of 55.6 m/s (108.1 knots) observed at 13.58 kilometers (44,540 ft) altitude. See Figure A-5.

#### A.4.4 Yaw Wind Component

The yaw wind velocity component (component normal to the horizontal projection of the flight path) at the surface was a wind from the left of 0.8 m/s (1.6 knots). The peak yaw wind velocity in the high dynamic pressure region was a wind from the left of 15.0 m/s (29.1 knots) at 12.98 kilometers (42,570 ft). See Figure A-6.

#### A.4.5 Component Wind Shears

The largest component wind shear ( $\Delta h = 1000$  m) in the altitude range of 8 to 16 kilometers (26,247 to 52,493 ft) was a yaw shear of  $0.0178 \text{ sec}^{-1}$  at 14.0 kilometers (45,850 ft). The largest pitch wind shear, in the lower levels, was  $0.0166 \text{ sec}^{-1}$  at 15.4 kilometers (50,610 ft). See Figure A-7.

#### A.4.6 Extreme Wind Data in the High Dynamic Region

A summary of the maximum wind speeds and wind components is given in Table A-4. A summary of the extreme wind shear values is given in Table A-5.

### A.5 THERMODYNAMIC DATA

Comparisons of the thermodynamic data taken at AS-508 launch time with the annual Patrick Reference Atmosphere, 1963 (PRA-63) for temperature, pressure, density, and Optical Index of Refraction are shown in Figures A-8 and A-9 and discussed in the following paragraphs.

#### A.5.1 Temperature

Atmospheric temperature differences were small, being 5 percent or less deviation from the PRA-63. Surface air temperature was slightly cooler than the PRA-63. Above 23.0 kilometers (75,460 ft) the temperature was warmer than the PRA-63. See Figure A-8.

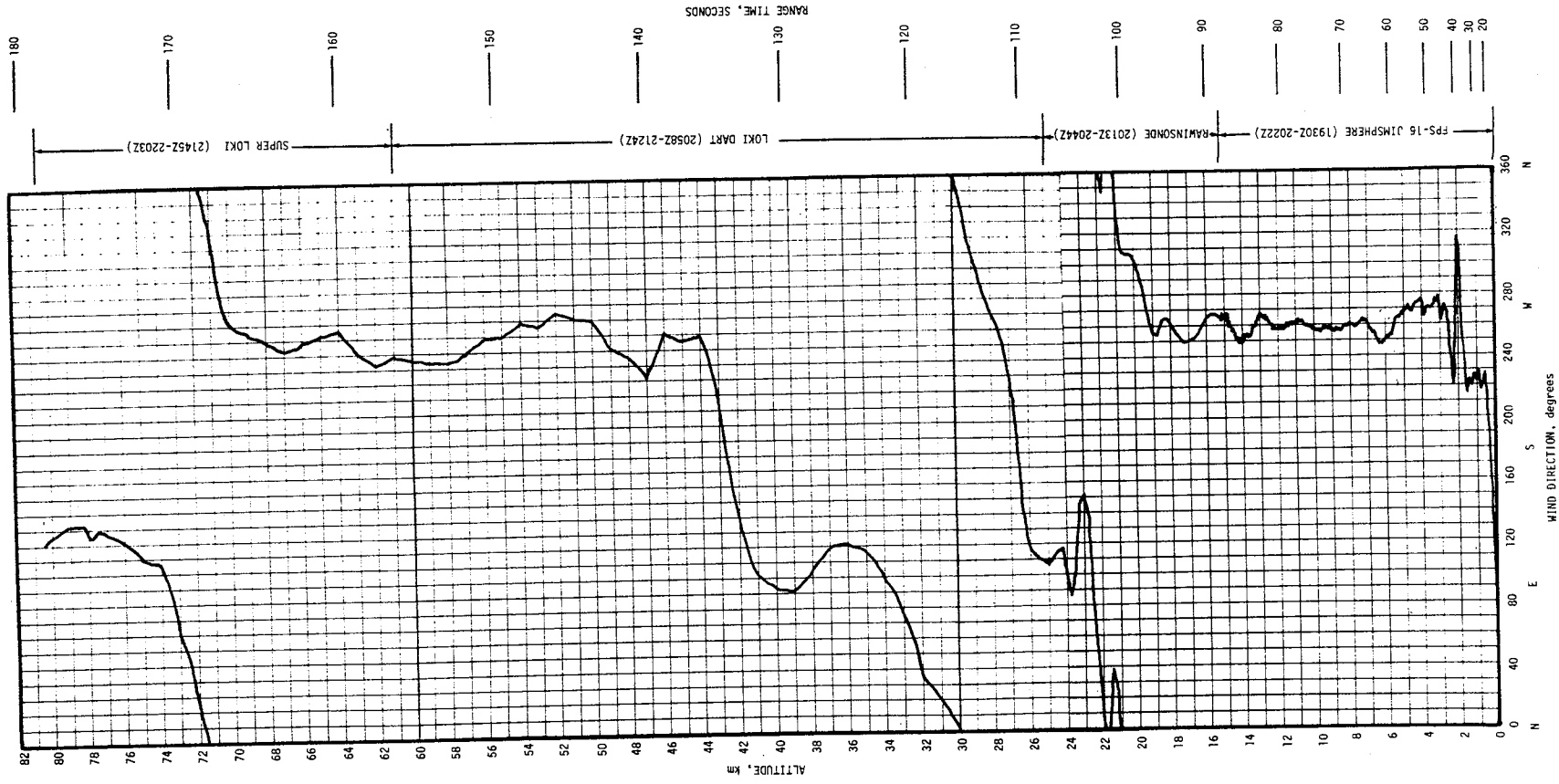


Figure A-4. Wind Direction at Launch Time of AS-508

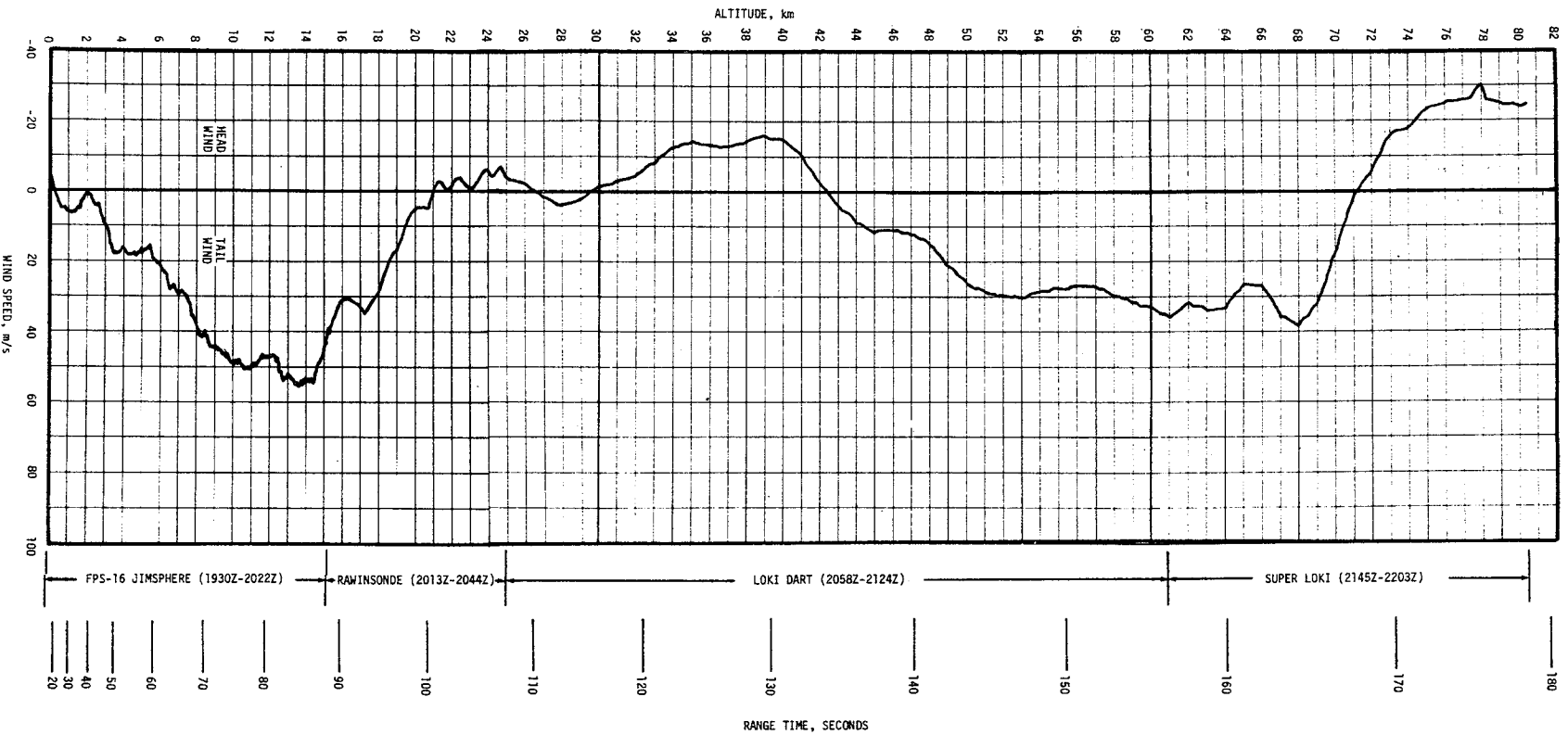


Figure A-5. Pitch Wind Velocity Component ( $W_x$ ) at Launch Time of AS-508

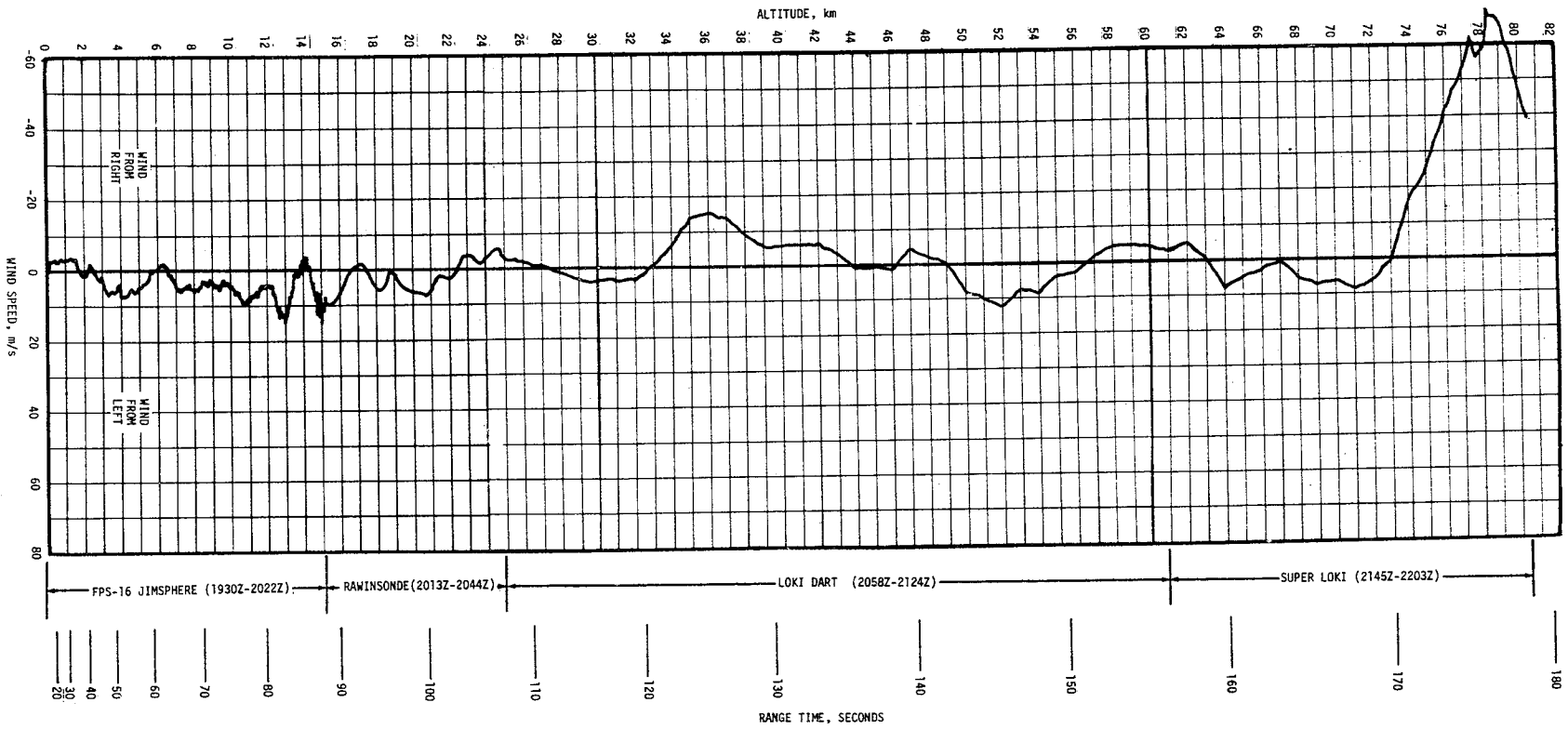


Figure A-6. Yaw Wind Velocity Component ( $W_z$ ) at Launch Time of AS-508

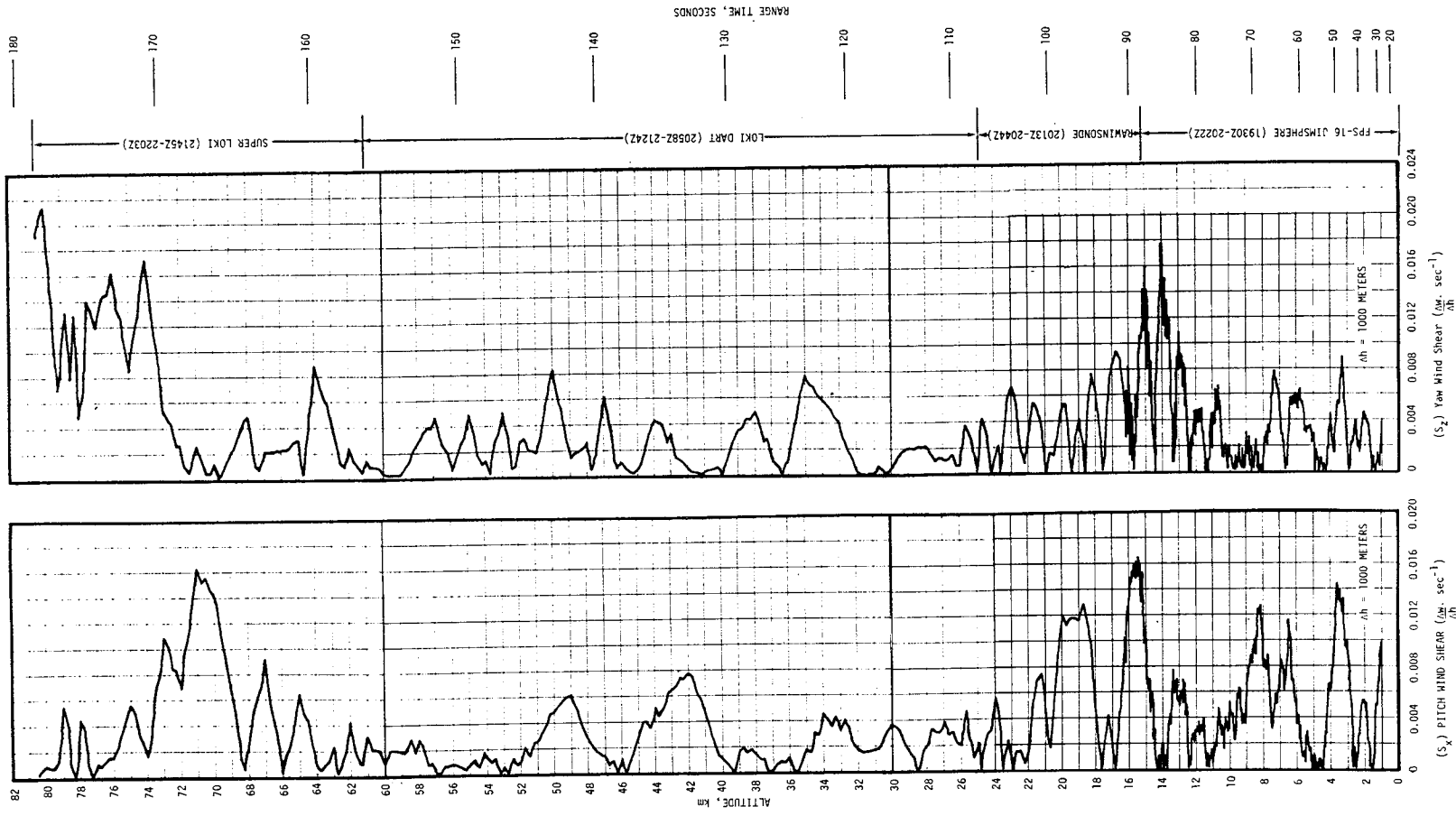


Figure A-7. Pitch ( $S_x$ ) and Yaw ( $S_z$ ) Component Wind Shears at Launch Time of AS-508

Table A-4. Maximum Wind Speed in High Dynamic Pressure Region for Apollo/Saturn 501 through Apollo/Saturn 508 Vehicles

VEHICLE NUMBER	MAXIMUM WIND			MAXIMUM WIND COMPONENTS			
	SPEED M/S (KNOTS)	DIR (DEG)	ALT KM (FT)	PITCH ( $W_x$ ) M/S (KNOTS)	ALT KM (FT)	YAW ( $W_z$ ) M/S (KNOTS)	ALT KM (FT)
AS-501	26.0 (50.5)	273	11.50 (37,700)	24.3 (47.2)	11.50 (37,700)	12.9 (25.1)	9.00 (29,500)
AS-502	27.1 (52.7)	255	12.00 (42,600)	27.1 (52.7)	12.00 (42,600)	12.9 (25.1)	15.75 (51,700)
AS-503	34.8 (67.6)	284	15.22 (49,900)	31.2 (60.6)	15.10 (49,500)	22.6 (43.9)	15.80 (51,800)
AS-504	76.2 (148.1)	264	11.73 (38,480)	74.5 (144.8)	11.70 (38,390)	21.7 (42.2)	11.43 (37,500)
AS-505	42.5 (82.6)	270	14.18 (46,520)	40.8 (79.3)	13.80 (45,280)	18.7 (36.3)	14.85 (48,720)
AS-506	9.6 (18.7)	297	11.40 (37,400)	7.6 (14.8)	11.18 (36,680)	7.1 (13.8)	12.05 (39,530)
AS-507	47.6 (92.5)	245	14.23 (46,670)	47.2 (91.7)	14.23 (46,670)	19.5 (37.9)	13.65 (44,780)
AS-508	55.6 (108.1)	252	13.58 (44,540)	55.6 (108.1)	13.58 (44,540)	15.0 (29.1)	12.98 (42,570)

Table A-5. Extreme Wind Shear Values in the High Dynamic Pressure Region for Apollo/Saturn 501 through Apollo/Saturn 508 Vehicles

( $\Delta h = 1000 \text{ m}$ )				
VEHICLE NUMBER	PITCH PLANE		YAW PLANE	
	SHEAR (SEC <sup>-1</sup> )	ALTITUDE KM (FT)	SHEAR (SEC <sup>-1</sup> )	ALTITUDE KM (FT)
AS-501	0.0066	10.00 (32,800)	0.0067	10.00 (32,800)
AS-502	0.0125	14.90 (48,900)	0.0084	13.28 (43,500)
AS-503	0.0103	16.00 (52,500)	0.0157	15.78 (51,800)
AS-504	0.0248	15.15 (49,700)	0.0254	14.68 (48,160)
AS-505	0.0203	15.30 (50,200)	0.0125	15.53 (50,950)
AS-506	0.0077	14.78 (48,490)	0.0056	10.30 (33,790)
AS-507	0.0183	14.25 (46,750)	0.0178	14.58 (47,820)
AS-508	0.0166	15.43 (50,610)	0.0178	13.98 (45,850)

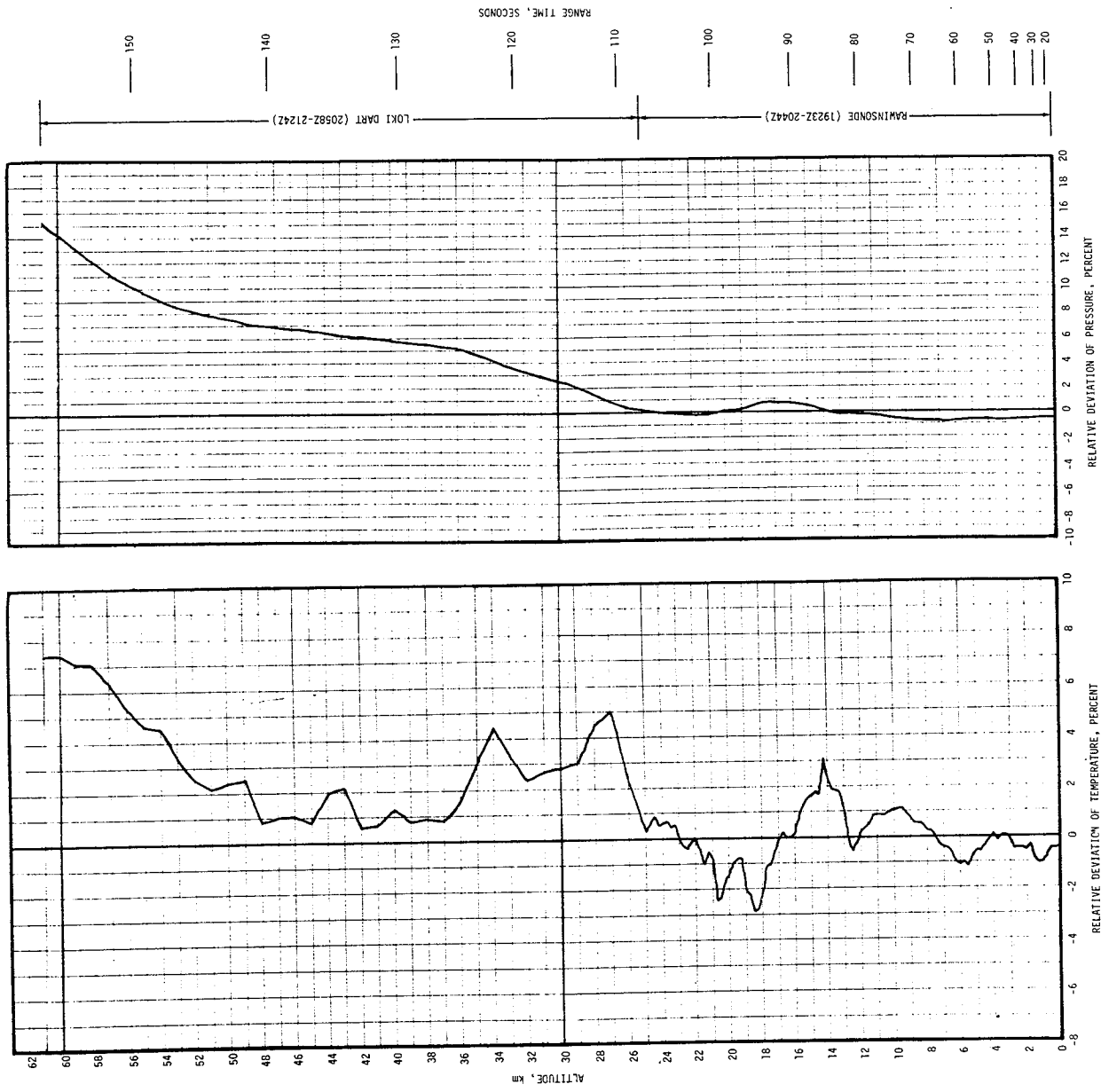


Figure A-8. Relative Deviation of Temperature and Pressure  
From the PRA-63 Reference Atmosphere, AS-508

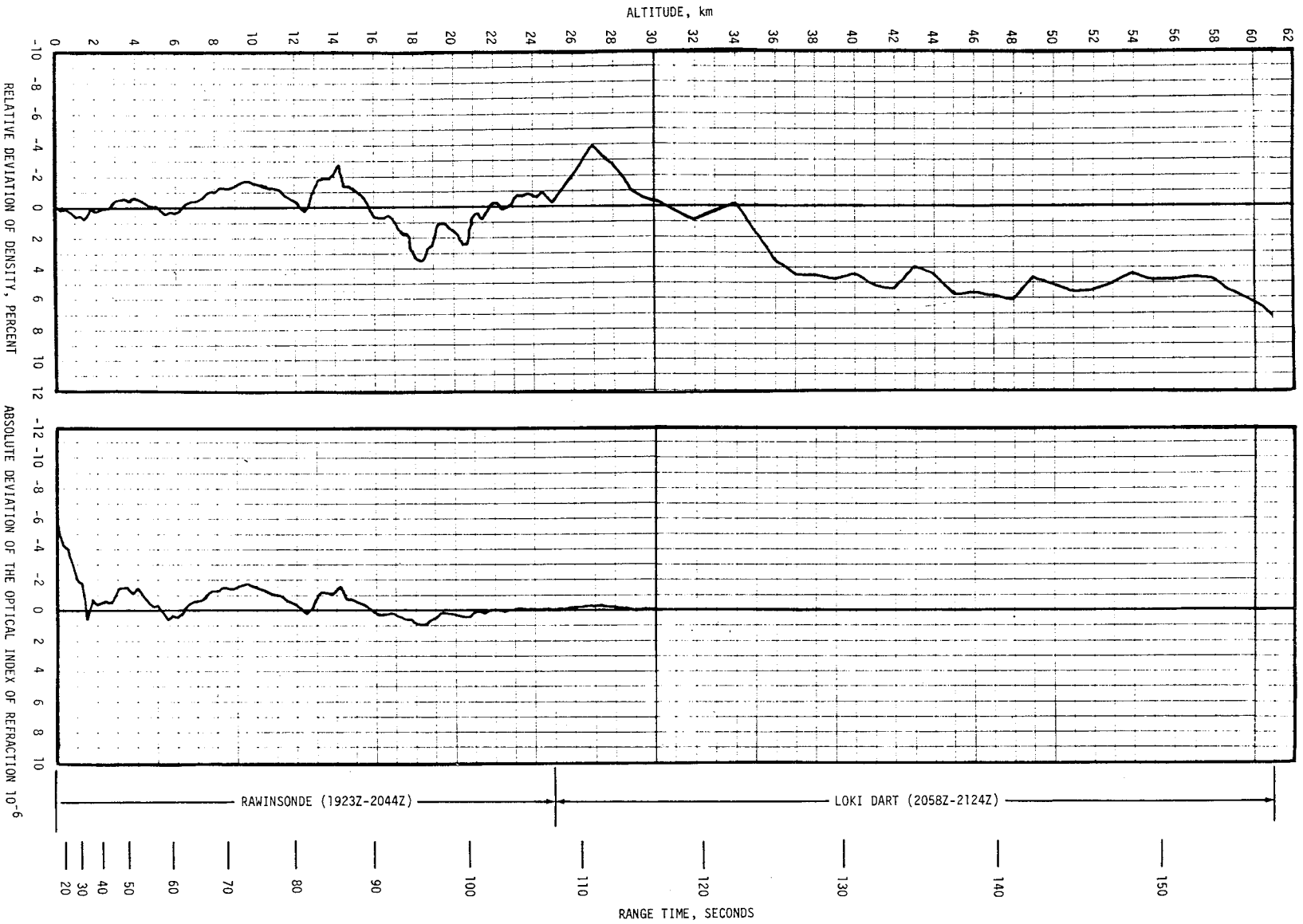


Figure A-9. Relative Deviation of Density and Absolute Deviation of the Index of Refraction From the PRA-63 Reference Atmosphere, AS-508

## A.5.2 Atmospheric Pressure

Atmospheric pressure deviations were less than one percent from the PRA-63 pressure values from the surface to 27.2 kilometers (89,160 ft) altitude. The pressure then became greater than +1 percent of the PRA-63 values with altitude, as shown in Figure A-8.

## A.5.3 Atmospheric Density

Atmospheric density deviations were small, being within 8 percent of the PRA-63 for all altitudes. See Figure A-9.

## A.5.4 Optical Index of Refraction

At the surface, the Optical Index of Refraction was  $5.65 \times 10^{-6}$  units lower than the corresponding value of the PRA-63. The deviation became less negative with altitude, and it approximates the PRA-63 at high altitudes as is shown in Figure A-9.

## A.6 COMPARISON OF SELECTED ATMOSPHERIC DATA FOR SATURN V LAUNCHES

A summary of the atmospheric data for each Saturn V launch is shown in Table A-6.

Table A-6. Selected Atmospheric Observations for Apollo/Saturn 501 through Apollo/Saturn 508 Vehicle Launches at Kennedy Space Center, Florida

VEHICLE NUMBER	VEHICLE DATA			SURFACE DATA						INFLIGHT CONDITIONS		
	DATE	TIME NEAREST MINUTE	LAUNCH COMPLEX	PRESSURE N/CM <sup>2</sup>	TEMPERATURE °C	RELATIVE HUMIDITY PERCENT	WIND*		CLOUDS	ALTITUDE KM	SPEED M/S	DIRECTION DEG
AS-501	9 Nov 67	0700 EST	39A	10.261	17.6	55	8.0	70	1/10 cumulus	11.50	26.0	273
AS-502	4 Apr 68	0700 EST	39A	10.200	20.9	83	5.4	132	5/10 stratocumulus, 1/10 cirrus	13.00	27.1	255
AS-503	21 Dec 68	0751 EST	39A	10.207	15.0	88	1.0	360	4/10 cirrus	15.22	34.8	284
AS-504	3 Mar 69	1100 EST	39A	10.095	19.6	61	6.9	160	7/10 stratocumulus, 10/10 altostratus	11.73	76.2	264
AS-505	18 May 69	1249 EDT	39B	10.190	26.7	75	8.2	125	4/10 cumulus, 2/10 altocumulus, 10/10 cirrus	14.18	42.5	270
AS-506	16 Jul 69	0932 EDT	39A	10.203	29.4	73	3.3	175	1/10 cumulus, 2/10 altocumulus, 9/10 cirrostratus	11.40	9.6	297
AS-507	14 Nov 69	1122 EST	39A	10.081	20.0	92	6.8	280	10/10 stratocumulus with rain	14.23	47.6	245
AS-508	11 Apr 70	1413 EST	39A	10.119	24.4	57	6.3	105	4/10 altocumulus 10/10 cirrostratus	13.58	55.6	252

\*Instantaneous readings from charts at T-0 from anemometers on launch pad at 18.3 m (60.0 ft) on launch complex 39 (A&B). Heights of anemometers are above natural grade.



## APPENDIX B

### AS-508 SIGNIFICANT CONFIGURATION CHANGES

#### B.1 INTRODUCTION

AS-508, eighth flight of the Saturn V series, was the sixth manned Apollo Saturn V vehicle. The AS-508 launch vehicle configuration was essentially the same as the AS-507 with significant exceptions shown in Tables B-1 through B-4. The basic AS-508 Apollo 13 spacecraft structure and components were unchanged from the AS-504 Apollo 9 configuration except Lunar Module (LM) crew provisions were accompanied by portable life support systems and associated controls required to accommodate extra vehicular surface activity, similar to AS-507, Apollo 12. The basic vehicle description is presented in Appendix B of the Saturn V Launch Vehicle Flight Evaluation Report, AS-504, Apollo 9 Mission, MPR-SAT-FE-69-4.

Table B-1. S-IC Significant Configuration Changes

SYSTEM	CHANGE	REASON
Propulsion	Engine No. 4 gas generator incorporates high $\Delta p$ LOX injector.	This type injector inhibits unstable combustion pressure oscillations (buzzing).
	Servoactuators redesigned to eliminate materials susceptible to stress corrosion.	Eliminate stress corrosion.
Environmental Control System	Aft compartment ECS reorificed.	To meet required temperatures at battery location
Data	Servoactuator return pressure and temperature measurements deleted.	R&D instrumentation which is no longer required.
GSE	Modified LOX dome purge and GN <sub>2</sub> primary regulation modules of pneumatic console.	Eliminate single point failures.
	Redesigned LOX dome purge regulator and added orifices to LOX dome purge module in pneumatic console.	Prevent sense tube failures and poppet deformation.

Table B-2. S-II Significant Configuration Changes

SYSTEM	CHANGE	REASON
Structure	Conversion to a flame retardant spray-on polyurethane foam insulation on LH <sub>2</sub> tank forward bulkhead, forward skirt, and LH <sub>2</sub> tank sidewall areas.	To reduce manufacturing costs, effect stage weight savings, improve insulation efficiency, and eliminate prelaunch helium purging and leak detection of these circuits.
	Redesign of LH <sub>2</sub> tank outlet feedline elbows using 2014-T6 aluminum alloy rings with 6061-T6 tube assemblies. These materials were machine welded together and welded onto the LH <sub>2</sub> tank lower cylinder.	To overcome previous stage problems with lap welds resulting in cracks and potential leak conditions.
Launch Vehicle Ground Support Equipment (LVGSE)	Deletion of prelaunch stage leak detection function for propellant tank common bulkhead, LH <sub>2</sub> tank forward bulkhead uninsulated area, and the tank J-ring area. Gas purging capability will be retained.	To eliminate the LVGSE leak detection equipment as a result of high confidence level in stage structural integrity. The remaining leak detection functions were eliminated by the above change to spray-on foam insulation.

Table B-3. S-IVB Significant Configuration Changes

SYSTEM	CHANGE	REASON
Propulsion	Installation of redundant cold helium shutoff valves to the LOX tank pressurization system.	To improve reliability and mission confidence by eliminating single point failure in the LOX pressurization system.
	Provided a backup helium supply to the J-2 engine start tank.	To make helium available from the LOX ambient repressurization sphere for the J-2 engine start tank in the event of start tank depletion during coast, and provide preprogramed recharge sequence for same.
	LH <sub>2</sub> prepressurization module orifice modifications.	Provides assurance of mission completion in the event the continuous vent regulator fails open and eliminates single point failure involving the regulator.
	Auxiliary Propulsion System forebody thermal isolation insulation	To maintain acceptable temperature limits of the Auxiliary Propulsion System forebody mounted components when flight mission time is increased for Lunar Impact Mission.
Electrical	Thermal protection of electrical components for Lunar Impact Mission.	To increase operating time for Lunar Impact Mission
	Added one event - Start Tank Recharge Valve Arm On K200-404.	To provide talkback on operation of start tank recharge backup system.

Table B-4. IU Significant Configuration Changes

SYSTEM	CHANGE	REASON
Emergency Detection	Modification of the EDS distributor. Automatic Abort Enable Backup to the Spacecraft Manual Abort Enable is provided for abort conditions prior to Time Base 7.	To provide ground control after spacecraft separation. This insures the ability to command from the ground.
Command and Communications	Changed Fail Safe position of CCS Coaxial Switch to the Omni Antenna from the Hi-Gain Antenna.	To allow tracking of the CCS to lunar impact.
Environmental Control	<p>Thermal radiation shrouds over cable trays and down inside of the IU over the components.</p> <p>Removal of thermal isolators between cold plate No. 24 and the IU structure. The cork outside the IU, in the area of cold plate No. 24, has been painted white.</p> <p>Thermal switch settings for S-IU-508 Environmental Control System (ECS) determine water valve operation:  Open at 59.2°F  Close at 60.0°F</p> <p>CCS components and 6D20 battery all on cold plate No. 24.</p> <p>Tape added to RTG.</p>	<p>To protect the cables, CCS, and other heat sensitive equipment from the direct solar radiation in space during Translunar Coast after spacecraft separation.</p> <p>To improve the heat flow from the cold plate to the IU structure especially for operation after loss of coolant flow during translunar coast. The white paint is to decrease the effect of external solar heating and heat loss to space when in shadow.</p> <p>Switch settings were determined from preflight test data.</p> <p>To help provide heat balance for the battery which will act as a heat sink for the CCS power amplifier.</p> <p>To increase radiative heat control especially after spacecraft separation.</p>
Instrumentation and Communications	<p>Note: CCS change and networks addition of fourth battery.</p> <p>Three platform vibration measurements were added to the DF1 telemetry link:  E7-603 VIB ST-124M SUPPORT, LONG  E8-603 VIB ST-124M SUPPORT, TANG  E9-603 VIB ST-124M SUPPORT, PERP</p> <p>Three platform accelerometer measurements were deleted from the DF1 telemetry link:  H17-603 Z ACCELEROMETER  H21-603 X ACCELEROMETER  H25-603 Y ACCELEROMETER</p>	<p>To allow tracking of the CCS to Lunar Impact.</p> <p>To measure low frequency vibrations transmitted to the platform support from the IU structure.</p> <p>To allow addition of the three vibration measurements on this telemetry link.</p>
Networks	<p>Add fourth battery 6D20. (See Instrumentation and Communications.)</p> <p>Cable modifications and additions.</p>	<p>To provide an independent power source for the CCS power amplifier and CCS transponder. This will add a nominal 84.8-hour operation capability for the CCS.</p> <p>In support of EDS, CCS changes, and additional vibration measurements on the ST-124M support.</p>

Table B-4. IU Significant Configuration Changes (Continued)

SYSTEM	CHANGE	REASON
Flight Program	<p>Accelerometer processing - Reasonableness test constants are changed at liftoff +10 seconds and are independent for each axis.</p> <p>The Evasive Maneuver Yaw Attitude is 40 degrees and signed opposite from yaw attitude during TD&amp;E.</p> <p>Lunar impact requirements -</p> <p>TLC orbital routines initialized at T<sub>7</sub> +150.9 seconds rather than T<sub>7</sub> +20 seconds.</p> <p>State vector is stored and the measured velocity components are zeroed at T<sub>7</sub> +150.9 seconds.</p> <p>Inertial hold attitude is maintained until T<sub>7</sub> +150.9 seconds when horizontal hold begins.</p> <p>Measured velocity component telemetry is continued after T<sub>7</sub> +150.9 seconds.</p> <p>DCS command for a second APS ullage burn has been added and includes variables for burn start time, burn duration, and attitude change before the burn.</p> <p>The Communications Maneuver and TD&amp;E Inhibit and Update Commands from T<sub>8</sub> have been deleted.</p>	<p>This change limits the maximum effect of possible accelerometer head contact with the mechanical stop.</p> <p>To guarantee at least a 40 degree angle of separation and increase the distance between the SC and S-IVB/IU.</p> <p>These changes increase the probability of lunar impact.</p>

APPROVAL

SATURN V LAUNCH VEHICLE FLIGHT EVALUATION REPORT  
AS-508, APOLLO 13 MISSION

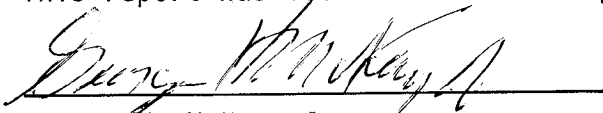
By Saturn Flight Evaluation Working Group

The information in this report has been reviewed for security classification. Review of any information concerning Department of Defense or Atomic Energy Commission programs has been made by the MSFC Security Classification Officer. The highest classification has been determined to be unclassified.



Stanley L. Fragge  
Security Classification Officer

This report has been reviewed and approved for technical accuracy.



George H. McKay, Jr.  
Chairman, Saturn Flight Evaluation Working Group



Herman K. Weidner  
Director, Science and Engineering



Roy E. Godfrey  
Saturn Program Manager

DISTRIBUTION:

MSFC:

Dr. E. Rees, DIR  
 Mr. J. Foster, DIR  
 Mr. R. Cook, DEP-M  
 Dr. E. Stuhlinger, AD-S

E

Mr. Maus, E-DIR  
 Mr. Smith, E-S

PA

Mr. B. Slattery, PA-DIR

PD

Dr. W. Lucas, PD-DIR  
 Mr. W. Mrazek, PD-DIR  
 Mr. E. Goerner, PD-DO-DIR  
 Mr. F. Digesu, PD-DO-E

PM

Mr. L. James, PM-DIR  
 Mr. C. Andressen, PM-PR-MGR  
 Dr. F. Speer, PM-MO-MGR  
 Mr. L. Belew, PM-AA-MGR  
 Mr. W. Brown, PM-EP-MGR  
 Mr. T. Smith, PM-EP-J  
 Mr. Norman, PM-MO  
 Mr. Boffola, PM-EP-F  
 Mr. R. Godfrey, PM-SAT-MGR  
 Mr. R. Smith, PM-SAT-MGR  
 Col. B. Montgomery, PM-SAT-MGR  
 Mr. L. Bell, PM-SAT-E  
 Mr. J. Moody, PM-SAT-Q  
 Mr. H. Hughes, PM-SAT-P  
 Mr. M. Urlaub, PM-SAT-S-IB/S-IC  
 Mr. W. Lahatte, PM-SAT-S-II  
 Mr. C. Meyers, PM-SAT-S-IVB  
 Mr. F. Duerr, PM-SAT-IU  
 Mr. R. Sparks, PM-SAT-G  
 Mr. G. Peters, PM-SAT-S-IVB  
 Mr. T. Ferrell, PM-EP-EJ  
 Mr. J. Stamy, PM-MA-MGR  
 Mr. Riemer, PM-MA-QP  
 Mr. J. Balch, PM-MT-MGR  
 Mr. H. Auter, PM-MT-T  
 Mr. C. Blevins, PM-SAT-S-IB/S-IC  
 Mr. A. Higgins, PM-SAT-S-IVB  
 Mr. C. Stover, PM-SAT-S-II  
 Mr. J. Reaves, PM-SAT-Q  
 Mr. A. Wheeler, PM-EP-F  
 Mr. W. Cushman, PM-SAT-T  
 Mr. M. Marchese, PM-MA-QR

S&E

Mr. H. Weidner, S&E-DIR  
 Mr. L. Richard, S&E-DIR  
 Dr. W. Johnson, S&E-R-DIR  
 Mr. G. McDonough, S&E-DIR

S&E-AERO

Dr. E. Geissler, S&E-AERO-DIR  
 Mr. W. Dahm, S&E-AERO-A  
 Mr. B. Dunn, S&E-AERO-ADV  
 Mr. R. Elkin, S&E-AERO-A1  
 Mr. H. Wilson, S&E-AERO-AT  
 Mr. I. Jones, S&E-AERO-AT  
 Mr. T. Reed, S&E-AERO-AU  
 Mr. S. Guest, S&E-AERO-AU (2)  
 Mr. R. Ryan, S&E-AERO-D  
 Mr. J. Cremin, S&E-AERO-MO (2)  
 Mr. J. Lindberg, S&E-AERO-M (10)  
 Mr. R. Jackson, S&E-AERO-P  
 Mr. R. Cummings, S&E-AERO-T  
 Mr. O. E. Smith, S&E-AERO-Y  
 Mr. J. Sims, S&E-AERO-P  
 Dr. J. Lovingood, S&E-AERO-D  
 Mr. W. Vaughan, S&E-AERO-Y (2)

S&E-CSE

Dr. W. Haeussermann, S&E-CSE-DIR  
 Mr. O. Hoberg, S&E-CSE-DIR  
 Mr. J. Aberg, S&E-CSE-S  
 Mr. W. Vann, S&E-CSE-A  
 Mr. R. Wolf, S&E-CSE-I  
 Mr. E. May, S&E-CSE-L  
 Mr. G. McKay, S&E-CSE-LF  
 Mr. C. Brooks, S&E-CSE-V  
 Mr. C. Hagood, S&E-CSE-A  
 Mr. R. Devenish, S&E-CSE-SC

S&E-ASTR

Mr. Stroud, S&E-ASTR-SC  
 Mr. Robinson, S&E-P-ATM (4487)  
 Mr. Dale, S&E-ASTR-SCC  
 Mr. S. Erickson, S&E-ASTR-SE  
 Mr. J. Darden, S&E-ASTR-SD  
 Mr. D. Justice, S&E-ASTR-SDA  
 Mr. D. Vallely, S&E-ASTR-SDC  
 Mr. E. George, S&E-ASTR-SDI  
 Mr. C. Jones, S&E-ASTR-SI  
 Mr. C. Mandel, S&E-ASTR-G  
 Mr. G. Ferrell, S&E-ASTR-GSQ  
 Mr. O. Duggan, S&E-ASTR-I  
 Mr. J. Boehm, S&E-ASTR-M  
 Mr. J. Lominick, S&E-ASTR-GMF  
 Mr. J. Taylor, S&E-ASTR-R  
 Mr. F. Wojtalik, S&E-ASTR-S

S&E COMP

Mr. W. Fortenberry, S&E-COMP-A  
 Mr. R. Cochran, S&E-COMP-R  
 Mr. R. Craft, S&E-COMP-RR

S&E-ME

Dr. M. Sievel, S&E-ME-DIR  
 Mr. H. Wuenschel, S&E-ME-DIR

S&E-ASTN

Mr. K. Heimburg, S&E-ASTN-DIR  
 Mr. E. Hellebrand, S&E-ASTN-DIR  
 Mr. R. Schwinghamer, S&E-ASTN-M  
 Mr. J. Earle, S&E-ASTN-SDD  
 Mr. K. Reilmann, S&E-ASTN-PJ  
 Mr. H. Fuhrmann, S&E-ASTN-EM  
 Mr. W. Cobb, S&E-ASTN-SA  
 Mr. P. Black, S&E-ASTN-SAS  
 Mr. C. Wood, S&E-ASTN-P  
 Mr. R. Hunt, S&E-ASTN-A  
 Mr. J. Riquelmy, S&E-ASTN-SDF  
 Mr. Katz, S&E-ASTN-SER  
 Mr. N. Showers, S&E-ASTN-A  
 Mr. J. Furman, S&E-ASTN-AA  
 Mrs. L. Mowell, S&E-ASTN-ADD  
 Mr. W. Grafton, S&E-ASTN-T  
 Mr. R. Lutonsky, S&E-ASTN-SAE  
 Mr. H. Sells, S&E-ASTN-SO  
 Mr. K. Rothe, S&E-ASTN-E  
 Mr. R. Griner, S&E-ASTN-XSJ (2)

S&E-QUAL

Mr. D. Grau, S&E-QUAL-DIR  
 Mr. H. Rushing, S&E-QUAL-PJ  
 Mr. P. Hughes, S&E-QUAL-P  
 Mr. J. Landers, S&E-QUAL-PC  
 Mr. S. Peck, S&E-QUAL-F  
 Mr. W. Brien, S&E-QUAL-Q (2)  
 Mr. A. Wittmann, S&E-QUAL-T

S&E-SSL

Mr. G. Heller, S&E-SSL-DIR  
 Mr. W. Sieber, S&E-SSL-S

A&TS-MS

A&TS-MS-H (2)  
 A&TS-MS-IP  
 A&TS-MS-IL (5)  
 A&TS-MS-D (2)

CC-P

Mr. Wofford, CC-P

KSC

Dr. K. Debus, CD  
 Dr. H. Gruene, LV  
 Mr. I. Rigell, LV-B  
 Mr. Sendler, IN  
 Mr. Mathews, AP  
 Gen. Morgan, AA  
 Dr. A. Knothe, RS  
 Mr. D. Edwards, LV-INS  
 Mr. L. Fannin, LV-MEC  
 Mr. Youmans, LV-OMO-3  
 Mr. J. Bell, LV-TMO-A  
 Mr. Lealman, LV-GDC (5)  
 Mr. Mizell, LV-PLN-12 (2)  
 Mr. O'Hara, LV-OMO  
 Mr. J. Perris, AP-SVO-3  
 Mr. Smith, AP-SVO  
 Mr. W. Jelen, IN-DAT-1

XTERNAL

Headquarters, National Aeronautics & Space Administration  
Washington, D. C. 20546

Dr. Petrone, MA  
Gen. Stevenson, MO  
Mr. Schneider, ML  
Capt. Holcomb, MAO  
Mr. White, MAR  
Mr. King, MAT  
Mr. Campbell, MAB  
Mr. Wagner, MAS (2 copies)  
Mr. Armstrong, MTX  
Mr. Lederer, MY

Director, Ames Research Center: Dr. H. Julian Allen  
National Aeronautics & Space Administration  
Moffett Field, California 94035

Director, Flight Research Center: Paul F. Bikle  
National Aeronautics & Space Administration  
P. O. Box 273  
Edwards, California 93523

Goddard Space Flight Center  
National Aeronautics & Space Administration  
Greenbelt, Maryland 20771  
Attn: Herman LaGow, Code 300

John F. Kennedy Space Center  
National Aeronautics & Space Administration  
Kennedy Space Center, Florida 32899  
Attn: Technical Library, Code RC-42  
Mrs. L. B. Russell

Director, Langley Research Center: Dr. Floyd L. Thompson  
National Aeronautics & Space Administration  
Langley Station  
Hampton, Virginia 23365

Lewis Research Center  
National Aeronautics & Space Administration  
21000 Brookpark Road  
Cleveland, Ohio 44135  
Attn: Dr. Abe Silverstein, Director  
Robert Washko, Mail Stop 86-1  
E. R. Jonash, Centaur Project Mgr.

Manned Spacecraft Center  
National Aeronautics & Space Administration  
Houston, Texas 77058  
Attn: Mr. J. McDivitt, PA  
Mr. D. Arabian, ASPO-PT (15 copies)  
Mr. G. Paulus, FC-5  
Mr. J. Hamilton, RL (MSFC Resident Office)  
G. F. Prude, CF-841 (2 copies)

Director, Wallops Station: R. L. Krieger  
National Aeronautics & Space Administration  
Wallops Island, Virginia 23337

Scientific and Technical Information Facility  
P. O. Box 5700  
Bethesda, Maryland 20014  
Attn: NASA Representative (S-AK/RKT) (25 copies)

Jet Propulsion Laboratory  
4800 Oak Grove Drive  
Pasadena, California 91103  
Attn: Ir1 Newlan, Reports Group (Mail 111-122)

Systems Engineering Group (RTD)  
Attn: SEPIR  
Wright-Patterson AFB, Ohio 45433

Office of the Asst. Sec. of Defense for Research  
and Engineering  
Room 3E1065  
The Pentagon  
Washington, D. C. 20301  
Attn: Tech Library

Director of Guided Missiles  
Office of the Secretary of Defense  
Room 3E131  
The Pentagon  
Washington, D. C. 20301

Central Intelligence Agency  
Washington, D. C. 20505  
Attn: OCR/DD/Publications (5 copies)

Director, National Security Agency  
Ft. George Mead, Maryland 20755  
Attn: C3/TDL

U. S. Atomic Energy Commission, Sandia Corp.  
University of California Radiation Lab.  
Technical Information Division  
P. O. Box 808  
Livermore, California 94551  
Attn: Clovis Craig

U. S. Atomic Energy Commission, Sandia Corp.  
Livermore Br, P. O. Box 969  
Livermore, California 94551  
Attn: Tech Library

Commander, Armed Services Technical Inf. Agency  
Arlington Hall Station  
Arlington, Virginia 22212  
Attn: TIPCR (Transmittal per Cognizant Act  
Security Instruction) (5 copies)

Commanding General  
White Sands Missile Range,  
New Mexico 88002  
Attn: RE-L (3 copies)

Chief of Staff, U. S. Air Force  
The Pentagon  
Washington, D. C. 20330  
1 Cpy marked for DCS/D AFDRD  
1 Cpy marked for DCS/D AFDRD-EX

Headquarters SAC (DPLBS)  
Offutt AFB, Nebraska 68113

Commander  
Arnold Engineering Development Center  
Arnold Air Force Station, Tennessee 37389  
Attn: Tech Library (2 copies)

Commander  
Air Force Flight Test Center  
Edwards AFB, California 93523  
Attn: FTOTL

Commander  
Air Force Missile Development Center  
Holloman Air Force Base  
New Mexico 88330  
Attn: Tech Library (SRLT)

Headquarters  
6570th Aerospace Medical Division (AFSC)  
U. S. Air Force  
Wright-Patterson Air Force Base, Ohio 45433  
Attn: H. E. Vongierke

AFETR (ETLLG-1)  
Patrick AFB, Florida 32925

EXTERNAL (CONT.)

Director  
U. S. Naval Research Laboratory  
Washington, D. C. 20390  
Attn: Code 2027

Chief of Naval Research  
Department of Navy  
Washington, D. C. 20390  
Attn: Code 463

Chief, Bureau of Weapons  
Department of Navy  
Washington, D. C. 20390  
1 Cpy to RESI, 1 Cpy to SP,  
1 Cpy to AD3, 1 Cpy to REW3

Commander  
U. S. Naval Air Missile Test Center  
Point Mugu, California 93041

AMSMI-RBLD; RSIC (3 copies)  
Bldg. 4484  
Redstone Arsenal, Alabama 35809

Aerospace Corporation  
Reliability Dept.  
P. O. Box 95085  
Los Angeles, California 90045  
Attn: Don Herzstein

Bellcomm, Inc.  
1100 Seventeenth St. N. W.  
Washington, D. C. 20036  
Attn: Miss Scott, Librarian

The Boeing Company  
P. O. Box 1680  
Huntsville, Alabama 35807  
Attn: S. C. Krausse, Mail Stop JD-12  
(20 copies)  
F. B. Williams, Mail Stop JA-51  
(1 copy)

The Boeing Company  
P.O. Box 58747  
Houston, Texas 77058  
Attn: H. J. McClellan, Mail Stop HH-05  
(2 copies)

The Boeing Company  
P. O. Box 29100  
New Orleans, Louisiana 70129  
Attn: E. R. Malthesen, Mail Stop LS-65  
(10 copies)

Mr. Norman Sissenwine, CREW  
Chief, Design Climatology Branch  
Aerospace Instrumentation Laboratory  
Air Force Cambridge Research Laboratories  
L. G. Hanscom Field  
Bedford, Massachusetts 01731

Lt/Col. H. R. Montague  
Det. 11, 4th Weather Group  
Eastern Test Range  
Patrick Air Force Base, Florida 33564

Mr. W. Davidson  
NASA Resident Management Office  
Mail Stop 8890  
Martin Marietta Corporation  
Denver Division  
Denver, Colorado 80201

Chrysler Corporation Space Division  
Huntsville Operation  
1312 N. Meridian Street  
Huntsville, Alabama 35807  
Attn: J. Fletcher, Dept. 4830 (2)

McDonnell Douglas Astronautics Company  
Missile & Space Systems Division/SSC  
5301 Bolsa Avenue  
Huntington Beach, California 92646  
Attn: G. J. Soldat (40 copies)

Grumman Aircraft Engineering Corp.  
Bethpage, Long Island, N. Y. 11714  
Attn: NASA Resident Office  
John Johansen

International Business Machine  
Mission Engineering Dept. F103  
150 Sparkman Dr. NW  
Huntsville, Alabama 35805  
Attn: C. N. Hansen (15 copies)

Martin Company  
Space Systems Division  
Baltimore, Maryland 21203  
Attn: W. P. Sommers

North American Rockwell/Space Division  
12214 South Lakewood Boulevard  
Downey, California 90241  
Attn: D. R. Binns (35 copies)

Radio Corporation of America  
Defense Electronic Products  
Data Systems Division  
8500 Balboa Blvd.  
Van Nuys, California 91406

Rocketdyne  
6633 Canoga Avenue  
Canoga Park, California 91303  
Attn: H. K. Georgius (10 copies)

Foreign Technology Division  
FTD (TDPSL)  
Wright-Patterson Air Force Base, Ohio 45433

Mr. George Mueller  
Structures Division  
Air Force Flight Dynamics Laboratory  
Research and Technology Division  
Wright-Patterson Air Force Base, Ohio 45433

Mr. David Hargis  
Aerospace Corporation  
Post Office Box 95085  
Los Angeles, California 90045

Mr. H. B. Tolefson  
DLA-Atmospheric Physics Branch  
Mail Stop 240  
NASA-Langley Research Center  
Hampton, Virginia 23365

Mr. Chasteen  
Sperry Rand  
Dept. 223  
Blue Spring Road  
Huntsville, Ala.

EXTERNAL (CONT.)

J. E. Trader  
NASA Resident Manager's Office  
McDonnell Douglas Astronautics Corp.  
5301 Balsa Avenue  
Huntington Beach, California 92646

L. C. Curran  
NASA Resident Manager's Office  
North American Rockwell/Space Division  
12214 Lakewood Blvd.  
Downey, California 90241

L. M. McBride  
NASA Resident Manager's Office  
North American Rockwell/Rocketdyne  
6633 Canoga Avenue  
Canoga Park, California 91303

C. M. Norton  
NASA Resident Manager's Office  
International Business Machines  
150 Sparkman Drive  
Huntsville, Alabama 35804

N. G. Futral  
NASA Resident Manager's Office  
North American Rockwell/Space Division  
69 Bypass NE  
McAllister, Oklahoma 74501

C. Flora  
McDonnell Douglas Astronautics Corp.  
Sacramento Test Center  
11505 Douglas Avenue  
Rancho Cordova, California 95670

W. Klabunde  
Northrop  
6025 Technology Drive  
Huntsville, Alabama 35804

David L. Christensen  
UARI, P. O. Box 1247  
Huntsville, Alabama 35807

A. T. Ackerman  
MAS-BELLCOM